Journal of RESIDUALS SCIENCE & TECHNOLOGY

VOLUME 12, SUPPLEMENT 1

JUNE 2015
ISSN (online): 2376-578X

SUPPLEMENT THEME

Residual Science and Technology for Environment Protection

GUEST EDITORS

Jerry Wu
Department of Environmental Engineering and Science
Feng Chia University

Jin Li
College of Chemica, Science and Engineering
Qingdao University

DES*tech* Publications, Inc.

Study on Modelling Infiltration Responses of Typical Top Soils Based on Infiltration Models

DEJUN YANG*, ZHENGFU BIAN, SHAOGANG LEI, SHOUGUO MU and JIBING XIONG
School of Environment Science and Spatial Informatics, China University of Mining and Technology, Xuzhou 221116, China

ABSTRACT: In this paper, we used Green-Ampt and Parlange models to simulate infiltration responses for five different typical European top soils. Different rainfall distribution types and surface storage capacity, with the same cumulative rainfall amount and rainfall interval were used to design four scenarios for simulating heavy rainfall condition in case 1. While nine scenarios were designed by different ponding depths and different functions of ponding depth with time, to simulate ponding condition in case 2. Numerical experiments showed that the sequence of soil infiltration capacity is coarse > fine > very fine > medium > medium fine, consistent to the sequence of soil saturated hydraulic conductivity K_s. Other variables, such as cumulative infiltration, runoff and the time when runoff occurs are also affected by K_s, soil water retention curve, and surface storage capacity. The parameters of soil water retention curve are the next most important factor. And more, h_s is also important for Green-Ampt model. Surface storage capacity can not only reduce the runoff but also lag the time of runoff occurrence. Reponses under different rainfall conditions vary largely, so exterior conditions should be paid more attentions when using Green-Ampt model. However, responses under different ponding distribution vary less. Thus, if ponding depth distribution is complex, constant ponding distribution type can be assumed for simplifying when Parlange model is used.

INTRODUCTION

MANY infiltration models have been proposed and developed through the past century, and these models can be categorized as empirical and theoretical-based models [1]. The empirical models usually have a simple form, and their parameters are derived by curve fitting of the equation to measurements of cumulative infiltration [1]. There are some widely-used empirical models, such as Kostiakov model [2], Kostiakov-Lewis model [3], and Horton model [4]. Compared with the numerical calculation of Richards equation, theoretical-based models are more convenient to be used [5]. Parameters of theoretical-based models can be obtained from soil properties, such as soil hydraulic conductivity, soil diffusivity, soil porosity, soil water pressure head and soil water content [1]. Thus, scientists have paid more attention to introducing and developing theoretical-based models.

Philip model [6] is based on a semi-analytical solution of Richards equation. The research [7] showed that this model was available for constant ponding head conditions. Mollerup and Hansen [8] introduced a power series solution to apply for falling ponding head infiltration with evaporation, and more generally, for variable ponding head infiltration [9]. The cumulative infiltration model, proposed by Parlange *et al.* [10] can be used as an infiltration model with variable ponding head conditions.

Another widely-used theoretical-based model is Green-Ampt model [11,12]. Many research of this model have been conducted for application in uniform [13,14,15] and layered soils [16,17], under unsteady rainfall conditions [18], and in irrigated systems [17]. Based on the Green-Ampt model, an algorithm was developed for determining the ponding condition, simulating infiltration into layered soil profile of arbitrary initial soil water distribution under unsteady rainfall, and partitioning the rainfall into infiltration, surface runoff and surface storage [19]. The Green-Ampt model was also used as a module in a GIS-based urban flood inundation model (GUFIM) [20], WEPP [21], ANSWERS [22] and SWAT [23].

Although many applications and parameter sensitivity analysis were conducted for infiltration models, exterior condition, which is of great importance for model input, has not been considered and studied. Different rainfall distribution with time can cause different infiltration input of prescribed time interval. Many

*Author to whom correspondence should be addressed.
E-mail: yangdj81@163.com; Tel: +86 15062116511

1544-8053/15/01 S001-09

doi:10.12783/issn.1544-8053/12/S1/1

models, such as WEPP, ANSWERS and SWAT, usually consider a constant rainfall distribution type with long time interval. For small rainfall intensity, it is reasonable, while for heavy rainfall intensity, it is not. Ponding depth distribution with time is very important for the input of infiltration models as well. Infiltration responses for different soils under different ponding depth distribution with time are still unknown, which is an obstacle for their usage as a module in the agro-hydrological models.

As discussed above, the algorithm of Green-Ampt model by Chu and Mariño [19] could simulate infiltration into layered soil profile of arbitrary initial soil water distribution under unsteady rainfall. As for the infiltration modeling under ponding conditions, Parlange model is easier to be used, thanks for the MATLAB solver [9]. And more, simulation results by Parlange model are more approaching to those by FEM and Philip's model [9]. Thus, these two models are potential module choices for the development of the agro-hydrological models.

In this paper, we explore different aspects of infiltration response based on the two infiltration models under different exterior conditions by numerical simulation. Here, we select five top soils for the numerical experiments [24] from Database of HYdraulic PRoperties of European Soils, and four scenarios under varying rainfall and nine scenarios under ponding conditions are designed for the five typical European top soils. The objectives of this study are: (1) to simulate infiltration responses to different soil types using two infiltration models; (2) to compare different responses under different exterior conditions; and (3) to investigate the effect of different soil hydraulic parameters on infiltration responses.

MATERIALS AND METHODS

The Green-Ampt Model by Chu and Mariño [19]

The soil profile is divided into N_c soil layers, with saturated hydraulic conductivity K_i and pressure head h_{si} at the i-th layer. When the wetting front reaches the layer n at location z ($z_{n-1} < z \le z_n$), the infiltration rate i_z, cumulative infiltration I_z and travel time t_z can be expressed as following:

$$i_z = \frac{z + h_{sn}}{\sum_{j=1}^{n-1} \frac{z_j - z_{j-1}}{K_j} + \frac{z - z_{n-1}}{K_n}} \tag{1}$$

$$I_z = I_{z_{n-1}} + (z - z_{n-1})(\theta_{sn} - \theta_{0n}) = \sum_{j=1}^{n-1}(z_j - z_{j-1})\theta_{fj} + (z - z_{n-1})\theta_{fn} \tag{2}$$

$$t_z = t_{z_{n-1}} + \frac{\theta_{fn}}{K_n}(z - z_{n-1}) + \theta_{fn}\left[\sum_{j=1}^{n-1} z_j \left(\frac{1}{K_j} - \frac{1}{K_{j+1}}\right) - \frac{h_{sn}}{K_n}\right] \ln\left(\frac{z + h_{sn}}{z_{n-1} + h_{sn}}\right) \tag{3}$$

where i_z (cm/h) is the infiltration rate; z (cm), h_{sn} (cm) and K_n (cm/h) are the depth of wetting front, the pressure head, and the saturated hydraulic conductivity of layer n, respectively; I_z (cm) is the cumulative infiltration; θ_{sn}, θ_{0n} and θ_{fn} (cm^3/cm^3) are the saturated soil water content, initial soil water content and the difference between θ_{sn} and θ_{0n} of layer n, respectively; t_z (h) is the travel time of wetting front.

Parlange Model

The infiltration model under ponding conditions [10] is written as following:

$$I - \frac{K_s H(\theta_s - \theta_i)(1 + \mu)}{i - (K_s - K_i)} = \frac{S_0^2}{2\delta(K_s - K_i)} \ln\left(1 + \frac{\delta(K_s - K_i)}{i - (K_s - K_i)}\right) \tag{4}$$

$$i = \frac{dI}{dt} \tag{5}$$

where I (cm) is cumulative infiltration; i (cm/h) is infiltration rate; H (cm) is ponding depth. We applied the MATLAB solver ode15i to solve Equation (4) [9].

S_0, δ and μ are calculated as following:

$$S_0^2 = \int_{\theta_i}^{\theta_s} D(\theta)(\theta_s + \theta - 2\theta_i)d\theta \tag{6}$$

$$\delta = \frac{1}{\theta_s - \theta_i} \int_{\theta_i}^{\theta_s} \left(\frac{K_s - K(\theta)}{(K_s - K_i)d\theta}\right) \tag{7}$$

$$\mu = \frac{1}{S_0^2 + 2K_s H_0(\theta_s - \theta_i)} \int_{\theta_i}^{\theta_s} (\theta_s - \theta) D(\theta) d\theta \tag{8}$$

where S_0 ($cm/h^{0.5}$) is sorptivity; δ is soil param-

Table 1. Initial Soil Water Content, Hydraulic Parameters and Physical Definitions of Five Soils [24,26].

Soil Type	θ_0 (cm^3/cm^3)	θ_s (cm^3/cm^3)	θ_r (cm^3/cm^3)	α (cm^{-1})	n	m	K_s (cm/d)	l	h_s (cm)	Physical Definitions
Coarse	0.1	0.403	0.025	0.0383	1.3774	0.2740	60.0	1.25	11.01	clay < 18%, sand > 65%
Medium	0.1	0.439	0.01	0.0314	1.1804	0.1528	12.061	–2.3421	16.68	18% < clay < 35%,15% < sand or clay < 18%,15% < sand < 65%
Medium Fine	0.1	0.430	0.01	0.0083	1.2539	0.2025	2.272	–0.5884	27.30	clay < 35%, sand < 15%
Fine	0.1	0.520	0.01	0.0367	1.1012	0.0919	24.8	–1.9772	8.89	clay < 35%, sand < 15%
Very Fine	0.1	0.614	0.01	0.0265	1.1033	0.0936	15.0	2.5000	16.68	60% < clay

eter related to conductivity, ranged from 0 to 1; μ is soil parameter related to ponding condition; $D(\theta)$ (cm^2/h) is diffusivity at soil water content θ; θ_s and θ_i (cm^3/cm^3) are the saturated and initial soil water content, respectively; K_s, K_i and $K(\theta)$ (cm/h) are the saturated hydraulic conductivity, initial hydraulic conductivity and hydraulic conductivity at soil water content θ; H_0 (cm) is the initial ponding depth.

Materials and Numerical Experiment

The hydraulic parameters [25], the initial soil water content and physical definitions of five soils are listed in Table 1.

The cumulative rainfall amount is 100 mm during 2 hours for Case 1. Figure 1(a) shows two rainfall distribution types. Rainfall distribution 1 refers the constant rainfall type, which is assumed as a usual rainfall type in agro-hydrological model. Rainfall distribution 2 increases linearly from 0 to a peak value, double average rainfall intensity from t = 0 to 1.4h, and decreases linearly to 0 at the end. Rainfall distribution 2 is usually used for storm profile when Rational Method is adapted to determine runoff in small catchment [27]. Four scenarios are designed for case 1 as following: C1 (rainfall distribution 1) and C2 (rainfall distribution 2) for storage storage = 0 cm, and C3 (rainfall distribution 1) and C4 (rainfall distribution 2) for storage storage = 1 cm. Figure 1(b) shows nine ponding depth distributions with time in Case 2 (P1~P9).

RESULTS AND DISCUSSION

Case 1

Figure 2 shows responses of infiltration and runoff rate with time for coarse soil under four scenarios. Under the same scenario, different soils have the similar trend of infiltration rate and runoff rate, indicating that they have the similar responses under the same scenario.

Under C1, the infiltration capacity is larger than rainfall rate, and the actual infiltration rate is equal to rainfall rate 5.0 cm/h, from beginning to 0.667 h. After 0.667 h, the actual infiltration rate begins to decrease, thus, runoff occurs due to no surface storage capacity. The actual infiltration rate decreases from 5.0 cm/h to 3.469 cm/h, while runoff rate increases from 0 to 1.531 cm/h at the end of the simulation.

The rainfall distribution of C2 causes a response quite different from that of C1. The actual infiltration rate increases to 5.907 cm/h linearly, and equals to rainfall rate before 0.827 h. At t = 0.827 h, the runoff oc-

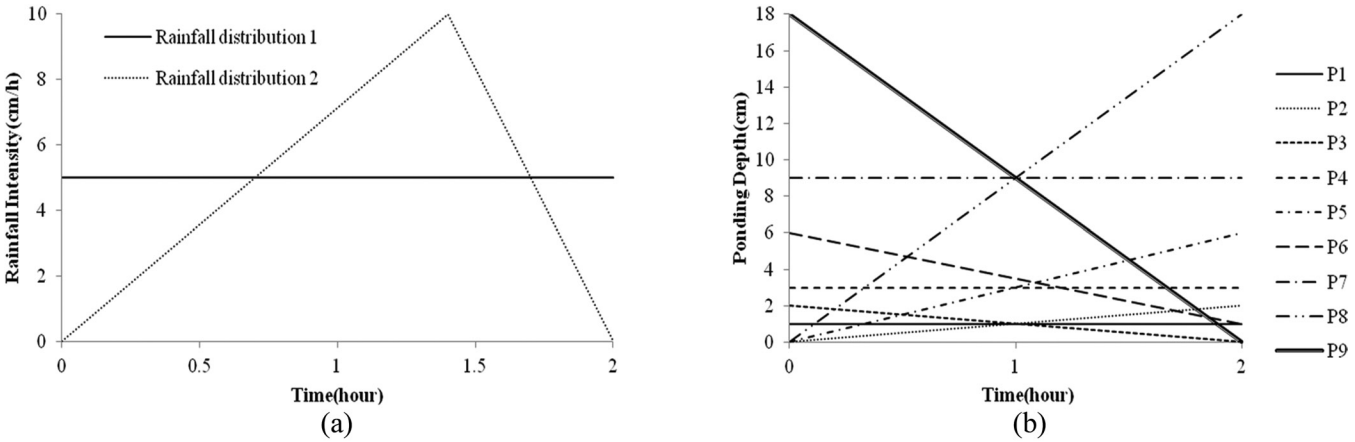

Figure 1. *(a) Different rainfall distributions for Case 1; and (b) Different ponding depth distributions for Case 2.*

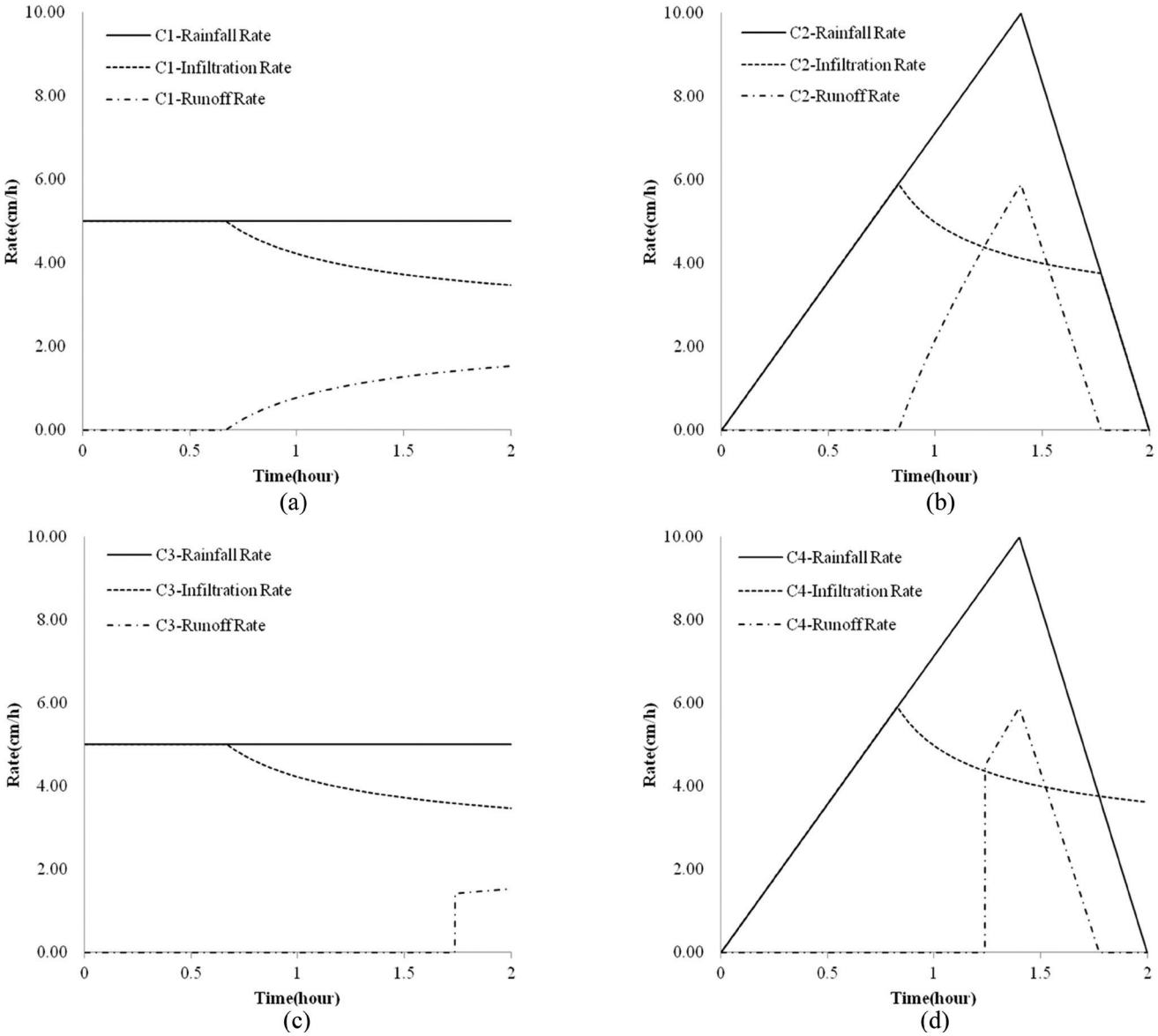

Figure 2. *Responses of infiltration and runoff rate for coarse soil under four scenarios (C1~C4 means scenario 1~4).*

curs. Then, the actual infiltration rate decreases to 3.75 cm/h during 0.827 h to 1.775 h, and again, equals to the rainfall rate after 1.775 h, when the runoff ceases. We note there are two periods during which the actual infiltration equals to the rainfall rate. The runoff rate increases to 5.884 cm/h at t = 1.4 h, when the rainfall rate peak occurs, and decreases to 0 cm/h at t = 1.775h. The runoff rate distribution curve is analogous to the rainfall distribution curve.

Under C3, the rainfall distribution is as same as that under C1, which makes the actual infiltration rate distribution curve the same as that under C1. However, there is 1cm surface storage capacity, which allows ponding to occur from 0.668 h to 1.737 h. At t = 1.737 h, the ponding process ceases, indicating the surface storage is full and runoff occurs. The runoff rate increases to 1.531cm/h at the end, same as that of C1.

Under C4, surface storage capacity allows ponding to occur from 0.827 h to 1.238 h, and runoff occurs from 1.238 h to 1.775 h. After 1.775 h, water stored in the surface, together with the rainfall, infiltrates into the soil profile. The final actual infiltration rate is 3.618 cm/h, different from 0 cm/h under C2.

For five soils under C4, the actual infiltration rate at the end is not zero when the rain ceases. This is due to the water stored in the surface transferring into infiltration. However, the actual infiltration rate at the end for five soils under C3 is as same as that under C1, when the rainfall is larger than the infiltration capacity, and surface storage is full or zero. For five soils under C1,

the actual infiltration rate at the end is larger than K_s for each soil, and less than the rainfall rate 5 cm/h. If the rainfall continues, the infiltration rate will decrease to the value of K_s.

Figure 3 shows the responses of cumulative infiltration and runoff with time for coarse soil under four scenarios. Different rainfall distribution and surface storage capacity produce different infiltration responses. See C1-Cumulative Infiltration and C2-Cumulative-Infiltration for instance, the variety for these two curves is mainly due to different rainfall distribution. As for C1-Cumulative Runoff and C2-Cumulative-Runoff, the surface storage capacity is the main reason for the difference of cumulative runoff amount.

As for responses for five soils under the same scenario, it is the soil hydraulic parameters (θ_s, K_s and h_s), which cause the responses different. Table 2 shows the cumulative infiltration, runoff, surface storage, the ratio between cumulative infiltration and rainfall, and cumulative runoff and rainfall at the end. For different soils, the responses for cumulative infiltration vary largely, from 1.83 cm to 8.60 cm, depending on the soil properties. As for different soils under C4, the cumulative surface storage for coarse is only 0.59 cm, while the cumulative surface storage is all above 0.89 cm for the other four soils. It is mainly because the K_s of coarse soil is much larger than other soils.

We can see the range of the ratio between cumula-

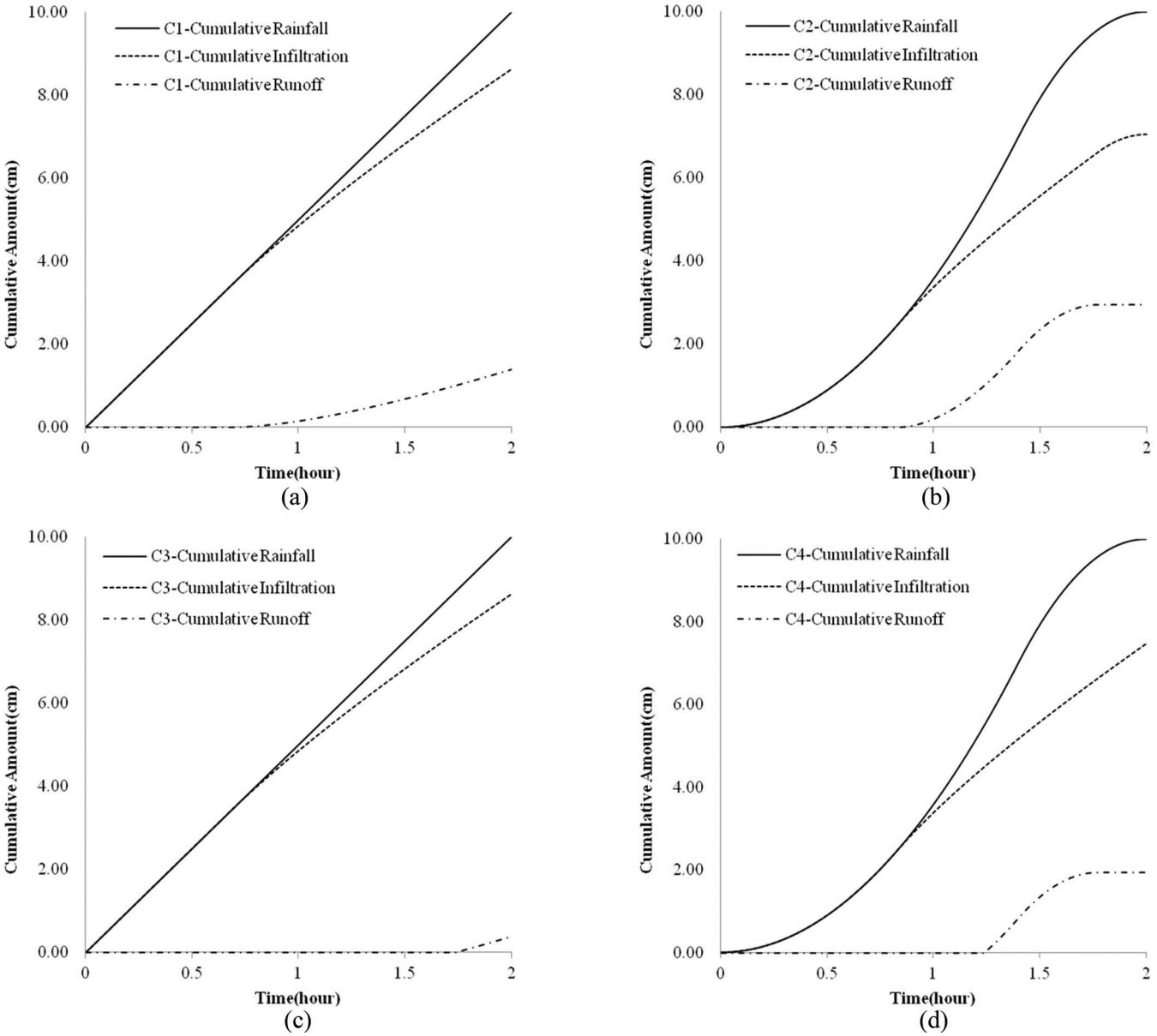

Figure 3. *Responses of cumulative infiltration and runoff amount for coarse soil under four scenarios (C1~C4 means scenario 1~4).*

Table 2. Cumulative Infiltration, Runoff, Surface Storage, the Ratio between Cumulative Infiltration and Rainfall, and Cumulative Runoff and Rainfall at the End.

Soil Type		Cumulative Infiltration (cm)	Cumulative Runoff (cm)	Cumulative Surface Storage (cm)	Infiltration/Rainfall	Runoff/Rainfall
Coarse	C1	8.61	1.39	–	0.86	0.14
	C2	7.05	2.95	–	0.71	0.29
	C3	8.61	0.39	1.00	0.86	0.04
	C4	7.46	1.95	0.59	0.75	0.19
	Average	**7.95**	–	–	**0.795**	**0.165**
Medium	C1	4.00	6.00	–	0.40	0.60
	C2	3.56	6.44	–	0.36	0.64
	C3	4.00	5.00	1.00	0.40	0.50
	C4	3.61	5.44	0.95	0.36	0.54
	Average	**3.80**	–	–	**0.38**	**0.57**
Medium Fine	C1	1.97	8.03	–	0.20	0.80
	C2	1.83	8.17	–	0.18	0.82
	C3	1.97	7.03	1.00	0.20	0.70
	C4	1.84	7.17	0.99	0.18	0.72
	Average	**1.90**	–	–	**0.19**	**0.76**
Fine	C1	5.25	4.75	–	0.53	0.47
	C2	4.54	5.46	–	0.45	0.55
	C3	5.25	3.75	1.00	0.53	0.37
	C4	4.65	4.46	0.89	0.46	0.45
	Average	**4.93**	–	–	**0.493**	**0.46**
Very Fine	C1	5.31	4.69	–	0.53	0.47
	C2	4.63	5.37	–	0.46	0.54
	C3	5.31	3.69	1.00	0.53	0.37
	C4	4.73	4.37	0.90	0.47	0.44
	Average	**4.98**	–	–	**0.498**	**0.455**

tive runoff and rainfall varies largely as well. The sequence of soil infiltration capacity corresponds to the sequence of soil K_s. The ratio of fine soil and very fine soil is very near, 0.493 and 0.498, respectively. The K_s of fine soil is 1.0333 cm/h, larger than that of very fine soil, which will lead to more cumulative infiltration for fine soil, while the h_s plays an opposite effect.

Case 2

Figure 4 shows the responses of infiltration rate for coarse soil under nine ponding scenarios. All infiltration rate curves can be divided into two stages: fast-falling rate stage and steady-falling rate stage.

Although three scenarios of each group have the same average ponding depth, the infiltration rate curve is different. The final infiltration rate for P1, P2, and P3 is 2.71 cm/h, 2.86 cm/h, and 2.52 cm/h, respectively. For different average ponding depth of the same distribution type with time, the final infiltration rate varies. The rate for P1, P4 and P7 is 2.71 cm/h, 2.93 cm/h, and 3.38 cm/h, with the infiltration rate at the end increasing with the average ponding depth.

From Table 3, we can see the final infiltration rate for five soils at the end under different scenarios. Under the same scenario, the final rate increased as the K_s increased. Under P1 for example, the final rate for coarse is the maximum, while the medium fine is the minimum. For the same soil under the same group, the infiltration rate under P3 is larger than that under P1 and P2 in the fast-falling stage, while the rate under P1 is larger than that under P2 and P3 in the steady-falling stage. Infiltration rate curve under P2 is between the curve under P1 and P3.

Figure 5 shows the cumulative infiltration with time for coarse soil under nine ponding scenes. Cumulative infiltration for each soil increases with time. During the fast-falling stage, the cumulative infiltration increases faster, when the infiltration rate is larger in this stage.

From Table 3, it is shown that, except for coarse sand, the cumulative infiltration amount of the other four sands under C1~C4 is all larger than that under

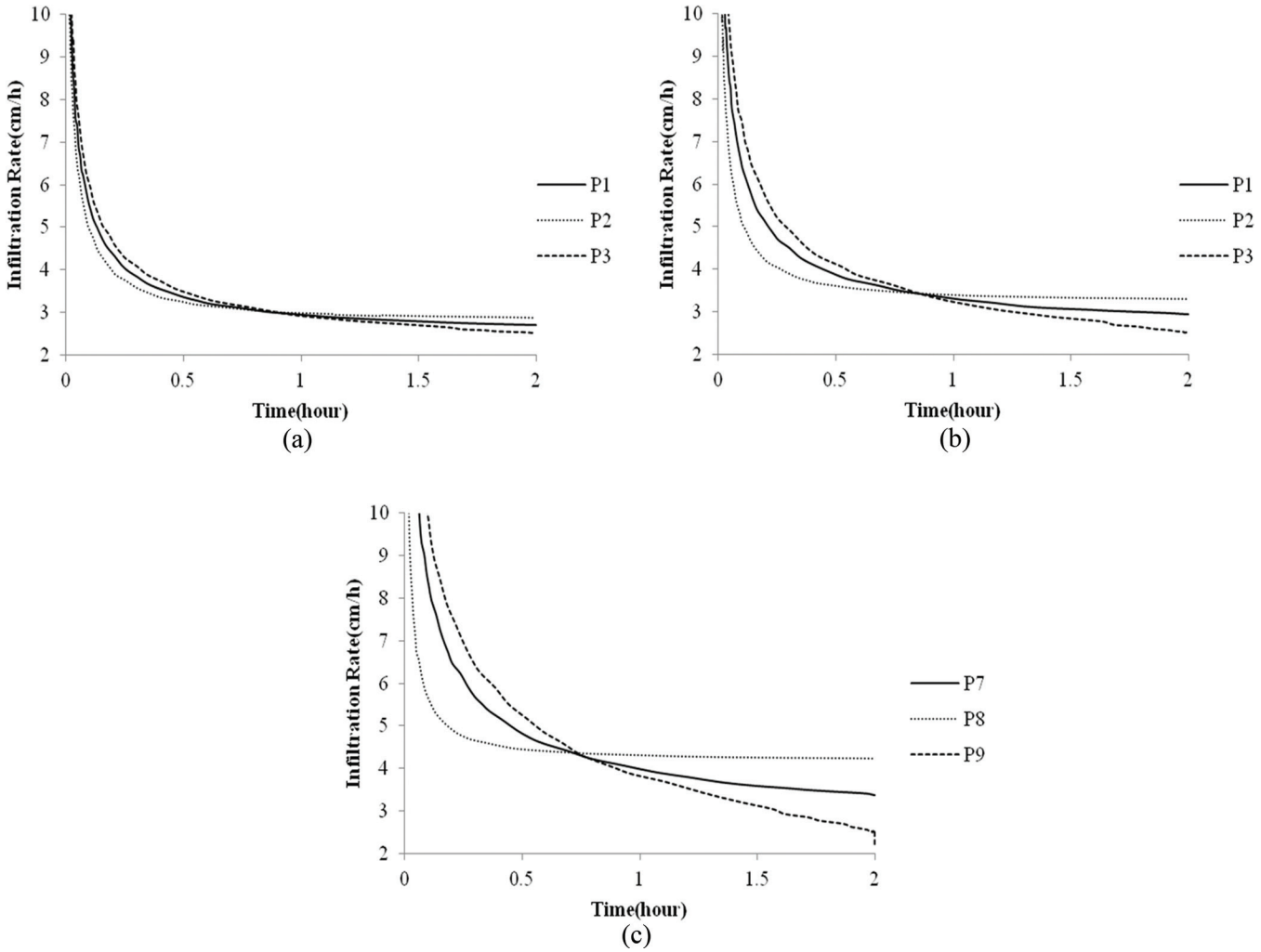

Figure 4. *Responses of infiltration rate with time for coarse soil under nine ponding scenarios (P1~-P9 means scenario 1~9).*

Table 3. The Final Infiltration Rate and Cumulative Infiltration Amount at the End for Five Soils Under Different Scenarios.

Soil Type	P1	P2	P3	P4	P5	P6	P7	P8	P9	C1	C2	C3	C4
The final infiltration rate (cm/h)													
Coarse	2.71	2.86	2.52	2.93	3.31	2.49	3.38	4.23	2.75	3.47	0	3.47	3.62
Medium	0.69	0.79	0.54	0.81	1.05	0.53	1.06	1.55	0.53	1.21	0	1.21	1.29
Medium Fine	0.37	0.39	0.34	0.39	0.46	0.32	0.47	0.64	0.28	0.53	0	0.53	0.56
Fine	1.21	1.38	1.03	1.42	1.79	1.05	1.8	2.59	1.14	1.77	0	1.77	1.86
Very Fine	0.81	0.99	0.64	1	1.36	0.64	1.35	2.06	0.65	1.64	0	1.64	1.76
The final cumulation infiltration amount(cm)													
Coarse	6.91	6.77	7.01	7.84	7.55	8.04	9.74	9.24	10.1	8.61	7.05	8.61	7.46
Medium	2.04	2.01	2.07	2.52	2.45	2.57	3.47	3.36	3.56	4	3.56	4	3.61
Medium Fine	1.36	1.36	1.36	1.47	1.46	1.46	1.74	1.73	1.74	1.97	1.83	1.97	1.84
Fine	3.16	3.01	3.25	4.01	3.78	4.15	5.6	5.31	5.81	5.25	4.54	5.25	4.65
Very Fine	2.34	2.26	2.4	3.07	2.94	3.16	4.44	4.26	4.55	5.31	4.63	5.31	4.73

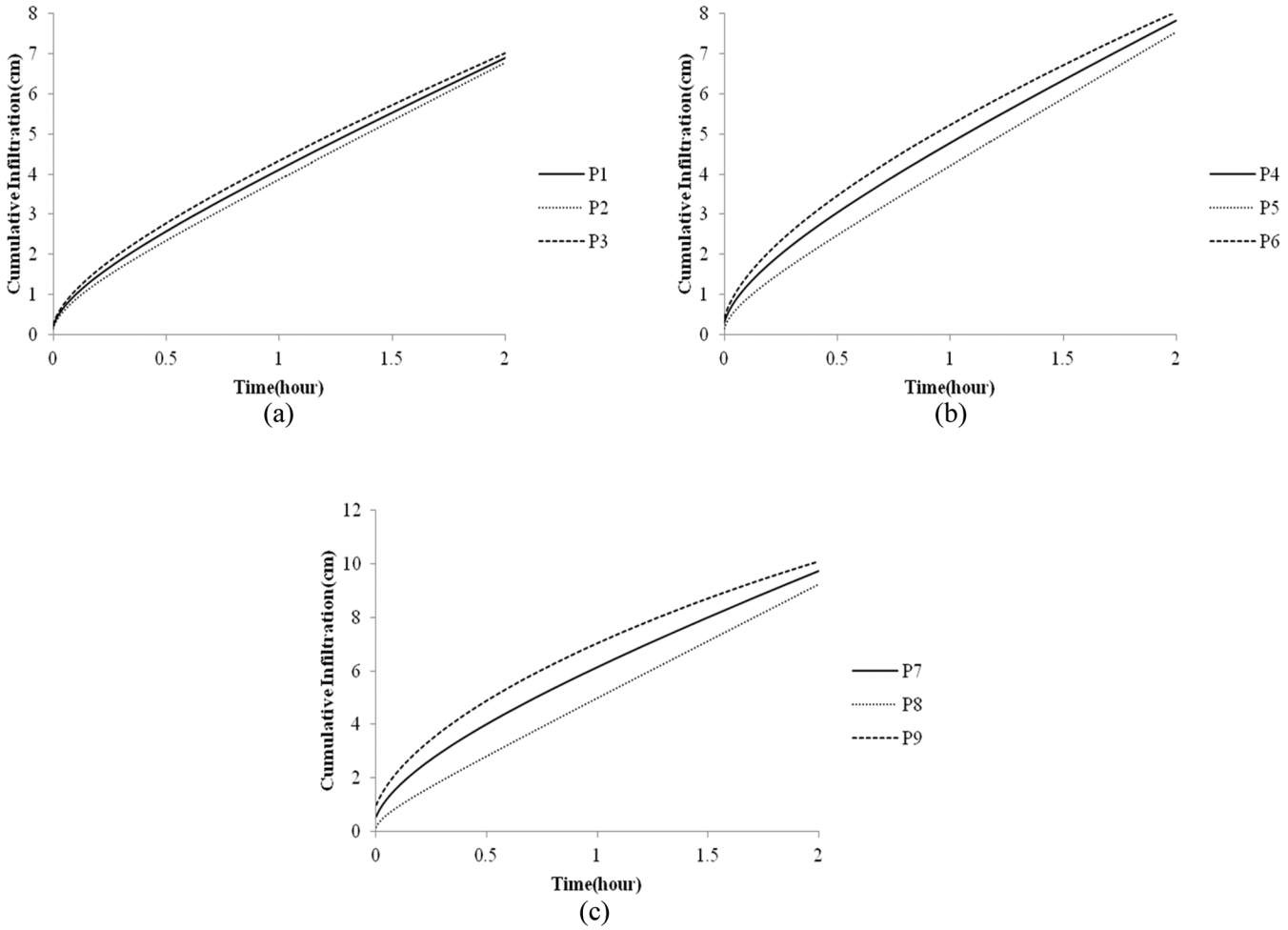

Figure 5. *Responses of cumulative infiltration with time for coarse soil under nine ponding scenarios (P1~-P9 means scenario 1~9).*

P1~P9. Cumulative infiltration amount under heavy intensity rainfall simulated by Green-Ampt model is larger than that under ponding conditions simulated by Parlange model for these four soils. The infiltration rate under C1, C2 and C4 is almost larger than that under P1~P7 and P9. This may be due to different parameters used in different models and different exterior conditions. Thus, usage of different models should be careful in choosing exterior conditions and parameters of models.

CONCLUSIONS

In this paper, we used two different infiltration models to simulate infiltration and runoff responses of five different typical European top soils. Hydraulic conductivity K_s, is the most influential parameter for both Green-Ampt model and Parlange model, as the larger the K_s is, the more water infiltrates. The parameters of soil water retention curve are the next most important factor. And more, h_s is also important for Green-Ampt model. Surface storage capacity can not only reduce the runoff but also lag the time of runoff occurrence.

Exterior conditions influence the responses differently. Reponses under different rainfall distributions with the same cumulative rainfall amount vary largely, especially for high K_s (such as coarse soil). But this is not considered in many models, which could results in error. However, responses of the same average ponding depth under different ponding depth distribution does not vary largely. If the ponding depth distribution is complex when using Parlange model, constant ponding distribution can be assumed for simplifying, with little error, especially for soil with low K_s.

Soil infiltration capacity is also found consistent by these two numerical experiments. The sequence is coarse > fine > very fine > medium > medium fine, whatever rainfall distribution and ponding depth distribution type is. Usage of different models should be careful in choosing exterior condition and parameters such as K_s, surface storage capacity and h_s of different models.

ACKNOWLEDGEMENTS

The work was supported by 973 Program (No.2013CB227904), the National Natural Science Foundation of China (No.U1361214) and the Fundamental Research Funds for the Central Universities (No. 2012QNB10). The authors gratefully thank experts for providing the data used in this study.

REFERENCES

1. Dashtaki, S.G., Homaee, M., Mahdian, M.H., Kouchakzadeh, M. Site-Dependence Performance of Infiltration Models. *Water Resources Management*, Vol. 23, No. 13, 2009, pp. 2777–2790.
2. Kostiakov, A.V. On the dynamics of the coefficient of water percolation in soils and on the necessity for studying it from a dynamics point of view for purposes of amelioration. *Transactions of the sixth commission of international society of soil science*, part A, 1932, pp. 15–21.
3. Mezencev, V.J. Theory of formation of the surface runoff. *Meteorolgia I gidrologia*, No. 3, 1948, pp. 33–46. (In Russian).
4. Horton, R.E. Approach toward a physical interpretation of infiltration capacity. *Soil Science Society of American Journal*, Vol. 5, No. 3, 1940, pp. 339–417.
5. Richards, L.A. Capillary conduction of liquids in porous mediums. *Physics*, Vol. 1, 1931, 318–333.
6. Philip, J.R. The theory of infiltration: 1. The infiltration equation and its solution. *Soil Science*, Vol. 83, 1957, pp. 345–357.
7. Philip, J.R. The theory of infiltration: 6. Effect of water depth over soil. *Soil Science*, Vol. 85, 1958, pp. 278–286.
8. Mollerup, M., Hansen, S. Power series solution for falling head ponded infiltration with evaporation. *Water Resources Management,* Vol. 43, No. 3, 2007, pp. W03425.
9. Mollerup, M. Philip's infiltration equation for variable-head ponded infiltration. *Journal of Hydrology*, Vol. 347, No. 1-2, 2007, pp. 173–176.
10. Parlange, J.Y., Haverkamp, R., Touma, J. Infiltration under ponded conditions: 1 optimal analytical solution and comparison with experimental observations. *Soil Science*, Vol. 139, No. 4, 1985, pp. 305–311.
11. Green, W.H., Ampt, G.A. Studies on soil physics: I. Flow of air and water through soils. *Journal of Agricultural Science*, Vol. 4, No. 1, 1911, pp. 1–24.
12. Ma, Y., Feng, S., Su, D., Gao, G., Huo, Z. Modeling water infiltration in a large layered soil column with a modified Green-Ampt model and HYDRUS-1D. *Computers and Electronics in Agriculture*, Vol. 71, No. S1, 2010, pp. S40–S47.
13. Dagan, G., Bresler, E. Unsaturated flow in spatially variable fields, 1. Derivation of models of infiltration and redistribution. *Water Resources Research*, Vol. 199, No. 2, 1983, pp. 413–420.
14. Govindaraju, R.S., Or, D., Kavvas, M.L., Rolston, D.E., Biggar, J. Error analyses of simplified unsaturated flow models under large uncertainty in hydraulic properties. *Water Resources Research*, Vol. 28, No. 11, 1992, pp. 2913–2924.
15. Govindaraju, R.S., Kavvas, M.L., Jones, S.E., Rolston, D.E. Use of Green-Ampt model for analyzing one dimensional convective transport in unsaturated soils. *Journal of Hydrology*, Vol. 178, No. 1-4, 1996, pp. 337–350.
16. Childs, E.C., Bybordi, M. The vertical movement of water in a stratified porous material, 1: Infiltration. *Water Resources Research*, Vol. 5, No. 2, 1969, pp. 446–459.
17. Rao, M.D., Raghuwanshi, N.S., Singh, R. Development of a physically based 1D-infiltration model for irrigated soils. *Agricultural Water Management*, Vol. 85, No. 1, 2006, pp. 165–174.
18. Chu, S.T. Infiltration during an unsteady rain. *Water Resources Research*, Vol. 14, No. 3, 1978, pp. 461–466.
19. Chu, X., Mariño, M.A. Determination of ponding condition and infiltration into layered soils under unsteady rainfall. *Journal of Hydrology*, Vol. 313, No. 3-4, 2005, pp. 195–207.
20. Chen, J., Hill, A. A., and Urbano, L. D. A GIS-based model for urban flood inundation. *Journal of Hydrology*, Vol. 373, No. 3, 2009, pp. 184–192.
21. Flanagan, D.C., Ascough II., J.C., Nearing, M.A., Laflen, J.M. 2001. The Water Erosion Prediction Project (WEPP) model. *In:* Harmon, R.S., Doe III, W.W. (Eds.), Landscape Erosion and Evolution Modeling. Kluwer Acad. Publ., Norwell, MA, pp. 145–199.
22. Bouraoui, F., and Dillaha, T. A. ANSWERS-2000: Runoff and sediment transport model. *Journal of Environmental Engineering—ASCE*, Vol. 122, No. 6, 1996, pp. 493–502.
23. Neitsch, S.L., Arnold, J.G., Kiniry, J.R., Williams, J.R. 2011. SWAT usermanual, version 2009. Texas Water Resources Institute Technical Report. A and M University, Texas, USA.
24. Wösten, J.H.M, Lilly, A., Nemes, A., Le Bas, C. Development and use of a database of hydraulic properties of European soils. *Geoderma*, Vol. 90, No. 3-4, 1999, pp. 169–185.
25. van Genuchten, M.Th. A closed-form equation for predicting the hydraulic conductivity of unsaturated soils. *Soil Science Society of American Journal*, Vol. 44, 1980, pp. 892–898.
26. Chu, X., Mariño, M. A. 2006. Simulation of infiltration and surface runoff: A Windows-based hydrologic modeling system HYDROL-INF. Graham, R. ed., *Proceedings of 2006 World Environmental and Water Resources Congress*, 1-8. Omaha, Nebraska, United States.
27. Christchurch City Council. 2011. Wetlands and Drainage Guide—Ko Te Anga Whakaora ma Nga Arawai Repa, Christchurch , New Zealand.

Heavy Metals Leaching from the Incinerator Bottom Ash Used for Road Pavement

WU MIN-HAO[1], HUANG WEI-CHIEH[1], LIN CHIOU-LIANG[1,*] and CHEN JIN-WEN[2]

[1]*Department of Civil and Environmental Engineering, National University of Kaohsiung, 700, Kaohsiung University Rd., Nanzih District, 811. Kaohsiung, Taiwan, R.O.C.*

[2]*Department of Civil Engineering, National Cheng Kung University, 1 University Rd., 701. Tainan City, Taiwan, R.O.C.*

ABSTRACT: This study analyzed the bonding strength of each kind of heavy metals by simulating the influence of pressure and acid rain when recycling incineration bottom ash from real factory as road building materials. Experimental results indicated that total leach quantity of heavy metals gradually reduced over time. After contrasting results of sequential extraction, it can be found that bonding forms of most heavy metals are organic matter state and residue state which are difficult to be leached, while the first three states are easy to be leached. The quantity of leach increased at the beginning due to the metal bonding of the first three states. In addition, compared with heavy metals in high pH value (2.88), leach quantity of all heavy metals is the largest in low pH value (1.1). However, different operating pressures have little effect on the leach of heavy metals. But if the aggregate size of bottom ash changes, it can be found that the large specific surface area of bottom ash with fine aggregate size is beneficial for the bottom ash to contact with filter liquor. Hence, leach concentration of heavy metals is higher than the bottom ash with coarse aggregate.

INTRODUCTION

DUE to increasing environmental awareness in recent years, recycling and reuse of incinerated ash has become an important trend. Nevertheless, most of the heavy metals mixed in waste were retained in bottom ash after the incineration. When the bottom ash is reused as an engineering material, some heavy metals may be released to the surrounding environment. There is scanty research on the relationship between pollution and environmental factors. Moreover, the total quantity and release velocity of heavy metals and pollutants in incinerated ash leached is closely related to environmental factors, such as pressure and pH value [1]. Leached heavy metals pose a serious threat to the environment and human health. Therefore, understanding the leaching process of heavy metals from bottom ash in different conditions is an important topic.

Sequential extraction procedure is a chemical analysis technology that selects proper acids to extract in sequence based on the mineral properties of the samples. It was first proposed by Tessier *et al.* [2]. In this method, heavy metals are often divided into five types including Exchangeable, Carbonate, Iron and Manganese oxides, Organic and Residual, of which Exchangeable, Carbonate and Iron and Manganese oxides are easy to be leached, while Organic and Residual are difficult to be leached. The sequential extraction method has been widely used in soil, bottom ash, flying ash and sludge [3–4].

To understand the impact of environmental factors on heavy metals leaching in reusing bottom ash as base material of road pavement or fill material, this study conducted an experiment in the self-made transparent high-pressure resistant test flume using the bottom ash. This study also discussed the effect of pH value, aggregate size and pressure on heavy metal leaching. Further, this study used sequential extraction method to discuss the bonding strength of each heavy metal in bottom ash when leached under different environmental conditions. The leaching sequence of each heavy metal was obtained for further analysis. Results of two experiments were compared to examine the possibility and safety of recycling of bottom ash in practical condition.

METHODS

To simulate the status of bottom ash in practical

*Author to whom correspondence should be addressed.
E-mail: cllin0407@nuk.edu.tw; Tel: 886-7-5919722; Fax: 886-7-5919376

1544-8053/15/01 S011-05

doi:10.12783/issn.1544-8053/12/S1/2

Table 1. Aggregate-Size Distribution of the Specimens.

Aggregate Size (sieve number)	Percentage of the Aggregates Passing Through the Sieve (wt%)	
	Fine Aggregate	Coarse Aggregate
37.5 mm (1-1/2″)	87–100	90–100
19.0 mm (3/4″)	45–90	50–85
4.75 mm (No. 4)	20–50	30–45
0.60 mm (No. 30)	6–29	10–25
0.075 mm (No. 200)	0–12	2–9

Table 2. Experimental Parameters.

Test No.	pH Value of the Solution	Pressure (kg/cm^2)	Aggregate Size
1	2.88	1.0	Fine
2	2.88	1.0	Coarse
3	2.88	0.5	Fine
4	2.88	0.5	Coarse
5	1.10	1.0	Fine
6	1.10	1.0	Coarse
7	1.10	0.5	Fine
8	1.10	0.5	Coarse

reuse, bottom ash from a reusable materials supplier (Ying Cheng Enterprise Co., Ltd.) was obtained. The bottom ash with an aggregate size below 75 mm is washed and screened with water. After water separation, magnetic separation, eddy current separation, winnowing, and vibration separation, the bottom ash with an aggregate size below 19 mm is chosen for further analysis.

Testing Heavy Metals Leached from Bottom Ash

The bottom ash was placed into a sieve shaker to separate bottom ash of different aggregate sizes after being fully screened. Specimens of different aggregate sizes were prepared for the experiment, as shown in Table 1. A transparent high-pressure resistant tube was designed to analyze the leaching of heavy metals from bottom ash (Figure 1). Specimens in various aggregate sizes were employed, and bottom ash aggregates with two aggregate-size distributions among a specific set of sieves were used in the experiments. The specimens were added to the tube at a fixed height to control the relative density of the aggregates. After the specimen models were completed, a test was conducted using solutions with different pH values to investigate the leaching behavior of bottom ash. Under the same pH values, two tube pressures and two aggregate sizes were examined. The filtrates were collected and separated at the tube outlet according to the aforementioned method to analyze the types and measure the total amounts of heavy metals leached from the filtrates. Eight tests were conducted. The parameters for each test are presented in Table 2.

Sequential Extraction Procedure

The sequential extraction method adopted in this study was modified from the method proposed by Tessier *et al.* [2]. The analytical method and parameters of this research were referred to a previous study [5]. First, 2.5 g of bottom ash was used for extraction according to the sequential extraction method. The solutions after extraction were treated with solid-liquid separation in high speed centrifugation (3000 rpm, 15 min). Supernatant was filtered and inductively-coupled plasma spectrograph (ICP) was used for concentration analysis of heavy metals.

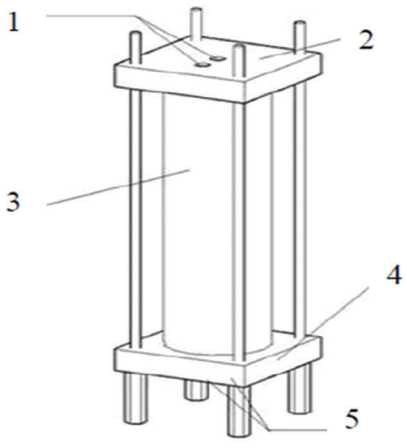

Graphic description:
1. Two holes for pressure injection or relief.
2. A square metal cap to ensure sealed experimental environment.
3. The test tube is a rounded transparent high-pressure acryl tubular column, with 9 cm for inner diameter and 11 cm for outer diameter.
4. A square metal cap to make environment sealed.
5. Two holes for solution collection or aeration injection.

Figure 1. High-pressure resistant tube.

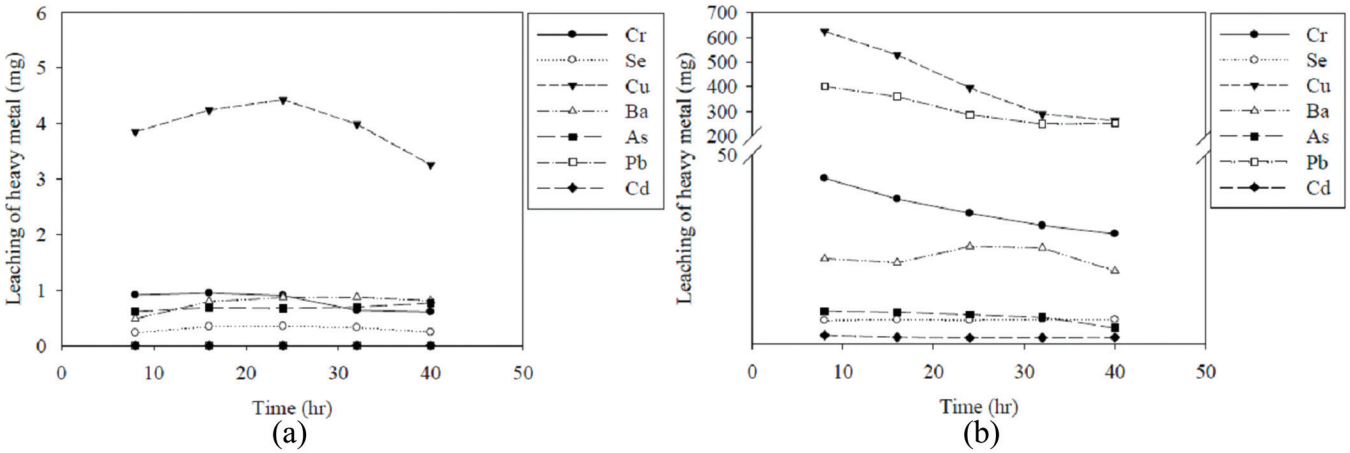

Figure 2. *Heavy metals leaching at different pH values: (a) pH = 2.88; and (b) pH = 1.10.*

RESULTS AND DISCUSSION

Influence of pH Value, Pressure and Aggregate Size on Heavy Metals Leached

Under different pH conditions, such as Runs 1 and 5 (Figure 2), the leaching amount of heavy metals in Run 5 [Figures 2(b)] was greater than those of the metals leached in Run 1 [Figure 2(a)]. The difference was significant for Cu and Pb, of which the leached amount was lower than the lower limit measured by ICP in Run 1. The leached amount, however, was very high in Run 5. Comparing the heavy metals leaching trend between the two groups, a declining trend over time was observed. This is possibly because the bottom ash leached in a large amount in the initial stage, but reduced over time. For Run 2 and Run 4, with the same aggregate size and pH condition, the pressure controlled by Run 2 was higher than that of Run 4. Comparing the leaching amount in these two runs, it was found that the amount of barium and copper leached from Run 2 (Figure 3(a)) was more than that from Run 4 (Figure 3 (b)). By comparing the leaching trend of heavy metals for these two runs, it was found that the leach amount gradually reduced over time. It can be concluded that different operating pressures had only a slight effect on the leaching of heavy metals.

Run 7 and Run 8 were operated with the same pH value and pressure but different aggregate sizes. Results reveal the total leach quantity of chromium, selenium, copper, and barium with fine aggregate size in Run 7 [Figure 4(a)] is more than those with coarse aggregate size in Run 8 [Figure 4(b)]. Leach quantity of lead and copper is far more than the other four types of metals. Herck *et al.* [6] and Kirk *et al.* [7] found that if physicochemical properties of ash are different, such as different aggregate sizes and different ingredients, the result of sequential extraction method could be easily influenced. Therefore, for two kinds of bottom ash with different aggregate sizes, specific surface area of

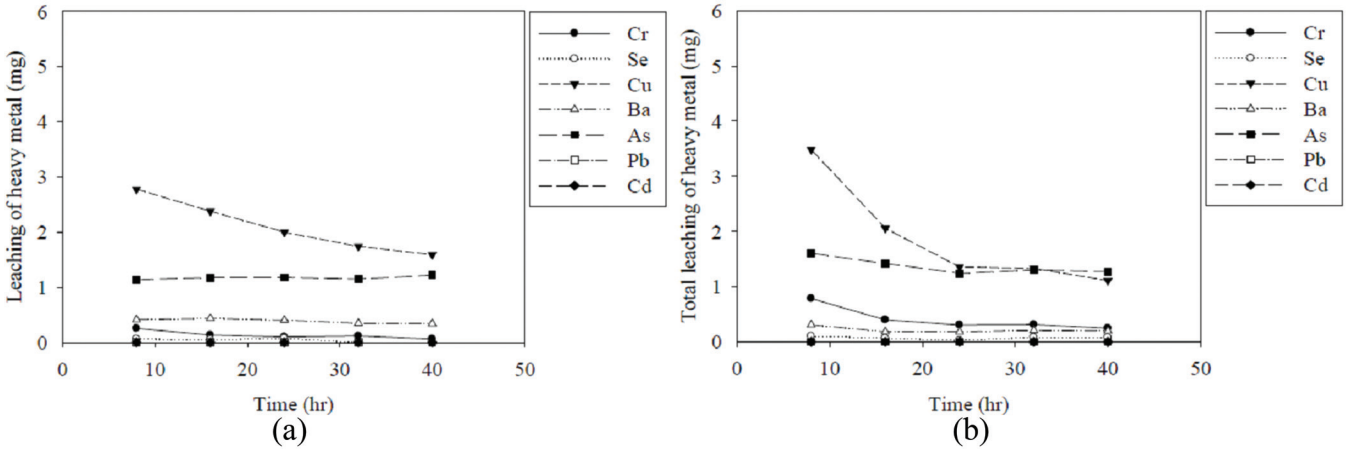

Figure 3. *Heavy metals leaching at different pressures: (a) p = 1.0 kg/cm^2; (b) p = 0.5 kg/cm^2.*

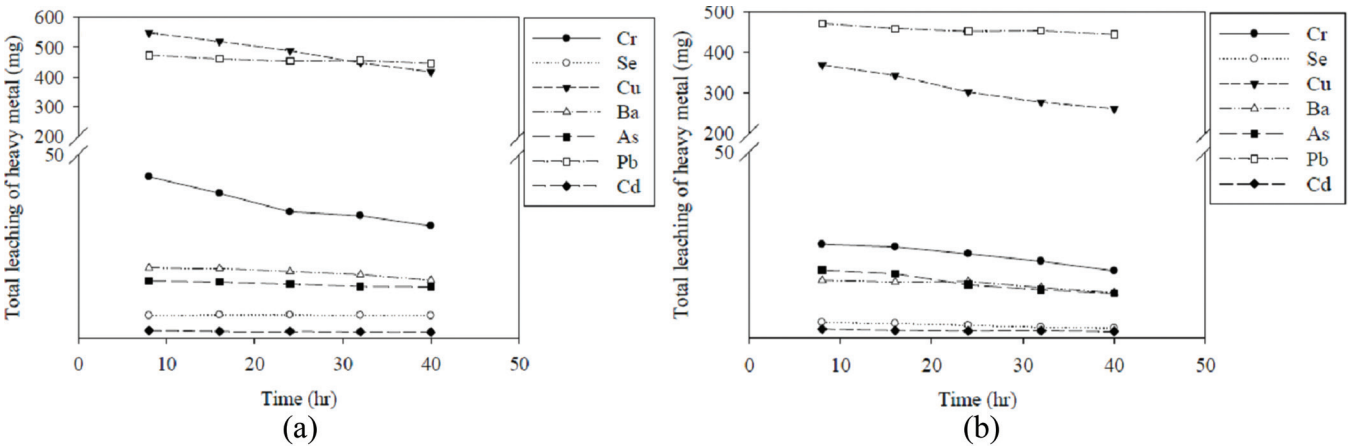

Figure 4. *Heavy metals leaching at different aggregate sizes: (a) Fine size; and (b) Course size.*

bottom ash with fine aggregate size in Run 7 is larger than that of Run 8 so that filter liquor can effectively contact with bottom ash to increase heavy metals leaching. Thus, total quantity of heavy metals leached from bottom ash with fine aggregate size in Run 7 is more than of Run 8 with course aggregate size.

Experimental Result of Sequential Extraction

After summarizing leach condition of six kinds of heavy metals, it can be found that for Cr, Se, Cu, Ba and Pb; most leached heavy metals are in the form of Fe-Mn oxide, organics and residue, while the latter two

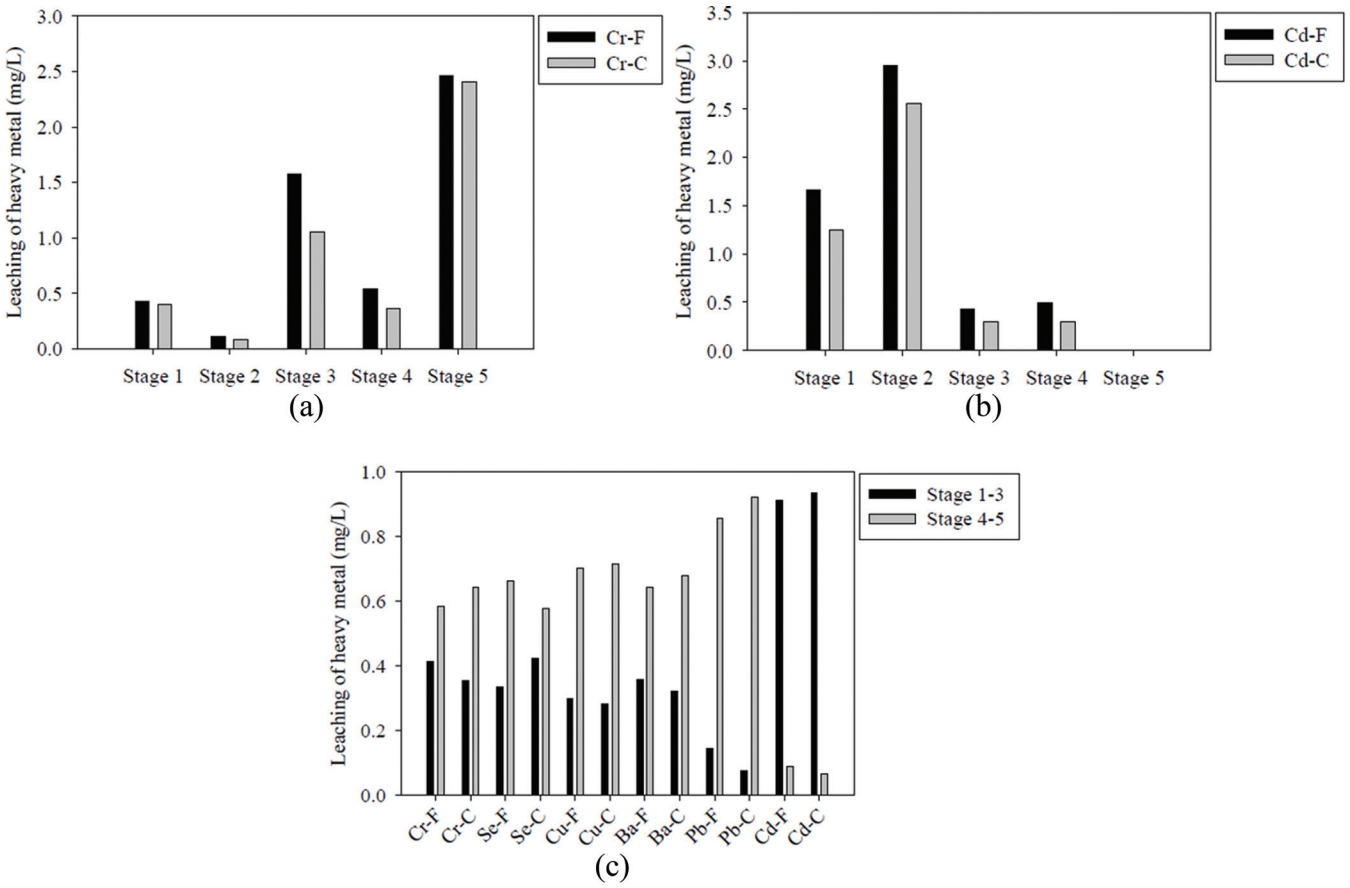

Figure 5. *Sequential extraction results: (a) Cr; (b) Cd; and (c) Ratios of various metals leached from in the first three phases to those in the final two phases.*

are the most common. For example, Figure 5(a) shows the result of heavy metal Cr as a representative. It can be estimated that it rarely moves in natural environment so that it is less harmful to nature. Among different forms of heavy metals, the proportion of the first three states of Cr, Se, Cu, Ba and Pb is not high. This might be due to the fact that the pre-processing procedure washed bottom ash before transporting bottom ash to the recycling plant. Washed bottom ash is much easier to leach heavy metals in the first three states. For Cd [Figure 5(b)], most leaching appeared in the exchangeable state and carbonized state and leach concentrates on the first three states. This indicates that Cd is more harmful to nature for its frequent moves in the natural environment. Compared with above mentioned heavy metals, the leach quantity of Cd is lower. This is probably because that Cd is of low boiling point (BP: 765°C) so that its volatility is high. In incineration processes, most Cd was volatilized and emitted into flue gases. Therefore, most Cd is in fly ash while Cd contained in bottom ash is less than other heavy metals with a higher boiling point.

Comparing bonding capability and leach sequence of heavy metals from the proportion of total leach amount of the first three states (exchangeable state, carbonized state, iron and manganese oxides states), it is found that dissociation capability of solution used in the first three states' representative test is weak and moderate (slightly alkaline). The dissociation capability of solution used in the latter two states' representative test is strong (slightly acid), which can easily break bonding within heavy metals. Comparing results from different aggregate sizes [Figure 5(c)], it can be found that the leach proportion of most heavy metals in the first three states leached from bottom ash with fine aggregate size is higher than that of bottom ash with coarse aggregate size. This indicates that a larger specific surface area of bottom ash with fine aggregate size increased the leach of heavy metal in bottom ash. As mentioned above, leach trend of heavy metals suggested that leach quantity gradually reduced over time. Comparing results of sequential extraction, it can be concluded that bonding forms of most heavy metals are in organic matter state and residue state which are difficult to be leached, while the first three states are easier to be leached. Therefore, the reason that leaches' quantity increased at the beginning is the metal bonding in the first three states, and then leach quantity gradually reduced after a period of time because only organic matter state and residue state are retained after leaching in the first three states.

CONCLUSIONS

The experimental results indicated that total leach quantity of heavy metals gradually reduced over time. Comparing results of sequential extraction, it can be found that bonding forms of most heavy metals are in organic matter state and residue state which are difficult to be leached while the first three states are easier to be leached. Therefore, the reason why leach quantity increased at the beginning is due to the metal bonding of the first three states, and then leach quantity gradually reduced over time because only organic matter state and residue state are retained after leaching the first three states. In addition, compared with heavy metals in high pH value (2.88), leach quantity of all heavy metals is higher in low pH value (1.1). However, different operating pressures have little effect on the leach of heavy metals. But if the aggregate size of bottom ash changes, it can be found that a larger specific surface area of bottom ash with fine aggregate size is beneficial for the contact between ash and filter liquor. Leach concentration of heavy metals, hence, is higher than bottom ash with coarse aggregate size.

REFERENCES

1. Wiles, C.C. 1996. "Municipal solid waste combustion ash: State-of-the-knowledge," *J. Hazard. Mater., 47*:325-344. http://dx.doi.org/10.1016/0304-3894(95)00120-4
2. Tessier, A., P. G. C. Campbell, and M. Bisson. 1979. "Sequential extraction procedure for the speciation of particulate trace metals," *Anal. Chem., 51*:844-854. http://dx.doi.org/10.1021/ac50043a017
3. Dermatas, D., G. Shen, M. Chrysochoou, D. G. Grubb, N. Menounou, and P. Dutko. 2006. "Pb speciation versus TCLP release in army firing range soils," *J. Hazard. Mater., 136*:34–46. http://dx.doi.org/10.1016/j.jhazmat.2005.11.009
4. Lin, C. F., C. H. Wu, and Y. C. Liu. 2007. "Long-term leaching test of incinerator bottom ash: Evaluation of Cu partition," *Waste Manage., 27*:954–960. http://dx.doi.org/10.1016/j.wasman.2006.07.004
5. Chou, J. D., M.Y. Wey, and S.H. Chang. 2009. "Evaluation of the distribution patterns of Pb, Cu and Cd from MSWI fly ash during thermal treatment by sequential extraction procedure," *J. Hazard. Mater., 162*:1000–1006. http://dx.doi.org/10.1016/j.jhazmat.2008.05.155
6. Herck, P. V. and C. Vandecasteele. 2001. "Evaluation of the use of a sequential extraction procedure for the characterization and treatment of metal containing solid waste," *Waste Manage., 21*:685–694. http://dx.doi.org/10.1016/S0956-053X(01)00011-3
7. Kirk, D. W., C. C. Y. Chan, and H. Marsh. 2002. "Chromium behavior during thermal treatment of MSW fly ash," *J. Hazard. Mater., B90*:39–49. http://dx.doi.org/10.1016/S0304-3894(01)00328-4

The Effect of Phosphate and Sulfate on Arsenate Desorption From Nano-TiO_2

TING LUO* and JIAJUN YU

School of Environmental Science and Engineering, 9 Xiwang Avenue, Yancheng Institute of Technology, Jiangsu 224051, China

ABSTRACT: The study focuses on the effect of phosphate and sulfate on As(V) desorption from nano-TiO_2. The results indicate that phosphate exhibits a strong influence on As(V) mobility. The desorption rate of As(V) increases according to the order: pH 9 > pH 8 > pH 7 > pH 6. The desorption rate of As(V) reaches the maximum value of 85% at pH 9, and the minimum value of 19% at pH 6. In addition, the desorption rate of As(V) increases according to the order: pH 7 > pH 8 > pH 9 > pH 6 in the presence of sulfate.

INTRODUCTION

ARSENIC (As) is a toxic and metalloid element. As contamination has become a serious threat to public health in the whole world. Inorganic forms of As, arsenite (As(III)) and arsenate (As(V)), are found in water and soil widely [1,2]. The toxicity of As(III) is 50 times more than As(V). Nevertheless, As(III) is easy to transform to As(V) in oxidizing conditions [2].

Recently, metal oxide nanomaterials have been developed as one of the most promising As removal technologies. The nanomaterials include nano-TiO_2 [3–6], zerovalent iron [7], and iron/manganese oxy-hydroxides [8–11]. It has been reported that nano-TiO_2 can be applied successfully in As adsorption from industrial wastewater and groundwater [3,12]. After these As-laden nanomaterials enter the natural environment, they may have the potential to release As to surface and groundwater under the influence of environmental factors.

Arsenic mobility is mainly controlled by microorganisms, adsorption/desorption, and coprecipitation reactions on a variety of engineered and natural nano-materials in the natural environment [13]. The adsorption/desorption reactions between As and nanoadsorbents are affected by a number of factors, such as ionic strength, pH, competing ions and the change of structure for solid phases. Competitive ions including sulfate, silicate, phosphate, and bicarbonate may influence the release of As from metal oxides, which commonly occurs in surface and groundwater [14–19]. Many studies have focused on the influence of sulfate and phosphate on As adsorption and desorption on metal oxides [16,17,20]. Previous studies have suggested that phosphate inhibits As adsorption due to competing for adsorption sites on metal oxides surfaces. Since As(V) and phosphate are both tetrahedral anions forming oxy anions in water, they have similar geochemical behaviors in the environment [21,22]. Hongshao and Stanforth [14] found that after phosphate addition, the initially adsorbed As(V) would desorb from FeOOH at pH 5, and the amount of desorbed As(V) was 6 μmol/g. Moreover, the competing role of sulfate has been investigated and found to be much less effective in causing As to desorb from metal oxides [20,23,24]. For example, Jain and Loeppert [16] observed that sulfate had no significant effect on As(V) adsorption on ferrihydrite at various pH values (from 3 to 10). Nevertheless, a few other studies reported that with the increasing sulfate concentration, the decrease of As(V) adsorption on iron oxide was observed [25].

Although many studies have been conducted on the competing role of phosphate and sulfate on As adsorption or desorption from metal oxides, only a few studies have explored the effect of sulfate and phosphate on As desorption from nanomaterials [26]. Tuutijärvi *et al.* [26] reported that phosphate had an significant impact on As(V) adsorption on nano-maghemite at pH 7. In addition, previous studies were primarily conducted with similar methods in which the competing anions and As were added to the adsorption system simultaneously (including metal oxide adsorbents). In this study, we aim to investigate how environmental competing anions affect the mobility of adsorbed As(V) on nano-

*Author to whom correspondence should be addressed.
E-mail: tluo@ycit.edu.cn, ting82333@126.com; Tel: +86 515 8829 8806;
Fax: +86 515 8829 8806

1544-8053/15/01 S017-07

doi:10.12783/issn.1544-8053/12/S1/3

TiO_2 in natural environment. Therefore, we performed the experiment with phosphate and sulfate anions added after As(V) adsorbed on nano-TiO_2 and equilibrated for 24 h.

The purpose of our study is to elucidate the effect of phosphate and sulfate on As(V) desorption from nano-TiO_2 after its adsorption reaches equilibrium. The experiment conditions were chosen to be at pH range of 6 to 9 and a series of competing anion concentrations.

MATERIAL AND METHODS

Nano-TiO_2 and Competing Anions Solution Preparation

Nano-TiO_2 used in this study was prepared with titanium sulfate. The basic properties of synthetic nano-TiO_2 can be found in previous work [3].

The salts (Na_2HAsO_4, Na_2SO_4, $Na_2HPO_4{\cdot}2H_2O$, NaCl) used in experiments were guaranteed reagents. Stock solutions of phosphate (HPO_4^{2-}, 1000 uM), sulfate (SO_4^{2-}, 5 g/L), As(V) ($HAsO_4^{2-}$, 50 mg/L), and chloride (Cl^-, 0.1 M) were prepared with the respective chemicals in deionized (DI) water. Stock solutions were diluted to working solutions for experiments.

Batch Experiment

Preadsorption experiment. Suspensions containing 50 mL As(V) (50 mg/L) and 1 g/L nano TiO_2 were prepared in a series of 50 mL centrifuge tubes. The background ion was 0.01 M NaCl. The pH of the batch experiment was adjusted to 6.0±0.1, 7.0±0.1, 8.0±0.1, and 9.0±0.1 using NaOH and H_2SO_4 solutions, respectively. pH values were chosen based on the pH of natural groundwater [2,27]. Suspensions were mixed on a rotator for 24 h, and then suspensions were centrifuged. The As-laden nano-TiO_2 loading As solid was thus obtained. The filtrate was filtered by a 0.22-μm membrane filter for soluble As(V) analysis. The final adsorption capacity of As(V) on nano-TiO_2 at different pH value was approximately 14.6 mg/g (pH 6), 11.1 mg/g (pH 7), 5.6 mg/g (pH 8), and 2.7 mg/g (pH 9) by mass balance calculation through soluble As(V) concentration.

Desorption experiment. After the As-laden nano-TiO_2 solids were obtained, one of the solids (As adsorption capacity 14.6 mg/g at pH 6) was transferred to a 50 mL centrifuge tube before 50 mL phosphate solution was added. The suspension was then rotated on a rotator for 24 h. The experiment solution was adjusted to pH 6.0±0.1 with NaOH and H_2SO_4. Subsequently, the suspension was filtered by a 0.22-μm membrane filter for soluble As(V) and phosphate analysis. The initially-added phosphate concentrations were 10, 20, 40, 80, 120, and 240 μM. For other As-laden nano-TiO_2 solids obtained at different pH (7, 8, 9), the desorption experiment procedure was the same as that of pH 6. For sulfate, the experiment procedure was the same as phosphate. The added sulfate concentrations were 50, 100, 250, 500, and 1000 mg/L. Background ion was 0.01 M NaCl in all batch experiments. The choice of phosphate and sulfate concentration in the study was based on typical levels of phosphate and sulfate in natural groundwater contaminated with As in Shanxi and Inner Mongolia, China [27,28].

Analysis

The concentration of dissolved As(V) in all samples was measured by an atomic absorption spectrometer (TAS-990, Puxi, China). The desorption rate was calculated according to the amount of As(V) adsorbed on nano-TiO_2 in the pre-adsorption experiment, and the amount of released As(V) from nano-TiO_2 in the desorption experiment. Phosphate and sulfate concentrations were measured using colorimetric methods [29].

RESULTS AND DISCUSSION

Effect of Phosphate Concentration and Solution pH on As(V) Desorption

Figure 1 and Figure 2 present the results of batch experiments of As(V) desorption with various phosphate concentrations from nano TiO_2 after 24 h equilibration. The results indicate that phosphate has a significant influence on the desorption of As(V) from nano-TiO_2. As shown in Figure 1(a), the concentration of desorbed As(V) increases from 0.8 to 7.8 mg/L with phosphate concentration increasing from 10 to 240 μM. The highest As(V) concentration is 7.8 mg/L, which is observed at phosphate concentration 240 μM and pH 6. The desorption rates of As(V) under different phosphate concentrations are shown in Figure 2A, which also increases with the increasing phosphate concentration. The lowest and highest desorption rate of As(V) are 19% and 85% at phosphate concentration 10 μM and 240 μM, respectively.

The results shown in Figure 2 and Figure 3 indicate that As(V) release from nano-TiO_2 is also influenced by pH in the presence of phosphate. The desorption

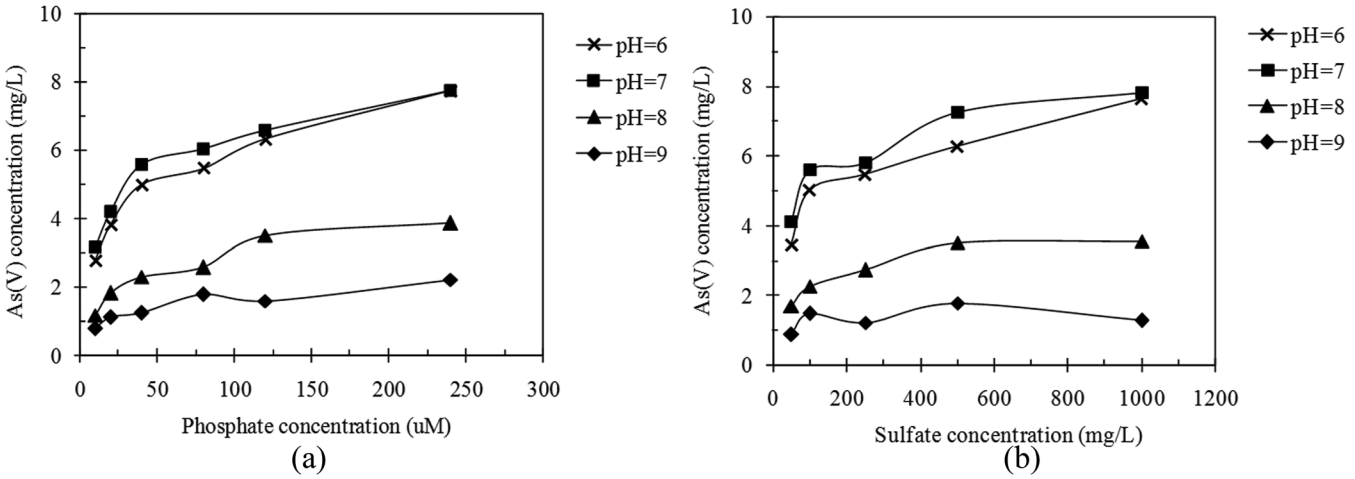

Figure 1. *Desorption of As(V) from nano-TiO_2 in the presence of: (a) phosphate; and (b) sulfate. Initial As adsorption capacity on nano-TiO_2 was 14.6 mg/g (pH 6), 11.1 mg/g (pH 7), 5.6 mg/g (pH 8), and 2.7 mg/g (pH 9). Background ion was 0.01 M NaCl.*

rate of As(V) increases with the increasing pH values (from 6 to 9). As(V) desorption rate reaches the highest value 85% at pH 9, and the lowest value 19% at pH 6 [Figure 2(a)]. In consistent with our results, the previous study reported that phosphate has an greater influence on As(V) adsorption at higher pH than at lower pH, and As(V) retention was greater at lower pH [16]. The As(V) desorption concentration also depends on pH values [Figure 3(a)]. The decrease of As(V) desorption concentration with the increasing pH values is observed, which is mainly due to the different initial adsorption capacities of As(V) on nano-TiO_2 at different pH values. According to previous studies, the adsorption behavior of As(V) on nano-TiO_2 depends on pH strongly [6]. The affinity of As(V) on metal oxide at lower pH is greater than that at higher pH, which is related to the surface charge of As(V) and metal oxide [6]. In this study, the lower desorption rate of As(V) at pH 6 instead of that at pH 9 [Figure 2(a)], which can thus be understood.

During the release of As(V) from nano-TiO_2 after addition of phosphate, the adsorption of phosphate onto nano-TiO_2 occurs (Figure 4). The adsorption rate of phosphate on nano-TiO_2 is shown in Figure 4, which is significantly affected by pH values. The maximum values of phosphate adsorption rate are 48% at pH 6, 41% at pH 7, 35% at pH 8, and 27% at pH 9, respectively. Although the phosphate concentration has no obvious influence on adsorption rate of phosphate, the amount of phosphate adsorbed on nano-TiO_2 increases with the increasing phosphate concentration (Table 1). The adsorption of phosphate on iron oxide with As(V) was also investigated in previous studies [20]. Jeong *et al.* [20] reported that the residue concentration of

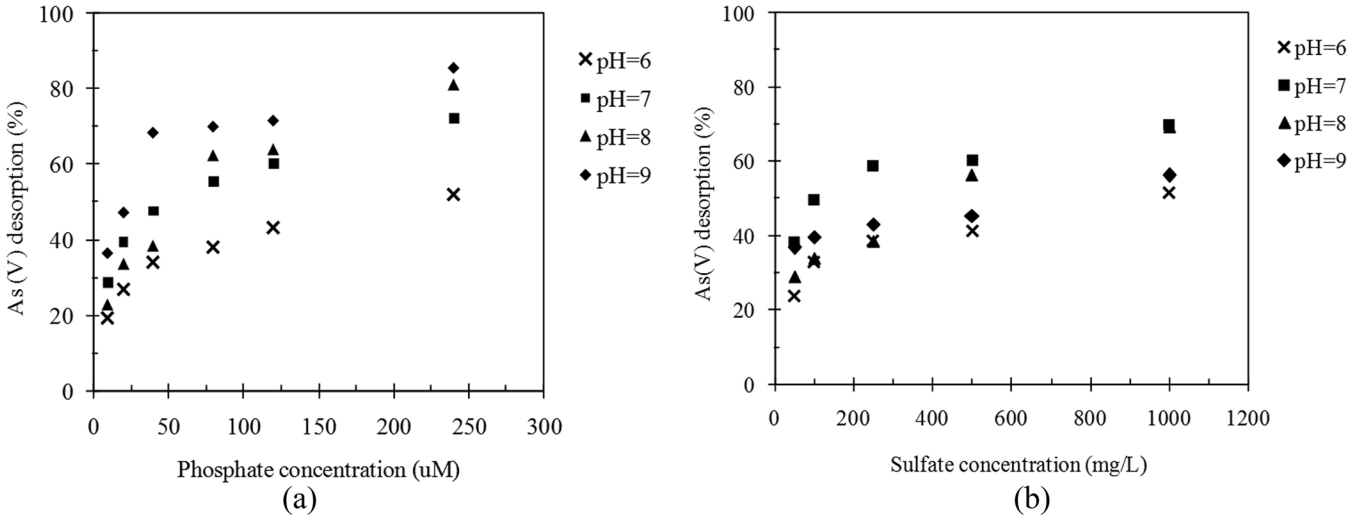

Figure 2. *Desorption rate of As(V) from nano-TiO_2 in the presence of: (a) phosphate; and (b) sulfate.*

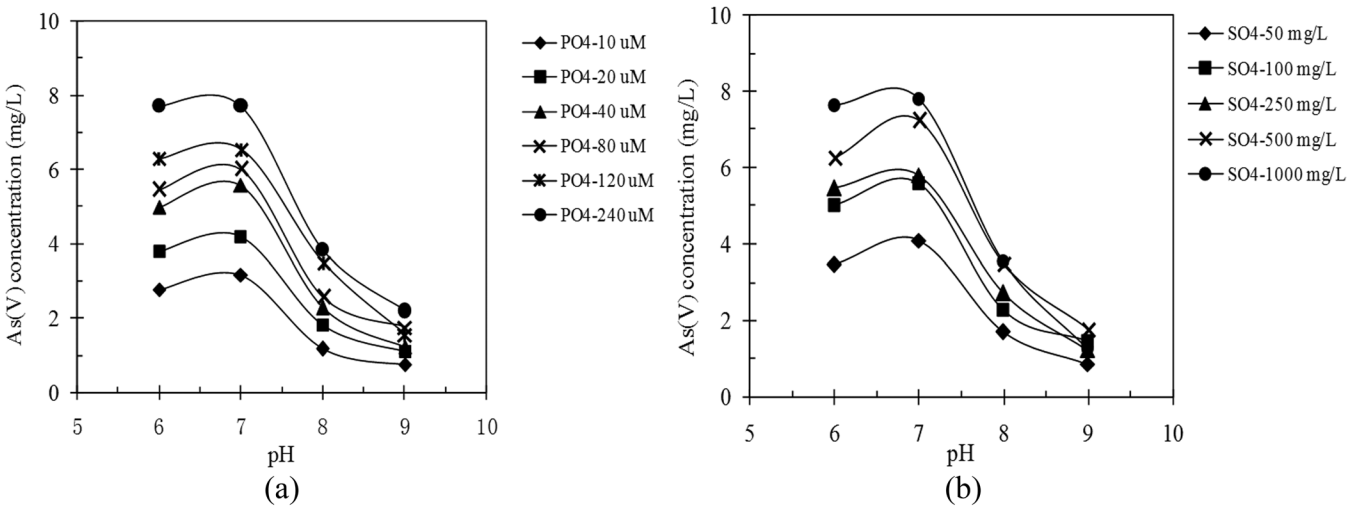

Figure 3. *Desorption of As(V) from nano TiO_2 in the presence of: (a) phosphate; and (b) sulfate as an function of pH.*

phosphate decreased significantly after adsorption by iron oxide. At initial concentration of 500 μg/L phosphate, Fe_2O_3 and Al_2O_3 adsorbed 78% and 25% of the phosphate anion respectively.

The results of desorption experiments can be explained considering the competing effect of dissolved phosphate with As(V), which means the capability of phosphate to displace As(V) previously adsorbed on the surface of nano-TiO_2 [24]. Based on the EXAFS analyses, As(V) adsorbed on nano-TiO_2 forms inner-sphere binuclear surface complexation [6]. The capability of phosphate to compete with As(V) for nano-TiO_2 surface sites can be expected given the structural resemblances between phosphate and As(V) [30–32]. Therefore, the adsorbed phosphate will presumably form an inner-sphere complex on nano-TiO_2 to compete with As(V) in this study.

Effect of Sulfate Concentration and Solution pH on As(V) Desorption

Sulfate concentration also has an influence on the release of As(V). The concentration of desorbed As(V) increases with the increasing sulfate concentration [Figure 1(b)]. The concentration of desorbed As(V) from nano-TiO_2 (Figure 1 and Figure 2) ranges between 0.7~7.7 mg/L with sulfate concentration changing from 50 to 1000 mg/L.

The result is coincident with previous studies. Wilkie and Hering [25] investigated the effect of sulfate on As(V) adsorption using iron oxide at different sulfate concentrations. They observed a considerable decrease in As(V) adsorption with sulfate, and the decreased amount became bigger with increasing sulfate concentration from 2.6 to 10 mmol/L. Nevertheless, in contrast to the result obtained in this study, Meng *et al.* [17] suggested that different sulfate concentrations (up to 300 mg/L) had no apparent influence on the removal of As(V) from ferric chloride.

In addition, As(V) release is affected by pH value in the presence of sulfate (Figures 2 and 3). The desorption rate of As(V) in the presence of sulfate [Figure 2(b)] increases according to the order: pH 7 > pH 8 > pH 9 > pH 6, which is different from the trend observed in the presence of phosphate [Figure 2(a)]. The highest concentration of desorbed As(V) is 7.7 mg/L at sulfate concentration 1000 mg/L and pH 7 [Figure 3(b)]. As mentioned before, As(V) adsorption/desorption depends on pH strongly, with higher desorption rate of As(V) occurring at higher pH. However, the desorption rate of As(V) reaches the maximum value of 69% at pH 7 instead of pH 9 in the presence of sulfate. A similar phenomenon is observed in a previous study which reported that an increased adsorption of As(V) was observed when pH > 7 at As(V)/SO_4 molar ratio of 1:50 [16]. The reason could possibly be the change of As(V) adsorption structure on nano-TiO_2 after sulfate addition.

As shown in Figure 4, the adsorption rate of sulfate is between 20%~45%. Meanwhile, the amount of sulfate adsorbed on nano-TiO_2 is calculated and shown in Table 2. The quantity of sulfate adsorbed on nano-TiO_2 increases with the increasing sulfate concentration except 1000 μM. The result is supported by other studies. Wijnja and Schulthess [33] observed that sulfate could adsorb on the surface of goethite and aluminum hydroxide. They found that both outer- and inner-sphere surface complexation of sulfate ions occurred on goe-

Table 1. The Amount of As(V) Release and Phosphate Adsorption on Nano-TiO_2 in the Presence of Phosphate.

Soil Type	Initial Phosphate Concentration (μM)	As(V) Release (mg/g)	Phosphate Adsorption Amount (mg/g)	Desorption Rate (%)
pH = 6	10	2.78	0.61	19
	20	3.81	1.16	27
	40	4.97	2.26	34
	80	5.46	4.86	38
	120	6.30	7.21	43
	240	7.72	15.67	52
pH = 7	10	3.16	0.55	29
	20	4.21	0.94	40
	40	5.57	1.79	48
	80	6.01	4.08	56
	120	6.56	6.11	60
	240	7.72	13.17	72
pH = 8	10	1.17	0.46	23
	20	1.81	0.78	34
	40	2.28	1.60	38
	80	2.57	3.30	62
	120	3.51	5.02	64
	240	3.85	11.29	81
pH = 9	10	0.77	0.27	37
	20	1.11	0.61	47
	40	1.23	1.30	68
	80	1.77	2.20	70
	120	1.58	3.45	72
	240	2.20	8.78	80

Table 2. The Amount of As(V) Release and Sulfate Adsorption on Nano TiO_2 in the Presence of Sulfate.

Soil Type	Initial Sulfate Concentration (μM)	As(V) Release (mg/g)	Sulfate Adsorption Amount (mg/g)	Desorption Rate (%)
pH = 6	50	3.46	4.91	24
	100	5.02	4.93	33
	250	5.46	12.44	39
	500	6.27	12.38	41
	1000	7.64	5.66	52
pH = 7	50	4.10	4.56	38
	100	5.59	4.24	50
	250	5.80	10.70	59
	500	7.24	10.87	60
	1000	7.82	4.92	70
pH = 8	50	1.69	4.16	29
	100	2.26	3.55	34
	250	2.72	8.80	38
	500	3.50	8.84	56
	1000	3.55	3.92	69
pH = 9	50	0.86	0.20	37
	100	1.47	2.64	40
	250	1.22	6.61	43
	500	1.78	7.21	46
	1000	1.27	2.94	56

thite and aluminum hydroxide surfaces through ATR-FTIR (attenuated total reflectance-Fourier transformed infrared) and Raman study.

Recently, many other researchers have studied the adsorption mechanism of sulfate. The results have suggested that sulfate can be adsorbed as outer-sphere [34] or inner-sphere complexation [35]. The type of bond formed may rely on experimental conditions including sulfate concentration and the order of anion addition [25,36,37]. Sulfate is adsorbed as outer-sphere complexation with sulfate concentration ≤ 0.05 M, while

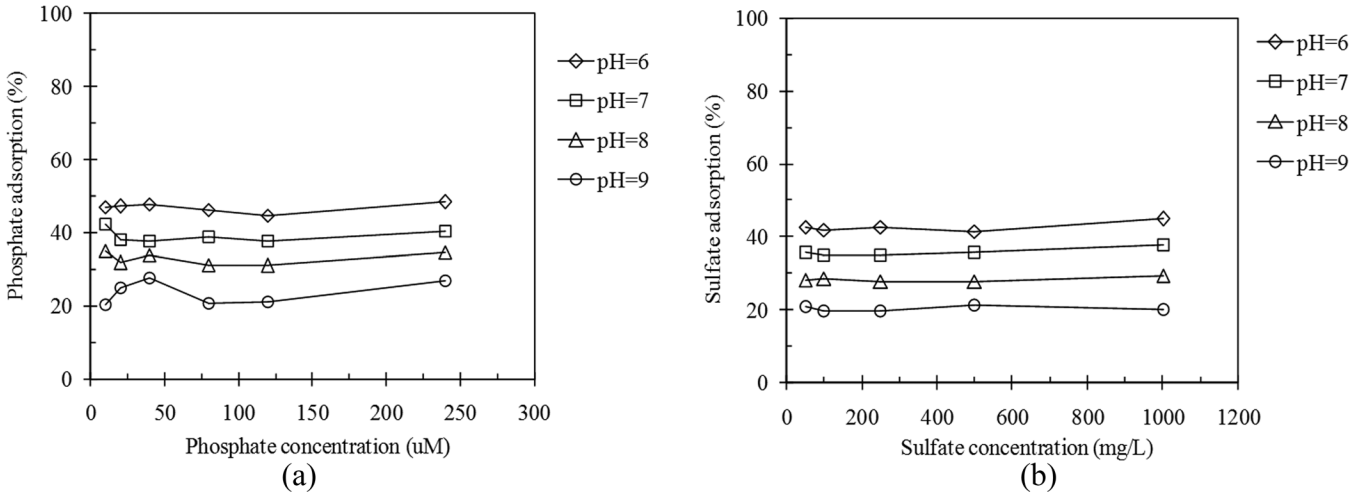

Figure 4. *Adsorption rate of (a) phosphate; and (b) sulfate on nano TiO_2. Background ion was 0.01 M NaCl.*

inner-sphere adsorption is the prevalent mechanism at higher sulfate concentrations [38]. In this study, the desorption rate of As(V) is between 23%~38% with low sulfate concentration (50 mg/L) at various pH values, and between 51%~69% with higher sulfate concentration of 1000 mg/L [Figure 2(b)].

The results indicate that sulfate adsorbed on nano-TiO_2 via inner-sphere complexation is possible with low sulfate concentrations. Therefore, the results of As(V) desorption from nano-TiO_2 induced by sulfate may be understood as sulfate forming both outer-sphere and inner-sphere complex on nano-TiO_2 surface at both low and high sulfate concentration. The results in this study are different from previous studies, which could be due to the different order of anion addition and the unique characteristics of nano-TiO_2. Violante *et al.* [36] and Ji [37] found that the order of addition affected the performance of competing ions. Oxalate was less capable to replace phosphate on goethite when the phosphate was added before oxalate, as opposed to when the two ions were added simultaneously or when oxalate was added first [36].

CONCLUSIONS

This study investigated the process of As(V) desorption from nano-TiO_2 in the presence of various phosphate and sulfate concentrations at different pH values. The phosphate exhibits a strong influence on As(V) mobility at pH 9. The highest value of As(V) desorption rate is 85% at pH 9, and the lowest value is 19% at pH 6 in the presence of phosphate. Meanwhile, phosphate adsorption on nano-TiO_2 occurs and the adsorption rate of phosphate is between 27%~48%. Sulfate also has an influence on As(V) desorption from nano-TiO_2. The desorption rate of As(V) reaches the maximum value of 69% at pH 7. The adsorption rate of sulfate on nano-TiO_2 is between 20%~45%.

More recently, the amount of used nano-materials has increased with the increasing application of nano-materials in the removal of As from contaminated waters. However, the effect of environmental competing anions including phosphate and sulfate on the mobility of adsorbed As on nano-materials is underestimated. Compared to previous studies that sulfate has no obvious effect on As mobility with low sulfate concentration, our results suggest that sulfate has a significant influence on As(V) desorption from nano-TiO_2. It sheds light on an important concern regarding the potential competing capability of sulfate, which deserves future study for deeper understanding.

ACKNOWLEDGEMENTS

We acknowledge the financial support of the National Natural Science Foundation of China (21407124), Natural Science Foundation of Jiangsu Province of China (BK20140465), State Key Laboratory of Environmental Chemistry and Ecotoxicology, Research Center for Eco-Environmental Sciences, Chinese Academy of Sciences (KF2013-10) and Foundation of Yancheng Institute of Technology (KJC2014021).

REFERENCES

1. Ferguson, J. F., and J. Gavis, ″A Review of the Arsenic Cycle in Natural Waters", *Water Res.*, Vol. 6, No. 11, 1972, pp. 1259–1274. http://dx.doi.org/10.1016/0043-1354(72)90052-8
2. Smedley, P. L., and D. G. Kinniburgh, ″A Review of the Source, Behaviour and Distribution of Arsenic in Natural Waters", *Appl. Geochem.*, Vol. 17, No. 5, 2002, pp. 517–568. http://dx.doi.org/10.1016/S0883-2927(02)00018-5
3. Luo, T., J. Cui, S. Hu, Y. Huang, and C. Jing, ″Arsenic Removal and Recovery from Copper Smelting Wastewater Using TiO_2", *Environ. Sci. Technol.*, Vol. 44, No. 23, 2010, pp. 9094–9098. http://dx.doi.org/10.1021/es1024355
4. Jegadeesan, G., S. R. Al-Abed, V. Sundaram, H. Choi, K. G. Scheckel, and D. D. Dionysiou, ″Arsenic Sorption on TiO_2 Nanoparticles: Size and Crystallinity Effects", *Water Res.*, Vol. 44, 2010, pp. 965-973. http://dx.doi.org/10.1016/j.watres.2009.10.047
5. Pena, M., G. P. Korfiatis, M. Patel, L. Lippincott, and X. Meng, ″Adsorption of As(V) and As(III) by Nanocrystalline Titanium Dioxide", Water Res., Vol. 39, No. 11, 2005, pp. 2327–2337. http://dx.doi.org/10.1016/j.watres.2005.04.006
6. Pena, M., X. Meng, G. P. Korfiatis, and C. Jing, ″Adsorption Mechanism of Arsenic on Nanocrystalline Titanium Dioxide", *Environ. Sci. Technol.*, Vol. 40, No. 4, 2006, pp. 1257–1262. http://dx.doi.org/10.1021/es052040e
7. Kanel, S. R., B. Manning, L. Charlet, and H. Choi, ″Removal of Arsenic(III) from Groundwater by Nanoscale Zero-valent Iron", *Environ. Sci. Technol.*, Vol. 39, No. 5, 2005, pp. 1291–1298. http://dx.doi.org/10.1021/es048991u
8. Deliyanni, E. A., D. N. Bakoyannakis, A. I. Zouboulis, and K. A. Matis, "Sorption of As(V) Ions by Akaganeite-type Nanocrystals," *Chemosphere*, Vol. 50, No. 1, 2003, pp. 155–163. http://dx.doi.org/10.1016/S0045-6535(02)00351-X
9. Mayo, J. T., C. Yavuz, S. Yean, L. Cong, H. Shipley, W. Yu, J. Falkner, A. Kan, M. Tomson, and V. L. Colvin, ″The Effect of Nanocrystalline Magnetite Size on Arsenic Removal", *Sci. Technol. Adv. Mat.*, Vol. 8, No. 1-2, 2007, pp. 71–75. http://dx.doi.org/10.1016/j.stam.2006.10.005
10. Tuutijärvi, T., J. Lu, M. Sillanpää, and G. Chen, "As(V) adsorption on maghemite nanoparticles", *J. Hazard. Mater.*, Vol. 166, No. 2–3, 2009, pp. 1415–1420. http://dx.doi.org/10.1016/j.jhazmat.2008.12.069
11. Tuutijärvi, T., J. Lu, M. Sillanpää, and G. Chen, ″Adsorption Mechanism of Arsenate on Crystal γ-Fe_2O_3 Nanoparticles", *J. Env. Eng.*, Vol. 136, No. 9, 2010, pp. 897–905. http://dx.doi.org/10.1061/(ASCE)EE.1943-7870.0000233
12. Jing, C., X. Meng, E. Calvache, and G. Jiang, ″Remediation of Organic and Inorganic Arsenic Contaminated Groundwater Using a Nanocrystalline TiO_2-based Adsorbent", *Environ. Pollut.*, Vol. 157, No. 8–9, 2009, pp. 2514–2519. http://dx.doi.org/10.1016/j.envpol.2009.03.011
13. Charlet, L., and D. A. Polya, ″Arsenic in Shallow, Reducing Groundwaters in Southern Asia: An Environmental Health Disaster", *Elements*, Vol. 2, No. 2, 2006, pp. 91–96. http://dx.doi.org/10.2113/gselements.2.2.91
14. Hongshao, Z., and R. Stanforth, ″Competitive Adsorption of Phosphate

and Arsenate on Goethite", *Environ. Sci. Technol.*, Vol. 35, No. 24, 2001, pp. 4753–4757. http://dx.doi.org/10.1021/es010890y

15. Anawar, H. M., J. Akai, and H. Sakugawa, "Mobilization of Arsenic from Subsurface Sediments by Effect of Bicarbonate Ions in Groundwater", *Chemosphere,* Vol. 54, 2004, pp. 753–762. http://dx.doi.org/10.1016/j.chemosphere.2003.08.030
16. Jain, A., and R. H., Loeppert, "Effect of Competing Anions on the Adsorption of Arsenate and Arsenite by Ferrihydrite", *J. Environ. Qual.*, Vol. 29, No. 5, 2000, pp.1422–1430. http://dx.doi.org/10.2134/jeq2000.00472425002900050008x
17. Meng, X., S. Bang, and G. P. Korfiatis, "Effects of Silicate, Sulfate, and Carbonate on Arsenic Removal by Ferric Chloride", *Water Res.,* Vol. 34, No. 4, 2000, pp. 1255–1261. http://dx.doi.org/10.1016/S0043-1354(99)00272-9
18. Meng, X., G. P. Korfiatis, S. Bang, and K. Bang, "Combined Effects of Anions on Arsenic Removal by Iron Hydroxides", *Toxicol. Lett.*, Vol. 113, No. 1, 2002, pp. 103–111. http://dx.doi.org/10.1016/S0378-4274(02)00080-2
19. Goldberg, S., "Competitive Adsorption of Arsenate and Arsenite on Oxides and Clay Minerals", Soil Sci. Soc. Am. J., Vol. 66, No. 2, 2002, pp. 413-421. http://dx.doi.org/10.2136/sssaj2002.4130
20. Jeong, Y., F. Maohong, J. Van Leeuwen, and J. F. Belczyk, "Effect of Competing Solutes on Arsenic(V) Adsorption Using Iron and Aluminum Oxides", *J. Environ. Sci.*, Vol. 19, No.8, 2007, pp. 910–919. http://dx.doi.org/10.1016/S1001-0742(07)60151-X
21. O'Reilly, S. E., D. G. Strawn, and D. L. Sparks, "Residence Time Effects on Arsenate Adsorption/desorption Mechanisms on Goethite", *Soil Sci. Soc. Am. J.*, Vol. 65, No. 1, 2001, pp. 67–77. http://dx.doi.org/10.2136/sssaj2001.65167x
22. Antelo, J., M. Avena, S. Fiol, R. López, and F. Arce, "Effects of pH and Ionic Strength on the Adsorption of Phosphate and Arsenate at the Goethite-water Interface", *J. Colloid Interface Sci.*, Vol. 285, No. 2, 2005, pp. 476–486. http://dx.doi.org/10.1016/j.jcis.2004.12.032
23. Goh, K. H., and T. T. Lim, "Arsenic Fractionation in a Fine Soil Fraction and Influence of Various Anions on Its Mobility in the Subsurface Environment", *Appl. Geochem.*, Vol. 20, No. 2, 2005, pp. 229–239. http://dx.doi.org/10.1016/j.apgeochem.2004.08.004
24. Frau, F., R. Biddau, and L. Fanfani, "Effect of Major Anions on Arsenate Desorption from Ferrihydrite-bearing Natural Samples", *Appl. Geochem.*, Vol. 23, No. 6, 2008, pp. 1451–1466. http://dx.doi.org/10.1016/j.apgeochem.2008.01.006
25. Wilkie, J. A., and J. G., Hering, "Adsorption of Arsenic onto Hydrous Ferric Oxide: Effects of Adsorbate/adsorbent Ratios and Co-occurring Solutes", *Colloid. Surface. A.*, Vol. 107, 1996, pp. 97–110. http://dx.doi.org/10.1016/0927-7757(95)03368-8
26. Tuutijärvi, T., E. Repo, R. Vahala, M. Sillanpää, and G. Chen, "Effect of Competing Anions on Arsenate Adsorption onto Maghemite Nanoparticles", *Chinese. J. Chem. Eng.*, Vol. 20, No. 3, 2012, pp. 505–514. http://dx.doi.org/10.1016/S1004-9541(11)60212-7
27. Luo, T., S. Hu, J. Cui, H. Tian, and C. Jing, "Comparison of Arsenic Geochemical Evolution in the Datong Basin (Shanxi) and Hetao Basin (Inner Mongolia), China", *Appl. Geochem.*, Vol. 27, No. 12, 2012, pp. 2315-2323. http://dx.doi.org/10.1016/j.apgeochem.2012.08.012
28. Guo, H., and Y. Wang, "Geochemical Characteristics of Shallow Groundwater in Datong Basin, Northwestern China", *J. Geochem. Explor.*, Vol. 87, No. 3, 2005, pp. 109–120. http://dx.doi.org/10.1016/j.gexplo.2005.08.002
29. Eaton, A. D., L. S. Clesceri, and A. E. Greenberg. 1995. Standard methods for the examination of water and wastewater, 19th, Washington, D C: American Public Health Association Publications.
30. Elkhatib, E., and A. M. Balba, "Arsenate Chemistry in Soils of Arid Ecosystems", *Alexandria Science Exchange*, Vol. 25, No. 1, 2004, pp. 229–261.
31. Arai, Y., and D. L. Sparks, "ATR-FTIR Spectroscopic Investigation on Phosphate Adsorption Mechanisms at the Ferrihydrite-water Interface", *J. Colloid. Interf. Sci.,* Vol. 241, No. 2, 2001, pp. 317–326. http://dx.doi.org/10.1006/jcis.2001.7773
32. Gao, Y., and A. Mucci, "Acid Base Reaction, Phosphate and Arsenate Complexation, and Their Competitive Adsorption at the Surface of Goethite in 0.7 M NaCl Solution", *Geochim. Cosmochim. Acta*, Vol. 65, No. 14, 2001, pp. 2361–2378. http://dx.doi.org/10.1016/S0016-7037(01)00589-0
33. Wijnja, H., and C. P. Schulthess, "Vibrational Spectroscopy Study of Selenate and Sulfate Adsorption Mechanisms on Fe and Al (Hydr)oxide Surfaces", *J. Colloid Interface Sci.*, Vol. 229, No. 1, 2000, pp. 286–297. http://dx.doi.org/10.1006/jcis.2000.6960
34. Zhang, P. C., and Sparks, D. L, "Kinetics and Mechanisms of Sulfate Adsorption/desorption on Goethite Using Pressure-jump Relaxation", Soil. Sci. Soc. Am. J., Vol. 54, 1990, pp. 1266–1273. http://dx.doi.org/10.2136/sssaj1990.03615995005400050011x
35. Peak, J. D., R. G. Ford, and D. L. Sparks, "An in situ ATR–FTIR Investigation of Sulfate Bonding Mechanisms on Goethite", *J. Colloid Interface Sci.*, Vol. 218, No. 1, 1999, pp. 289–299. http://dx.doi.org/10.1006/jcis.1999.6405
36. Violante, A., C. Colombo, and A. Buondonno, "Competitive Adsorption of Phosphate and Oxalate by Aluminum Oxides", *Soil Sci. Soc. Am. J.*, Vol. 55, 1991, pp. 65–70. http://dx.doi.org/10.2136/sssaj1991.03615995005500010011x
37. Ji, G. L., "Competitive Adsorption of Phosphate and Fluoride on Iron Oxide", *Acta Pedologica Sinica*, Vol. 23, 1986, pp. 220–227.
38. Kinjo, T., and P. F. Pratt, "Nitrate Adsorption: II. Competition with Chloride, Sulphate and Phosphate", *Soil Sci. Soc. Am. Proc.*, Vol. 32, 1971, pp.725–728. http://dx.doi.org/10.2136/sssaj1971.03615995003500050028x

The Analysis of Impact Factors for Dissolved Oxygen Concentration in Wastewater Treatment System Using an Adaptive Modeling Method

AIMIN AN*, LICHUN QI, HAOCHEN ZHANG and YONGXIN CHOU
College of Electrical and Information Engineering, Lanzhou University of Technology, Lanzhou, 730050, Gansu, China

ABSTRACT: The dissolved oxygen concentration (DOC) in water is an important indicator of self-purification capacity of water in wastewater treatment system. In this study, the operating processes of wastewater treatment systems are modeled based on the mechanism model. Meanwhile, different factors that influence the DOC are analyzed. The adaptive dynamic model of DOC is established in the Matlab environment considering white noise in the model input. The effect of the input variables (e.g., aeration tank) and load variables (e.g., oxygen consumption) on the DOC is analyzed in detail when white noise is considered in the model input. The transform transient characteristics of DOC are obtained after leaving out outliers of the input variables. As an on-line outlier's detection method, abnormal value detection is used to remove the inferior quality data in order to ensure the reliability of the efficiency of the developed model. Results demonstrate that the adaptive dynamic simulation model can be used to improve both the accuracy of modeling and the ability of modeling system dynamics.

INTRODUCTION

WASTEWATER treatment system is a nonlinear system with time-varying, strong-coupling characteristics. Its performance could be affected by many factors, e.g., water flow, the sludge load and uncertain mixed composition in sewage inflow. Also, the dissolved oxygen concentration (DOC) in the wastewater treatment system has nonlinear, time-varying, serious interference characteristics [1–2]. There are strong coupling relationships among the concentration of dissolved oxygen, water components and biochemical pool components. The DOC is one of the most significant control variables in treatment processes for activated sludge. Some efficient operation and control technologies have been widely investigated in order to obtain optimal DOC under the premise that qualified effluent quality could be achieved. By doing this, one can minimize operating costs [3].

For the control strategies for DOC in the wastewater treatment processes, many studies have been done in the literature. Holmberg *et al.* have studied a dynamics model, which can be used to estimate biochemical oxygen demand (BOD) of the inflow and BOD of the effluent [4]. A recursion method is used to estimate the oxygen transfer coefficients and oxygen uptake rate (OUR). Estimation of oxygen transfer coefficient and OUR according to oxygen transfer model is proposed by Olsson and Andrews, *et al.* [5–8]. The Kalman filtering technique was used in the work by Olsson; Andrews *et al.* took into account the dissolved oxygen for the constant manipulation. Its differential coefficient was found close to zero; thus transient characteristics of transmission model can be ignored. The least square method is used to estimate these parameters when the system is at steady-state. Marsili-libelli *et al.* [9] have used the least squares technique to estimate oxygen transfer coefficient and OUR in real time according to the dynamic characteristics of the air flow and dissolved oxygen. Controlling DOC in the processes of wastewater treatment is, however, still an operational challenge [10]. A key question for this is what the primary factors that influence the DOC are.

According to the characteristics of biochemical sewage treatment processes, an adaptive dynamic model is built by using the module of SIMULINK in Matlab to simulate DOC, based on a previous study [11]. Combined with the self-tuning control theory, such simulation model can be used to simulate the effect of the input variables (aeration tank to provide oxygen capacity) and the load variable (necessary oxygen con-

*Author to whom correspondence should be addressed.
E-mail: anaiminll@163.com; Tel: 13519602893; Fax: 0931-2973506

1544-8053/15/01 S025-06

doi:10.12783/issn.1544-8053/12/S1/4

sumption) on the DOC; even white noise exists in the input variables. Meanwhile, a detection method is used to detect outliers of the input variables; the transient change characteristics of DOC are also examined.

WASTEWATER TREATMENT PROCESSES DESCRIPTION

DOC plays an important role in biological wastewater treatment process. The aeration tank of oxygen deficiency or excess will lead to the deterioration of activated sludge's living environment. If the oxygen is insufficient, filamentous bacteria can breed, leading to the final sludge expansion in the aeration tank. On the other hand, effluent water quality could be affected due to the decreased growth rate of other bacteria. When oxygen is excessive, it will cause sedimentation variation of suspended solids due to the destruction of the flocculant. At the same time, the cost of wastewater treatment could be increased by high energy consumption.

A biochemical pool generally is also named as an aeration tank, where aerobic biological oxidation occurs. Activated sludge process is a complex system occurring in an aeration tank. But if only considering the DOC, the processes in the aeration tank are comprised of two components, namely water and dissolved oxygen. Dissolved oxygen can be provided to the system either through water containing dissolved oxygen or through oxygen mass transfer occurring in the interface of gas and liquid. Generally, oxygen should be transferred from gas phase to the surface of the water, and then dissolved in water before it is transferred to the main body of liquid phase from the water surface.

In order to improve the applicability of the simulation results, the BSM1 model that is internationally recognized by the international water association (IAWQ) was selected to simulate the biological processes. Wastewater treatment processes are composed of one biological reaction tank and two sedimentation tanks, as shown in Figure 1. The biological reaction tank is composed of five units and a stirring device where the denitrification reaction occurred, followed by the aeration pool. The oxygen charging device is at the bottom of the three units, where the oxidation reaction of carbon and nitrogen nitrification occurred. The analysis presented in this study is mainly for reactions occurring in the three units.

MATHEMATICAL MODEL OF DOC

Dynamics of DOC

The BSM1 contains 13 kinds of components, 8 reaction processes and 19 parameters. It could be affected by many factors, such as the complex structure of the model itself, model parameters, various processes in sewage treatment plants and the capabilities of instruments measuring water quality parameters. In practice, justified assumptions are often needed to establish a simplified BSM1 model.

Due to the strong turbulence associated with wastewater flow in the treatment of plants, it is reasonable to assume that the oxygen is saturated in both the gas phase and liquid phase. Therefore, the dynamics of DOC can be represented in Equation (1):

$$V\frac{dC}{dt} = Q_{IN}C_{IN} - Q_{OUT}C + V \cdot K_L a(C_{SAT} - C) - OUR \tag{1}$$

where V is volume of aeration tank in m^3; Q_{IN} is water flow in m^3/h; Q_{OUT} is effluent flow in m^3/h; C is

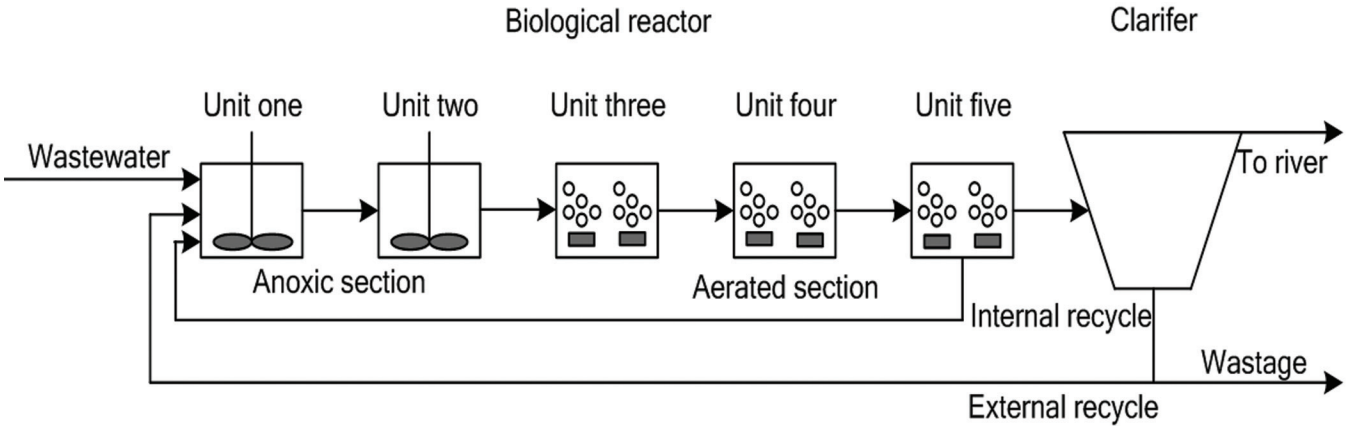

Figure 1. *BSM1 benchmark layout.*

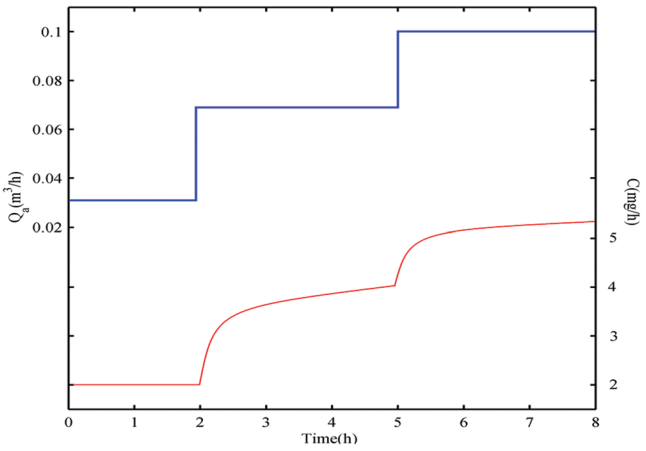

Figure 2. *Aeration tank air flow changes and dissolved oxygen response curves.*

DOC in mg/L; C_{IN} is the DOC in the water in the unit of mg/L; C_{OUT} is saturated DOC in mg/L; K_La is dissolved oxygen mass transfer coefficient in the unit of h^{-1}; and OUR is oxygen absorption rate associated with the substrate in the water.

Assuming the pool is thoroughly mixed and its capacity is constant, Equation (1) can be simplified to Equation (2):

$$\frac{dC}{dt} = \frac{Q_{IN}}{V}(C_{IN} - C) + V \cdot K_a Q_a (C_{SAT} - C) \quad (2)$$

Where K_a is a constant in the unit of m^{-3}; Q_a is air flow in the unit of m^3/h.

Simulation results of the input—output response of the aeration tank from this model is shown in Figure 2. It can be seen that DOC at the outlet of the aeration tank was slowly increasing and reached steady state gradually [11], when air flow fed to the aeration tank was increased by a step change. The product of the air flow and the DOC is not linear with air flow, where a nonlinear relationship was observed.

Dynamic Model Construction

In wastewater aeration tank, the amount of transient oxygen is obtained through ordinary differential equations (ODE). The oxygen concentration is varied with time, but not with position. For reason of a simpler presentation, the transfer process of oxygen is simplified to a transient process. For simulating the transient process, which is chosen as input process of the aeration tank, the Laplace transformations to differential equations are applied to generate operator equations and the corresponding transfer functions.

The dynamic model depends on the sensitivity and inertia index. In this paper, the mathematical model is studied by a graphic simulation model. The steady state equation of dissolved oxygen and the transfer function were used in mathematical modeling. The Simulink module in the Matlab software is used to model the transient processes, using empirical analysis of sensitivity of sewage aeration tank and inertia index variables.

DOC of the steady-state equation can be further simplified in Equation (3):

$$C = C_{ox} - \frac{L \cdot k_1(h, \lambda_1, \delta_s)}{R_g \cdot k_2(T, h)} \quad (3)$$

Using the formulations from reference [12], the calculation results about the DOC linear model were derived. k_1 and k_2 are correction coefficients, and the values are 1.12, and 1.53; respectively; C_{ox} is oxygen solubility, the value is 13.0 g/m^3; K_{a0} is transfer coefficients, its value is 0.18 $(g/m_3)/(m_3/min)$, and K_{q0} is –0.012 $(g/m^3)/(m^3/min)$.

The interpretation and description about all the parameters associated with the DOC model are shown in Table 1.

In general, the dynamic process occurs in the aeration tank, since the K_a (R_g, L), K_q (R_g) and the process inertia constants change with the transition of oxygen, and these parameters are time-varying. The inertia time constants and the transfer coefficients separately are defined as inertia indexes and sensitivity indexes.

Table 1. Parameters, Symbols and Meanings.

Parameters, Symbols	Meanings	Unit
C_{ox}	oxygen solubility	g/m^3
T	wastewater temperature	°C
h	submerging depth of air diffusors	m
$L = Q(R_a - R_t)$	oxygen consumption in wastewater treatment as a required load	g/min
Q	wastewater afflux	m^3/min
R_a	total pollution control of the oxygen demand	g/m^3
R_t	oxygen demand in effluent wastewater	g/m^3
R_g	the amount of air provided to the aeration tank	m^3/min
$K_1(h, \lambda_d, \delta_s)$	aeration unit estimating coefficient of oxygen concentration	/
λ_d	with a disk export airflow intensity	m^3/h
δ_s	disk density of the floor area of aeration tank	/
$K_2(T, h)$	oxygen transfer coefficient of activated sludge	/

In the transient process, the sensitivity and inertia indexes are mathematically defined as follows:

$$K_a(R_g, L) = \frac{L \cdot k_1(h, \lambda_d, \delta_s)}{R_g^2 \cdot k_2(T_0, h)}$$

and

$$K_q(R_g) = -\frac{k_1(h, \lambda_d, \delta_s)}{R_g \cdot k_2(T_0, h)} \quad (4)$$

$$T_a(R_g) = \frac{V \cdot k_1(h, \lambda_d, \delta_s)}{R_g \cdot k_2(T_0, h)}$$

and

$$T_q(L, C) = \frac{V \cdot C.k_2(T_0, h)}{L \cdot k_1(h, \lambda_d, \delta_s)} \quad (5)$$

Coefficient k_1 (h, λ_1, δ_s) is a function of the variable λ_d. Though k_1 changes only 3% of k_{10}, it can be assumed that k_1 and k_{10} are of the same value, 1.12. Water temperature, T, is 10°C; submerging depth of air diffusers, h, is 4 m; disk density of the floor area of aeration tank δ_s is 0.063; with a disk export airflow intensity, λ_d, is 1.5 m^3/h; and wastewater volume in aeration tank, V, is 1200 m^3.

The mathematical model of the oxygen concentration $C(t)$ in the process of the transient could be obtained by Laplace transform, as shown in Equation (6). [13]:

$$C(s) = Y_a(s) \cdot \Delta R_g(s) + Y_q(s) \cdot \Delta L(s) + C_0 \quad (6)$$

$$Y_a(s) = \frac{K_a(R_g, L)}{T_a(R_g) \cdot s + 1}, \quad Y_q(s) = \frac{K_q(L_g)}{T_q(L, C) \cdot s + 1} \quad (7)$$

where $C(s)$ is the result of the oxygen concentration processed by Laplace transform in the dynamic model; $Y_a(s)$ is the transfer functions of an input impact channel, and $Y_q(s)$ is taken as the transfer functions of a load impact channel.

As the oxygen transient process of transfer function is steady, the equations can't be directly solved. Numerical results, however, can be obtained using Matlab.

Abnormal Value Detection Method

Due to the characteristics of strong nonlinear, time-varying parameters in the sewage treatment process, the process operated in a dynamic complex disturbance environment, uncertain disturbance will make the data inferior. At the same time, the incorrect operation or measurement instrument failure, abnormal measurement could be recorded. The presence of such outliers can often affect the prediction performance of the model. Therefore, an on-line outliers detection method was developed. The 3δ rule is the simplest method for outlier detection. However, as the mean and standard deviation could be easily affected by outliers, practical application of the 3δ rule is limited. Hampel used the median absolute deviation (*MAD*) and median (*Med*) instead of the standard deviation and mean and developed a more robust detection method [14]. Given a set of measuring sequence x :{ x (t), t = 1, 2,…, L}, if

$$|x(t) - Med(x)| > 3 \times MAD(x) \quad (8)$$

Among them

$$MAD(x) = 1.4826 \times Med(x - Med(x)) \quad (9)$$

Based on the definition of Hampel method, $x(t)$ are marked as outliers [15].

In this study, the measurement data is defined as a moderate outlier if it meets Equation (8) and does not meet Equation (10). A measurement data is defined as a severe abnormal value if it meets Equation (10).

$$|x(t) - Med(x)| > 6 \times MAD(x) \quad (10)$$

The rest of the measurement data is defined as normal data.

Through detecting the input variables and excluding the abnormal value, the correctness of input data quality can be ensured. This will relieve the high interference problem in the wastewater treatment process.

SIMULATION RESULTS

The initial value of transfer coefficient for the dynamic model, K_{a0}, is 0.18(g/m^3)/(m^3/min), and K_{q0} is –0.012(g/m^3)/(m^3/min) [16–18]. At the same time white noise was added to the model input. Simulation results are shown in Figure 3.

Initial values for the following were set to model sensitivity and inertia index. Sewage aeration capacity L_{g0} is 60 m^3/min; Oxygen consumption load q_0 is 900 g/m^3; Oxygen concentration C_0 is 2 g/m^3. At the same time white noise was added to the model input. The sensitivity and inertia index of the dynamic model are shown in Figure 4.

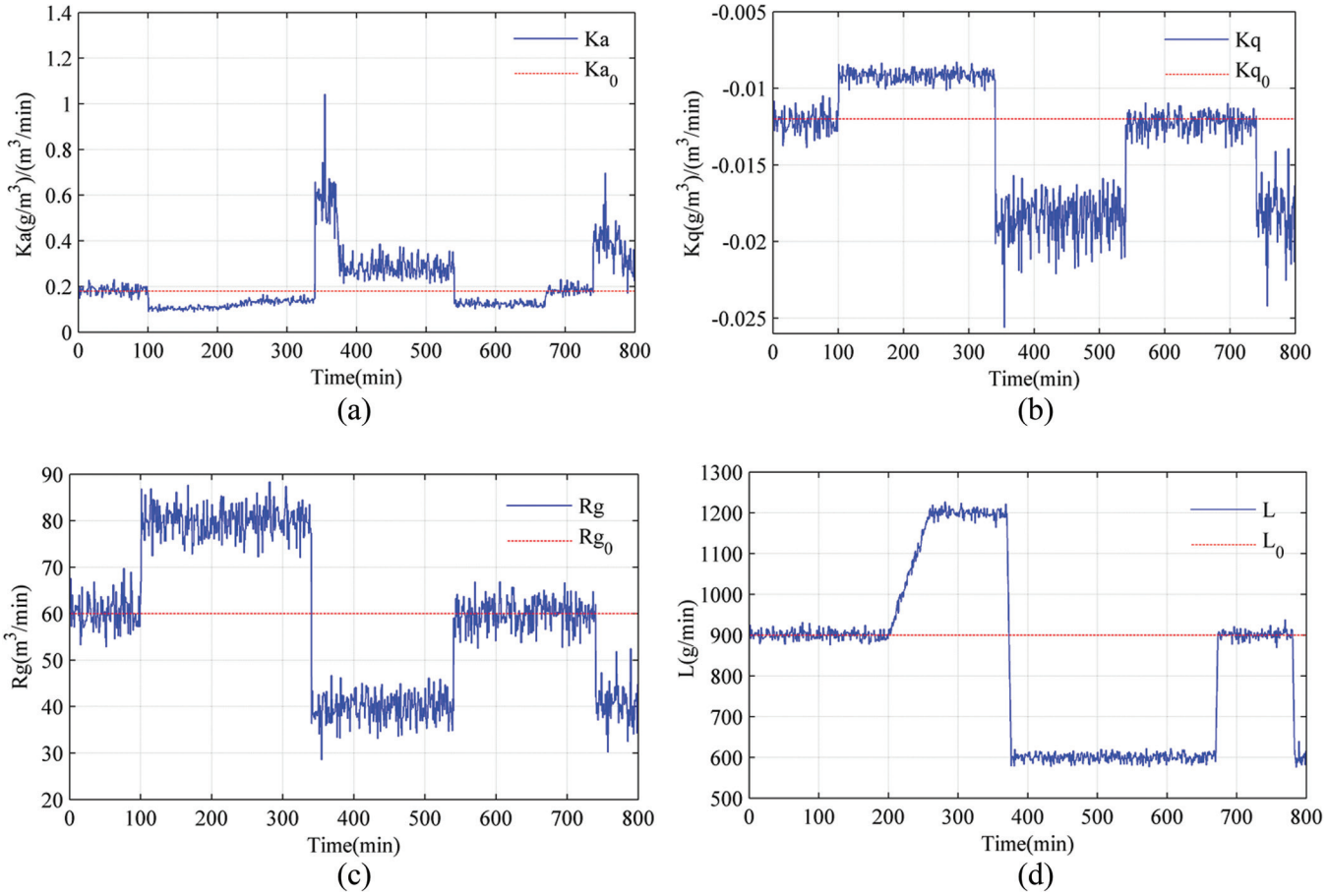

Figure 3. *The variation profile of the relevant parameters: (a) The sensitivity index profile under aeration variation; (b) The sensitivity index profile under load variation; (c) Oxygen expenditure as a load; and (d) Aeration rate.*

The constant setting load, L, is 600 g/min, while air supply to the sewage aeration tank reduced from its maximum (80 m^3/min) to its minimum (40 m^3/min). The sensitive index K_a changed from its minimum ($0.07(g/m^3)/(m^3/min)$) to its maximum ($0.31(g/m^3)/(m^3/min)$). As can be seen from Figure 8, the dynamic model of the DOC (C_n) remained at around 2 g/m^3, which is more accurate and stable than the DOC under steady state model (C_s).

At the time of the peak load (L), oxygen capacity of the aeration tank (R_g) reached its maximum value to maintain a certain DOC. When the load was low, the

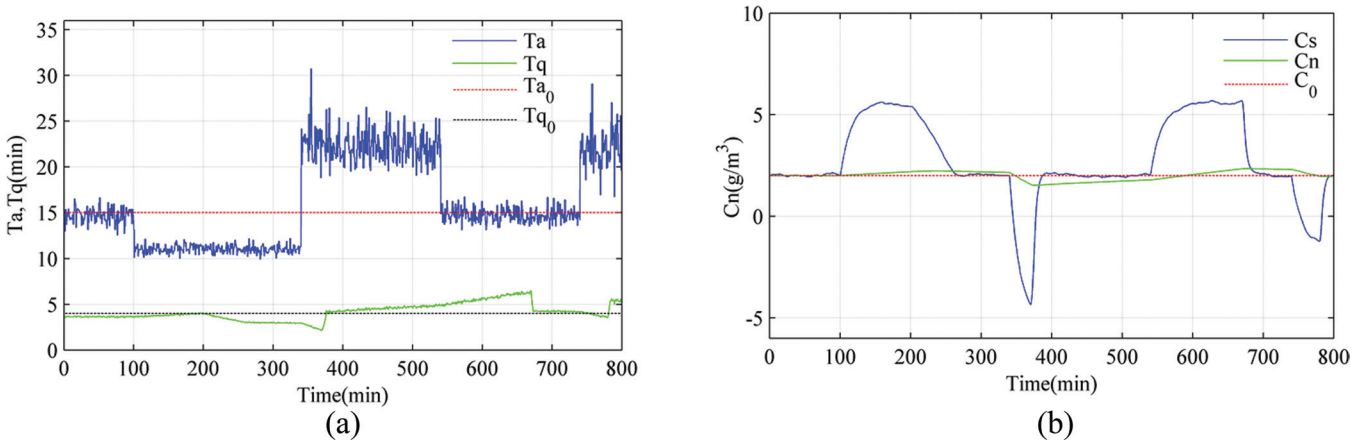

Figure 4. *The performance comparison of the steady and dynamic models: (a) Characteristics of sensitivity and inertia indexes for steady and dynamic models; and (b) Oxygen concentration for steady and dynamic models.*

aeration capacity decreased. The increase and decrease of the oxygen aeration capacity and load can lead to the variations of the DOC. Sensitive index (K_a) around the average initial value is 0.18 (g/m^3)/(m^3/min), the change range of which is plus or minus 50%. Therefore, the dynamic model can adapt to changes in index variables. As sewage aeration tank sensitivity and inertia index change significantly, the dynamic model can ensure the accuracy of the simulated DOC.

CONCLUSIONS

Based on the analyses of the dynamic model of the DOC in sewage treatment, an outlier detection method and Laplace transform are used to solve the steady-state equation of DOC. The adaptive dynamic model of DOC was established in the Matlab environment considering white noise in the model input. The primary impact factors on the DOC are analyzed, where both the load and oxygen capacity of the aeration pool have an effect on the DOC. At the same time, results demonstrate that the adaptive dynamic model can improve modeling accuracy of DOC. An extension of this study could focus on optimal control strategies for DOC in wastewater treatment processes.

ACKNOWLEDGEMENT

This work is supported by the Natural Science Foundation of China (Grant No. 61064003, 51165024 and 61364004) and the Natural Science Foundation of Gansu Province (Grant No.145RJZA024 and No.145RJYA313). The authors also thank the anonymous reviewers for greatly improving the presentation and quality of this work due to their valuable comments and suggestions.

REFERENCES

1. Du S. X., ″Modeling and control of biological wastewater treatment processes”, *Control Theory and Applications,* Vol. 19, No. 5, 2002, pp. 660–666.
2. Ko, Y. J., B. C. McInnis, and G. C. Goodwin, ″Adaptive Control and Identification of the Dissolved Oxygen Process”, *Automatica*, Vol. 18, No. 6, 1982, pp. 727–730. http://dx.doi.org/10.1016/0005-1098(82)90062-0
3. Marsili, L. S., R. Giardi, and M. Lasagni, ″Self-tuning Control of the Activated Sludge Process”, *Environmental Technology*, Vol. 6, No. 12, 1985, pp. 576–583. http://dx.doi.org/10.1080/09593338509384378
4. Holmberg, A, ″Modelling of the Activated Sludge Process for Microprocessor-based State Estimation and Control”, *Water Research*, Vol. 16, No. 7, 1982, pp. 1233–1246. http://dx.doi.org/10.1016/0043-1354(82)90142-7
5. Holmberg, U., and G. Olsson, ″Simultaneous On-line Estimation of Oxygen Transfer rate and Respiration rate”, *Modelling and Control of Biotechnological Processes*, 1985, pp. 185–189.
6. Olsson, G., L. Rundqwist, L. Eriksson, and L. Hall, ″Self-tuning Control of the Dissolved Oxygen Concentration in Activated Sludge Systems”, *Instrumentation and Control of Water and Wastewater Treatment and Transport Systems,* 1985, pp. 473–480.
7. Goto, M., ″On-line Estimation of Oxygen Uptake Rate for the Activated Sludge Process”, *Dissertation Abstracts International Part B: Science and Engineering*, 1985, Vol. 46, No.6.
8. Andrews, J. F., ″Dynamic Models and Control Strategies for Wastewater Treatment Processes”, *Water Research,* Vol. 8, No. 5, 1974, pp. 261–289. http://dx.doi.org/10.1016/0043-1354(74)90090-6
9. Marsili-Libelli, S. 1990. ″Adaptive Estimation of Bioactivities in the Activated Sludge Process”, presented in *IEE Proceedings D* (Control Theory and Applications), Vol. 137, No. 6, 1990, pp. 349–356.
10. Wen, Q., Y. Wu, L. X. Zhao, Q. Sun, and F. Y. Kong, ″Electricity Generation and Brewery Wastewater Treatment from Sequential Anode-Cathode Microbial Fuel Cell”, *Journal of Zhejiang University SCIENCE B*, Vol. 11, No, 2, 2010, pp. 87–93. http://dx.doi.org/10.1631/jzus.B0900272
11. Sotomayor, O. A., S. W. Park, and C. Garcia, ″Software Sensor for Online Estimation of the Microbial Activity in Activated Sludge Systems”, *ISA transactions*, Vol. 41, No. 2, 2002, pp. 127–143. http://dx.doi.org/10.1016/S0019-0578(07)60073-1
12. Sniders, A., A. Laizans, ″Computer Aided Modelling of Wastewater Aeration”, *In:* The 3rd International Scientific Conference on Rural Development, Lithuanian University of Agriculture, Kaunas, 2007.
13. Sniders, A., A. Laizans, ″Adaptive Model of Wastewater Aeration Tank”, Scientific Journal of Riga Technical University. *Environmental and Climate Technologies*, Vol. 6, No. 1, 2011, pp. 112–117.
14. Xie, L., Y. Zhao, D. Aziz, X. Jin, L. Geng, E. Goberdhansingh, and B. Huang, ″Soft Sensors for Online Steam Quality Measurements of OTSGs”, *Journal of Process Control*, Vol. 23, No. 7, 2013, pp. 990–1000.http://dx.doi.org/10.1016/j.jprocont.2013.05.006
15. Waewsak, C., A. Nopharatana, and P. Chaiprasert, ″Neural-fuzzy Control System Application for Monitoring Process Response and Control of Anaerobic Hybrid Reactor in Wastewater Treatment and Biogas Production”, *Journal of Environmental Sciences,* Vol. 22, No. 12, 2010, pp. 1883–1890. http://dx.doi.org/10.1016/S1001-0742(09)60334-X
16. Saeed, T., A. Al-Muyeed, R.Afrin, H. Rahman, and G. Sun, ″Pollutant Removal from municipal Wastewater Employing Baffled Subsurface Flow and Integrated Surface Flow-Floating Treatment Wetlands”, *Journal of Environmental Sciences,* Vol. 26, No. 4, 2014, pp. 726–736. http://dx.doi.org/10.1016/S1001-0742(13)60476-3
17. Kobayashi, T., Y. Tang, T. Urakami, S. Morimura, and K. Kida, ″Digestion Performance and Microbial Community in Full-Scale Methane Fermentation of Stillage from Sweet Potato-Shochu Production”, *Journal of Environmental Sciences,* Vol. 26, No. 2, 2014, pp. 423–431. http://dx.doi.org/10.1016/S1001-0742(13)60423-4
18. Belaid, C., M. Khadraoui, S. Mseddi, M. Kallel, B. Elleuch, and J. F. Fauvarque, ″Electrochemical Treatment of Olive Mill Wastewater: Treatment Extent and Effluent Phenolic Compounds Monitoring Using Some Uncommon Analytical Tools”, *Journal of Environmental Sciences*, Vol. 25, No. 1, 2013, pp. 220–230. http://dx.doi.org/10.1016/S1001-0742(12)60037-0

Double Consolidation Technology for the Stabilization of Heavy Metal Ions in the Fly Ash Generated by the Incineration of Municipal Solid Waste

SUN JIA-YING*, YANG YI-FAN and ZHENG MING
Research Center of Green Building Material and Waste Resources Reuse, Ningbo Institute of Technology, Zhejiang University, Ningbo 315100, China

ABSTRACT: In this paper, a new consolidation technology is proposed for solidifying the fly ash from municipal solid waste; moreover, the safety of the solidified fly ash for practical applications is investigated. This approach aims to address the high levels of heavy metals, such as Pb and Zn, in the fly ash from municipal solid waste, which exceed the national emission standards for solid waste and water discharge in China. This consolidation method was found to increase the compressive strength (after 28 days) of fly ash concrete from municipal solid waste to values greater than 40 MPa. Furthermore, the asphalt mixture prepared with the fly ash concrete offered some excellent advantages, such as better residual Marshall Values and rutting resistance, which are beneficial when laying roads. Additionally, the leaching toxicity of the asphalt mixture was well within the limits prescribed by the national emission standards, which implies that the heavy metal ions were effectively bound in the asphalt mixture and the aggregate was stably solidified.

INTRODUCTION

THE rapid increase in the rate of municipal solid waste (MSW) production, which is typically between 10–12% a year in countries like China, has necessitated the development of effective technologies for its disposal. At present, methods such as landfilling, incineration, composting and recycling are still the chief ways of treating and disposing of MSW. However, it has been seen over the past few decades that these waste disposal practices can be inefficient and cause pollution. Furthermore, each processing technology has its limitations, which cannot be ignored. For example: gases and leachates are generated by landfilling; incineration produces dioxins and furan and attracts mosquitoes; and the quality of the obtained compost is affected by the presence of glass and other impurities [1–2].

In order to make effective use of the existing treatment facilities and address the challenge of efficiently treating MSW, a novel technology, which combines incineration and double consolidation with inorganic gelling materials and asphalt, is proposed in this paper. Using this technology, the toxic hazardous substances in MSW, such as fly ash, and in particular the heavy metal ions, are effectively bound and stably solidified so that the resulting sludge is unpolluted by these substances. It is noteworthy that an asphalt mixture prepared by concentrating MSW fly ash offers excellent advantages, such as better mechanical properties than those of common asphalt mixtures and improved performance when used for laying roads. The stability imparted by the presence of heavy metal ions in the asphalt mixture, which was prepared by concentrating MSW fly ash, was evaluated using the toxicity characteristic leaching procedure (TCLP) and multilevel extraction technology to check whether it complies with the Chinese national emission standards, GB5086.2-1997 [3], and the United States (U.S.) Environmental Protection Agency (EPA) standards, SW-846.

EXPERIMENTAL METHODS

Raw Materials

The following raw materials were used in the experiments.

- *Slag*: The ground slag for the experiments was pro-

*Author to whom correspondence should be addressed.
E-mail: jakys@163.com; Tel: 13454710396

1544-8053/15/01 S031-07

doi:10.12783/issn.1544-8053/12/S1/5

Table 1. Chemical Composition of Slag and Steel Slag Powder (wt%) Used in the Experiments.

Sample	SiO_2	Al_2O_3	Fe_2O_3	CaO	MgO	SO_3	Loss on Combustion
Slag	32.3	14.3	0.2	39.0	7.7	1.0	1.89
Steel slag	14.7	3.4	21.0	45.0	9.0	0.4	1.65

cured from New Building Materials Co. Ltd. Shanghai Baotian. The slag had a specific data of 460 m^2/kg and its chemical composition is shown in Table 1.

- *Steel slag*: The ground steel slag for the experiments was procured from Shanghai BaoSteel Metallurgy Construction Company. The slag had a specific data of 500 m^2/kg and its chemical composition is shown in Table 1.
- *Curing agent*: The curing agent used in the experiments was prepared in-house.
- *MSW fly ash*: The MSW fly ash produced by the solid waste incineration plant in Ningbo, China, was used in the experiments.
- *Asphalt:* Sinopec Asphalt70# was used in the experiments. The overall performance of the asphalt is shown in Table 2.

The results of the experimental AC-16I gradation of the asphalt mixture are shown in Table 3. The asphalt aggregate ratio was 4.8%.

Method

After drying, the MSW fly ash was mixed with the curing agent in ratios of 1:2, 1:2.5, and 1:3. The size of each sample was 40 mm × 40 mm × 160 mm, and samples were kept in a standard curing room before their bending and compressive strengths were measured according to the GB/T50081-2002 standards. Subsequently, the samples were divided into 120 categories, and then the asphalt mixture was prepared by powder concretion with the MSW fly ash, or with limestone dust.

The mechanical properties of the asphalt mixtures obtained were evaluated using the Marshall test according to the JTJ052-2000 (T0709) standards; moreover, the results obtained for an asphalt mixture with MSW fly ash were compared with those obtained for the mixture with limestone dust. The influence of the different proportions of the MSW fly ash on the water solubility of the asphalt mixture was evaluated by performing a freeze-thaw splitting test according to the JTJ052-2000 (T0729) standards.

Additionally, the influence of the different proportions of MSW fly ash on the high-temperature stability of the asphalt mixture was evaluated by performing a wheel rutting resistance test according to the JTJ052-2000 (T0719) standards.

The toxicity level, i.e., the heavy metal content, in the asphalt mixture prepared with the MSW fly ash was tested according to the GB5086.2-1997 national standards. Furthermore, the maximum leaching toxicity of heavy metals using the TCLP was also tested according to the US EPA standards, SW-846 [4].

RESULTS AND DISCUSSION

The Leaching Toxicity of MSW Fly Ash Concrete

In order to understand the influence of the double consolidation technology on the safety of the asphalt mixture prepared with MSW fly ash concrete, the leaching toxicity of the mixture was measured. The experimental results are shown in Figure 1.

The leaching toxicity of the heavy metal ions in the asphalt mixture with the MSW fly ash, which was prepared using the double consolidation method, was tested using the fly ash level oscillation method. The leaching toxicity was found to be lower than the national emission standards for solid waste and water discharge. Furthermore, the maximum leaching toxicity of the heavy metal ions, as determined using the TCLP, was also lower than these national emission standards.

Table 2. The Performance of the Asphalt70#.

Test		Asphalt70#	Test		Asphalt70#
Penetration/0.1 mm	15°C	23.0	Thin Film Oven Test (TFOT)	Penetration (25°C)/0.1 mm	41.5
	25°C	71.3		Ductility (10°C)/cm	18.0
	30°C	138		Softening point/°C	51.4
Ductility/cm	5°C	not measured	Penetration ratio (10°C)/%		58.2
	7°C	not measured	Mass loss/%		0.71
	10°C	58	T_{800}/°C		45.0058
Softening point/°C		47.4	$T_{1.2}$/°C		–9.8272

Table 3. Experimental AC-16I Gradation of the Asphalt Mixture.

	Percentage (%) Gradation for the Following Sieve Sizes (mm)									
Gradation	**0.075**	**0.15**	**0.3**	**0.6**	**1.18**	**2.36**	**4.75**	**9.5**	**13.2**	**16.0**
Upper limit	8	15	21	28	37	50	63	78	90	100
Lower limit	4	7	11	16	22	32	42	58	75	95
Experimental gradation	3	11	16	22	29.5	41	52.5	68	82.5	97.5

However, the leaching toxicity of the heavy metal ions in the MSW fly ash, when tested alone, was higher than these emission standards. The fractions of metal ions from the MSW fly ash remaining in the asphalt mixture were 98%, 99%, 97%, 99%, 98%, and 100% for Pb, Zn, Cd, Cr, Cu, and Ni, respectively. Therefore, the heavy metal ions present in the MSW fly ash were effectively stabilized in the asphalt mixture by the double consolidation method.

The Mechanisms for the Stabilization of Heavy Metal Ions in the Asphalt Mixture Prepared by the Concretion of MSW Fly Ash

The heavy metal ions of Pb, Zn, Cr, and Cd that were present in the asphalt mixture, which contained the MSW fly ash prepared using the double consolidation method, could be analyzed using a multistage extraction process. This experiment was carried out to confirm the long-term stability of the asphalt mixture prepared using the double consolidation method; the results are shown in Figure 2.

In the multistage extraction process, 10% of the Pb, as a representative heavy metal, was acid soluble and found in the form of heavy metal carbonates and hydroxides. The heavy metal ions of all types in this form leached readily; however the percentages remaining in the aqueous solution were less than 10%, which is below the national discharge standards prescribed. In addition, the amount of Pb present in the amorphous ferric oxide was 15%, and was mainly in the form of heavy metal sulfates and elemental heavy metals. The

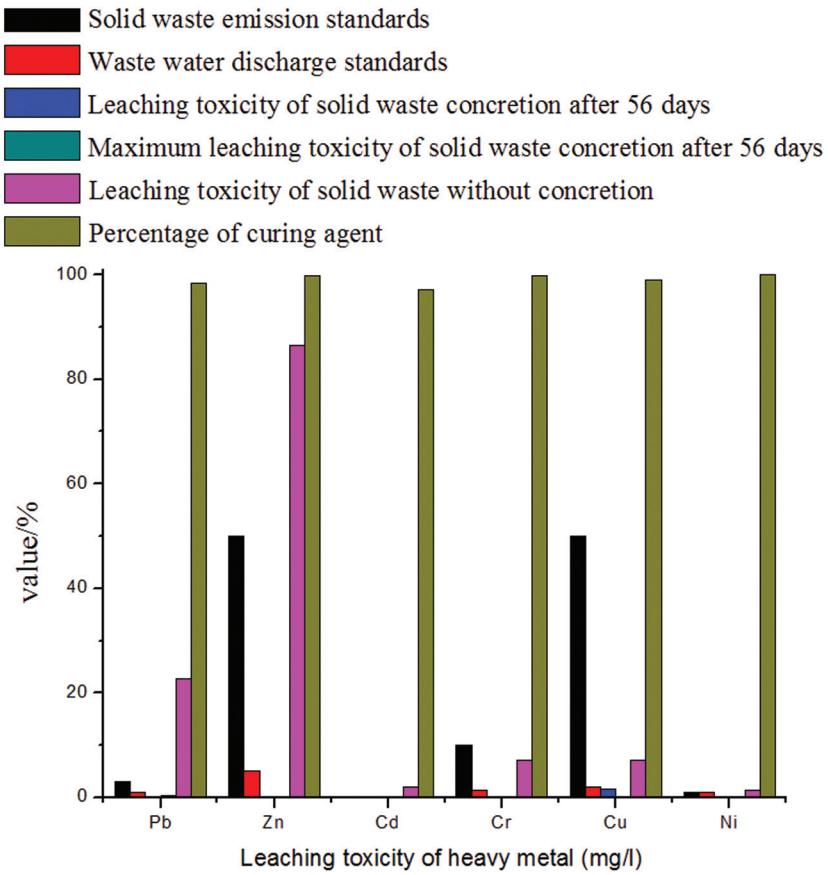

Figure 1. *The results of the toxicity testing to determine the heavy metal content in the asphalt mixture prepared with MSW fly ash.*

heavy metal ions found in heavy metal sulfates, oxides, and chromates were hardly leached under these conditions, and the amount of Pb found in the crystalline ferric oxide was 52%. The remaining 18% of the Pb was retained as residuals owing to the minimal leaching of heavy metal ions in the silicate or aluminum silicate families, or in elemental or oxide forms. More than 88% of the Zn, Cd, and Cr in the asphalt mixture was in the form of bound organics, amorphous ferric oxides, crystalline ferric oxides, or residuals. This shows that the physical and chemical reactions triggered in the asphalt mixture during concretion produced stable mineral phases, such as heavy metal sulfates, elemental heavy metals, oxide or chromate salts, silicates, and aluminum silicates.

These heavy metal ions were hardly leached under the conditions prescribed by the national testing standards. Therefore, the double consolidation of the asphalt mixture prepared with MSW fly ash can be applied safely for practical purposes.

The Replacement of the Limestone Dust in a Common Asphalt Mixture Containing MSW Fly Ash Concrete and a Comparison of the Stability

The compositional analysis of the different asphalt mixtures indicated that the CaO content in the MSW fly ash concrete was much higher than that in the limestone dust mixture. Thus, the limestone dust was replaced with MSW fly ash concrete to improve the alkalinity and adhesion of the aggregate and the asphalt.

The MSW fly ash concrete produced for the experiments was fully ground to pass through a 0.0075 mm standard test sieve. The grade of the asphalt mixture was at the medium level, according AC-16I. In the common asphalt mixture, the ratio of limestone dust is 6%, and in the experiments in this paper 25%, 50%, 75%, or 100% of this limestone dust was replaced by MSW fly ash concrete. The performance index of the asphalt mixture after the replacement was determined by the Marshall Stability test. The results of this sta-

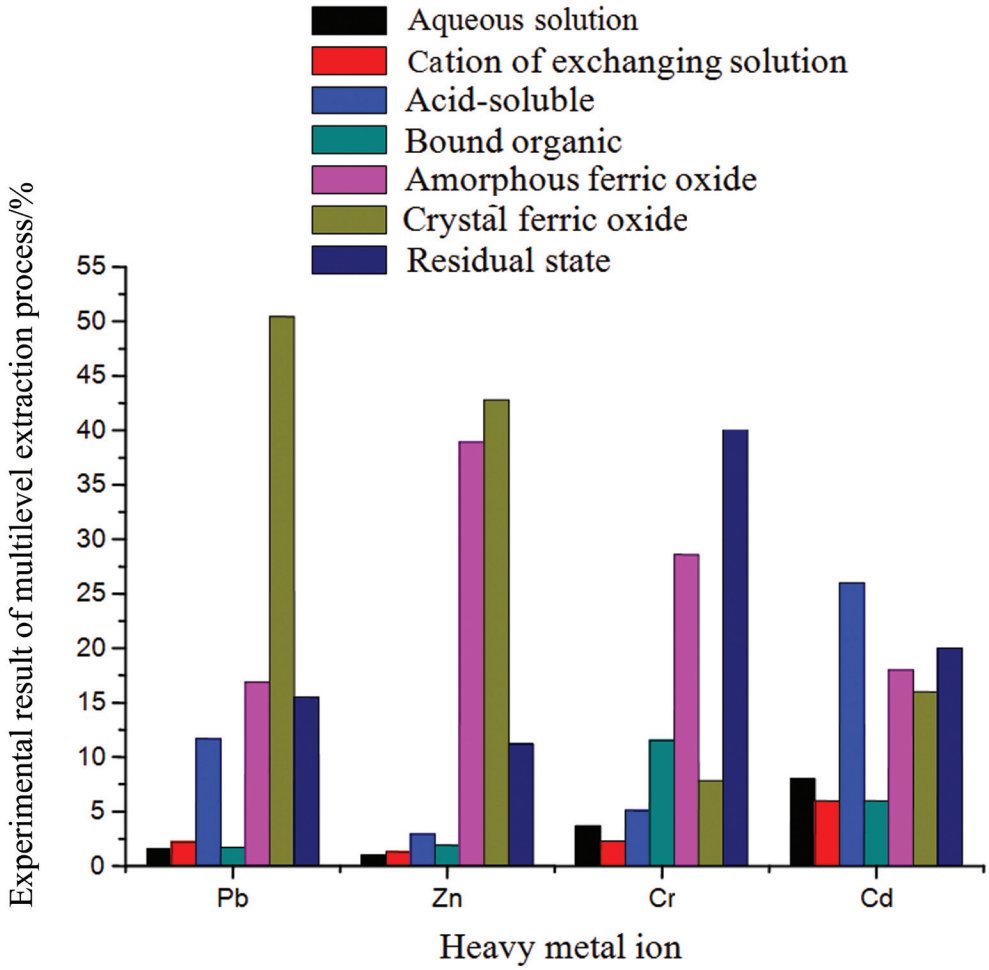

Figure 2. *The results of the multilevel extraction.*

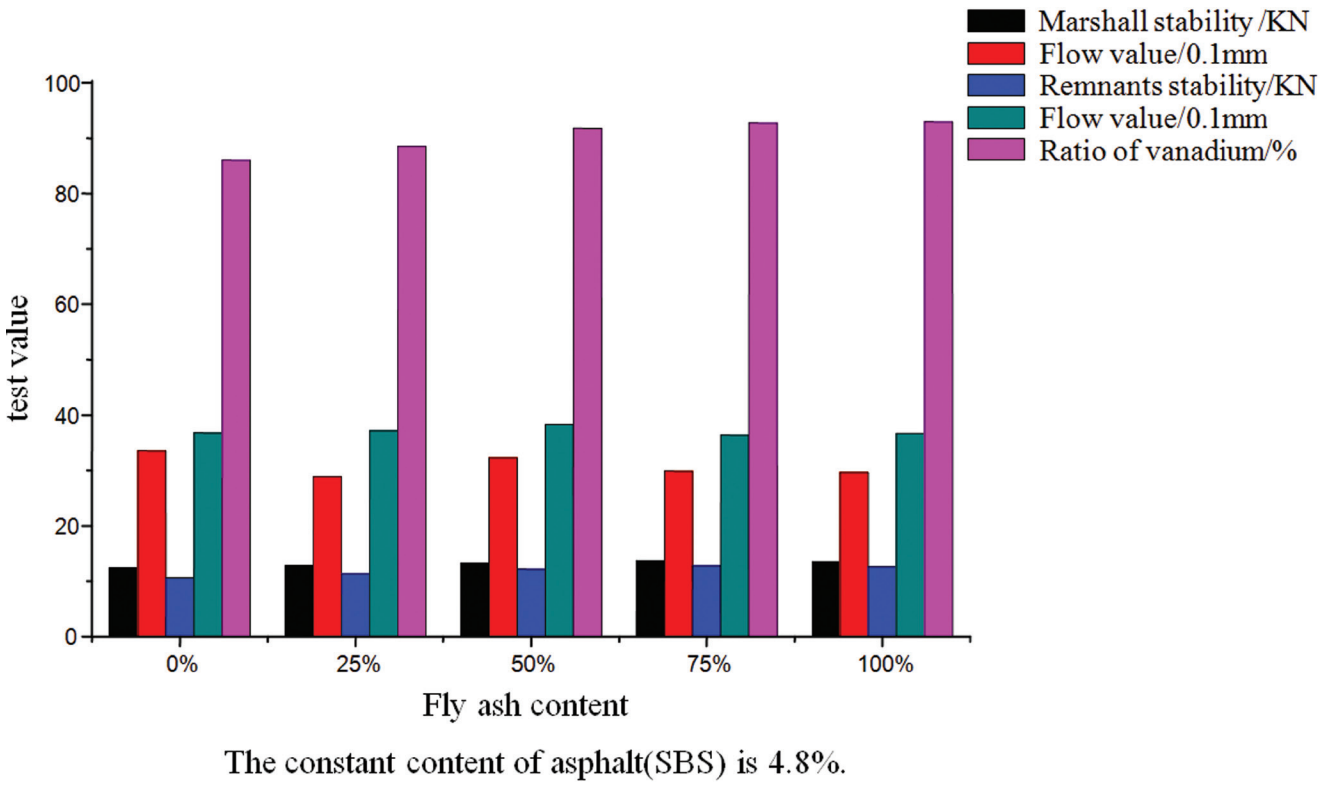

Figure 3. *The results of the Marshall stability test of the MSW fly ash concrete mixture.*

bility test for the MSW fly ash concrete mixture are shown in Figure 3.

These results show that replacing the limestone dust with MSW fly ash concrete can improve the stability of the aggregate and the asphalt. As the amount of the MSW fly ash concrete increased, the stability and its residual stability gradually increased, with the stability being maximized when 75% of the limestone dust was replaced with the MSW fly ash. However, when the amount of fly ash was increased further, the stability decreased marginally.

According to the chemical reaction theory, the alkalinity of the MSW fly ash concrete is higher than that of the limestone dust. Therefore, the acidic materials in the asphalt reacted completely with the alkaline MSW fly ash concrete, which could improve the adhesion between the asphalt and the aggregate. The maximum stability obtained when 75% of the limestone dust was replaced with MSW fly ash may be attributed to the complete reaction of the asphalt mixture (of defined contents) with the alkaline materials in the MSW fly ash concrete, much like the reaction with CaO. When the amount of fly ash was increased further, it is possible that the reaction was incomplete, which explains why the Marshall stability did not increase further. However, further experimental evidence, specifically with regard to the exact compositions of the asphalt and MSW fly ash concrete, as well as their acidity and alkalinity, are required to unambiguously confirm this reasoning.

The Water Stability of the Asphalt Mixture Containing MSW Fly Ash Concrete Prepared by Double Consolidation [5]

Fresh water, seawater, and sulfate liquor with 5% of Na_2SO_4 were employed in the freeze-thaw splitting tests, with the test results displayed in Figures 4(a) and 4(b).

The test results show that the addition of MSW fly ash concrete improved the water stability of the asphalt mixture; this was due to the alkaline nature of the fly ash. The asphalt, which contained carboxylic acid and sulfoxides, acted as a weak acid. Therefore, when the MSW fly ash concrete was evenly distributed in the asphalt mixture, the compounds reacted to form neutral and stable products. These products adhered to the surface of the aggregate and were difficult to remove, thus improving the water stability of the asphalt mixture.

Furthermore, the test results also show that the water stability of the asphalt mixture prepared with MSW fly ash concrete significantly differed depending on the

test medium employed. The stability of the asphalt mixture was more pronounced in fresh water, for which the test results (TSR) exceeded 75%. The TSR in seawater was also high, while the minimum TSR was observed in sulfate liquor.

The High-temperature Stability of Asphalt Mixture Containing MSW Fly Ash Concrete Prepared by Double Consolidation

The results of the wheel rutting test of the asphalt mixture are shown in Figure 5, where it can be seen that the dynamic stability of the asphalt mixture increased significantly by increasing the MSW fly ash content. However, the increase in the dynamic stability of the asphalt mixture was not very significant when more than 75% of the limestone dust was replaced with the MSW fly ash concrete.

CONCLUSIONS

The following conclusions can be drawn from this study.

- The heavy ions present in MSW fly ash concrete were stabilized in the asphalt mixture during the double consolidation, which included the addition of the curing agent and asphalt. The leaching toxicity of heavy metal ions, as tested using the flat oscillation method or the TCLP, in the asphalt mixture prepared with the MSW fly ash concrete was far less than the limits prescribed by the national solid waste emission standards. Furthermore, because the binding between the heavy metals and the MSW fly ash concrete was significantly strengthened, the leaching toxicity of the heavy metals decreased.
- The multilevel extraction experiments demonstrated

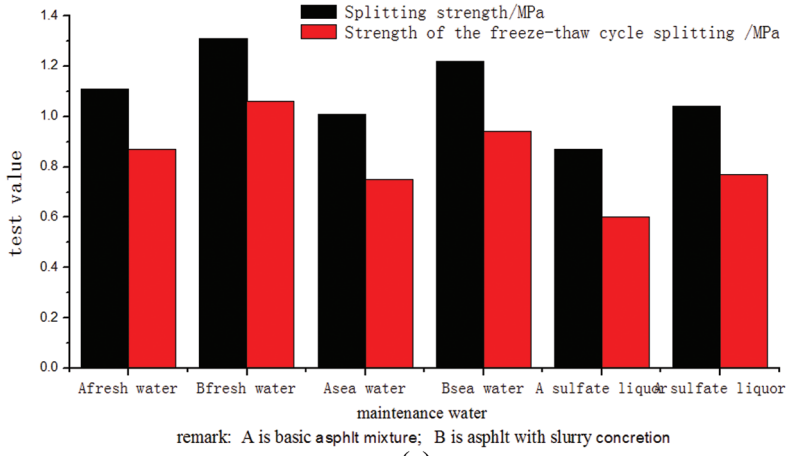

(a)

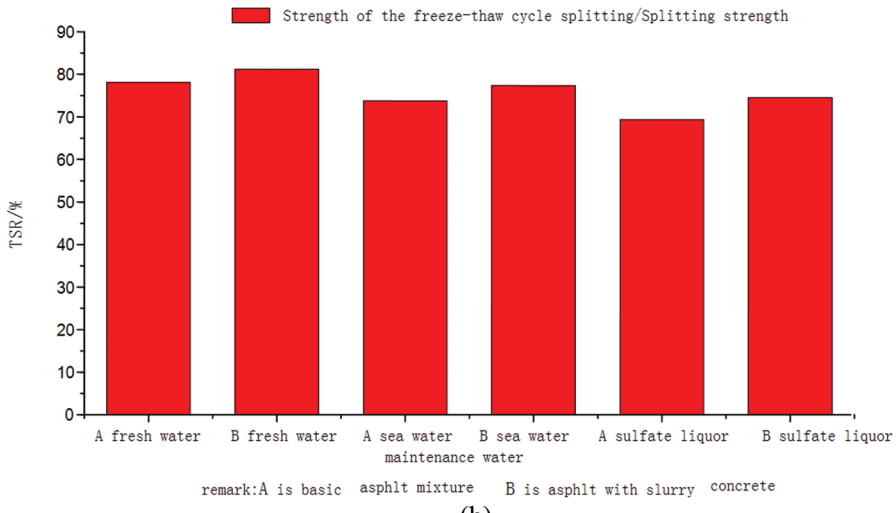

(b)

Figure 4. *(a) The water stability of the asphalt mixture; and (b) The water stability of the asphalt mixture.*

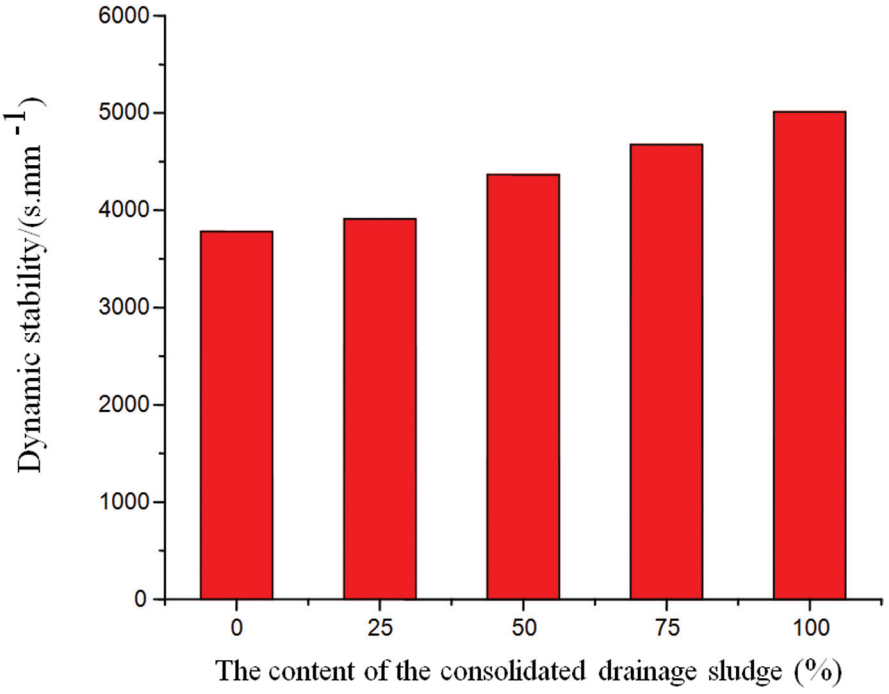

Figure 5. *The results of the wheel rutting test carried out with the asphalt mixture.*

that the heavy metal ions in the MSW fly ash concrete were stable in the asphalt mixture. The stabilization of the heavy metal ions during the preparation of the asphalt mixture is attributed to a combination of chemical bonding and physical encapsulation.

- The results of the freeze-thaw splitting tests and wheel rutting tests of the asphalt mixtures, which were produced using the double consolidation technology, showed that the water stability and rutting resistance of the MSW fly ash concrete were better than those of common asphalt mixtures. Thus, the MSW fly ash subjected to the double consolidation method could be used to prepare asphalt mixtures that can be used safely for practical purposes.

REFERENCES

1. Yao, Y. and J. Tang. 2003. "The significance and countermeasures of realizing the waste reduction and recycling (in Chinese)." EB/OL. Forum 2003:25–29.
2. Tang, J. and H. Ma. 2000. "The exploration of municipal solid waste resources' utilization (In Chinese)." EB/OL. Renew Resour Forum 4:31–33.
3. GB5086.2-1997. 1997. "The leaching-out toxicity methods of solid waste-level oscillation method." S. 225–227.
4. Kosson, D. S., H. A. van Der Sloot, T. Homes and C. Wiles. 1991. "Leaching properties of untreated residues tested in the USEPA program for evaluation of treatment and utilization technologies of municipal waste combustor residues," in Waste Materials in Construction, Gouumans JJJM, van Der Sloot HA, Aalbers TG, eds. the Netherlands: Elsevier, pp. 119–134.
5. Hao, P. and D. Zhang. 1997. "The influence of asphalt mixture's water stability on building stones," *J. Chongqing Jiaotong Univ.*, 16(1):80–85.

Test Study of Enhanced Coagulation for Conventional Treatment with Low Temperature and Low Turbidity

W. C. SONG[1,2], X. LI[1,*], S. H. SUN[2], Y. L. YANG[1] and R. B. JIA[2,*]
[1]*College of Architecture and Civil Engineering, Beijing University of Technology, Beijing, 100124, China*
[2]*Shandong Water and Wastewater Monitoring Center, Jinan, 250021, China*

ABSTRACT: Sole use of polymeric aluminum ferric chloride (PAFC) and its combination with composite polymeric aluminum ferric chloride/poly-dimethyl-diallyl- ammonium chloride coagulant (PAFC-PDMDAAC), chlorine dioxide (ClO_2) and composite potassium permanganate (PPC) were tested for treating retrieved water from the Yellow river during the period of low temperature and low turbidity. Such tests were carried out under full load operation in a water plant with conventional process. Results showed that the combined use of PPC and PAFC-PDMDAAC was more effective in treating influent with low temperature and low turbidity than the other coagulants. The turbidity, oxygen consumption, total trihalomethanes (THM) and absorbable organic halogens (AOX) in the effluent were compared with effluent under the sole treatment of PAFC, reduced by 76.8%, 14.2%, 60.8% and 19.4%, respectively. The operation cost, however, was only increased by 0.024 yuan/m^3, denoting that it is a cost-effective method.

INTRODUCTION

FOR many years, the Yellow River of China has alleviated the pressure of local urban water demand for cities along its main stream and ensured local economic and social development. In order to ensure water availability, most of the downstream towns of the Yellow River have built Yinhuang reservoirs. The turbidity of the Yellow River water was reduced after pre-sedimentation. Low turbidity, high nitrogen and phosphorus content and high residence time of water in the Yinhuang reservoir water lead to low turbidity and high algae.

At present, most of the water supply treatment plants using Yinhuang reservoirs as water sources have adopted conventional treatment process. The treatment is often ineffective and effluents from treatment plants fail to meet the water quality standard during the period of winter and spring when water is at low temperature and of low turbidity. The study has shown that conventional technology can remove more than 60% of the oxygen consumption in the raw water, so it is a promising method for water treatment [1]. The conventional technology is mainly to improve and optimize the conventional processes or to add new treatment processes to remove turbidity, viruses, microorganisms and organic pollutants to meet the new quality standards of drinking water. It mainly includes chemical oxidation, enhanced coagulation and improved filtering, etc. Among them the optimization of coagulants and preoxidation, etc. is usually given high priorities. Such operation improvement is simple and economic. The effectiveness of enhancing treatment of water with low turbidity through permanganate oxidation, polyacrylamide (PAM) aided coagulation and sludge recycling was investigated through continuous bench studies [2]. Compared with ferric chloride coagulation, sole use of recycling sedimentation sludge was ineffective in treating water with low turbidity. PAM with recycled sludge showed improved effects, and additional permanganate dosing could lead to much lower effluent turbidity and oxygen consumption (COD_{Mn}). Studies showed that the addition of aluminium sulphate and polyaluminium chloride (PAC) coagulants could remove turbidity of water in the typical upstream of the Yellow River in the winter with low temperature and low turbidity. But such processes could lead to excess aluminium. The combined use of PAC and $FeCl_3$ could also increase the iron residue [3]. The combined use of polymeric ferric chloride (PFC) and a small dose of dimethyl diene propyl chloride homopolymer (PDMDAAC) has a better flocculation effect on surface drinking water than that by sole use of PFC or PDMDAAC [4]. A chlorine dioxide (ClO_2) preoxidation process could enhance the coagulation effect of the conventional pro-

*Authors to whom correspondence should be addressed.
E-mail: lixing@vip.163.com; jiaruibao68@126.com; Tel. +8653155589618; Fax. +8653155589600

1544-8053/15/01 S039-09

doi:10.12783/issn.1544-8053/12/S1/6

cess and increase the removal rate of chromaticity and turbidity. It also improves the removal rate of algae and its intracellular pollutants and effectively inhibits the formation of disinfection by-products [5]. Comparative pilot tests were conducted to investigate the coagulation-aiding effects of combined preoxidation by potassium permanganate composites with chlorine and preozonation [6]. Results showed that it could further improve the quality of treated water by the synergistic effect of the intermediate such as hydrous manganese dioxide, which was generated by potassium permanganate. The addition of composite potassium permanganate could significantly increase the size and density of the flocculation mass, improve the effect of static precipitation and enhance the removal rate of turbidity [7]. The addition of potassium permanganate coagulant aids could also help PFC-PDMDAAC composite flocculants increase the removal rate of permanganate index [4]. Sun Yunkai *et al.* [8] focused on treating water from the Danjiangkou reservoir by optimizing the dosage and precipitation time of three kinds of commonly used coagulants, namely $FeCl_3$, PAC and aluminum sulfate (AS). The adaptability test with the optimal coagulant was carried out in a pilot study. Results from Sun *et al.* revealed that the coagulant had a good adaptability. The strengthening of the conventional process with carefully selected chemicals has drawn increasing attention in the research community. Very few studies focused on the production test of actual operation of a water treatment plant. In this paper, a production test for strengthening the conventional process with added chemicals was conducted for Yinhuang water plant.

EXPERIMENTAL PROCEDURE AND MATERIALS

Quality of Raw Water

The main water quality indexes of the raw water are listed in Table 1.

Experimental Materials

Polymeric aluminum ferric chloride (PAFC) produced by Shandong Zibo Water Purifier Plant is used in this study. Its main parameters are listed as following. Its relative density is 1.24 (20°C); alumina content is 10.5–11.26; iron oxide content is 2–4% and its basicity is 70–92%. The unit price is 800 yuan per ton.

Composite polymeric aluminum ferric chloride/poly-dimethyl-diallyl-ammonium chloride coagulant (PAFC-PDMDAAC) comprised of PAFC and PDMDAAC (2%) at the price of 1200 yuan per ton is produced by the Chemical factory of Jinan Quancheng Water co., LTD.

The characteristics of Chlorine dioxide (ClO_2) produced by Zibo Huarun Trade co., LTD. is described as following. Its raw liquor concentration is 6% and its ClO_2 purity is greater than 99%. Its price is 5400 yuan per ton. It is often activated using a complete set of activator and added by water ejector.

Potassium permanganate composite agents (PPC) are compounded with food grade coagulant aids and water quality regulator. Concentration of potassium permanganate is 5% and its price is 1600 yuan per ton. It is produced by the chemical reagent factory of Shengli Oilfield Water Supply Company.

Water Treatment Plant

Raw water of the plant was retrieved from the Yinhuang reservoir. The design capacity of the water treatment plant was 400000 m^3/d. Conventional treatment processes include coagulation, sedimentation, filtration and disinfection (As shown in Figure 1). PAFC was used as coagulant and a static mixer and a folded plate were used to facilitate coagulation. The flat flow type of sedimentation basin with length of 120 m and residence time of 2 h was used. The v-shaped filter, with filtration rate of 8 m/h and combined recoil with gas and water, was employed. Liquid chlorine was adopted for disinfection. Comparison between the strengthening with the composite coagulant (PAFC-PDMDAAC) and the enhancing by pre-oxidation with ClO_2 or PPC conventional process was optimized to treat with low temperature and low turbidity.

Methodology

The production tests were divided into four stages,

Table 1. Quality Conditions of Raw Water During the Period with Low Temperature and Low Turbidity.

pH	COD_{Mn} (mg/L)	Turbidity (NTU)	Algae (million/L)	Chlorophyll a (μg/L)	Ammonia nitrogen (mg/L)	Temperature (°C)
7.8–8.3	2.1–3.5	< 5	< 20	2.0–5.2	0.1–0.2	1–3

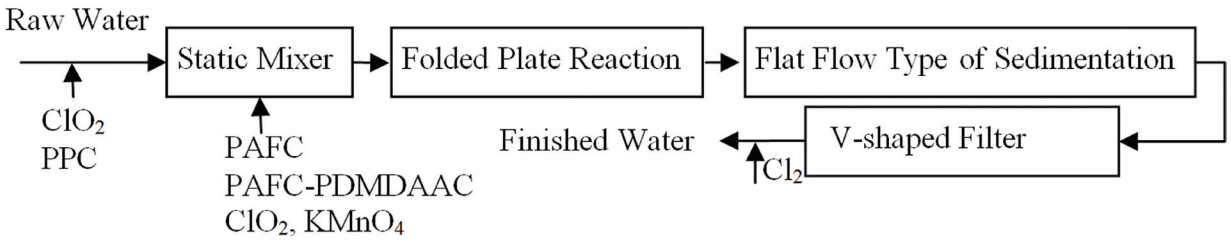

Figure 1. *The process of experimental water plant.*

and each stage was defined as a working condition, as shown in Table 2. The tests were carried out during the period with low temperature and low turbidity between December and January. The samples were collected at each treating process and analyzed after 5-day running of the water treatment plant under each condition. The average values of 5 days during the test were taken to investigate the efficiency of water purification under different working conditions. The switch interval between the working conditions was 2 days.

Water Quality Analysis

pH value was measured by HI8424 portable pH meter. Turbidity was measured by Hach 2100P turbidity meter. COD_{Mn} was analyzed using potassium permanganate method. UV254 was tested by UV2100 ultraviolet spectrophotometer. Total algae were observed under the microscope. The chlorophyll a (Chl-a) was measured using spectrophotometric method. Total trihalomethane (THM) was measured by head space-gas chromatography. TOC was analyzed by TOC-VCPH total organic carbon analyzer. Absorbable organic halides (AOX) was analyzed by Multi X 2500 total organic halogen analyzer. Water temperature was measured by thermometer.

RESULTS AND DISCUSSION

Removal Effect of Turbidity

Removal effect of turbidity under different conditions is shown in Figure 2. Both turbidities in the water under condition 1 and condition 2 are more than 1 NTU. However the turbidities was reduced to 0.6 NTU after preoxidation and precipitation with ClO_2 and PPC. It should be noted that for effective removal of turbidity in the coagulation process, reduction of filter load and the strengthening of the coagulation precipitation are important [1]. The turbidities of the effluent under the four conditions were 0.56, 0.4, 0.22, 0.13 NTU, respectively. The turbidities of the effluent under condition 2, condition 3 and condition 4 were reduced by 28.6%, 60.7% and 76.8% respectively, compared to that under condition 1.

On the one hand, hydrolysis effect of conventional coagulants at low temperature is not ideal due to some disadvantages, e.g., slow Brownian motion, limited effective collision between particles, larger viscosity coefficient of water, higher zeta potential, larger exclude potential energy between particles, lower flocculation reaction speed and slow formation of flocs. In the low-temperature water, the colloid presents solvent state because of the hydration around the particles, which is unfavorable for the formation of flocculating body. On the other hand, low turbidity means less contaminant particles in water. A colloidal dispersion system with low turbidity has strong dynamic stability and coagulation stability and only a handful of colloid particles are negatively charged, which was not conducive to the formation of flocs. Therefore, the turbidity of water with low temperature and low turbidity was difficult to remove.

PAFC-PDMDAAC composite coagulant improves the coagulation effect compared to PAFC because it could increase inorganic coagulants in hydrolysis of polynuclear hydroxy complex compounds, leading to the increased coagulation efficiency [9]. PDMDAAC is a kind of cationic flocculant with high positive charge, which can destabilize the negatively charged colloid particles in water with low temperature and low turbidity and less colloid particles at the same time, and can enhance the PAFC abilities of charge neutrality and adsorption bridging, resulting in enhanced coagulation [4].

Table 2. Working Condition of the Production Tests.

			Oxidation Agent	
Working Condition	**Coagulant Type**	**Dosage (mg/L)**	**Type**	**Dosage (mg/L)**
Condition 1	PAFC	20	–	–
Condition 2	PAFC-PDMDAAC	20	–	–
Condition 3	PAFC-PDMDAAC	20	ClO_2	0.5
Condition 4	PAFC-PDMDAAC	20	PPC	0.5

The condition 3 further reduces the turbidity of sediment by the synergistic effects of ClO_2 oxidation and PAFC-PDMDAAC. This is partially due to the fact that ClO_2 is a strong oxidant and can change the size and the shape of the electric charge on the surface, as well as the surface characteristics of the suspended solids in water, which is advantageous to the coagulation [10].

The condition 4 has significantly strengthened coagulation and improved filtration efficiency. The oxidation of PPC could destroy the protection of organic matters in water to colloid material, and strengthen the colloid stability off, resulting to the improved coagulation. New ecological hydrated manganese dioxide colloid can be formed due to that the reduction of potassium permanganate could form relatively compact flocs. Such flocs usually have large specific surface area and high formation speed, leading to the settling down of particulate matters in the water [11].

Removal Effect of Organics

The removal effect of COD_{Mn} and TOC under different conditions is shown in Figure 3. The removal rate of COD_{Mn} under condition 2 was the largest and it was about 10% for the other three conditions during sedimentation stage. The removal rate of COD_{Mn} under the four conditions was about 10% during filtration stage. The concentration of COD_{Mn} in effluent under the four conditions was 1.76, 1.56, 1.52, 1.51 mg/L respectively. Concentration of COD_{Mn} in the effluent under condition 2, condition 3 and condition 4 was reduced by 11.4%, 13.6% and 14.2% respectively compared with that under condition 1. The removal efficiency of TOC under the four conditions was poor, and the TOCs contained in the effluent were 2.21, 2.12, 2.03 and 1.95 mg/L respectively. TOCs in the effluent under condition 2, condition 3 and condition 4 were reduced by 4.1%, 8.1% and 11.8%, respectively, compared with that under condition 1.

Previous studies showed that the removal of organic matter is mainly through chelating reaction with iron and aluminum coagulant [12]. For condition 2, Iron, Aluminum and PDMDAAC components of PAFC-PDMDAAC composite coagulant create synergies, which increase the organic matter removal efficiency.

The organic matter removal of the condition 3 is improved by the synergistic effects of ClO_2 oxidation, enhanced coagulation and PAFC-PDMDAAC. ClO_2 can lead to the instability and aggregation of colloidal solids. The macromolecular organic matter could then turn into small molecule organic matter, which is beneficial for coagulation [10].

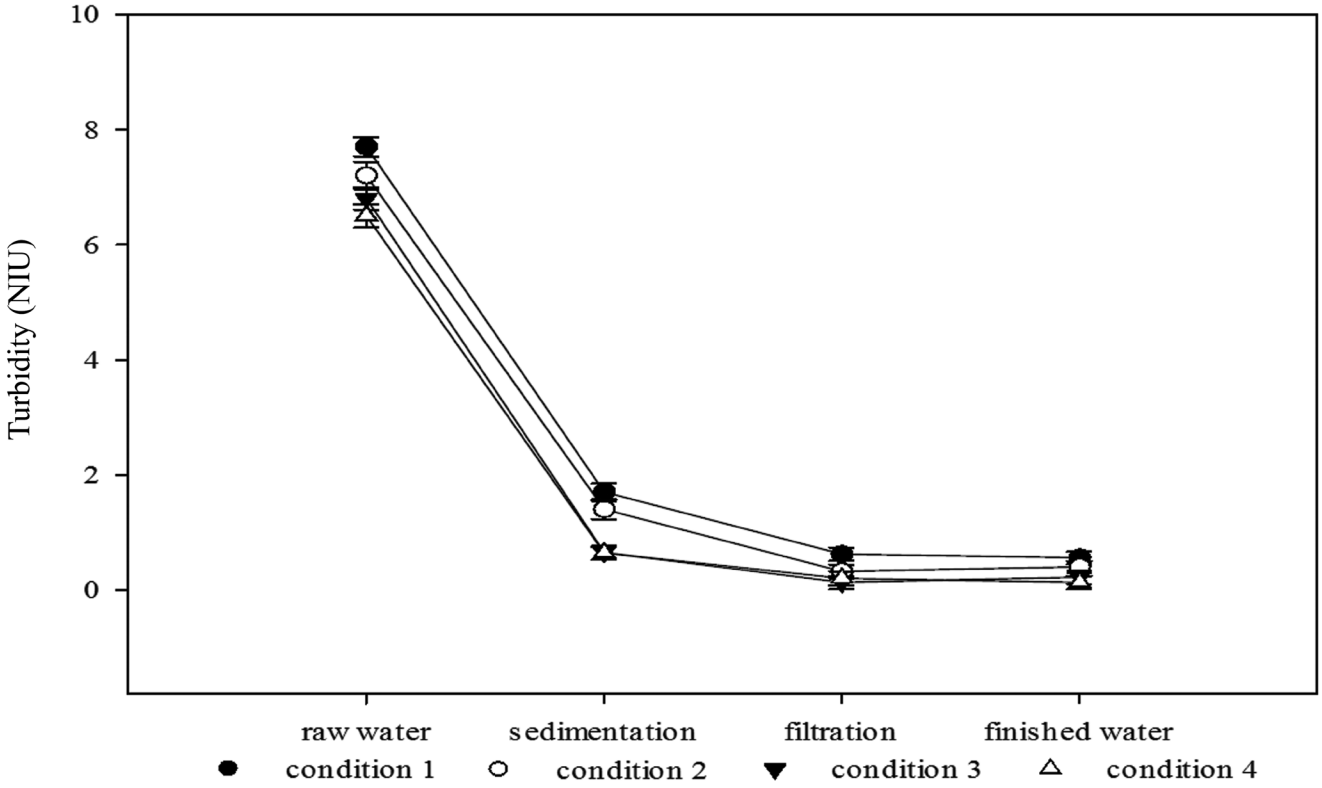

Figure 2. *Removal effect of turbidity under different conditions.*

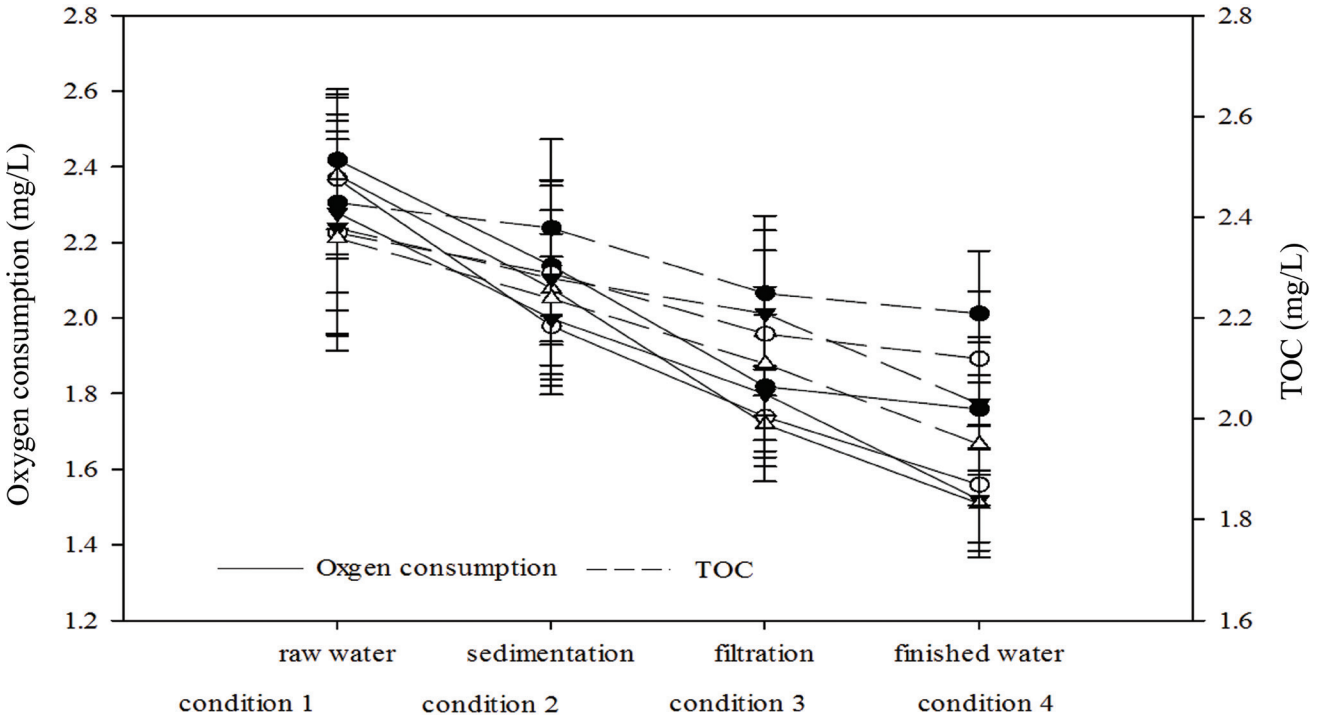

Figure 3. *Removal effect of organics under different conditions.*

The condition 4 has greatly increased the removal rate of organic matter by the synergistic effects of PPC oxidation, adsorption, enhanced coagulation and PAFC-PDMDAAC. PPC could enhance the removal rate of organic matter [13]. The oxidation of PPC could change the structure of some organic materials, for some oxidized substances can be oxidized to inorganic substance. Dysoxidized organic matter is mainly removed through the adsorption and package of MnO_2 colloid.

Removal of Algae

The removal rates of the total algae and Chl-a under different conditions are shown in Figure 5. The removal rates of total algae and Chl-a under condition 1 and condition 2 were low during coagulation precipitation, denoting that the total algae and Chl-a were mainly removed during filtration process and so filter loading was heavy. However, the removal capacities of total algae and Chl-a under condition 1 and condition 2 were improved due to the preoxidation by adding ClO_2 and PPC during coagulation precipitation. This indicates that the filter load was reduced. The total algae in the effluent under the four conditions were not detected but the Chl-a was measured to be 0.35, 0.23, 0.08 and 0.07 μg/L, respectively. The Chl-a in the effluent under condition 2, condition 3 and condition 4 was, compared with that under condition 1, reduced by 34.3%, 77.1% and 80%, respectively.

Previous studies showed that physiological and ecological structures of algae, algae activities, surface charge and algae metabolites are the primary factors that affect coagulation [14,15]. It is also found that there is a positive correlation between the removal rate of algae and turbidity removal [16].

The algae removal rate under the condition 3 is higher than the above two. ClO_2 could enter into the cells of algae in the form of a single molecule. The structure of chlorophyll and protein could then be changed; the algal cells systems were damaged and died eventually [17]. The activities of the algae were inhibited; the gathered algal cells were dissipated and cracked, leading to destruction of the surface structure of the algal cells. Therefore, the algae were removed by the synergistic effect of ClO_2 and PFAC-PDMDAAC [5,18].

Algae removal effect under condition 3 is the best due to a proper amount of PPC and PFAC-PDMDAAC synergy coagulation. The appropriate amount of PPC could maintain the integrity of the cell structures without releasing intracellular substances [19]. At the same time, the extracellular substances of algae are oxidized, resulting in declined algal activities. MnO_2 is attached on the surface of algae, which could increase the proportion of algae, under the coagulation of PFAC-PDMDAAC, as well as the algae removal efficiency [11,13].

Removal Effect of DBPs and AOX

During chlorination, chlorine may react with some organic and inorganic substances to form a series of halogenated organic by-products, most of which pose potential threat to human health [20]. The AOX refers to the chlorination, brominating and iodination of organics. It could cause distortion, cancer and catastrophe [21]. Among 129 kinds of priority pollutants put forward by the United States Environmental Protection Agency (USEPA), organic halides account for about 60%. The organic halide characterized by AOX has become one of the international water quality indexes. The concentration of THM and AOX in the effluent after chlorination under different conditions are shown in Figure 5. It can be known from Figure 5 that the total THM and AOX concentration in the finished water under condition 1 were the highest with 0.79 mg/L and 0.78 mg/L, respectively. Concentration of THM and AOX in the effluent under condition 2, condition 3 and condition 4 were effectively decreased by 45.6%, 54.4%, 60.8% and 7.8%, 12.9%, 19.4%, respectively, compared with those under condition 1.

Previous studies found that TOC concentration and by-products generation after disinfection has a good linear relationship [22]. Therefore, THM and AOX production in the effluent under different working conditions are mainly related to the removal rate of organic matters. THM and AOX production under condition 2 were primarily reduced by the coagulation of PAFC—PDMDAAC which removed disinfection by-products precursor.

Under condition 3, THM and AOX production is mainly reduced by the effect of ClO_2 selectivity oxidizing. ClO_2 could oxidize the locus that could be easily attacked by chlorine, and reduce the production of chlorinated disinfection by-products [23].

Under condition 4, THM and AOX production is mainly reduced by the synergistic effect of PPC oxidation, adsorption, and enhanced coagulation, resulting in increased removal of disinfection by-products precursors. The oxidation of potassium permanganate may damage some disinfection by-products precursors. MnO_2 serving as agglomeration adsorption core could remove some disinfection by-products precursors and improve removal efficiency of organic matters.

Technical and Economic Analysis

Technical and economic analyses of the four conditions were conducted and results were shown in Tab. 3. It can be found from Table 3 that water quality of

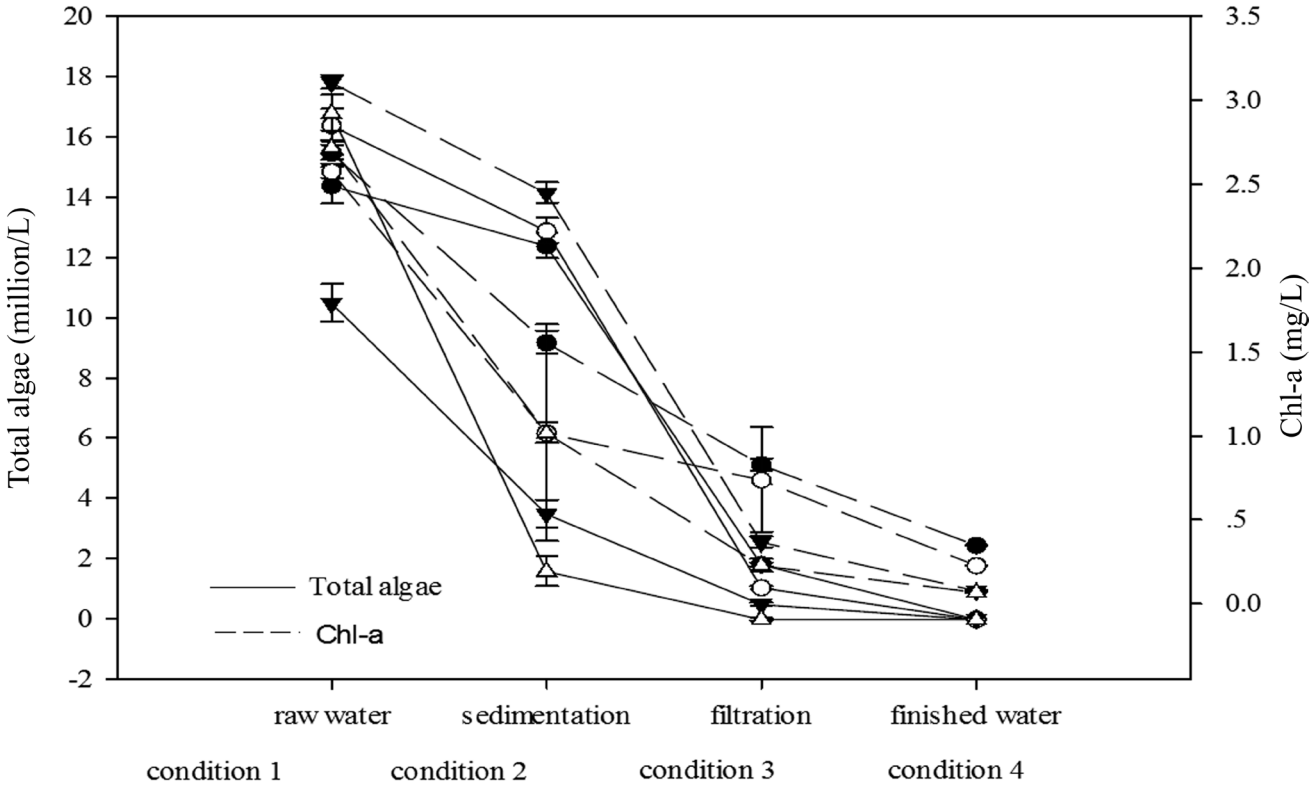

Figure 4. *Removal effect of algae under different conditions.*

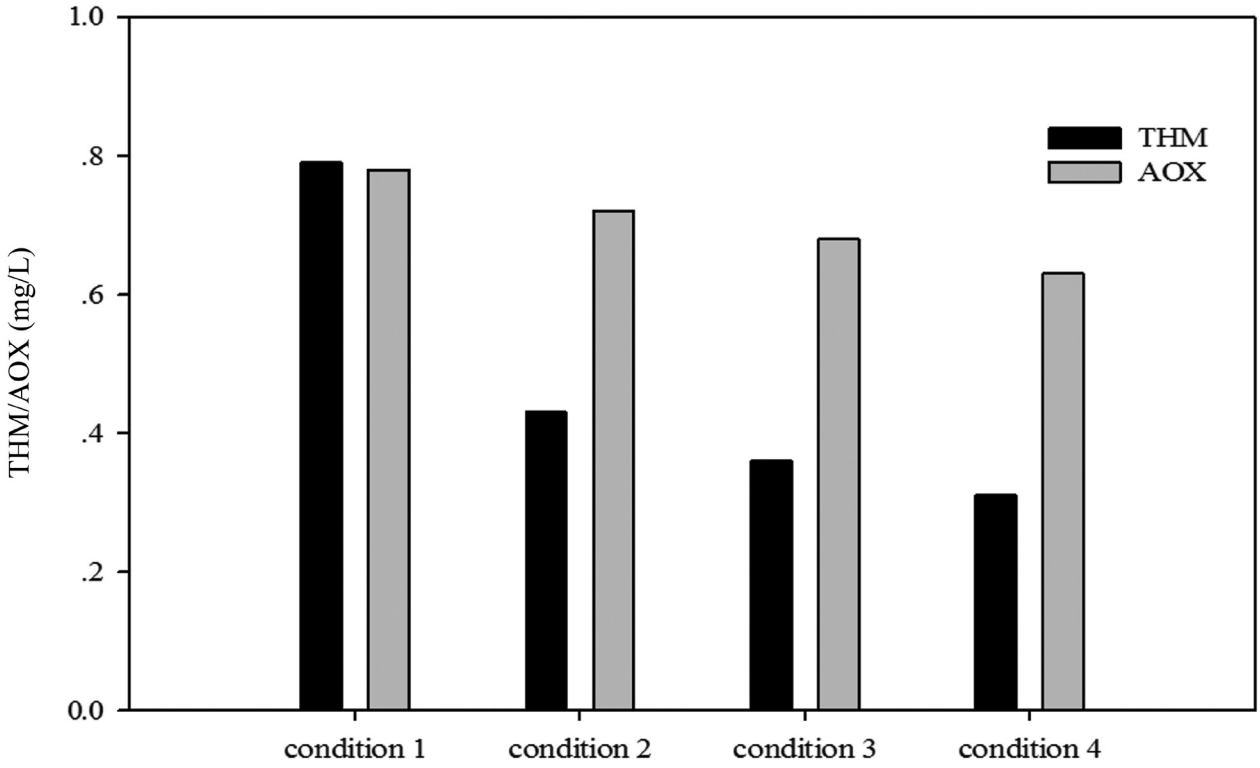

Figure 5. *Removal effects of THM and AOXe under different conditions.*

effluent under condition 2, 3 and 4 were improved compared with that under condition 1. Compared with condition 1, turbidity, COD and total THM in the effluent under condition 4 declined more significantly, i.e., 76.8 %, 14.2 % and 60.8 %, respectively. The increased cost for condition 3 (0.051 yuan/m^3) was the highest, followed by 0.024 yuan/m3 for condition 4 and 0.008 yuan/m^3 for condition 2. The condition 4 can effectively improve the quality of the effluent and therefore it is suitable for the water plant during the period of low temperature and low turbidity.

CONCLUSIONS

Compared with the sole use of PAFC coagulant, joint use of the composite PAFC-PDMDAAC coagulant, as well as combined use of the composite PAFC-PDMDAAC with chlorine dioxide or composite potassium permanganate could increase the removal efficiencies of turbidity and organics, reduce the formation of disinfection by-products and improve the quality of effluent. It should be pointed out that the combined use of the composite potassium permanganate and composite PAFC-PDMDAAC coagulant was the most effective to the operation of a conventional water treatment plant when influent is of low temperature and low turbidity.

ACKNOWLEDGEMENTS

This work was financially supported by China water pollution control and treatment national science and technology major project (Grant No. 2012ZX07404-

Table 3. Technical Analysis for Different Conditions.

	Water Quality Parameters						Economic Indexes	
	Turbidity (NTU)		COD_{Mn} (mg/L)		THM (mg/L)			
Type of Condition	Value	Descend Range %	Value	Descend Range %	Value	Descend Range %	Agent Fee (yuan/m^3)	Increased Agent Fee (yuan/m^3)
Condition 1	0.56	–	1.76	–	0.79	–	0.016	–
Condition 2	0.4	28.6	1.56	11.4	0.43	45.6	0.024	0.008
Condition 3	0.22	60.7	1.52	13.6	0.36	54.4	0.059	0.051
Condition 4	0.13	76.8	1.51	14.2	0.31	60.8	0.032	0.024

003), China science and technology program for public wellbeing (Grant No. 2013GS370202), project of mount Taishan scholar of Shandong province for drinking water safety ensuring technology (Grant No. ts200640025), Jinan science and technology program of major project (Grant No. 201307010).

REFERENCES

1. Shi Mingyan, Cui Fuyi, Zhang Hailong, *et al.* Pollutants removal by conventional drinking water treatment technique and optimal selection of coagulants [J]. *Journal of Harbin Institute of Technology,* 2002, 34(6):762–766 (in Chinese).
2. Gao Ya, Bi Zhe, Wang Dongsheng, *et al.* Optimization of coagulation performance and residual aluminium control for Yellow River water with low temperature and low turbidity [J]. *Chinese Journal of Environmental Engineering*, 2013, 7(10):3737–3742 (in Chinese).
3. Sun Li-hua, Lv Mou, Yang Yan-ling, *et al.* Enhanced treatment of water with low turbidity: combined effects of permanganate, PAM and recycled sludge [J]. *Journal of harbin institute of technology (new series)*, 2009, 16(6):863–868 (in Chinese).
4. Gao Baoyu, Wei Jincheng, Wang Yan, *et al.* Study on PolyFerric–Organic Composite Flocculants for Treatment of Surface Water [J]. *China Water and Wastewater*, 2006, 22(7):57–61 (in Chinese).
5. Jia Ruibao, Li li, Li Shijun, *et al.* Study on strengthened treatment of algae- contained reservoir with Chlorine dioxide [J]. *China Water & Wastewater*, 2003, 19(13):93–95 (in Chinese).
6. Liang Heng, Zhang Wen-yu, Gong Wei-jia, *et al.* Comparative study on combined preoxidation by potassium permanganate composites with chlorine and preozontion [J]. *Journal of harbin institute of technology (new series)*, 2009, 16(6):849–853.
7. Gu Qiaohong, Rong Guodong. Potassium permanganate composite and powered activated carbon for the treatment of algae-laden Yellow River water [J]. *Water Technology*, 2009, 3(1):36–39 (in Chinese).
8. Sun Yunkai, He Wenjie, Sun Ying, *et al.* Optimal selection of coagulants for treating low temperature and low turbidity Danjiangkou Reservoir water [J]. *Water Technology*, 2014, 8(1):1–6 (in Chinese).
9. Wang Y, Gao B Y, Yue Q Y. The characterization and flocculation efficiency of composite flocculant iron salts-polydimethyldiallylammonium chloride [J]. *Chem. Eng. Jour.*, 2008, 142(2): 175–181. http://dx.doi.org/10.1016/j.cej.2007.11.022
10. Yang Tao, Fu Jin-xiang, Liang Jian-hao Research on Chlorine Dioxide Pre-oxidation of Low Temperature Slight-polluted Water [J]. *Liaoning Chemical Industry*, 2005, 34(8): 348–349 (in Chinese).
11. Ma Jun, Chen Zhonglin, Li Guibai, *et al.* Enhanced coagulation of stabilized surface water with high organic contents by permanganate chemical [J]. *China Water & Wastewater*, 1999, 15(9): 1–3 (in Chinese).
12. Zhang Sheng, Xie Shuguang, Zhang Xiaojian, *et al.* The study progress of the control of natural organic matter in raw water by enhanced coagulation. *Techniques and Equipment for Environmental Pollution Control* 2003, 4(8): 19–22 (in Chinese).
13. LI Xing, YANG Yan-ling. Polluted raw water treatment by pre-oxidation of potassium permanganate composite [J]. *Journal of Harbin University of Commerce (Natural Sciences Edition)* 22 (1):20–23 (in Chinese).
14. Henderson R K, Baker A, Parsons S A, *et al.* Characterisation of algogenic organic matter extracted from cyanobacteria, green algae and diatoms [J]. *Water Research*, 2008, 42(13): 3435–3445. http://dx.doi.org/10.1016/j.watres.2007.10.032
15. Takaara T, Sano D, Konno H, *et al.* Cellular proteins of Microcystis aeruginosa inhibiting coagulation with polyaluminum chloride [J]. *Water Research*, 2007, 41 (8):1653–1658. http://dx.doi.org/10.1016/j.watres.2007.01.035
16. ZHAO Xiao-lei, ZHANG Yue-jun, LI Xiao-xiao, *et al.* Algae removal effects of PAC/PDM on Tailu lake prechlorination algae-rich water in summer [J]. *Journal of Nanjing University of Science and Technology (Natural Science)*, 2010, 34 (4): 570–574 (in Chinese).
17. LIU Jie-sheng, YANG Wei -dong, ZHANG Heng, WU Yan. Effects of chlorine dioxide on contents of chlorophyll a, proteins and DNA in phaeocystis globosa [J]. *Journal of Tropical and Subtropical Botany*, 2006, 14(5):427–432 (in Chinese).
18. Wang Lining, Fang Jingyun, Ma Jun, *et al.* Effect of pre-oxidation on algal cell morphology and algal removal by enhanced coagulation process [J]. *Journal of Southeast University (Natural Science Edition)*, 2005, 35 (S1): 182–185 (in Chinese).
19. Drikas M, Chow C W K, House J, *et al.* Using coagulation, flocculation, and settling to remove toxic cyanobacteria[J]. *J Am Water Works Assoc*, 2001, 93(2) : 100–111.
20. Miles A W, Singer P C, Ashley D L, *et al.* Comparison of trihalomethanes in tap water and blood [J]. *Environ Sci. Technol*, 2002, 26(8): 1692–1698. http://dx.doi.org/10.1021/es001991j
21. Jiang Mei, Shen Xinqiang, Chao Gai, *et al.* Toxity of AOX Bleaching Effluent to Eggs and Larvae of Sparus Macrocepgalus [J]. *Research of Environmental Science*, 2004, 19(2):27–31 (in Chinese).
22. Sdrodes J B, Rodriguez M J, Li H, Bouchard C. Occurrence of THMs and HAAs in experimental chlorinated waters of the Quebec City area(Canada) [J]. *Chemosphere*, 2003, 5 1(4): 253–263.
23. Wang Li-kun, Wang Qi-shan, LIU Yan-fang, *et al.* THMFP control of drinking water via preoxidation of chlorine dioxide[J]. *Journal of Tianjin University*, 2009(12): 1118–1122 (in Chinese).

Study on Anaerobic Ammoniumoxidation (ANAMMOX) Sludge Immobilized in Different Gel Carriers and Its Nitrogen Removal Performance

GUANGHUI CHEN[1], JUN LI[1,*], HAILIANG DENG[1], QIANQIAN DONG[2], YANZHUO ZHANG[1], ZHAOMING ZHENG[1] and AIYUE HOU[1]

[1]*Key Laboratory of Beijing for Water Quality Science and Water Environment Recovery Engineering, Beijing University of Technology, Beijing 100124, China*

[2]*Architectural and Civil Engineering Institute, Beijing University of Technology, Beijing 100124,China*

ABSTRACT: To maintain Anammox biomass, different materials were used as carriers to immobilize Anammox sludge. The adsorptive property, anaerobic ammonia oxidation activity, and stability of the particles were evaluated. The results indicated waterborne polyurethane (WPU) was the most suitable immobilizing material. In a continuous flow experiment, we further investigated the resistance to impact load and the anaerobic ammonia oxidation activity by increasing the influent load. It was found that for WPU-immobilized particles, no effluent SS or particles fracture was observed during the 66-day operation, and the WPU-immobilized particles showed a strong capability to retain sludge and good stability in the long-term.

INTRODUCTION

THE ANAMMOX process is an effective microbial pathway to treat wastewater. In this process, NO_2^--N acts as the electron acceptor, and NH_4^+-N becomes oxidized to N_2 under anaerobic conditions [1]. Compared with the conventional nitrogen removal system (nitrification-denitrification [2]), the ANAMMOX process has clear advantages: it does not require organic carbon and oxygen and produces less surplus sludge; these advantages all reduce operational cost [3–5]. However, ANAMMOX bacteria are autotrophic bacteria—they grow slowly and have a low cell yield; in addition, ANAMMOX bacteria are also affected by environmental conditions [6–7]. It is difficult for ANAMMOX biomass to remain in a reactor. Thus, there is difficultly in starting an ANAMMOX reactor, which limits its development [8]. Researchers have conducted extensive studies on the ANAMMOX technique and proposed techniques on starting an ANAMMOX reactor, such as the biological fluid bed and fed-batch [9–10]. However, the results from using these techniques are not ideal [11]. Therefore, retaining microbes and ensuring the biomass of ANAMMOX bacteria have become a primary direction in developing the ANAMMOX technique [12].

The embedded immobilization technique may be able to solve this problem, which is a new microbe immobilization technique in the modern bioengineering field. The embedded immobilization technique immobilizes free cells or enzymes in a constrained area through immobilization material such that the activity of cells or enzymes can be maintained and reused; the embedded immobilization technique provides a good retaining effect on microbes [13–15]. Using the embedded immobilization technique to immobilize ANAMMOX sludge can effectively prevent the loss of ANAMMOX bacteria and maintain the biomass in the reactor, and thus, this technique appears promising [16–18]. However, there are disadvantages with using the existing immobilization materials, such as insufficient mechanical strength, low bioactivity, and lack of stability during long-term operation [19–21]. This study uses waterborne polyurethane (WPU) [22], polyethylene glycol (PEG), carboxymethyl cellulose (CMC), and polyvinyl alcohol (PVA) as materials to immobilize ANAMMOX sludge, and the long-term mechanical stability, ANAMMOX performance, and shock-loading resistance were evaluated to provide a

*Corresponding author: Jun Li
E-mail: lijunbjut@163.com; Tel: +8613611249208; Fax: +8601067391645

1544-8053/15/01 S047-08

doi:10.12783/issn.1544-8053/12/S1/7

basis for further study on the rapid start-up and stable operation of the embedded immobilized technique-based ANAMMOX process.

MATERIALS AND METHODS

Immobilization Materials

Sludge concentrate: the ANAMMOX sludge was obtained from a sequential batch reactor (SBR) in a laboratory that had been in stable operation for one year. The sludge taken from the reactor was first washed three times in deionized (DI) water to remove the residues on the surface of the sludge. Afterwards, the sludge was centrifuged at 500 $r \cdot m^{-1}$ for 20 min. Analytically pure immobilization agents (PEG, WPU, CMC, PVA) and crosslinking agents/initiators ($CaCl_2$, H_3BO_3, potassium persulfate (KPS), and tetramethylethylenediamine (TMEDA)) were used.

Water Quality

Synthetic wastewater was used. Table 1 lists the main components of the wastewater. Trace elements I and II followed reference [23]. The pH of the water ranged from 7.1 to 7.84.

Preparation of Immobilized Granules

The preparation methods for all the immobilized granules are as follows (mass percentage):

- *WPU-immobilized granules*: 10% WPU solution and ANAMMOX sludge concentrate of equivalent volume were mixed homogeneously. The initiators TMEDA and KPS were added, and the solution was rapidly stirred. Approximately 30 min later, the mixed solution became a gel.
- *PEG-immobilized granules*: 10% PEG solution and equivalent volume ANAMMOX sludge were mixed. The initiators TMEDA and KPS were added after the mixed solution became a gel. The solid gel was cut into 3 × 3 × 3 mm cubes, and WPU-immobilized granules were obtained.
- *CMC-immobilized granules*: Equivalent volumes of 3% CMC solution and ANAMMOX sludge concentrate were mixed. The mixed solution was added to 4% $CaCl_2$ solution drop by drop using a pipette. The solution was then stored in a 4°C refrigerator for crosslinking for 12 h to obtain spherical CMC-immobilized granules.

Table 1. Composition of the Synthetic Wastewater.

Main Components	Mass Concentration ($mg \cdot L^{-1}$)
KH_2PO_4	32
$CaCl_2$	142
$MgSO_4 \cdot 7H_2O$	283
$KHCO_3$	802
NH_4Cl	372
$NaNO_2$	502
Trace element I	1 $ml \cdot L^{-1}$
Trace element II	1 $ml \cdot L^{-1}$

- *PVA-immobilized granules*: Equivalent volume of 8% PVA solution and ANAMMOX sludge concentrate were mixed homogeneously. The mixed solution was added to saturated H_3BO_3 solution drop by drop using a pipette. The solution was then stored in a 4°C refrigerator for crosslinking for 12 h to obtain spherical PVA-immobilized granules.

The prepared immobilized granules were collected and used for batch culture to determine their activity [24]. After 1 week of activation, the immobilized granules were removed for later use.

Mechanical Stability

To determine the mechanical stability of the immobilized granules, the mechanical strength, expansion coefficient, and swelling properties were used as evaluation indices. Mechanical strength: 30 immobilized granules of similar size of each material type were selected and placed in a 500-mL conical flask. Then, 400 mL of DI water was added to the reactor. The mixture was magnetically stirred at 500 r/min for 24 h, after which the ratio of intact immobilized granules to the original number of immobilized granules was determined. Expansion coefficient: 20 immobilized granules from each of the four material types were added to a 500-mL conical flask (400 mL DI water). The flask was slowly shaken at 30°C for 72 h; then, the diameters of the immobilized granules before and after treatment were measured by a vernier caliper. The ratio of the mean diameter of the immobilized granules after 72 h of treatment to the mean diameter of the original immobilized granules was the expansion coefficient. Swelling properties: 20 immobilized granules from each of the four material types were added to a 500-mL conical flask (400 mL synthetic wastewater). The flask was slowly shaken at 32°C for 1 week. The changes in the immobilized granules were observed.

ANAMMOX Performance

The ANAMMOX performance of the immobilized granules was measured in a serum bottle. A total of 40 mL of activated immobilized granules (including approximately 20 mL of concentrated sludge) of each material type was added to a 500-mL serum bottle, which was covered with black plastic bags. Then, 400 mL of synthetic wastewater was added to the serum bottle. The bottle was magnetically stirred at 100 r/min. The serum bottle was air-stripped with purity N_2 for 20 min to ensure an anaerobic environment, and the temperature was controlled at 30°C. The pH was not controlled. Sampling was conducted every 8 h from the serum bottle. A total of 20 mL of un-immobilized ANAMMOX sludge concentrate was used as the control group for the same experiments. The experiment was repeated twice, and the results were averaged.

Continuous-flow Experiment

The continuous-flow experiment used an up-flow anaerobic sludge blanket (UASB) reactor (Figure 1), which used the material polymethyl methacrylate (PMMA). The reactor contains three phase separators in the upper section with an effective volume of 17 L. A mesh was placed at the water outlet to prevent the immobilized granules from flowing out with the water. There was a water bath layer on the external wall of the reactor. The temperature in the reactor was maintained at 30°C with a water bath outside. After activation, immobilized granules (the amount was based on 20% of the volume fill ratio) were added to the reactor. The wastewater used in experiment was synthetic. The concentration of NH_4^+-N was between 40 and 200 mg/L, and the concentration of NO_2^--N was between 50 and 180 mg/L; the concentrations of the other components are listed in Table 1. During the experiment, the hydraulic retention time (HRT) was 8h; such indices as NH_4^+-N, NO_2^--N, and NO_3^--N in the effluent were determined every day.

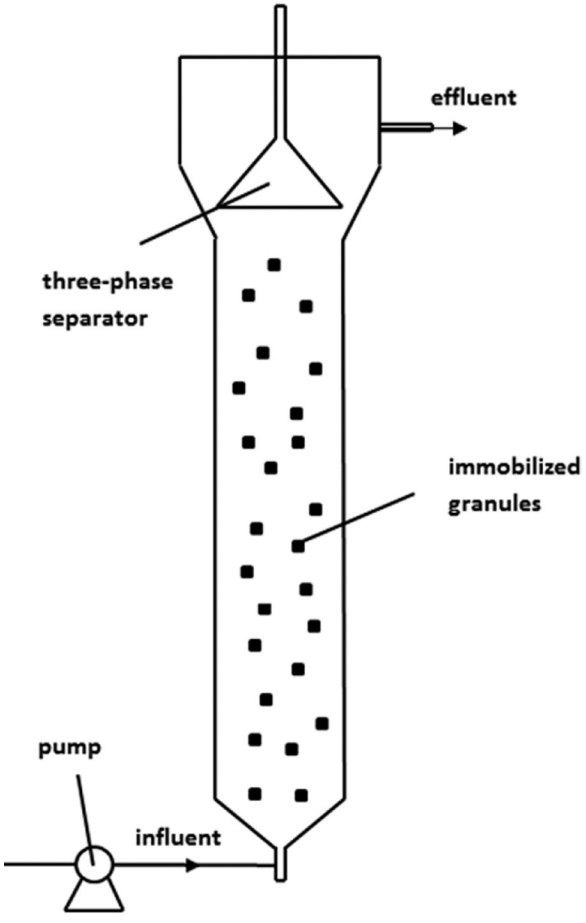

Figure 1. *Up-flow anaerobic sludge blanket (UASB) reactor.*

Scanning Electron Microscopy (SEM)

SEM analysis of immobilized granules: immobilized granules were removed from the reactor and washed, and 25% pentanediol was used to immobilize the granules for 1.5 h. Afterwards, the granules were washed three times in PBS. Subsequently, the granules were dehydrated in an ascending series of ethanol (volume fraction: 50%, 70%, 80%, 90%, and 100%); the duration of dehydration was 10–15min. Lastly, isoamyl acetate was used for displacement. After the granules were freeze-dried for 24 h, a 1500-nm thick metallic membrane layer was electroplated on the surfaces of the samples. A Hitachi S-4300 SEM was used for observation.

Testing Methods

The standard method was used to determine NH_4^+-N, NO_2^--N, NO_3^--N, TN, MLSS, and MLVSS [25]. A WTW/Multi 3420 multiparameter was used to determine the pH and temperature.

RESULTS AND DISCUSSION

Adsorption Properties

Figure 2(a) shows the adsorptions of NH_4^+-N on the different granules. The WPU granules had the highest adsorption rate for NH_4^+-N; their adsorption rates were 7.1% at 32 h and 7.3%, at 40 h. The PVA granules had

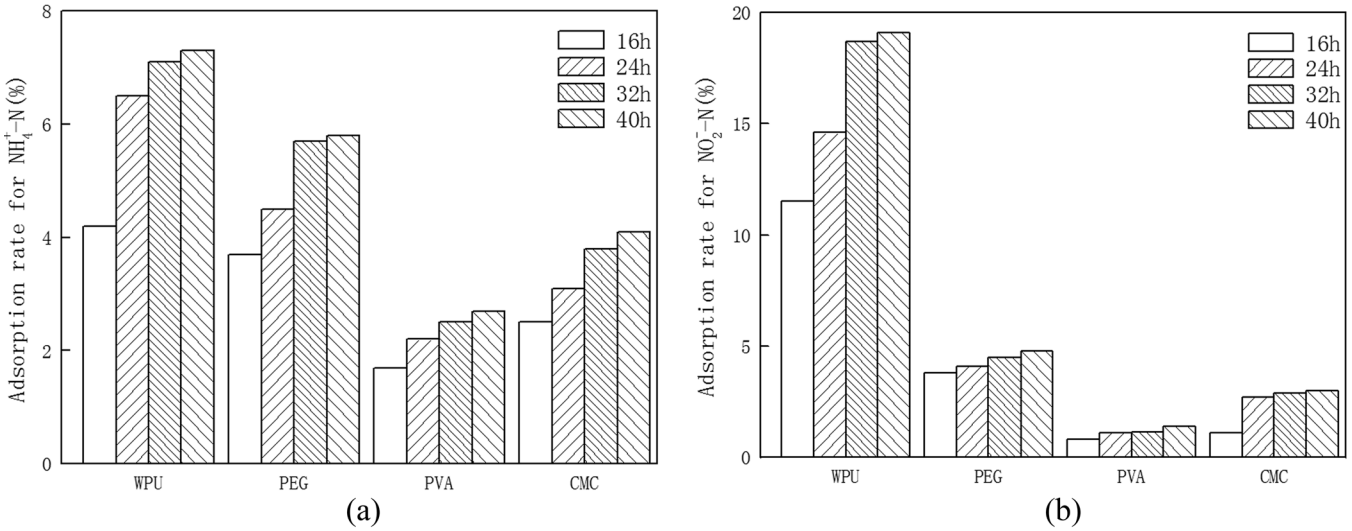

Figure 2. *Adsorptions of NH_4^+-N and NO_2^--N on different immobilized granules: (a) Adsorptions of NH_4^+-N; and (b) Adsorptions of NO_2^--N.*

the lowest adsorption rate for NH_4^+-N; their adsorption rate was only 2.7% at 40 h. Figure 2(b) shows that there were significant differences among the materials in terms of the adsorption of NO_2^--N. The WPU granules' adsorption rate reached 19.1% at 40h; the PEG, PVA, and CMC granules all had extremely low adsorption rates for NO_2^--N that did not surpass 5%, and the PVA granules had the lowest adsorption rate, which was only 1.1% at 40 h.

The experiments revealed that the four types of immobilization materials all had certain adsorption properties for NH_4^+-N and NO_2^--N; however, the adsorption rates were not high and reached equilibrium rapidly. Therefore, after 1 week of activated culture, all types of immobilized granules reached their adsorption equilibrium for NH_4^+-N and NO_2^--N. As a result, the adsorption properties had only a slight impact on the subsequent experimental results; therefore, the properties could be neglected.

Stability of the Immobilized Granules

Table 2 lists the mechanical stability indices of the four types of immobilized granules. After 1 week of stirring in synthetic wastewater, the CMC-immobilized granules and the PVA-immobilized granules became soft and fragile. The mechanical strength of the CMC-immobilized granules was the lowest; after 24 h of high-speed rotation, almost all the CMC-immobilized granules had broken. The WPU-immobilized and PEG-immobilized granules exhibited the best stability; after 1 week of stirring, these granules exhibited essentially no change. The expansion coefficient of the WPU-immobilized granules was 1.02; after 24 h of high-speed rotation, no granules had broken. The PEG-immobilized granules also exhibited relatively good stability, though the stability was less than that of the WPU-immobilized granules; after high-speed rotation, 14% of the granules had broken. The expansion coefficient of the PVA-immobilized granules was 1.31; the PVA-immobilized granules also exhibited good stability. However, a phenomenon was observed in the PVA-immobilized granules in which the granules stacked together. Thus, considering all indices, the order of the mechanical stability from strongest to weakest was WPU > PEG > PVA > CMC.

Table 2. Stability of Immobilized Granules.

Immobilized Granules	Mechanical Strength	Expansion Coefficient	Swelling Properties
PEG	0.86	1.04	—
WPU	1.00	1.02	—
CMC	0.07	1.82	++
PVA	0.73	1.31	+

Notes: (—) – unchanged; (+) – slightly softened and loosened; (++) – softened and fragile.

The differences in the mechanical stability were primarily caused by the properties of the different immobilization materials. PVA is a synthetic polymer and has good physical properties; as an immobilization material, the PVA-immobilized granules inherited the merits of PVA. However, these granules contain many hydrophilic hydroxyl groups in their chemical structure, which results in the PVA-immobilized granules exhibiting certain water swelling properties and autocondensing tendencies [26]. Therefore, PVA-immobi-

lized granules tended to conglutinate, which decreased the specific surface area of the immobilized granules and thus affected their stability. CMC-immobilized granules have no clear spherical shell, and thus, these granules exhibit a good mass transfer performance but have a loose chemical structure; the CMC-immobilized granules had the lowest stability and are not well-suited as an immobilization material. PEG and WPU are synthetic polymeric material and thus exhibit good biocompatibility and excellent mechanical strength [27]. When cross-linked, these materials form a stable gel. However, the materials have a different relative molecular mass and chemical structure; the space of the WPU three-dimensional network structure is relatively small, which not only ensures the mechanical strength of the WPU-immobilized granules but also absorbs less water when swelling. Therefore, the WPU-immobilized granules exhibited a better mechanical stability than the PEG-immobilized granules and are considered the best material among the four types.

ANAMMOX Performance of the Immobilized Granules

Figure 3(a) shows the variation curve of the removal rate of NH_4^+-N with respect to time for the different immobilized granules. The removal rate of NH_4^+-N increased first rapidly and then slowly in both the control group and the immobilization group, which was because the initial concentration of NH_4^+-N was high and the ANAMMOX rate was fast; later, the substrate concentration decreased, which decreased the reaction

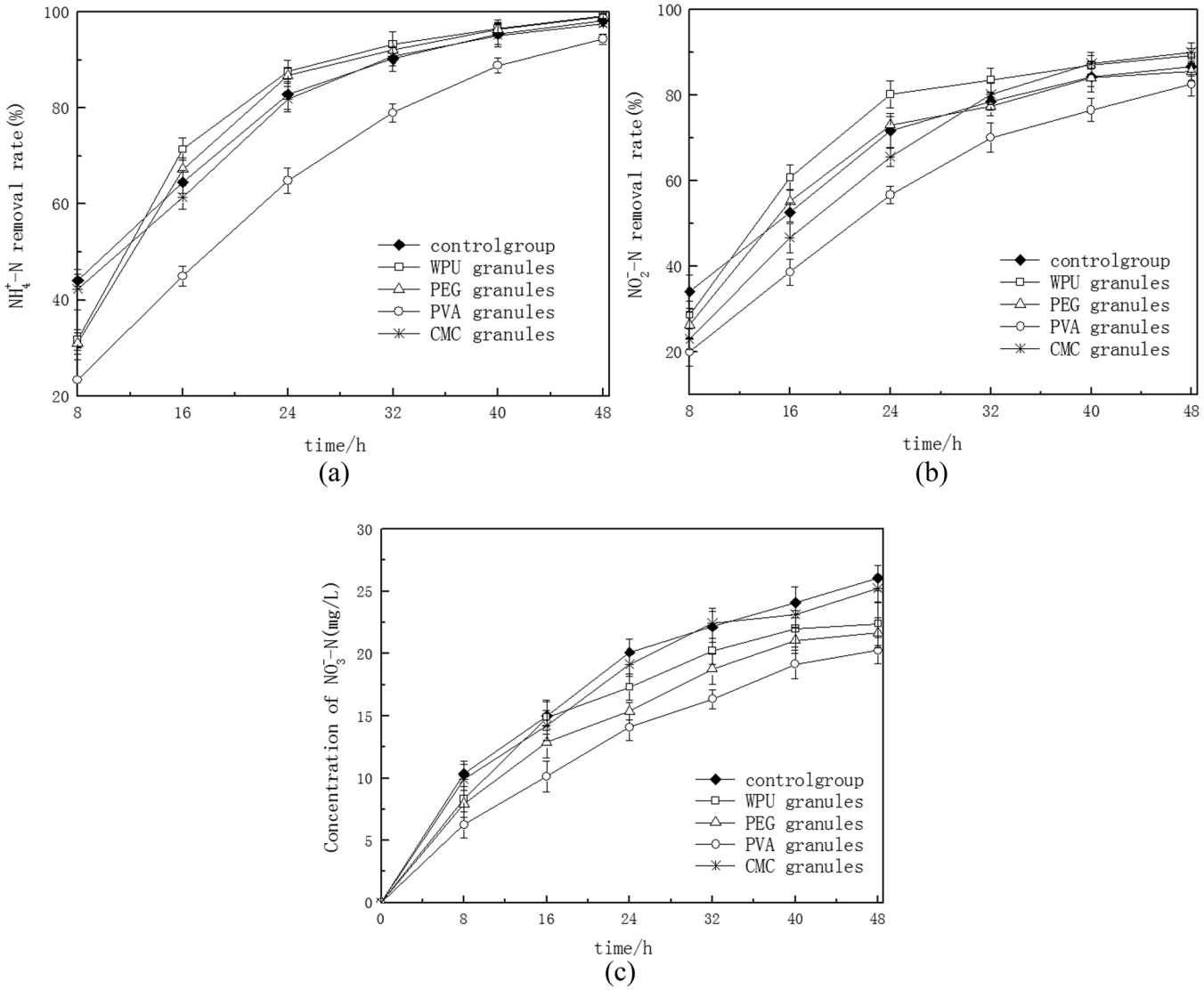

Figure 3. *Variation curves of NH_4^+-N, NO_2^--N, and NO_3^--N with respect to time: (a) NH_4^+-N; (b) NO_2^--N; and (c) NO_3^--N.*

rate. Between 0 and 8 h, the removal rate of NH_4^+-N in the control group and CMC-immobilized granules increased the fastest. After 16 h, the removal rate for the WPU- and PEG-immobilized granules surpassed the removal rate of the control group and CMC-immobilized granules. After 40 h, the removal efficiency decreased in both the control group and the immobilization group. Eventually, at 50 h, the NH_4^+-N in all the reactors was completely removed. The variation pattern of the concentration of NO_2^--N was essentially the same as the variation pattern of NH_4^+-N. Between 0 and 8h, the removal rates for NH_4^+-N and NO_2^--N in the control group (and CMC group) were greater than in the immobilization group, which was primarily because the immobilization material prevented mass transfer between the materials in the water and the ANAMMOX bacteria in the immobilized granules. After 16 h, the removal rates for NH_4^+-N and NO_2^--N in the WPU- and PEG-immobilized granules were greater than in the control group, which benefited the more concentrated biomass in the immobilized granules and resulted in a higher activity of the ANAMMOX bacteria.

Between 8 and 32h, the substrate completely dispersed into the immobilized granules. An analysis was performed for this period, and the average removal rates for NH_4^+-N and NO_2^--N were as follows (from fastest to slowest): WPU > PEG > CMC > PVA. By comparison with the variation curve of the yield of NO_3^--N with respect to time in Figure 3(c), the ratios of the removed amount of NO_2^--N to the removed amount of NH_4^+-N of the WPU-, PEG-, PVA-, and CMC-immobilized granules were 1.204, 1.292, 1.328, and 1.537, respectively. The ratios of the yield of NO_3^--N to the removed amount of NH_4^+-N were 0.337, 0.325, 0.185, and 0.229, respectively, which were both extremely similar to the ratios of the control group. Thus, these immobilized granules exhibited good ANAMMOX performance.

The ANAMMOX properties of the different immobilized granules are related to the different chemical structures and the form of the cross-linked immobilized granules. For each PVA-immobilized granule, there was a homogenous spherical shell; the exterior was relatively dense, and thus, the mass transfer resistance was large. In addition, the conglutination of granules resulted in a decrease in specific area, which resulted in a poor mass transfer property; therefore, the ANAMMOX performance of the PVA-immobilized granules was the poorest. The spherical shell formed on the surface of each CMC-immobilized granule was relatively thin, and the mass transfer resistance was relatively small. After crosslinking, the size of the network structure formed inside was relatively large. However, because CMC-immobilized granules have no stable structure, they easily shatter; shattered granules lose the immobilized advantages, and thus the performance of CMC-immobilized granules is similar to that of un-immobilized ANAMMOX sludge. The WPU- and PEG-immobilized granules contained no clear shell on the surface of each immobilized granule and therefore had good mass transfer performance and contained a looser three-dimensional network structure. The WPU-immobilized granules exhibited a better ANAMMOX performance compared with the PEG-immobilized granules. Figures 4(a) and 4(b) show × 4.0 k and × 8.0 k SEM images of the surfaces of the WPU-immobilized granules. Figure 4(a) shows that there are many channels on the surface of each WPU-immobilized granule; bacteria were divided into different areas by the channels. Figure 4(b) shows that these bacteria had a spherical shape, and there were volcanic crater-like concaves on the two sides of each bacterium, which indicates that these were typical ANAMMOX bacteria. Figure 4(c) shows the SEM image of the inside of a WPU-immobilized granule after being cut open; it can be seen that a large amount of ANAMMOX bacteria grew along the channels inside of the granule. There-

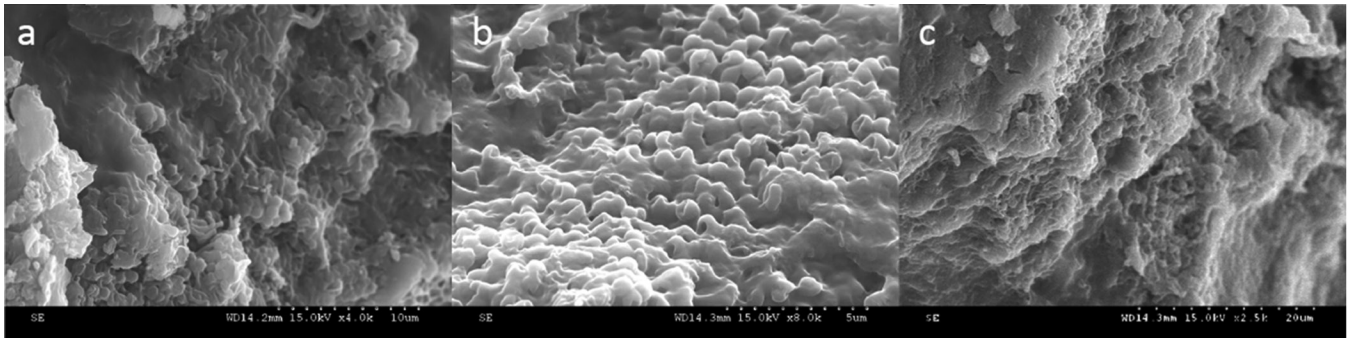

Figure 4. *SEM images of the WPU-immobilized granules: (a) surface × 4.0 k; (b) surface × 8.0 k; and (c) inside × 2.5 k.*

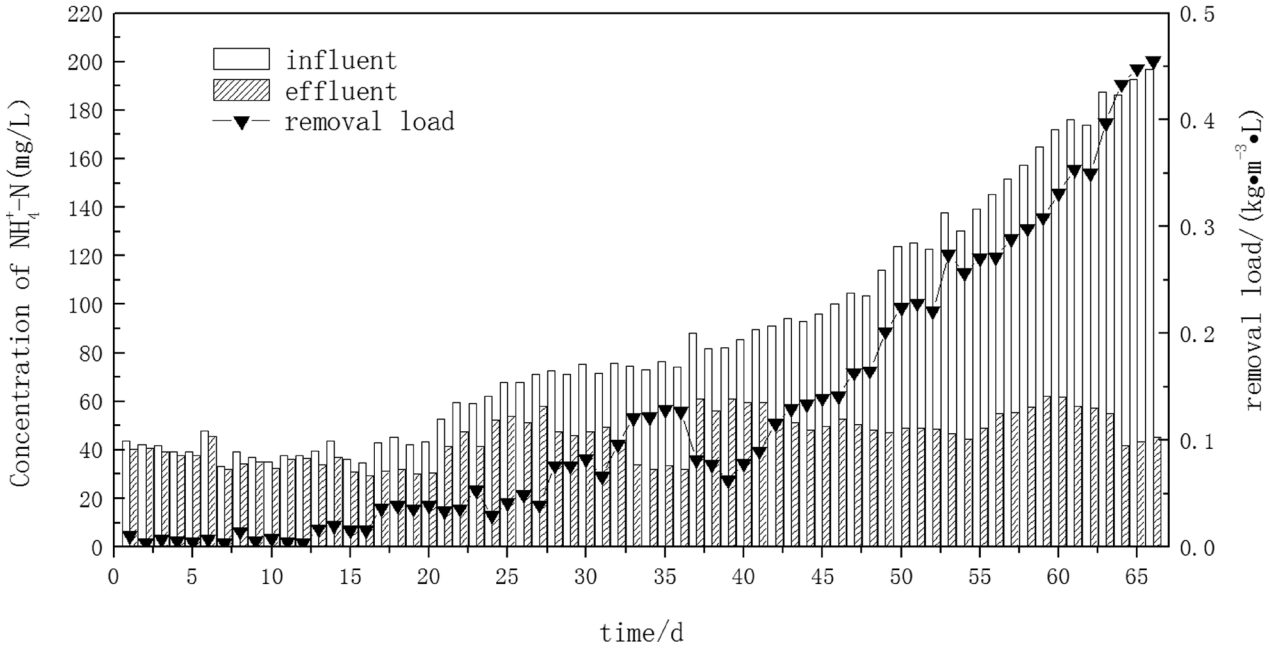

Figure 5. *Variation curves of the concentrations and removal load of NH_4^+-N with respect to time.*

fore, the WPU-immobilized granules had the best mass transfer property and ANAMMOX activity.

Continuous-flow Experiment

To study the nitrogen removal performance and stability of WPU-immobilized granules during long-term operation, a continuous-flow experiment was developed. The HRT was 8h, the influent NH_4^+-N was varied between 40 and 200 mg/L, and NO_2^--N was varied between 50 and 180 mg/L. Using NH_4^+-N as a metric, Fig. 5 shows that between 0 and 20 days, the removal load of NH_4^+-N was less than 0.5kg·m^{-3}/L because the immobilized granules were under a domestication period. Then, the activity of the immobilized granules increased. The influent concentration increased the removal load of NH_4^+-N, which had also been increasing. On the 66th day, the removal load of NH_4^+-N was 0.455 kg·m^{-3}/L, and the removal rate was up to 77%. In addition, the effluent of the reactor was always clear during the experimentation period, and no suspended solids (SS) were detected. None of the immobilized granules broke. The WPU-immobilized granules exhibited a good sludge retaining ability and mechanical stability.

CONCLUSIONS

By comparing WPU-, PEG-, PVA-, and CMC-immobilized granules, the WPU-immobilized granules exhibited an extremely strong shock-loading resistance and mechanical stability during long-term operation, in which none of the WPU-immobilized granules broke. The WPU-immobilized granules exhibited good sludge retaining ability and mechanical stability. WPU has significant advantages compared with the other materials and is suitable for use as an immobilization material for ANAMMOX sludge.

ACKNOWLEDGMENTS

This research was supported bythe National Critical Project for Science and Technology on Water Pollution Prevention and Control of China (Nos. 2014ZX07201-011).

REFERENCES

1. Van de Graaf A A, Bruijn P de, and Robertson L A. "Metabolic pathway of anaerobic ammonium oxidation on the basis of 15N studies in a fluidized bed reactor", *J. Microbiology*, Vol. 143, No. 7, 1997, pp. 2415–2421. http://dx.doi.org/10.1099/00221287-143-7-2415
2. Van D. U., Jetten M., and Van L. M. "The SHARON®-Anammox® process for treatment of ammonium rich wastewater", *J. Water Science and Technology*, Vol. 44, No. 1, 2001, pp. 153–160.
3. Chou W. P, Tseng S. K, and Ho C. M. "Anaerobic ammonium oxidation improvement via a novel capsule bioreactor", *J. Environmental Technology*, Vol. 33, No. 18, 2012, pp. 105–110.
4. Winkler M K H, Kleerebezem R and Van Loosdrecht M C M. "Integration of anammox into the aerobic granular sludge process for main stream wastewater treatment at ambient temperatures", *J. Water Research*, Vol. 46, No. 1, 2012, pp. 136–144. http://dx.doi.org/10.1016/j.watres.2011.10.034
5. Jetten M S, Wagner M, and Fuerst J, "Microbiology and application of

the anaerobic ammonium oxidation ('anammox') process." *J. Current Opinion in Biotechnology*, Vol. 12, No. 3, 2001, pp. 283–288. http://dx.doi.org/10.1016/S0958-1669(00)00211-1

6. Tang C J, Zheng P, and Chen T-T, "Enhanced nitrogen removal from pharmaceutical wastewater using SBA-ANAMMOX process." *J. Water Research*, Vol. 45, No. 1, 2011, pp.201-210. http://dx.doi.org/10.1016/j.watres.2010.08.036
7. Mahmood Q, "Effect of substrate concentration on stability of anammox biofilm reactors." *J. Journal of Central South University of Technology*, Vol. 17, No. 1, 2010, pp.79–84. http://dx.doi.org/10.1007/s11771-010-0014-6
8. Tang Chongjian, and Xiong Lei, "WANG Yunyan.Kinetic Characteristics of High-rate ANAMMOX Granules". *J. Environmental Science*, Vol. 34, No. 9, 2013, pp. 3544–3551.
9. Van der Star W R, Abma W R, and Blommers D, "Startup of reactors for anoxic ammonium oxidation: experiences from the first full-scale anammox reactor in Rotterdam". *J. Water Research*, Vol. 41, No. 18, 2007, pp. 4149–4163. http://dx.doi.org/10.1016/j.watres.2007.03.044
10. Wett B. "Solved upscaling problems for implementing deammonification of rejection water". *J. Water Science & Technology*, Vol. 53, No. 12, 2006, pp. 121–128. http://dx.doi.org/10.2166/wst.2006.413
11. Zu Bo, Zahang Daijun, and Yan Qing. "Effect of Trace NO_2 and Kinetic Characteristics for Anaerobic Ammonium Oxidation of Granular Sludge". *J. Environmental Science*, Vol. 29, No. 3, 2008, pp. 683–687.
12. Qiao S, Tian T, and Duan X, "Novel single-stage autotrophic nitrogen removal via co-immobilizing partial nitrifying and anammox biomass". *J. Chemical Engineering Journal*, Vol. 230, 2013, pp. 19–26. http://dx.doi.org/10.1016/j.cej.2013.06.048
13. Chen Y., Zhou T., and Yao S., "Ethanol production by repeated batch and continuous fermentations by Saccharomyces cerevisiae immobilized in a fibrous bed bioreactor". *J. Journal of Microbiology and Biotechnology*, Vol. 23 No. 4, 2013, pp. 511–517. http://dx.doi.org/10.4014/jmb.1209.09066
14. Zhang Changli, Yang Hong, and Wang Jingjing, "Preparation and Pervaporation Performance of Silazane Hydrophobically Modified Mesoporous Molecular Sieves Filled PDMS Hybrid Composite Membrane", *J. Journal of Bei Jing University of Technology*, Vol. 39, No. 11, 2013, pp. 1700–1715.
15. Dan Zhang, Yu Zhang, and FeiShen,"Removal of cadmium and lead from heavy metals loaded PVA–SA immobilized Lentinusedodes", *J. Desalination and Water Treatment*, (ahead of print), 2013, pp. 1–10.
16. Qiao X, Liu Z, and Liu Z, "Immobilization of activated sludge in poly (ethylene glycol) by UV technology and its application in micro-polluted wastewater". *J. Biochemical Engineering Journal*, Vol. 50, No. 1, 2010, pp. 71–76.
17. Dong Y M, Zhang Z J, and Jin Y W, "Nitrification performance of nitrifying bacteria immobilized in waterborne Polyurethane at low ammonia nitrogen concentrations", *J. Journal of Environmental Sciences,* Vol. 23, No. 3, 2011, pp. 366–371. http://dx.doi.org/10.1016/S1001-0742(10)60418-4
18. Riham S, and Muftah H E., "Biological treatment of wastewater contaminated with p-cresol using Pseudomonas putida immobilized in polyvinyl alcohol (PVA) gel", *J. Journal of Water Process Engineering*, Vol. 1, 2014, pp. 84–90. http://dx.doi.org/10.1016/j.jwpe.2014.03.008
19. Magri A,Vanotti M B, and Szogi A A.,"Anammox sludge immobilized in polyvinyl alcohol (PVA) cryogel carriers", *J. Bioresour Technol,* Vol. 114, 2012, pp. 231–240. http://dx.doi.org/10.1016/j.biortech.2012.03.077
20. Zhou Y Z, Yang J, and Wang X L, "Bio-beads with immobilized anaerobic bacteria, zero-valent iron, and active carbon for the removal of trichloroethane from groundwater", *J. Environmental Science and Pollution Research*, 2014, pp. 1–10.
21. Zhong C. H., Liu P., and Zhang W. D., "PVA-immobilized beads modified by carrageenan and bentonite", *J. Chinese Journal of Environmental Engineering,* Vol. 7, No. 8, 2013, pp. 2837–2843.
22. Dong Y M, Zhang Z J, and Jin Y W, "Nitrification characteristics of nitrobacteria immobilized in waterborne Polyurethane in wastewater of corn-based ethanol fuel production", *J. Journal of Environmental Sciences,* Vol. 24, No. 6, 2012, pp. 999–1005. http://dx.doi.org/10.1016/S1001-0742(11)60893-0
23. Strous M, Gerven E V, and Zheng P, "Ammonium removal from concentrated waste streams with the anaerobic ammonium oxidation (anammox) process in different reactor configurations", *J. Water Research*, Vol. 31, No. 8, 1997, pp. 1955–1962. http://dx.doi.org/10.1016/S0043-1354(97)00055-9
24. Zhu G L, Hu Y Y, and Wang Q R., "Nitrogen removal performance of anaerobic ammonia oxidation co-culture immobilized in different gel carriers", *J. Water Sci Technol*, Vol. 59, No. 12, 2009, pp. 2379–2386. http://dx.doi.org/10.2166/wst.2009.293
25. Federation, W. E. 2005. Standard methods for the examination of water & wastewater. Washington, DC: American Public Health Association (APHA).
26. Tacx J, Schoffeleers H, and Brands A, "Dissolution behavior and solution properties of polyvinyl alcohol as determined by viscometry and light scattering in DMSO, ethylene glycol and water", *J. Polymer,* Vol. 41, No. 3, 2000, pp. 947–957. http://dx.doi.org/10.1016/S0032-3861(99)00220-7
27. Lee S, Lee S K, and Kim B., "Synthesis and Properties of Thermosensitive Poly (N-Isopropylacrylamide)/Waterborne Polyurethane Graded Concentration Hybrid Films", *J. Journal of Macromolecular Science, Part B,* Vol. 53, No. 2, 2014, pp. 254–264. http://dx.doi.org/10.1080/00222348.2013.832617

Advanced Treatment and Reuse of Papermaking Effluent by Membrane Separation

SEN WANG[1,2,*], ANLONG ZHANG[1] and SUFENG ZHANG[1]
[1]*Shaanxi University of Science & Technology, Xi'an, Shaanxi Province, 710021, China*
[2]*State Key Laboratory of Pulp and Paper Engineering, South China University of Technology, Guangzhou, Guangdong Province, 510640, China*

ABSTRACT: The paper focuses on identifying optimal conditions of fly ash and advanced treatment conditions for papermaking effluent, using Membrane Separation technology. Results show the pretreatment effect is the best when fly ash is 80 mg/L and the speed of mixing is 200 r/min for 1h. The operation pressure of ultrafiltration membrane process is 0.04 ~ 0.1 MPa. After fly ash adsorption and Membrane Separation advanced treatment, both COD_{Cr} and salinity in the effluent are below 10 mg/L, and Chroma is less than 15 times; SS and electrical conductivity are lower. The COD_{Cr} in the concentrated water is below 85 mg/L after the RO treatment and is in accordance with the new National Emission Standard for Papermaking Industry (GB3544-2008).

INTRODUCTION

WITH the rapid development of pulp and papermaking industry, how to treat papermaking effluent and its possible reuse has become an increasingly significant problem. Most small and medium-sized paper mills in China have utilized Level 1 precipitation with secondary biochemical disposal and other facilities to treat papermaking effluent. Although water quality of the reused water has been substantially improved in the past few years, the concentration of COD_{Cr} in the water is still relatively high. Reuse may accumulate different organic and inorganic substances, which leads to the problems of deposition in the system, e.g., electrochemical corrosion. To reduce or eliminate the corrosion and deposition of the devices and pipes caused by papermaking effluent and to further lower water consumption per unit of production, it is necessary to use advanced treatment technology for treating papermaking effluent, focusing on eliminating salt and lowering the molecular weight organics [1]. This study uses fly ash adsorption as pretreatment technology and adopts membrane separation technology to treat papermaking effluent after secondary biochemical process.

*Author to whom correspondence should be addressed.
Email: wangsenly@163.com; Phone: 86-029-86168575; Fax: 86-029-86168238

EXPERIMENT SETUP

Origin and Water Quality of Effluent

The effluent is obtained from the second pond of a papermaking mill in Shaanxi Province. This mill mainly uses waste paper and semi-chemical pulp of misc to produce corrugating and its annual production capacity is about 150,000 tons. The effluent still contains inorganic salt, organic matters with low molecular weight and other soluble solids after secondary biochemical disposition. Water quality parameters of the effluent are shown in Table 1.

Main Chemicals and Experimental Equipment

The main chemical is fly ash and the following equipment is used in the experiment: conductivity meter (DDS-307A), pH (pHS-3C), and COD (HACH DR2800).

Fly ash is obtained from self-contained plant of the papermaking mill. The main ingredients of the fly ash are illustrated in Table 2.

Process and Equipments of the Membrane

To dispose and reuse the papermaking effluent, removing inorganic salt and reducing molecular organics and other soluble solids is important. Although mem-

1544-8053/15/01 S055-06

doi:10.12783/issn.1544-8053/12/S1/8

Table 1. Parameters of the Effluent Value.

Project	pH	COD_{Cr}, mg/L	Chromaticity, time	SS, mg/L	Salinity, mg/L	Electrical Conductivity, S/cm
No.	7.57	321	193	225	2150	3.64

brane separation technology, especially reverse osmosis, is effective in removing inorganic salts and other solids, the untreated effluent cannot meet the requirements of the reverse osmosis. This may lead to membrane pollution. Therefore, reverse osmosis is usually not used alone and it is advisable to use pretreatment first before adopting membranes to dispose the effluent [2]. In this study, fly ash is used in pretreatment and microfiltration or ultra-filtration and reverse osmosis are used as the main processes [3], as shown in Figure 1.

After the disposition of fly ash, effluent flows to the sand filter and the infusion pump. It is then pumped to microfiltration of membrane components. The reject is retained in UF inside tank, while the condensed liquor is counter-flowed to the MF inside tank. The effluent in UF inside tank is pumped to UF membrane module. The reject is retained in RO inside tank after the disposition of UF, while the condensed liquor is counter-flowed to the UF inside tank. The effluent in RO inside tank is pumped to the reverse osmosis membrane components by the infusion pump and the pressure pump. The reverse osmosis condensed water flowing through the valve control can realize the full discharge or part of the return in order to improve the RO system recovery. RO water directly flows into the RO water production tank. The positive washing operation of MF or UF membrane is to use the infusion pump to pump the MF or UF water to membrane components. The negative operation is to use the reversed washing pump to pump the MF or UF water to be further treated [4].

Table 2. Chemical Components of the Fly Ash.

Components	Mass Fraction, %
SiO_2	51.88
Al_2O_3	37.35
Fe_2O_3	3.37
CaO	2.61
MgO	0.43
SO_3	0.71
Na_2O	0.31
K_2O	0.78
TiO_2	0.95
Run-off Quantity	1.86

Description of Membrane Modules

The parameters and the functions of three membrane modules are illustrated in Table 3.

Experiment and Investigated Means

In order to meet the requirements of the UF water, fly ash is used in Step 1 to dispose the second pond water in the laboratory. Step 2 is to apply membrane separation technology to pretreat the effluent of MF, UF and RO extended process. It aims to investigate main parameters according to the water and waste water monitoring methods [5]. The main investigated items are COD_{Cr}, SS, chromaticity, and salinity.

RESULTS AND DISCUSSION

Pretreatment Experiment Using Fly Ash

Due to the large specific surface area of fly ash and abundant active points of aluminum and silicon, fly ash is selected in a variety of processes including floccula-

Table 3. Parameters and Functions of Three Membrane Modules.

Membrane Modules	Parameters and Functions
MF	MF test uses membrane module 40*300mm MF-01 whose micro-membrane aperture 0.2 μm and the effective film covers an area of 0.1 m^2. The flux of pure water is 20~30 L/h polypropylene microfiltration membrane and can bear corrosion. The chemistry stability is good, but the price is lower.
UF	The form of UF membrane module is the hollow fiber structure Ø40*300mm PS-50, and its effective membrane area is 0.1 m^2, the nominal molecular weight intercepting value is 50,000. The throughput of pure water is 10~15 L/h at 25°C and 0.1 Mpa. The material is polysulfone which has good antioxidation and mechanical intensity, and the chemistry stability is good.
RO	RO uses the module Ø40*300mm, the effective membrane area is 0.1 m^2, and the desalination rate is more than 95%. The pure water throughput ranges from 12 to 15 L/h at 25°C and 0.6 MPa. The reverse osmosis membrane is made of aromatic polyamide, its range of pH is wide, and it can achieve a good treatment when the pH value is between 4 and 11.

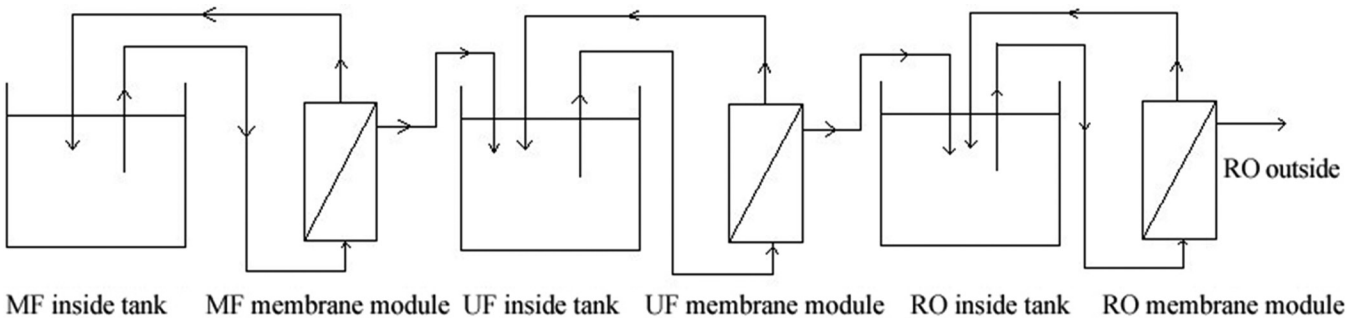

Figure 1. *Schematic diagram of the membrane.*

tion, filtration, natural cleaning and adsorption, etc. [6] However, different parameters, e.g., dosages, temperature, pH, agitated time and other conditions, all could influence the effect of the treatment. Among all the factors, dosage and the agitated time are the most important in the experiment [7].

Dosage Effects

Different dosages of fly ash are prepared in six 500 ml beakers for 200 ml of original effluent. Each is agitated at 200 r/min for 60 min at the normal temperature and the pH value is 7.57. After one hour, the supernatant fluid is analyzed. Results are shown in Figure 2.

According to Figure 2, the removal rate of chromaticity and COD_{Cr} increases as the dosage of the fly ash increases; similarly, the removal rate of SS increases with the increase of the amount of fly ash at first, and then slightly decreases. When the dosage of the fly ash gradually increased to 80 g/L, the removal effect of the effluent with suspended solids was the best. The removal rate of SS, COD_{Cr} and chromaticity is 86.2%, 62.1% and 90.5%, respectively. However, with further increased dosage of fly ash, the removal rate of COD_{Cr} and chromaticity increased, but decreased for SS. This is because fly ash has strong adsorption capacity for the flocculation of organic matter. Hence, pollutants in the papermaking effluent can deposit more easily, while the residue is so little that it cannot be removed by deposition. What's worse, when the dosage of the fly ash increased, the cost for effluent management and the yield of slurry could be increased [8].

Effects of Agitated Time

Six beakers of 250 mL including 20 g of fly ash and 100 mL of originated effluent are prepared, meanwhile agitating is at normal temperature and the agitated velocity is 200 r/min. From 15 to 90 min, in the interval of every 15 minutes, each beaker is kept still for 1h. Analytical results of the supernatant fluid are determined, as shown in Figure 3.

As shown in Figure 3, the mixing time is within 90 min. With the increased mixing time, fly ash adsorption gradually increased and so did the removal rates of COD_{Cr}, chromaticity and SS. The primary reason is that the differences of organic matter consistencies of fly ash between inlet and outlet are substantial at the beginning of adsorption; the adsorption power is intensive at the beginning and the velocity is rather high [9]. Along with the adsorption reaction, the concentra-

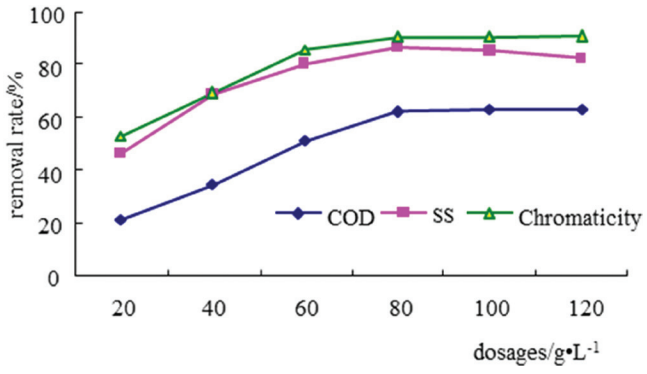

Figure 2. *Effects of fly ash dosages on removal rates.*

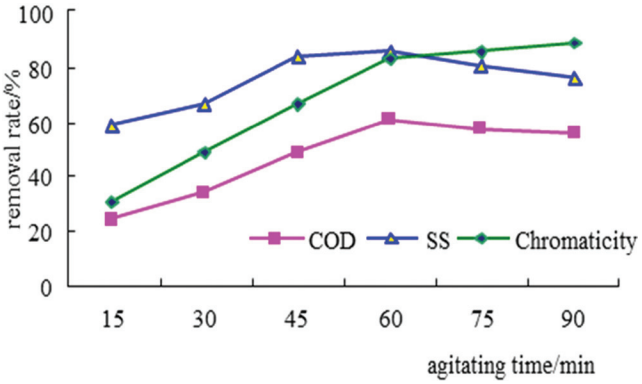

Figure 3. *Effects of agitating time on removal rates.*

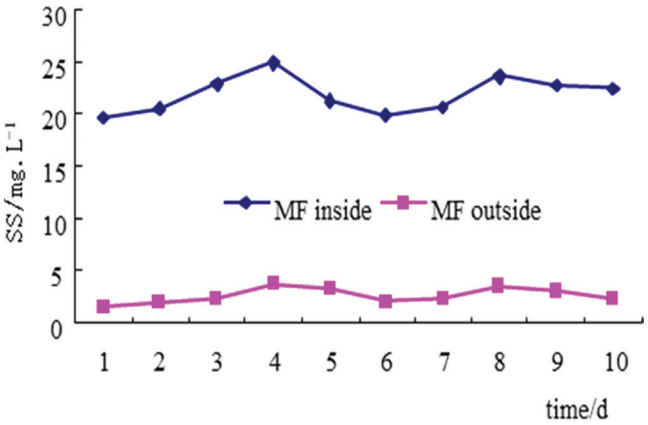

Figure 4. *Effects of micro fitter on treating SS.*

tion difference of the fly ash between the inside and the outside becomes smaller and thus the adsorption power is lower. When fly ash adsorption is no longer changed with the time, adsorption balance can be achieved [10]. When it is over 60 min, removal rates of COD_{Cr} and SS decrease slowly as the mixing duration increases. This is because different processes including adsorption, flocculation and filtration are involved. Longer agitated time is harmful to flocculation and precipitation and it can disperse the formed flocculation and have an effect on the managed effects [11].

Membrane Separation

MF Experiment

Micro-filter is used to deal with treated effluent which has been pretreated by fly ash and the results are shown in Figure 4 and Figure 5.

As shown in Figure 4, feed consistency of SS in MF is 16~29 mg/L and its reject consistency is 5 mg/L. The removal rates of SS in fly ash adsorption and flocculation reaction are 80.2%~85.7%, and the removal rate of MF for SS is 85.7%~94%. Thus it can be seen that micro-filter effect is better in the fly ash pretreatment compared with the suspended solids removal [12].

According to figure 5, COD_{Cr} consistency of MF feed effluent is 89.6~143.8 mg/L and the reject consistency is 70.8~108.5 mg/L. The average removal rate of MF for COD_{Cr} is 21.3%. The mechanism for COD_{Cr} removal is mainly physical entrapment and it is related to the feed water quality (including consistency, composition and so on). It is found in the literature [7] that most molecular weight of soluble COD_{Cr} is below 1,000 or higher than 100,000. The feed water of MF is the reject in the second pond, which is pretreated by fly ash. The feed COD_{Cr} in MF water is mainly empty, and its molecular weight is below 1,000 or higher than 10,000,000. However, the particle diameter of microfiltration membrane entrapment is between 0.05~10 μm. Additionally, the intercept nominal molecular weight is greater than 1-million-high polymer material. Hence, removing COD_{Cr} by MF is not the most effective method.

UF Experiment

Operation Pressure on the Influence of UF Throughput

Ultra-filtration is a type of pressure in the film, so water throughput is related to filtration pressure [13]. The impact of operating pressure on UF membrane throughput is shown in Figure 6.

As shown in Figure 6, the higher the operating pressure, the larger the throughput. When the operation pressure is up to 0.12 Mpa, the change of water throughput of the membrane is smaller. This is because

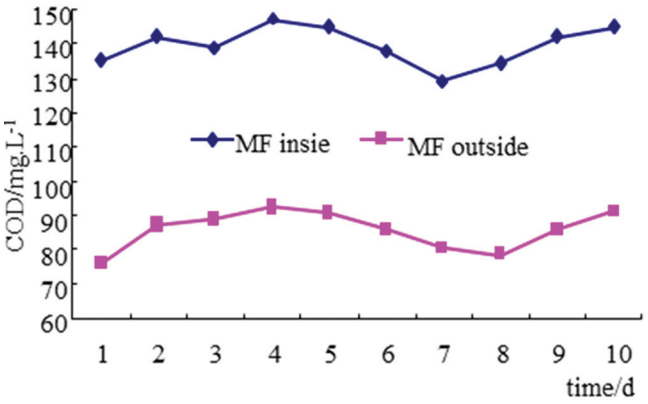

Figure 5. *Effects of MF on treating COD_{Cr}.*

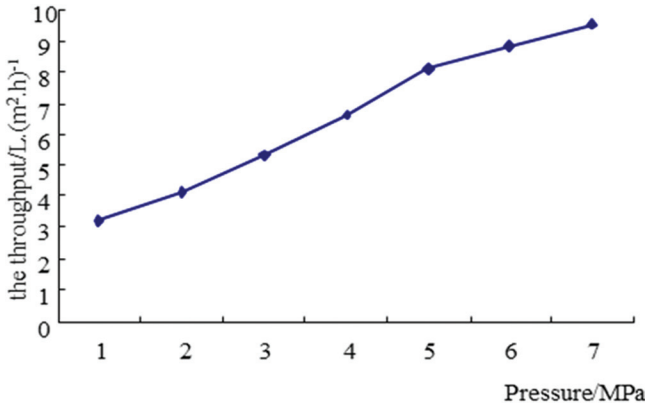

Figure 6. *Effects of pressure on treating results.*

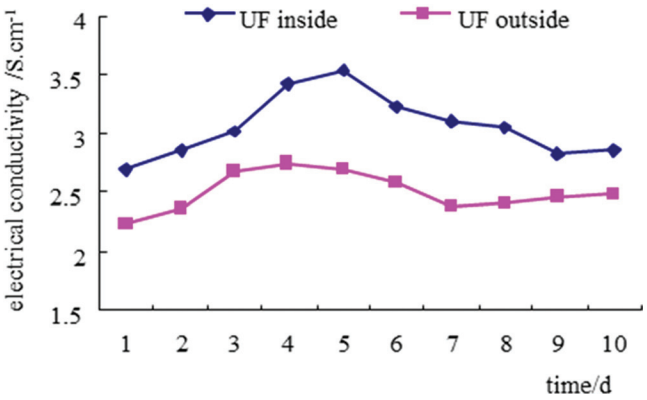

Figure 7. *Effects of UF on treating results.*

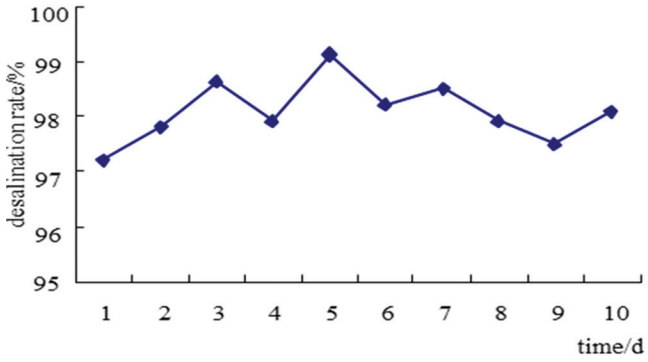

Figure 8. *RO desalination rate.*

at the beginning of the experiment, the concentration polarization phenomenon is not obvious. As the pressure increases, the permeable rate of the membrane is higher. When the pressure reaches a certain level, the consistency gradient of the membrane surface increases, and the permeable pressure is also improved, which in turn leads to the changes of concentration polarization. When the solute concentration of membrane surface is up to its saturation concentration, the gel layer is formulated on the surface of the membrane, which leads to the increase of the mass transfer resistance so that the membrane permeable rate decreases. In other words, the membrane throughput is lower [14]. Choosing a reasonable pressure can not only decrease the membrane pollutants but also produce a larger amount of matter to the throughput. Operation pressure of ultra-filtration membrane is within the range of 0.04 to 0.10.

Effects of UF Experiment

Because COD_{Cr} in UF outlet water is mainly with the form of empty soluble COD_{Cr} and suspended solids, which can hardly get through the ultra-filtration membrane. Most studies in the literature paid attention to the electrical conductivity [15]. The results of this study are shown in Figure 7.

From Figure 7, it can be seen that the electrical conductivity of UF rejects ranges from 2.36 to 3.13 ms/cm and removal rate is low. The solution conductivity is an indicator of the total ion in the solution. The higher the conductivity, the more the ions in solution. The ultra-filtration membrane mainly entraps the macromolecular organic matters, suspended substances, colloids, microorganisms and other materials. The solution of dissolved ions has no intercepting effect; hence the UF water conductivity is higher [16].

Reverse Osmosis Experiment

Salts in the effluent are mainly the soluble solids, although the quantity is relatively small, they can be accumulated after the circulation process. While the removal rate of MF and UF is low, solids can only be removed by RO [17]. The effect is illustrated in Figure 8.

As is shown in Figure 8, RO desalination rates are over 97%. This is because the pore size of the reverse osmosis membrane is less than 1 nm. It only allows solvent and water to pass through and intercept organic matters of small molecules and inorganic salts.

Processing Effects of Combination

Under the optimal processing condition, the effects

Table 4. Treating Results Under the Optimal Conditions.

Project	COD_{Cr}, mg/L	Chromaticity, time	SS, mg/L	Salinity, mg/L	Electrical Conductivity, S/cm
Untreated water	286~340	151~185	181~26	1500~2500	2.0~4.35
Fly ash pretreatment	114~136	21~32	25~37	—	—
RO outside	≤ 10	≤ 15	≤ 3	≤ 10	≤ 0.05
RO slopped water	60~85	18~25	22~31	—	—
Clean water	≤ 10	≤ 10	≤ 5	≤ 15	≤ 0.01

Notes: "—" stands for the unchecked item.

of combination process for second pond water treatment are shown in Table 4.

From Table 3, it can be seen that organic matter COD_{Cr}, inorganic SS and chromaticity, or salinity and conductivity in the water have been significantly reduced since the disposition of combination process. This is because the pore size of the reverse osmosis membrane is less than 1 nm, which allows solvent and water to pass through and intercept small-molecule organic matters and salt. The water quality of effluent can reach at least the same as water quality standard. COD_{Cr} in RO heavy consistency water is under 85 mg/L (or ≤ 100) which meets National Newly Emission Standard for paper industry (GB3544-2008).

CONCLUSIONS

Using fly ash to pre-treat the second pond reject, the optimum dosage of the fly ash is 80 g/L, agitating duration is 1h at the speed of 200 r/min. The removal rate of COD_{Cr}, chromaticity and SS are 62.1%, 90.5% and 86.2%, respectively. After the disposition of MF, UF and RO, the consistency of COD_{Cr} and salinity of fly ash pretreated water is less than 10 mg/L, chromaticity is less than 15 times and both SS and conductivity are very small. Water quality after disposition is similar to or better than the quality of pure water, which fully meets the quality standards of reused water. COD_{Cr} concentration after RO treatment in water is less than 85 mg/L, which also satisfies National Newly Emission Standard for paper industry.

By using fly ash membrane separation disposition, the treatment effect is good while the operation is simple and the processing cost is low. More importantly, fly ash adsorption, flocculation and filtration are integrated processes in this method.

ACKNOWLEDGMENTS

The authors are grateful for the financial support from Doctor's Scientific Foundation Research Funded Project of Shaanxi University of Science & Technology (Grant No: BJ14-09), Open Fund of State Key Laboratory of Pulp and Paper Engineering of South China University of Technology (Grant No: 201455).

REFERENCES

1. Y.-L. He, Waste paper pulping and papermaking waste water closed circulation and zero discharge, *China Pulp & Paper,* Vol. 31, No. 2, 2001, pp. 13-14.
2. N-song C., Soon-ouk B. and Chung-hak L., Effects of membrane fouling on solute rejection during membrane filtration of activated sludge, *Process Biochemistry*, Vol. 36, No. 9, 2001, pp. 855–860.
3. Lshiguro K. and Imai SS., Effects of biological treatment conditions on permeate flux of UF Membrane in a membrane/activated sludge wastewater treatment system, *Desalination*, Vol. 98, No. 3, 1994, pp. 119–126. http://dx.doi.org/10.1016/0011-9164(94)00136-7
4. Mariola R., Michal Bodzek Krystyna Konieezny, Schematic diagram of the laboratory Scalecross flow filtration system (with Pretreatment and/or final treatment) and liquid circulation. *Desalination*, Vol. 23, No. 9, 2009, pp. 100–110.
5. State environmental protection administration. 2002. The water and waste water monitoring method board of water and waste water monitoring method. The fourth edition and enlarged edition. Beijing, China environmental science press, Inc.
6. C.-B. Xia, X.-Z. He and D.-L. Li, Comparative sorption studies of toxic cresol on fly ash and impregnated fly ash, *Technol. Equip, Environ Pollute Control*, No. 2, 2000, pp. 82–86.
7. Sen A. K., Adsorption of mercury (II) by coal fly ash, *Water Research*, Vol. 21, No. 8, 1987, pp. 885–888. http://dx.doi.org/10.1016/S0043-1354(87)80003-9
8. C.-H. Huang and G.-L. Su, Fly ash base coagulant performance research, *Environmental Science*, Vol. 16, No. 2, 1995, pp.: 47.
9. Erol M., Kagak B., and Smerigboyu A E, Removal of Cu^{2+} and Pb^{2+} in aqueous solutions by fly ash, Energy. *Converse Manage*, Vol. 46, No. 8, 2005, pp. 1319–1331. http://dx.doi.org/10.1016/j.enconman.2004.06.033
10. Cetin S., and Pehlivan E., The use of fly ash as a low cost, environmentally friendly alternative to activated carbon for the removal of heavy metals from aqueous solutions, *Colloid Surface A*, Vol. 298, 2007, pp. 83–87. http://dx.doi.org/10.1016/j.colsurfa.2006.12.017
11. Shigemoto N., Hayashi H., Selective formation of Na-X zeolite from coal fly ash by fusion with sodium hydroxide prior to hydrothermal reaction, *Journal of Material Science*, Vol. 28, 1993, pp. 478l–4786. http://dx.doi.org/10.1007/BF00414272
12. Amokrane A., Landfill leachates pretreatment by coagulation, *Water Res*, Vol. 31, No. 11, 1997, pp. 2775.http://dx.doi.org/10.1016/S0043-1354(97)00147-4
13. Z., Wang. 2000. *The Basis of Membrane Separation Technology*. Beijing: Chemical Industry Press, Inc.
14. Philip J. E., Michael R. B., and Arto P., The influence of hydrophobicity roughness and charge upon ultrafiltration membranes for black tea liquor clarification, *Journal of Membrane Science,* Vol. 31, No. 3, 2008, 250–262.
15. Tansel B., Baoandl W.Y., and Tansel N., Characterization of fouling kinetics in ultrafiltration systems by resistance in series model, *Desalination*, Vol. 129, 2000, pp. 7–14.
16. Crozes G.F., J-G Jacangelo, Anselme C., and Laine J.M., Impact of ultrafiltration operating conditions on membrane irreversible fouling. *Journal of Membrane Science*, Vol. 124, 1997, pp. 63–76. http://dx.doi.org/10.1016/S0376-7388(96)00244-X
17. Takeshi S., and Yasuhiko L., Effects of activated sludge properties on water flux of ultrafiltration Membrane used for human excrement treatment, *Water Science and Technology*, Vol. 23, No. 7, 2009, pp. 1601–l608.

Thermodynamic Analysis of a Sludge Drying and Incinerating Process System

XIAOYING HU[1,2,*], LINGNAN WU[1,3] AND CHANGQING DONG[1]

[1]*National Engineering Laboratory for Biomass Power Generation Equipment, North China Electric Power University, Beijing, China*

[2]*Key Laboratory of Energy Thermal Conversion and Control of Ministry of Education, Nanjing, China*

[3]*School of Energy Power, and Mechanical Engineering, North China Electric Power University, Beijing, China*

ABSTRACT: This paper presents a study on a sludge disposing system using exergy analysis approach and energy utilization diagram methodology. The results showed that, among the main equipment of the system, the furnace has the largest irreversibility (about 49.46% of the total exergy input) and the heat recovery steam generator (or HRSG) has the lowest exergy efficiency (about 23.80%). Suggestions are accordingly provided on heat transfer enhancement and thorough mixing of fuels.

INTRODUCTION

THE output of dried sludge from sewage treatment plants is about 200,000 tons per year in China (about 3.8~5.5 million tons of wet sludge), which increases 10%~20% annually [1]. Proper utilization of sludge as a useful resource has attracted wide attention in the world. Incineration could achieve three Rs (Recycle, Reuse and Reduce) in sludge treatment and utilization. Incineration provides a nice method to reduce sludge's mass and volume, as well as to recover energy. However, the process needs to be highly controllable, and there remains significant opportunity for further improvement in order to make it a clean technology and compatible with sustainable development.

Li [2] and Huang [3] analyzed the development and application of incineration disposal of sludge. Economy, problems and measures of the disposal method were discussed based on the influencing factors of incineration disposal [4,5]. Sludge with a dried solid content of 20% to 35% is considered to be appropriate for co-incineration in coal power plants [6]. Experiments of co-firing of sludge and coal or polyethylene showed that, by adding assistant fuel and changing conditions of the incineration combustor, not only incineration of sludge was stabilized but also the pollutants in flue gas were reduced [7]. The sewage sludge was incinerated and its experiment showed that heavy metals in slag were stable due to their reactions with minerals in sewage sludge [8]. The characteristics of sludge incineration were analyzed through a fluidized bed incinerator platform and thermal gravity balance experiment [9,10]. The incineration experiment of dried sludge in fluidized bed incinerator indicated that the percentage of volatile heavy metals in flue gas was influenced by temperature, moisture content and sludge addition [11–16]. In this paper, the heat flow and exergy flow in sludge were analyzed respectively with the aim to improve the efficiency of sludge incineration.

DESCRIPTION OF THE SLUDGE DISPOSING PROCESS

As shown in Figure 1, the system consists of a flash dryer, a furnace, a heat recovery steam generator (HRSG) and an air heat exchanger. The material streams are divided into solid stream, flue gas stream, steam stream and air stream.

1. Solid stream: raw sludge was dried in flash dryer and the dried sludge was burned in furnace. Sludge was heated up through thermal convection and radiation.
2. Flue gas stream: the hot flue gas produced in furnace was cooled down by feed water in HRSG and by air stream in air exchange system.
3. Steam stream: feed water was heated up by flue gas.
4. Air stream: air was heated by flue gas in air heat exchanger.

Three hypotheses were made: (1) ambient temperature was 15°C; (2) the system worked for about 10

*Author to whom correspondence should be addressed.
E-mail: huxy@ncepu.edu.cn; Tel: +86-10-61772457; Fax: +86-10-61772031

1544-8053/15/01 S061-06

doi:10.12783/issn.1544-8053/12/S1/9

Table 1. Physical Parameters of Raw Sludge.

Element Analysis (%)							Initial Parameters		
C	H	S	N	O	*	Ash	Mass Flow (kg/s)	Moisture Content (%)	Low Level Heat Value (MJ/kg)
41	6	1	3	22.5	1.5	25	11.11	70	4.79

Note: * represented the metallic elements.

hours per day; (3) 400 tons of dried sludge could be disposed per day. Compositions of raw sludge and flue gas 1 are shown in Table 1 and Table 2, respectively. Parameters of material streams, such as temperature and mass flow rate, are shown in Table 3. Based on black box model, the heat flow and the exergy flow were analyzed.

ANALYSIS AND DISCUSSION

Thermal Efficiency Analysis

The heat value of sludge is expressed by:

$$Q_f = G * llhv \tag{1}$$

where Q_f is mass flow, t/h; *llhv* means lower heat value in MJ/kg.

The enthalpy of steam is calculated by:

$$H_w = G_w * h_w \tag{2}$$

The enthalpy of air and flue gas is calculated according to:

$$Q = G * C_p * t \tag{3}$$

where C_p is specific heat at constant pressure, t is temperature. The ratio of heat absorbed by cold streams to heat released by hot streams within thermal efficiency of dryer, HRSG and air heat exchanger is defined as:

$$\eta_t = \frac{\Delta Q_{cold}}{\Delta Q_{hot}} \tag{4}$$

The thermal efficiency of furnace is defined in the following equation.

$$\eta_f = \frac{Q_{useful}}{Q_{in}} \tag{5}$$

As Table 4 and Table 5 show, the efficiencies of dryer, furnace, HRSG and air heat exchanger in the system are all more than 70%. In comparison among them, the efficiency of furnace and flash dryer is higher than that of the other equipment, with the values of 87.61% and 86.17% respectively.

Analysis with Exergy Approach

The following assumptions were made:

1. All gases involved were treated as ideal gas in the parameter range of equipments.
2. While the energy losses of equipment were considered, their heat losses were neglected.

The exergy of sludge is expressed as the following:

$$E_f = H^o_{L,f} = llhv * G \tag{6}$$

The exergy of steam is calculated by:

$$E(T,P) = G * ((H - H_0) - T_0(S - S_0)) \tag{7}$$

The exergy of material with respect to ambient temperature is expressed as:

$$E = G * C_p * \left((T - T_0) - T_0 \ln \frac{T}{T_0} \right) \tag{8}$$

Efficiency of flash dryer, HRSG and air heat exchanger is calculated by:

$$\eta_t = \frac{\Delta E_{cold}}{\Delta E_{hot}} \tag{9}$$

where ΔE_{cold} is the exergy change of cold streams and ΔE_{hot} is the exergy change of hot streams.

Table 2. Components of Flue Gas 1.

Components	N_2	O_2	CO_2	H_2O	H_2S
Molar mass	28	32	44	18	34
Mass Fraction (%)	67.1	7.7	12.9	12.1	0.2

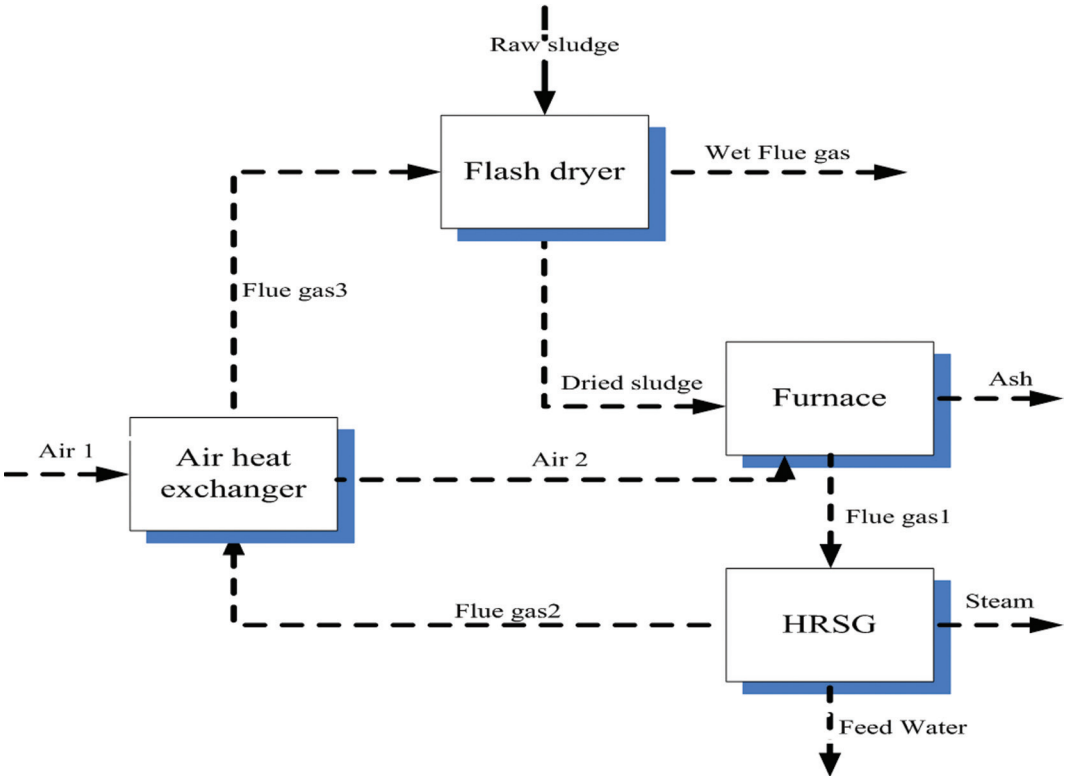

Figure 1. *The sludge drying and incineration system.*

The exergy efficiency of furnace is expressed by:

$$\eta_f = \frac{E_{fluegas} - E_{air}}{E_{sludge}} \tag{10}$$

where $E_{fluegas}$, E_{air} and E_{sludge} denote the exergy of flue gas, air and sludge in furnace, respectively.

The results calculated by Equation (6) to Equation (10) are shown in Table 6 and Figure 2. As shown in Figure 2, the system efficiency is improved by recycling of flue gas exergy in flash dryer and air-to-air heat exchanger.

Exergy Analysis with Energy Utilization Diagram

The energy utilization diagram method has been comprehensively applied to graphically present the thermodynamic properties of different chemical processes or thermal processes used the A (energy level) – ΔH (energy transformation quantity) diagrams. The horizontal axis ΔH represents the quantity of transformed energy in relation to the first thermodynamics law, while the vertical axis A denotes the energy level of processes relevant to energy transformation, which is related to the second thermodynamics law [17–19].

Exergy change ΔE is defined as the following equation.

$$\Delta E = \Delta H - T_0 \Delta S \tag{11}$$

While, energy level A is

$$A = \frac{\Delta E}{\Delta H} = \frac{\Delta H - T_0 \Delta S}{\Delta H} = 1 - T_0 \frac{\Delta S}{\Delta H} \tag{12}$$

As far as a system is concerned, the device releasing energy is called energy donor and is expressed as 'ed'; while the one receiving energy is called energy accep-

Table 3. Temperature and Mass Flow of Material Streams in the Process.

	Material Streams									
Parameters	**Raw Sludge**	**Dried Sludge**	**Flue Gas 1**	**Flue Gas 2**	**Flue Gas 3**	**Wet Flue Gas**	**Air 1**	**Air 2**	**Ash**	**Steam**
Temperature (°C)	15	95	1628	1355	1340	200	15	300	1400	527
Mass Flow Rate (t/h)	39.996	15.012	105.048	105.048	105.048	130.068	91.728	91.728	2.988	9.52

Table 4. Rate of Heat Flow of Material Streams in the System.

	Material Streams									
	Raw Sludge	**Dried Sludge**	**Flue Gas 1**	**Flue Gas 2**	**Flue Gas 3**	**Wet Flue Gas**	**Air 1**	**Air 2**	**Ash**	**Steam**
Rate of Heat Flow (MW)	53.8	70.99	69.36	56.54	45.75	25.80	0.38	8.18	0.86	9.35

tor and is expressed as 'ea'. Since the energy change of the acceptor $\Delta H_{ea} > 0$, this leads to $A_{ed} \geq A_{ea}$. When ΔH_{ea} is limited, the exergy loss of system is given by the following:

$$EXL = -\sum_i \Delta E_i = \int_0^{H_{ea}} (A_{ed} - A_{ea}) dH_{ea} \qquad (13)$$

Thus, a plot depicted by energy donor (A_{ea}) and energy acceptor (A_{ea}) against the transformed energy (ΔH_{ea}) is given. As a result, the area between the energy donor (A_{ed}) curve and the energy acceptor (A_{ea}) curve indicates the exergy losses of the corresponding process in the system.

As Figure 3 shows, the energy utilization diagram is divided into four parts (a)-(d), which represent the dryer (a), furnace (b), HRSG (c) and air heat exchanger (d) of the system. In the dryer, energy transformation is shown by the curves of A_{ed} and A_{ea}. When the temperature of flue gas 3 was changed from 1613K (A = 0.8215) to 473K (A = 0.391), raw sludge was dried to a temperature of 368K. The required energy ΔH was 17.11MW. The plot area ΔE between A_{ed} and A_{ea} shows exergy losses of drying process. In the furnace, dried sludge was incinerated to flue gas and its temperature was increased to 1901K, which was presented by curve $A_{ea,\ sludge}$. The temperature change of air was depicted by curve $A_{ea,air}$. In HRSG, heat of flue gas 1 was released and its temperature was decreased from 1901K (A = 8485) to 1628K (A = 0.823). On the other side, the heat acceptor feed water has been heated, vaporized and then superheated. As to air heat exchanger, air was heated by flue gas and its temperature was increased from 288K to 573K. The diagram shows that the furnace has the largest exergy loss in the system.

Discussion

As shown in Figure 2 and Figure 3, the result of traditional exergy analysis and calculation was in agreement with EUD analysis. The furnace has the largest exergy loss, followed by the flash dryer, HRSG and air heat exchanger.

The distribution of exergy loss fractions is pre-

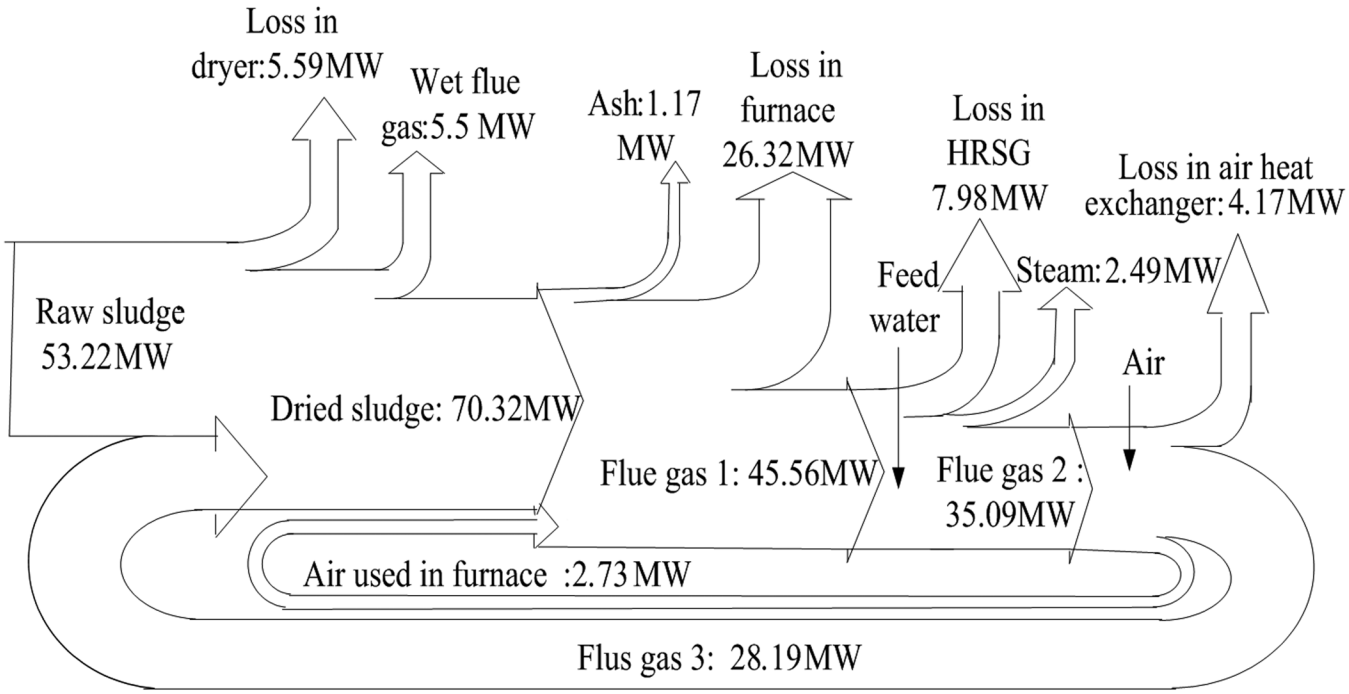

Figure 2. *The exergy flow diagram of sludge drying and incineration process.*

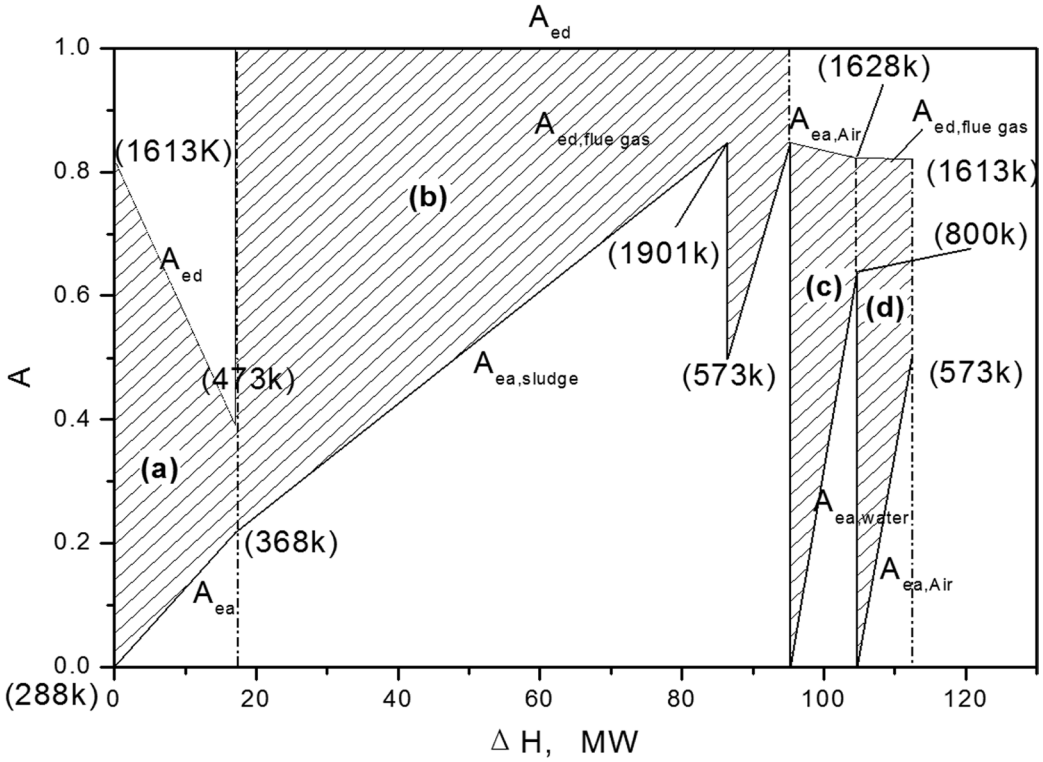

Figure 3. *Energy utilization diagrams of the four components of the system: (a) Flash dryer; (b) Furnace; (c) HRSG; (d) Air heat exchanger.*

sented in Figure 4. Although the highest thermal efficiency (87.61%) was achieved in the furnace, it was also responsible for the largest percentage of exergy loss (49.46%). The percentages of exergy loss in the HRSG, flash dryer and air heat exchanger were 14.99%, 10.50% and 7.84% respectively.

In the furnace, exergy losses were caused by irreversible processes of chemical reaction and heat transfer. The irreversible loss of chemical reaction in the furnace was inevitable. Thus, it was suggested to improve the heat transfer ability and mixing of fuels in order to reduce the exergy loss.

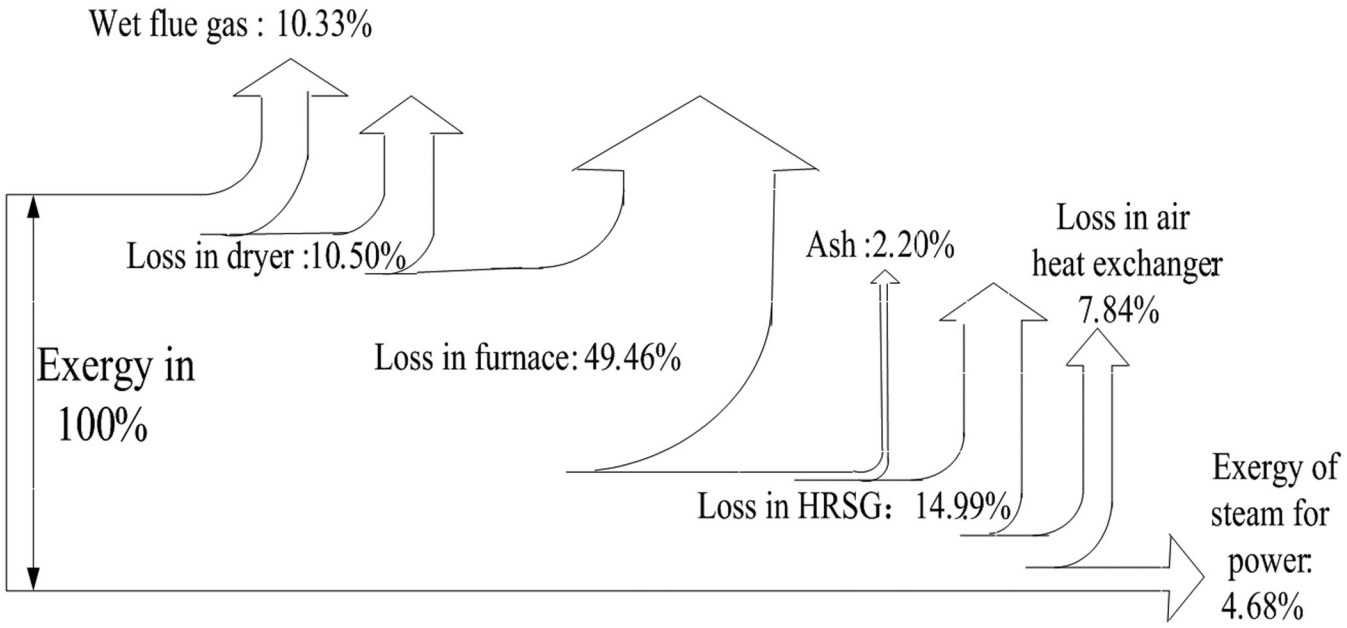

Figure 4. *The distribution of exergy loss fractions in the system.*

Table 5. Heat Loss and Thermal Efficiency of Equipment.

Equipment	Input (MW)	Output (MW)	Loss of Heat Flow Rate (MW)	Thermal Efficiency (%)
Dryer	99.55	96.79	2.76	86.17
Furnace	79.17	71.22	7.95	87.61
HRSG	69.36	65.89	3.47	72.93
Air heat exchanger	56.92	53.93	2.99	72.29

Thermal efficiency and exergy efficiency of components were shown in Table 5, in which it can be noted that the air heater and HRSG had an exergy efficiency of about 30%. Therefore, it is an effective way to improve exergy efficiency of heat exchanger by reducing the average temperature difference of the heat exchanger.

CONCLUSIONS

Thermal analysis, exergy analysis and energy utilization diagram methodology was performed for analyzing the sewage incineration system. The exergy loss of the furnace was about 49.46% of the total energy input. The exergy efficiency of HRSG was about 23.80%, which was the lowest one. As the irreversible loss of chemical reaction in the furnace was inevitable, improvements in heat transfer ability and thorough mixing of fuels and air were suggested. The exergy loss of the furnace could be reduced by some techniques such as a circulating fluidized bed, which helps to improve heat transfer and mixing. For the heat exchanger, a suitable temperature difference should be attained to improve the exergy efficiency.

ACKNOWLEDGEMENT

The authors are grateful for the support of the National Natural Science Foundation of China (51206046), the Major State Basic Research Development Program of China (973 Program)(2015CB251501), the Ph.D. Programs Foundation of Ministry of Education of China (20120036120007), the Open Research Fund Projects of Key Laboratory of Energy Thermal Conversion and Control of Ministry of Education.

REFERENCES

1. Http: //www.chinaep.net/feishui_shili/feishui_shili-097.htm.
2. Li, Y., "Progress of the Technology of Fluidized Bed Incineration in the Sewage Sludge Treatment", *Energ. Conserv. Environ. Prot.*, No.2, 2004, pp. 24–26.
3. Huang, L., H. Du, C. Lu, G. Huang., "Application and Development of Sludge Drying and Incineration in Europe", *Water Wastewater Eng.*, No. 29, 2003, pp. 19–22.
4. Zhang, N., Q. Zhou, X. Rui, "Burning technology of mud", *Energ. Res. Util.*, No. 1, 2003, pp. 35–37.
5. Li, J., Z. Wang, N. Zhang, X. Yang, W. Song, Chen G., "The Study on the Wastewater Sludge Incineration Technology", *Environ. Eng.*, No. 23, 2005, pp. 48–53.
6. Stefan, J. Technical Options for Sewage Sludge Disposal. The Sewage Sludge Disposal Workshop between China and Germany. Beijing, June 28, 2007.
7. Jiao, W., Y. Na, M. Zheng, Q. Lv., "Experimental study on pollutant emissions of sewage sludge incineration", *Tech. Eq. Environ. Pollut. Control.*, No. 7, 2006, pp. 74–77.
8. Han, J., M. Xu, H. Yao, Y. Xia., "Experiment on sewage sludge incineration in melting furnace", *J. Huazhong Univ. Sci. and Tech. (Nature Science Edition)*, No. 34, 2006, pp. 108–110.
9. Qiu, J., J. Cheng., "The characteristics of sewage sludge during incineration process and its chemical kinetics analysis", *J. Huazhong Univ. Sci. and Tech. (Nature Science Edition)*., No. 33, 2005, pp. 25–33.
10. Khiari, B., F. Marias, F. Zagrouba, J. Vaxelaire., "Use of a transient model to simulate fluidized bed incineration of sewage sludge", *J. Hazard. Mater. B.*, Vol. 135, No. 1–3, 2006, pp. 200–209. http://dx.doi.org/10.1016/j.jhazmat.2005.11.068
11. Liu, Y., "Study on the Combustion Characteristics and Heavy Metal Emission Characteristics of Municipal Sewage Sludge in Fluidized Bed", Zhejiang University, Master Degree Thesis. 2004.
12. Li, A., Y. Qu, W. Yao, Z. Wang, Y. Wei., "An Experimental Study on Remains Property of Heavy Metals in the Bottom Ash", *Tech. Eq. for Environ. Pollut. Control.*, No. 3, 2002, pp. 20–24.
13. Zhang, Y., Y. Chi, J. Li, X. Li, J. Yan, K. Cen., "An Experiment Study on Distribution of Heavy Metals in the Incineration of Sludge", *Power Syst. Eng.* No. 21, 2005, pp. 27–29.
14. Han, J., M. Xu, H. Yao, Y. Xia., "Study of partition of heavy and alkali metals during sewage sludge incineration", *J. Huazhong Univ. Sci. and Tech. (Nature Science Edition)*. No. 34, 2006, pp. 106–108.
15. Oliver, M., W. Joachim. "Modeling the adsorption of mercury in the flue gas of sewage sludge incineration", *Chem. Eng. J.*, Vol. 96, No. 1–3 2003, pp. 197–205. http://dx.doi.org/10.1016/j.cej.2003.08.018
16. Hidekichi Y., U. Kohei., "Mutagenic activities of exhaust gas and ash from sludge incineration plants", *Sci. Total Environ.*, Vol. 215, No. 1-2, 1998, pp. 41–49. http://dx.doi.org/10.1016/S0048-9697(98)00120-X
17. Masaru I., J. Jun., "Graphical Exergy Study on Single Stage Absorption Heat Transformer," *Appl. Therm. Eng.*, Vol.19, No.11, 1999, pp. 1191–1206. http://dx.doi.org/10.1016/S1359-4311(98)00117-3
18. Jin, H., H. Zhao, Z. Liu, R. Cai. "A novel EFHAT system and exergy analysis with energy utilization diagram", *Energy*, Vol. 29, No. 12–15, 2004, pp. 1983–1991. http://dx.doi.org/10.1016/j.energy.2004.03.009
19. Gao, L., H. Jin, Z. Liu, D. Zheng. "Exergy analysis of coal-based polygeneration system for power and chemical production", *Energy,* Vol. 29, No. 12–15, 2004, pp. 2359–2371. http://dx.doi.org/10.1016/j.energy.2004.03.046

Effect of Long Sludge Retention Time on Biological Phosphorus Removal in A2/O Process

WANG CHANGWEN[1], LI JUN[1,*], ZHAO BAIHANG[1], YUE YAODONG[1] and WANG YONGLEI[1,2]
[1]*Key Laboratory of Beijing for Water Quality Science and Water Environment Recovery Engineering, Beijing University of Technology, Beijing 100124, China;*
[2]*College of Municipal and Environmental Engineering, Shandong Jianzhu University, Jinan 250101, China*

ABSTRACT: Sludge retention time is an important parameter to the biological phosphorus removal system. This paper investigated the effect of long sludge retention time on biological phosphorus removal in Anaerobic/Anoxic/Aerobic process (A2/O). The results showed that prolonging sludge retention time (SRT) of the A^2/O system had no significant impact on biological phosphorus removal efficiency, which slightly decreased from 92.9% (at an SRT of 12 d) to 92.1% (at an SRT of 30 d). Scanning Electron Microscope-Energy Dispersive Spectrometer (SEM-EDS) analysis demonstrated the relative content of phosphorus in dry activated sludge increased from 2.27% to 4.36%, which explained the excellent phosphorus removal performance at long SRT. At the same time, the average particle size increased from 201.57 μm to 256.99 μm, and the flocs at longer SRT had a more spherical and compact structure relative to that at shorter SRT. Our results demonstrated that long SRT was a sustainable way for biological phosphorus removal in A^2/O process.

INTRODUCTION

MANY efforts have been made recently to enhance biological phosphorus removal, including developing new processes, improving current processes and advancing the phosphorus microbiology (van Loosdrecht *et al.*, 1998; Lu *et al.*, 2006; Wang *et al.*, 2009; Whang *et al.*, 2006). However, most wastewater treatment plants were built many years ago, and it is very expensive for them to develop new processes or advance the phosphorus microbiology. Consequently, it makes more practical sense to enhance biological phosphorus removal to improve current processes and optimize the operations.

Various wastewater treatment processes have been applied to reduce the amount of the discharged nutrients. In the past few years, A2/O process has been widely used to achieve simultaneous biological removal of nitrogen and phosphorus (Ma *et al.*, 2009; Zeng *et al.*, 2010; Ge *et al.*, 2010), but few investigations about the long sludge retention time in the process have been conducted.

Sludge retention time (SRT) is one of the most important control parameters in advanced biological nutrient removal (BNR). However, the relationship between SRT and phosphorus removal still has great controversies. The United States Environmental Protection Agency (EPA, 1987) claimed that when SRT increased, phosphorus removal efficiency dropped because of the decrement of biomass yield rate. In contrast, Wentzel *et al.* (1991) reported that phosphate accumulating organisms (PAOs) were predominant in the long SRT system, which could retain more phosphorus than normal bacteria due to its relatively lower decay rate than that of other microorganisms. Randall *et al.* (1992) found that the phosphorus content in biomass increased with increasing SRT but phosphorus removal efficiency showed almost no change.

In this paper, the effect of long sludge retention time on biological phosphorus removal in A2/O process was investigated based on theoretical analysis. Through our work, it is expected to provide a recommendation about long SRT in A2/O process for the upgradings and operation optimizations of the current wastewater treatment plants.

MATERIALS AND METHODS

Wastewater and seed sludge

This study was carried out in the laboratory of Bei-

*Author to whom correspondence should be addressed.
E-mail: jglijun@bjut.edu.cn

1544-8053/15/01 S067-07

doi:10.12783/issn.1544-8053/12/S1/10

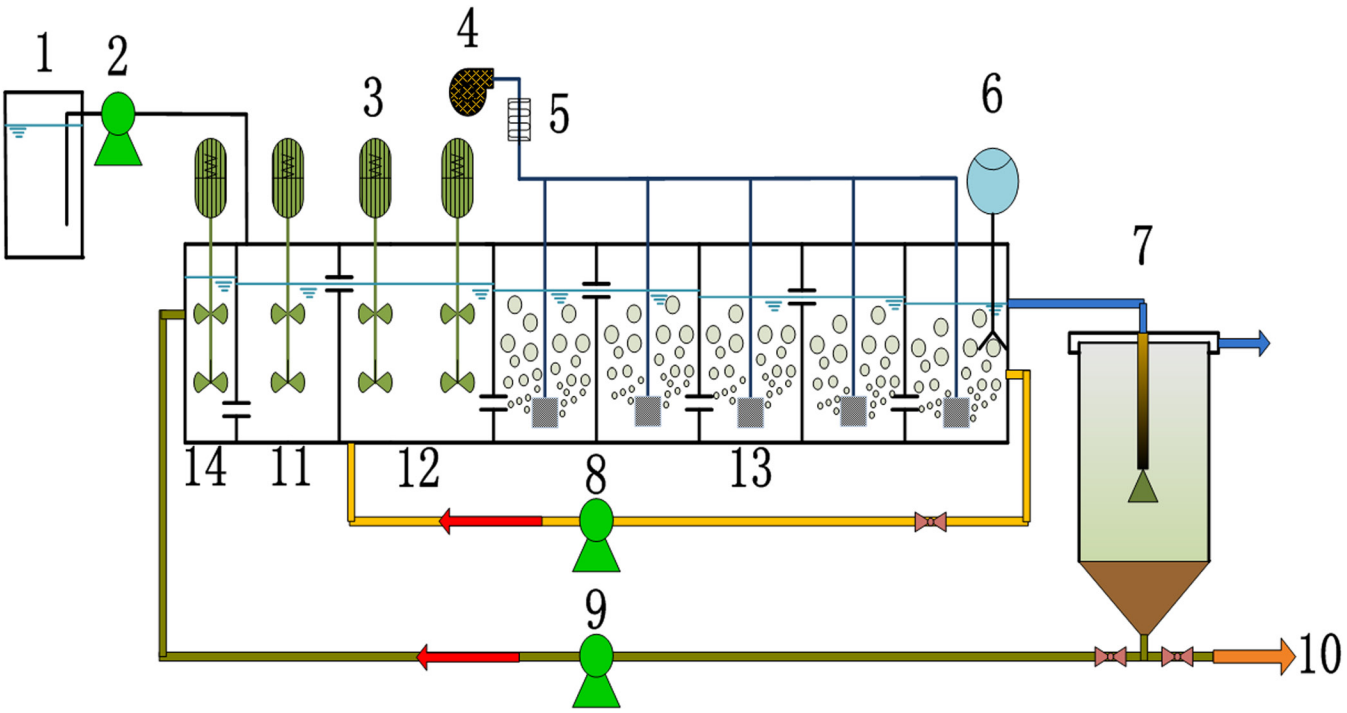

Figure 1. *Schematic diagram of the A^2/O reactor. 1: feed tank; 2: influent pump; 3: stirrer; 4: air pump; 5: gas flowmeter; 6: DO probe; 7: settler; 8: internal recycle pump; 9: sludge return pump; 10: waste sludge; 11: anaerobic zone; 12: anoxic zone; 13: aerobic zone; 14: pre-anoxic zone.*

jing University of Technology in Beijing, China and lasted from July to August. Moreover, the pilot reactor was located in an experiment room, so that the wastewater temperature could be kept at 20~25°C.

The wastewater used in this study was collected from the sewers of campus residential area and its characteristics are summarized in Table 1. Apparently, the wastewater was of typically low COD level, which would severely influence the simultaneous nitrogen and phosphorus removal in A2/O process. Seed sludge was collected from Gaobeidian full-scale WWTP (1,000,000 m^3/d) with A2/O process in Beijing, where biological phosphorus removal with auxiliary chemical phosphorus removal was employed.

Reactor and Operation

Figure 1 shows the schematic diagram of the used A2/O reactor in this study. The reactor, made from acrylics, consisted of pre-anoxic zone, anaerobic zone, anoxic zone and aerobic zone (the volume ratio was 1:2.5:5.5:12). The hydraulic retention time was 15h and the external return flow ratio was 0.62. The return sludge was pumped into the pre-anoxic zone first and then flowed into the anaerobic zone with the influent wastewater. Fine air bubbles were diffused through sand disc into the aerobic zone and the average dissolved oxygen was kept at 2.0 mg/L and MLSS was kept at 5000 mg/L. The internal return flow ratio was 2.14. SRT was set at 12d from day 0 to day 18 and then prolonged to 30d from day 19 to day 63.

Analytical Methods

All samples were analyzed after filtration with 0.45 μm membrane. Chemical Oxygen Demand (COD), Ammonia Nitrogen (NH_4^+-N), Total Phosphorus (TP), Sludge Volume Index (SVI), Mixed Liquid Suspended Solids (MLSS) and volatile MLSS (MLVSS) were measured according to Standard Methods (APHA, 1999). Microscopic examination was performed using an Olympus-BX41 (Olympus, Japan). A laser particle size analysis system (Malvern Mastersizer 2000, Malvern, UK) was used to measure the particle size of activated sludge.

SEM-energy dispersive X-ray (EDX) analysis was

Table 1. The Characteristics of Feeding Wastewater.

COD (mg/L)	NH_4^+-N (mg/L)	TN (mg/L)	TP (mg/L)	pH	Temperature (°C)
221.80 ± 23.83	77.17 ± 5.72	93.35 ± 6.82	5.52 ± 0.73	7.0~7.8	20~25

carried out by virtue of a Hitachi S-4700 field emission scanning electron microscope equipped with an EDX detector to observe the spatial distribution of selected elements within a granule. C, N, O, Na, Mg, Al, Si, P, S, K and Ca were selected for content determination, and every element was quantified by the weight percentage of the total 11 elements.

Mathematical Analysis

Figure 2 illustrates the phosphorus mass balance in A^2/O process. Compared with nitrogen, phosphorus mainly presents in water and activated sludge. The influent phosphorus firstly transfers from wastewater phase to sludge phase and then is discharged from the system as waste sludge to achieve the phosphorus removal (Tchobanoglous *et al.*, 2002). According to the phosphorus mass balance (Ge *et al.*, 2010), the influent phosphorus is equal to the effluent phosphorus plus the phosphorus in waste sludge [Equation (1)] (Nowak, 1999). The effluent phosphorus and the phosphorus in waste sludge can be calculated respectively using Equations (2) and (3) (Ge *et al.*, 2010), and the discharged sludge flow q can be expressed by Equation (4) (USEPA, 1987). Thus, the phosphorus removal efficiency η can be calculated using Equatiom (5). For a given system, the phosphorus removal efficiency η can be determined by θ_c and f_p.

$$TP_{inf} = TP_{eff} + TP_w \quad (1)$$

$$TP_{inf} = QS_{inf} \quad (2)$$

$$TP_w = qX_w f_p \quad (3)$$

$$Pq = \frac{VX}{\theta_c} \quad (4)$$

$$\eta = \frac{TP_{inf} - TP_{eff}}{TP_{inf}} = \frac{VXX_w f_p}{, _c QS_{inf}} \times 100\% \quad (5)$$

where,

η = the phosphorus removal efficiency, %
TP_{inf} = the influent phosphorus, g/d
TP_{eff} = the effluent phosphorus, g/d
TP_w = the phosphorus in waste sludge, g/d
Q = the influent flow, L/d
q = the waste sludge flow, L/d

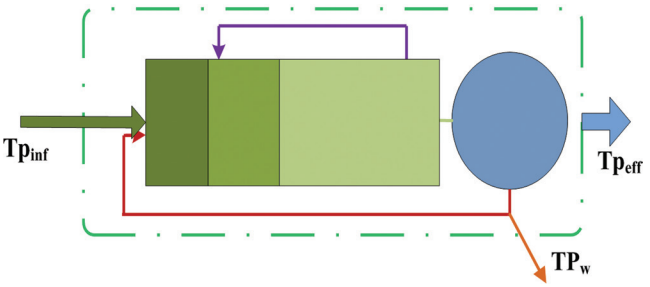

Figure 2. *Phosphorus mass balance of the A^2/O system.*

V = the reactor volume, L
X = the mixed liquor suspended solids, g/L
X_w = the discharged sludge mixed liquor suspended solids, g/L
θ_c = The sludge retention time (SRT), d
f_p = the phosphorus proportion of the waste sludge dry weight, g phosphate/g dry waste sludge, %
S_{inf} = the influent phosphorus concentration, g/L

RESULTS AND DISCUSSION

Effect of SRT on Biological Phosphorus Removal

As shown in Figure 3, when SRT was changed from 12 d to 30 d, MLSS of the system increased from 3000 mg/L to 5000 mg/L. In contrast, the extension of SRT had no significant effect on phosphorus removal. As can be seen, when SRT was 12 d, the effluent phosphorus was 0.42 mg/L on average and the removal efficiency was 92.9%; when SRT was 30 d, the effluent phosphorus and removal efficiency was 0.47 mg/L and 92.1%, respectively. According to Equation (5), the phosphorus removal efficiency η of a given system is determined by SRT and f_p. For the phosphorus removal process with a longer SRT, its removal efficiency almost had no change, which implied that f_p increased simultaneously.

Variations of Sludge Characteristics with SRT Prolonging

MLSS, MLVSS and SVI

Figure 4 shows the variations of sludge characteristics at two SRT stages. At SRT of 12 d, MLSS was about 2500 mg/L, and MLVSS/MLSS was 0.79 on average. Besides, its SVI was 72 on average, indicating the activated sludge had a good settleability. When SRT was prolonged to 30 d, MLSS increased gradually at the initial days and reached about 5000 mg/L

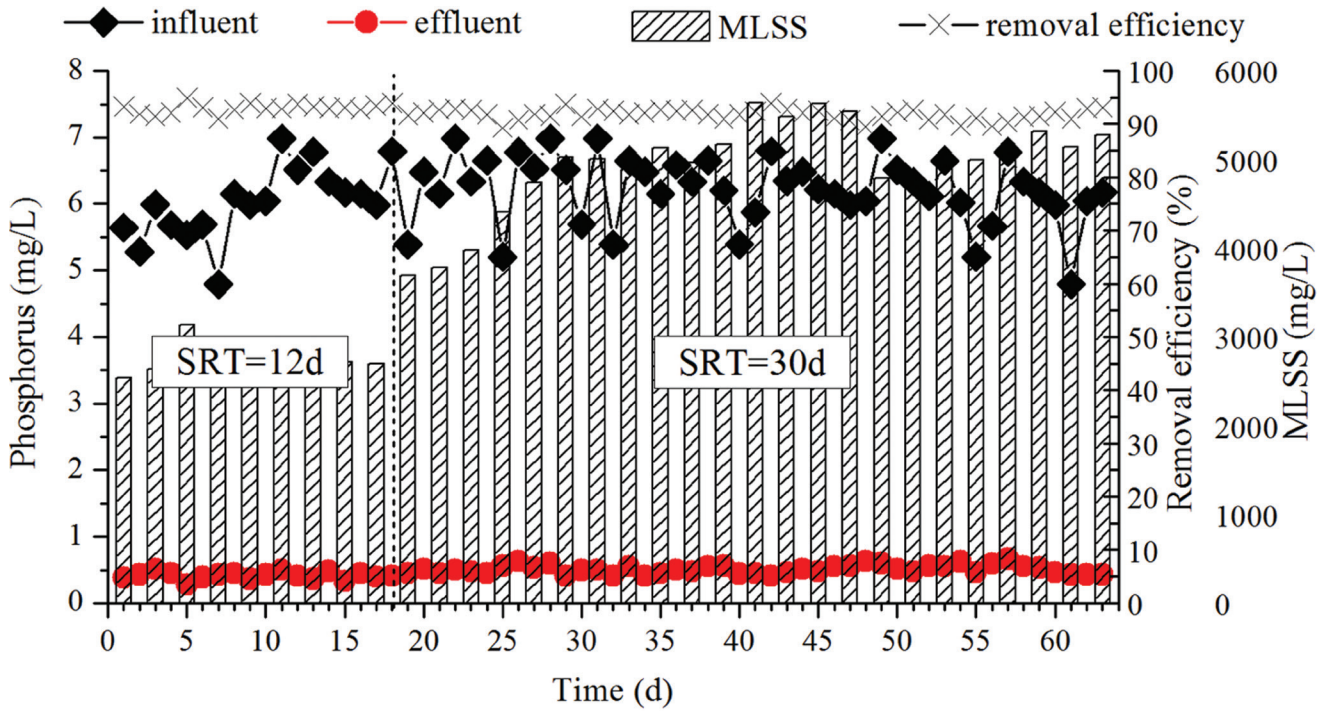

Figure 3. *Phosphorus removal and MLSS variations at SRT of 12 d and 30 d.*

at the steady state. At the same time, MLVSS/MLSS decreased from 0.79 to 0.73 due to the accumulation of inorganic substances in activated sludge at long SRT. Accordingly, SVI also dropped to 65 on average. In this experiment, the settleability of activated sludge was not deteriorated but improved. Obviously, long SRT can reduce the amount of waste sludge; namely, the sludge treatment cost can be cut down.

The Relative Content of Phosphorus in Dry Activated Sludge

According to the wavelength and intensity of characteristic X-rays emitted by various elements, SEM-EDX can determine the existent elements in tested samples. In recent years, SEM-EDX has been applied to investigate the roles of various elements in activated

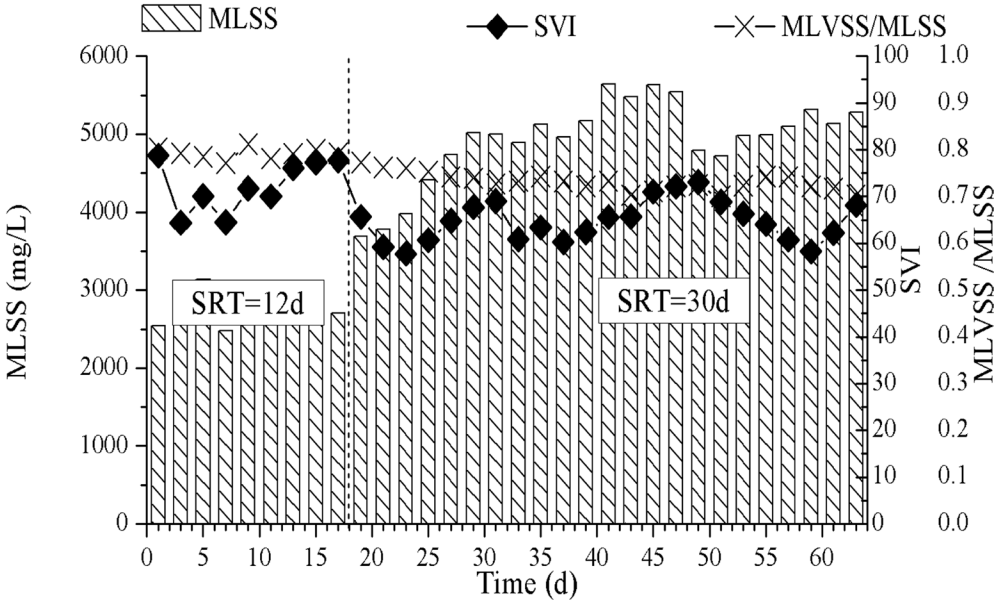

Element	SRT = 12d Wt %	SRT = 30d Wt %
C K	31.69	25.94
N K	20.27	16.84
O K	41.00	46.57
Na K	00.38	00.20
Mg K	00.81	02.15
Al K	00.22	00.12
Si K	00.41	00.43
P K	02.27	04.36
S K	01.19	00.91
K K	00.27	00.93
Ca K	01.48	01.56

Figure 4. *Variations of sludge characteristics at SRT of 12 d and 30d.*

sludge flocs settleability (Liu *et al.*, 2005). In this study, it was used to detect the relative content of phosphorus in dry activated sludge so as to determine f_p. Figure 4 shows the results of SEM-energy dispersive X-ray (EDX) analysis. As can be seen, the relative content of phosphorus in dry activated sludge increased from 2.27% to 4.36% when SRT was prolonged from 12d to 30d. Although the amount of waste sludge was reduced because of the extension of SRT, the amount of phosphorus discharged from the system was not reduced significantly. As a result, the phosphorus removal efficiency was not deteriorated obviously.

In analysis of mass balance in A2/O process, the total phosphate content in dry waste sludge ratio was generally assumed as 3% (Randall, *et al.*, 1997; Ge *et al.*, 2010). Moreover, the ratio was usually considered as a constant when the operation parameters were changed. However, based on the results in this study, the above assumptions did not meet the actual situation. For a more accurate mass balance analysis, the total phosphate content in dry waste sludge should be measured.

Particle Size Distribution and Sludge Morphology

Figure 6 shows the particle size distribution at SRT of 12 d and 30 d respectively. Sludge operating at long SRT (30 d) tended to have a larger particle size, and the average particle size increased from 201.57

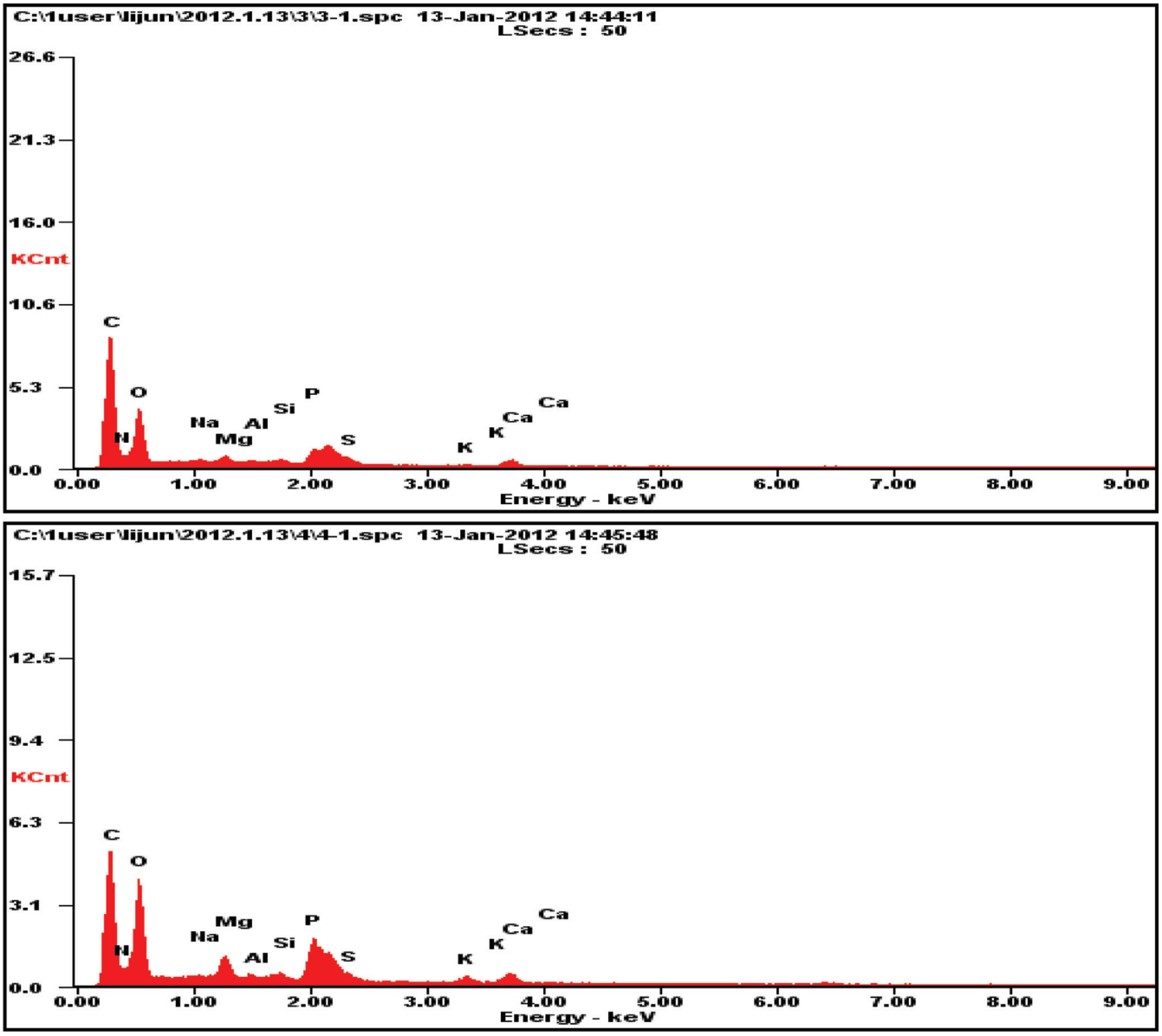

Figure 5. *EDX results of dry activated sludge at SRT of 12d and 30d.*

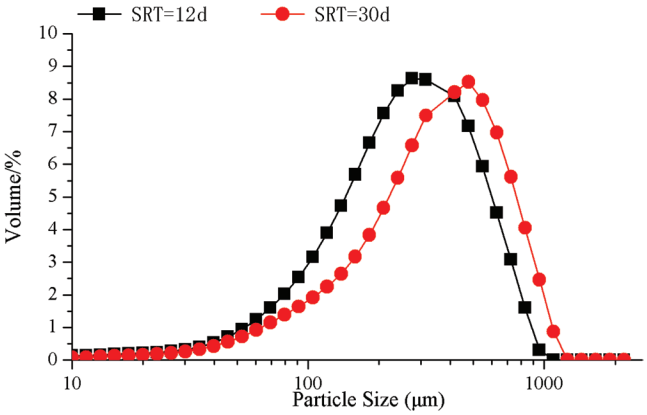

Figure 6. *Particle size distributions of activated sludge at SRT of 12 d (a) and 30 d (b).*

μm to 256.99 μm. Andreakakis (1993) indicated that sludge flocs with larger particle size had lower density and larger specific surface area than sludge flocs with smaller particle size, so the sludge flocs with larger particle size had a poor settleability. However, the particle size had no direct relationship with the settling velocity. Jin *et al.* (2003) reported that flocculating ability and surface properties of the sludge flocs played important roles in sludge compressing and settling abilities. Generally speaking, larger and denser sludge flocs had a good settleability.

As shown in Figure 7, the activated sludge at an SRT of 12d presented a loose and irregular shape, whereas that at an SRT of 30d was dense and regular. The activated sludge at an SRT of 30d had a good settleability, and its SVI was about 65 (Figure 7). Liss *et al.* (2002) also found that flocs at lower SRTs (4 and 9 days) presented an irregular shape, while that at higher SRTs (16 and 20 days) had a more spherical and compact structure. Besides, they suggested that cells under nutrient rich conditions could give rise to a more complex microcolony and colony morphology. When the influent flow kept constant, prolonging SRT meant reducing the organic load. The stability of flocs particle size distribution and morphologies at different SRTs might be explained by the cell growth rate. Under lower SRTs, more substrates were available for sludge microorganism growth. Therefore, more microcolonies were formed on the surface of flocs until the mass of flocs was big enough to disintegrate into smaller flocs. While under higher SRTs, the limited substrate and starved conditions produced a more stable biomass (Liao *et al.*, 2006).

CONCLUSIONS

Prolonging SRT in the A^2/O system had no significant impact on biological phosphorus removal. The removal efficiency decreased slightly from 92.9% at a SRT of 12d to 92.1% at a SRT of 30d, due to the increase of the relative content of phosphorus from 2.27% to 4.36% in dry activated sludge. At the same time, the average sludge particle size increased from 201.57 μm to 256.99 μm, and the flocs at longer SRT had a more regular and compact structure relative to that at shorter SRT. The results indicated that long SRT not only led to good phosphorus removal efficiency, but also generated a smaller amount of waste sludge which was more stable.

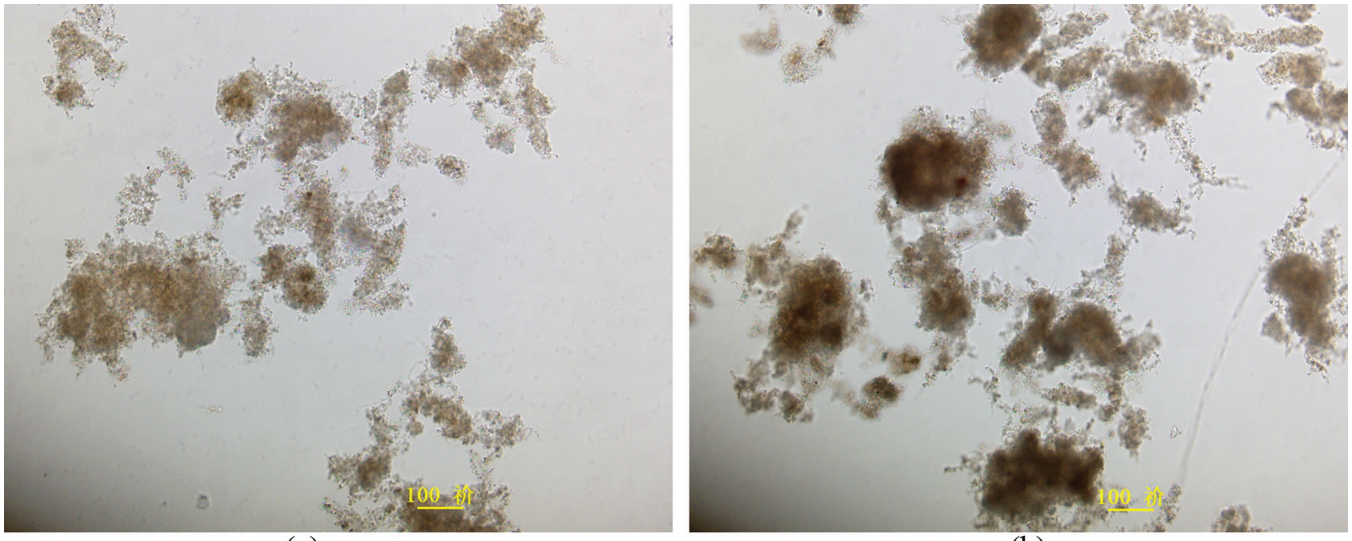

Figure 7. *Optical micrographs of activated sludge at SRT of: (a) 12 d and (b) 30 d.*

ACKNOWLEDGMENTS

This study was supported by the National Natural Science Foundation of China (51078008), the Beijing Municipal Education Commission general program (KM2012- 10005028), and the Beijing University of Technology Doctoral Scientific Research Foundation (X0004011201102).

REFERENCES

Andreadakis A., 1993. Physical and chemical properties of activated sludge floc. *Water Science and Technology, 27*(12): 1707–1714.

APHA (American Public Health Association), AWWA (American Water Works Association), and WEF (Water Environment Federation), 1999. Standard methods for the examination of water and wastewater (20th ed.). Washington DC, USA.

Barnard, J. L., 1983. Design consideration regarding phosphate removal in activated sludge plants. *Water Science and Technology, 15*(3-4): 319–328.

Ge S. J., Peng Y. Z., Wang S. Y., Guo J. H., Ma B., Zhang L., Cao X., 2010. Enhanced nutrient removal in a modified step feed process treating municipal wastewater with different inflow distribution ratios and nutrient ratios. *Bioresource Technology, 101*(23): 9012–9019. http://dx.doi.org/10.1016/j.biortech.2010.06.151

Ge S. J., Peng Y. Z., Zhang L., Wang X.M., Wang S. Y., 2010. Performance and material balance of modified UCT step feed enhanced biological nitrogen and phosphate removal process. *CIESC Journal, 61*(4): 1009–1016. (in Chinese)

Jin Bo, Britt-Marie Wilén, Paul Lant, 2003. A comprehensive insight into floc characteristics and their impact on compressibility and settleability of activated sludge. *Chemical Engineering Journal, 93*(1-3): 221–234.

Liao B. Q., Droppo I. G., Leppard G. G., Liss S. N., 2006. Effect of solids retention time on structure and characteristics of sludge flocs in sequencing batch reactors. *Water Research, 40*(13): 2583–2591. http://dx.doi.org/10.1016/j.watres.2006.04.043

Liss S. N., Liao B. Q., Droppo I. G., Allen D. G., Leppard G. G., 2002. Effect of solids retention time on floc structure. *Water Science and Technology*, *46*(1-2): 431–438.

Liu Y, Lin Y M, Tay J H, 2005. The elemental compositions of P-accumulating microbial granules developed in sequencing batch reactors. *Process Biochemistry, 40*(10): 3258–3262. http://dx.doi.org/10.1016/j.procbio.2005.03.002

Lu H., Oehmen A., Virdis B., Keller J., Yuan Z. G., 2006. Obtaining highly enriched cultures of Candidatus Accumulibacter phosphatis through alternating carbon sources. *Water Research, 40*(20): 3838–3848. http://dx.doi.org/10.1016/j.watres.2006.09.004

Ma Y, Peng Y Z, Wang X L, 2009. Improving nutrient removal of the AAO process by an influent bypass flow by denitrifying phosphorus removal. *Desalination, 246* (1-3): 534–544. http://dx.doi.org/10.1016/j.desal.2008.04.061

Nowak O. Parameter estimation for activated sludge Models with the help of mass balances, 1999. *Water Science Technology, 39*(4): 113–120. http://dx.doi.org/10.1016/S0273-1223(99)00065-7

Randall C. W., Barnard J. L., and Stensel H. D., 1992. *Design and retrofitting of wastewater treatment plants for biological nutrient removal.* Technomic Publishing, CRC Press, Lancaster, Florida, USA .

Randall A. A., Benefield L. D., Hill W. E., 1997. Induction of Phosphorus Removal in an Enhanced Biological Phosphorus Removal Bacterial Population. *Water Research, 31* (11): 2869–2877. http://dx.doi.org/10.1016/S0043-1354(97)00140-1

Tchobanoglous G., Burton F. L., Stensel H. D., 2002. *Wastewater Engineering: Treatment and Reuse*, fourth ed. Metcalf & Eddy Inc., Mc Graw-Hill Science Engineering, NY, USA.

United States Environmental Protection Agency, 1987. Design manual-phosphorus removal, EPA/625/1-87/001. Environmental Protection Agency, Washington D C, USA.

van Loosdrecht M. C. M., Brandse F. A., de Vries A. C., 1998. Upgrading of wastewater treatment processes for integrated nutrient removal-the BCFS (R) process. *Water Science and Technology, 37*(9): 209–217. http://dx.doi.org/10.1016/S0273-1223(98)00290-X

van Loosdrecht M. C. M., Henze M., 1999. Maintenance, endogenous respiration, lysis, decay and predation. *Water Science and Technology, 39* (1): 107–117. http://dx.doi.org/10.1016/S0273-1223(98)00780-X

Wang Y. Y., Peng Y. Z., Stephenson T., 2009. Effect of influent nutrient ratios and hydraulic retention time (HRT) on simultaneous phosphorus and nitrogen removal in a two-sludge sequencing batch reactor process. *Bioresource Technology, 100*(14): 3506–3512. http://dx.doi.org/10.1016/j.biortech.2009.02.026

Wentzel M. C., Ekama G. A., and Marais G. R., 1991. Kinetics of nitrification denitrification biological excess phosphorus removal systems-a review. *Water Science and Technology, 23*(4-6): 555–565.

Whang L. M., Park J. K., 2006. Competition between polyphosphate and glycogen- accumulating organisms in enhanced biological phosphorus-removal systems: effect of temperature and sludge age. *Water Environmental Research, 78*(1): 4–11. http://dx.doi.org/10.2175/106143005X84459

Zeng W., Li L., Wang Y. Y., Wang S. Y., Peng Y. Z., 2010. Nitritation and denitritation of domestic wastewater using a continuous anaerobic-anoxic-aerobic (A2O) process at ambient temperatures. *Bioresource Technology. 101*(21): 8074–8082. http://dx.doi.org/10.1016/j.biortech.2010.05.098

Rice Husk Bio-ash Impacts Redox Status and Rice Growth in a Flooded Soil from Southwestern China

XING-CHENG HUANG[1], QIU-JU JIANG[1], SHUAI ZHONG[1], YUE-QIANG ZHANG[1,2] and XIAO-JUN SHI[1,2,*]

[1]*College of Resources and Environment, Southwest University, Chongqing 400716, PR China*

[2]*National Monitoring Station of Soil Fertility and Fertilizer Efficiency on Purple Soils, Chongqing 400716, PR China*

ABSTRACT: This paper reports a soil-based bioassay of rice husk bio-ash impacts on redox properties and rice production. Bio-ash was produced during the pyrolytic process of rice husk as a boiler fuel, after which it was applied as an amendment to a flooded soil. Bio-ash was amended before rice transplanting at different mass rates including 0%, 0.1%, 1% and 5%, which was defined as T1, T2, T3, and T4 respectively. Results show that rice husk bio-ash in flooded soil could increase soil Eh value, pH value and organic matter content (OM), and also reduce reductant amount and activity. The numbers of rice white roots of T2 and T3 increased by 30% and 8% compared to that of T1 in the tillering stage. Increased grain yields due to bio-ash amendments at the rate of 0.1% and 1% were 3.43% and 11.8% higher than that of T1.

INTRODUCTION

BIO-ASH or biochar is the product of pyrolysis and carbonization, whereby organic materials are heated in a low or zero oxygen environment [1]. It can be produced from a wide range of organic sources including wood, agricultural residues, animal manure, rice husks and other waste materials [2,3]. In China, a lot of agricultural residues are burned, causing serious environmental problems. The development and utilization of biomass resources is of great significance to reduce environmental pollution and improve resource utilization [4,5]. Rice husk, the waste product, causes environmental problems during rice production, but it is potentially used in the remediation of soil [6,7] as the bio-ash. Bio-ash is a highly stable form of Carbon which may remain in soil for thousands of years and can act as low-carbon products for carbon sinks in agricultural soils [8,9]. It has a high cation exchange capacity, relatively large surface area and different kinds of nutrients. Therefore, application of bio-ash can also increase existing nutrient content and nutrient holding capacity [10,11,12]. However, no consensus regarding the role of bio-ash in influencing plant growth and yield as both increased [9,13,14] and decrease [15,16] plant growth and yield were reported in the literature. This study focuses on examining the role of bio-ash in plant growth and how possibly does it influence growth yield.

Bio-ash has the potential as a soil amendment to improve soil quality and crop productivity. Continuously flooded fields, widely distributed in southwestern China, are of low-yield. Long-term waterlogged soil environment has resulted in strong soil reduction, low nutrient, nutrient imbalance and soil acidification, which have negative impact on rice seedlings and root growth. Hence, these fields are often of low crop yields [17].

A practical and meaningful question to ask is whether rice husk bio-ash can optimize the soil redox potential and soil fertility and promote rice growth. In this paper, the impact of different rates of rice husk bio-ash on redox potential, soil chemical properties and rice growth in a flooded soil was comprehensively examined.

MATERIALS AND METHODS

Soil and Bio-ash Characteristics

The flooded soil (0–20 cm surface layer) was collected from Jiangjin District (106.2°E, 29.1°N), Chongqing City, China, and sieved through a 2-mm mesh screen after air-drying in shade. The basic characteristics and nutrient concentrations of the soil were analyzed using standard methods as presented in Table 1.

*Author to whom correspondence should be addressed.
E-mail: shixj@swu.edu.cn; Tel: 86 23 68250146; Fax: 86 23 68250444

1544-8053/15/01 S075-04

doi:10.12783/issn.1544-8053/12/S1/11

Table 1. Physical and Chemical Properties of the Soil.

pH	OM (g kg^{-1})	Total N (g kg^{-1})	Total P (g kg^{-1})	Total K (g kg^{-1})	Available P (mg kg^{-1})	Available K (mg kg^{-1})	Relaxed K (mg kg^{-1})	Clay (< 2 mm, g kg^{-1})
5.1	14.3	1.0	0.14	18.8	7.5	136	342	330

Bio-ash used in this study was produced by burning rice husks in a boiler at 500°C, The pH of bio-ash was measured in water at 1:5 (w/v) ratios. Carbon, Phosphorus, Potassium contents of bio-ash were determined by dry combustion analysis using element analyzers (Flash EA 1112/conflo, element, Italy; UV2310, UV, China; TAS-990, AAS, China). The pH of bio-ash solution was pH (H_2O) 10.4, and the concentration of C, P and K is 23.97%, 0.013%, and 0.043%, respectively.

Treatments

Four levels of bio-ash rate, 0, 1, 10 and 50 t ha^{-1}, equivalent to mixing separately with soil at the rates of 0%, 0.1%, 1%, 5%, are defined as T1, T2, T3, T4 respectively [18]. The soil, thus amended was used to fill pots at 8.0 kg of soil per pot. Each pot contained the same weight of soil and each plant was repeatedly treated for eighteen times. The input of chemical N totaled 150 kg N ha^{-1} with 100 kg N ha^{-1} compound fertilizer ($N:P_2O_5:K_2O$ = 15:15:15) as the base fertilizer and 50 kg N ha^{-1} urea, 60% of which was fertilized during elongation stage and the other 40% during the heading stage. The seedlings were transplanted on 3rd May, and harvested on 25th of August. Regular cultivation and management were carried out for rice growth period. Rice crop management was taken following by Liu [19].

MEASUREMENTS AND SAMPLINGS

Samplings were carried out separately at the tillering stage (TS, 30 DAP), elongation stage (ES, 60 DAP), heading stage (HS, 80 DAP) and maturation stage (MS, 100 DAP). The three pots were sampled each time. The pH and total organic matter of soil samples were measured. Then 6 pots were used to investigate the yield indices including panicle number, filled grains and grain weight etc., at maturity. At the tillering stage, the redox potential was measured by potential difference method; the reductant (include organic reductant, Fe^{2+}, S^{2-}, etc) activity and amount were measured by volumetric method. All the measurements of soil basic properties were taken following the methods described by Lu [20].

Duncan differential significance analysis method at $p < 0.05$ between treatments was analyzed using SPSS17.0 software.

Table 2. Effects of the Bio-ash on Physicochemical Property of the Soil at the Tillering Stage (30 DAP) of Rice.

Treatment	Reduzate Activity (cmol kg^{-1})	Reduzate Amount (cmol kg^{-1})	Redox Potential Eh (mv)		
			5 cm	10 cm	20 cm
T1	3.28a	6.95a	86b	62b	–16b
T2	2.78b	6.42ab	95b	72ab	–10b
T3	2.60b	5.90ab	111a	81ab	11a
T4	2.53b	5.77b	124a	89a	13a

RESULTS

Effects of Rice Husk Bio-ash on Soil Redox Properties

Effects of bio-ash on soil redox properties at the tillering stage are shown in Table 2. The rank of the redox potential is T4, T3, T2, and T1 in the descending order, although the potential of T2 was not significantly different from that of T1. The soil reductant activity following bio-ash amendment was always lower than the control (T1) and was significantly different from T1. The reductant amount in various treatments appears to have no significant difference in different levels of bio-ash except the T1 treatment.

The bio-ash treatment has remarkably reduced the reductnat activity therefore it could increase soil redox potential.

Dynamic Changes of Soil pH and OM

Soil pH is one of the important indices that indirectly reflect physical form, transfer process and nutrient availability. Figure 1 shows the dynamic change of soil pH in various stages after bio-ash was added into the soil. The soil pH in various growth periods is all higher than T1. The magnitude of pH change in various growth periods is T4, T3, T2 and T1 in the descending order. At the heading stage, soil pH is reduced to

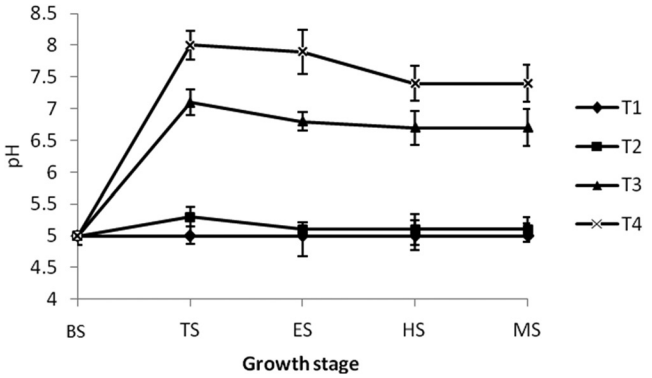

Figure 1. *Effect of rice husk bio-ash on soil pH.*

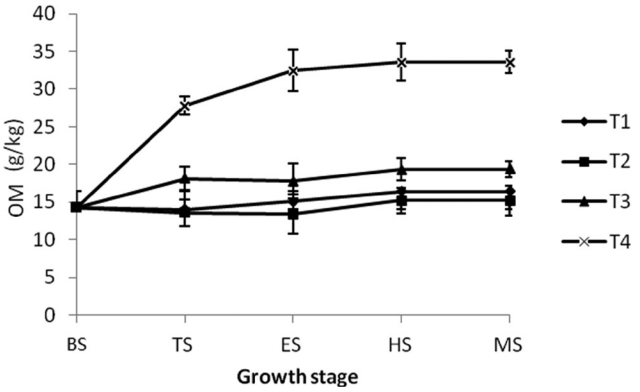

Figure 2. *Effect of rice husk bio-ash on soil OM.*

a stable range. Bio-ash can thus increase soil pH value and could be used to treat acid soil.

Figure 2 shows the dynamic change of soil OM in various stages of rice growth. The tendency of OM change in various growth periods is ranked T4, T3, T1 and T2 in descending order. Except T2, the OM of bio-ash treatment was all higher than the control. It can be concluded that bio-ash treatments could significantly increase soil organic matter into a certain rate, because it can increase the biomass of roots.

Effects of Bio-ash on Rice Root Growth

The numbers of rice root in treatments T2 and T3 were significantly higher than that of T1. The number of black roots in treatments T2 and T3 were 30% and 8%, respectively, less than that of T1. T4 has the minimum total number of roots and the maximum number of black roots.

Effects of Bio-ash on Rice Yield and Yield Components

The rice yield of T4 (5% Bio-ash amendment) was the least which was significant less than the rest treatments, all seeds are empty grain. Rice yield of the control was increased by 3.43% and 11.8% in the use of 0.1% and 1% bio-ash amendments, respectively.

DISCUSSION

Amendment with bio-ash can remarkably inhibit the reductant activity. At the same time, it could increase the soil redox potential at the tillering stage.

With the addition of a small amount bio-ash to the soil, no obvious effect on soil organic issue and soil pH value could be detected. Even in the early stage of the rice growth, soil organic matter content is less than the control treatment. This may due to the fact that bio-ash has promoted the decomposition of soil organic matter [21], leading to a decline in the organic matter content. The medium and high treatments, however, significantly increased the amount of soil carbon concentration and pH value. Interestingly, other studies have also reported that pH and Eh are negatively correlated with bio-ash in soils [22,23]. In this study, both pH and Eh increased due to the addition of bio-ash. This may due to the high pH of bio-ash that could reduce the production of Fe^{2+}, CH_4 and other reduzate in an alkaline environment [24].

In the early growth stage of rice, the addition of a small amount of bio-ash increased the number of roots and the percentage of white root rate. Therefore, bio-ash at recommended rate can increase root number and its activity. An overdose of bio-ash could kill the roots and seedlings for the high pH value; then it will lead to the reduction of rice yields.

Table 3. Rice Root Growth in the Tillering Stage.

Treatment	Total (No./pot)	White Root (No./pot)	Yellow Root (No./pot)	Black Root (No./pot)
T1	401b	57b	294b	50b
T2	431a	82a	314a	35c
T3	419ab	61b	312a	46bc
T4	315c	21c	226c	68a

Table 4. Effect of Rice Husk Bio-ash on Rice Yield.

Treatment	Panicle Number (No./Pot)	Grain Number (No./ spike)	Seed Setting Rate (%)	1000-grain wt. (g)	Yield (g/pot)
T1	18.3a	189.07b	75.0b	26.36b	68.19c
T2	20.3a	185.33b	74.0b	27.46a	76.27a
T3	18.3a	187.39b	78.0a	26.22b	70.53b
T4	12.5b	264.11a	0.0	0.00	0.00

Further, a small amount of bio-ash amendment could increase grain weight to 1000-grain and increase seed setting rate. Rice husk bio-ash has strong adsorption capacity, huge physical structure and large surface area. It can promote the ion exchange and adsorption capacity of the soil and enhance the content of soil nutrients, resulting in higher crop yields [25].

REFERENCES

1. Antal M. J., Grønli M., 2003. The Art, Science, and Technology of Charcoal Production. *Industrial & Engineering Chemistry Research 42*(8), 1619–1640. http://dx.doi.org/10.1021/ie0207919
2. Kwapinski W., Byrne C. M. P., Kryachko E., *et al.*, 2010. Biochar from biomass and waste. *Waste and Biomass Valorization 1*(2), 177–189. http://dx.doi.org/10.1007/s12649-010-9024-8
3. Streubel J. D., Collins H. P., Garcia-Perez M., *et al.*, 2011. Influence of contrasting biochar types on five soils at increasing rates of application. *Soil Science Society of America Journal 75*(4), 1402–1413. http://dx.doi.org/10.2136/sssaj2010.0325
4. Cuiping L., Chuangzhi W., Haitao H., 2004. Study on the distribution and quantity of biomass residues resource in China. *Biomass and bioenergy 27*(2), 111–117. http://dx.doi.org/10.1016/j.biombioe.2003.10.009
5. Jiang D., Zhuang D., Fu J., *et al.*, 2012. Bioenergy potential from crop residues in China: Availability and distribution. *Renewable and Sustainable Energy Reviews 16*(3), 1377–1382. http://dx.doi.org/10.1016/j.rser.2011.12.012
6. Zhang A. F., Bian R. J., Pan G. X., *et al.*, 2012. Effects of biochar amendment on soil quality, crop yield and greenhouse gas emission in a Chinese rice paddy: a field study of 2 consecutive rice growing cycles. *Field Crop Res 127*, 153–160. http://dx.doi.org/10.1016/j.fcr.2011.11.020
7. Agusalim M., Wani H. U., Syechfani M. S., 2004. Rice Husk Biochar for Rice Based Cropping System in Acid Soil 1. The Characteristics of Rice Husk Biochar and Its Influence on the Properties of Acid Sulfate Soils and Rice Growth in West Kalimantan, Indonesia. *Fuel Processing Technology 85*(11), 1273–1282.
8. Gaunt J. L., Lehmann J., 2008. Energy balance and emissions associated with biochar sequestration and pyrolysis bioenergy production. *Environmental Science and Technology 42*(11), 4152–4158. http://dx.doi.org/10.1021/es071361i
9. Chan KY., Van Zwieten L., Meszaros I., *et al.*, 2007. Agronomic values of greenwaste Biochar as a soil amendment. *Australian Journal of Soil Research 45*, 629–634. http://dx.doi.org/10.1071/SR07109
10. Brown R., 2009. Biochar production technology. Biochar for environmental management: *Science and technology* 127–146.
11. Liang B., Lehmann J., Solomon D., *et al.*, 2006. Black carbon increases cation exchange capacity in soils. *Soil Science Society of America Journal 70*(5), 1719–1730. http://dx.doi.org/10.2136/sssaj2005.0383
12. Kishimoto S., Sugiura G. Charcoal as a soil conditioner. *Int Achieve Future*, 1985, 5, 12–23.
13. Steiner C., Teixeira W. G., Lehmann J., *et al.*, 2007. Long term effects of manure, charcoal and mineral fertilization on crop production and fertility on a highly weathered Central Amazonian upland soil. *Plant and Soil 291*(1-2), 275–290. http://dx.doi.org/10.1007/s11104-007-9193-9
14. Novak J. M., Busscher W. J., Laird D. L., *et al.*, 2009. Impact of Biochar amendment on fertility of a southeastern coastal plain soil. *Soil Science 174*(2), 105–112. http://dx.doi.org/10.1097/SS.0b013e3181981d9a
15. Deenik J. L., McClellan T., Uehara G., *et al.*, 2010. Charcoal volatile matter content influences plant growth and soil nitrogen transformations. *Soil Science Society of America Journal 74*(4), 1259–1270. http://dx.doi.org/10.2136/sssaj2009.0115
16. Chan K. Y., Van Zwieten L., Meszaros I., *et al.*, 2008. Using poultry litter Biochars as soil amendments. *Soil Research 46*(5), 437–444. http://dx.doi.org/10.1071/SR08036
17. Chai J. J., Liao M., Xu P. Z., *et al.*, 2012. Feature Analysis on Nutrients Restrictive Factors of Major Low Productive Waterlogged Paddy Soil in China. *J. Soil Water Conserv 23*(2), 157–162.
18. Morrison D. A., Morris E. C., 2000. Pseudoreplication in experimental designs for the manipulation of seed germination treatments. *Austral Ecol, 25*, 292–296. http://dx.doi.org/10.1046/j.1442-9993.2000.01025.x
19. Liu X. Y., Qu J. J., Li L. Q., *et al.*, 2012. Can biochar amendment be an ecological engineering technology to depress N2O emission in rice paddies? A cross site field experiment from South China. *Ecol. Eng 42*, 168–173. http://dx.doi.org/10.1016/j.ecoleng.2012.01.016
20. Lu, R.K., 2000. Methods of Soil and Agro-chemical Analysis. China Agricultural Science and Technology Press.
21. Wardle D. A., Nielsson M. C., Zackrisson O., 2008. Fire-derived char-coal causes loss of forest humus. *Science 320*, 629. http://dx.doi.org/10.1126/science.1154960
22. Bohrerova, Z., Stralkova, R., Podesvova, J., Bohrer, G., Pokorny, E., 2004. The relationship between redox potential and nitrification under different sequences of crop rotations. *Soil and Tillage Research 77*(1), 25–33. http://dx.doi.org/10.1016/j.still.2003.10.006
23. Von der Kammer, F., Thöming, J., Förstner, U., 2000. Redox buffer capacity concept as a tool for the assessment of long-term effects in natural attenuation/intrinsic remediation. In Redox Springer Berlin Heidelberg, 189–202.
24. Wang Z. P., Delaune R. D., Patrick W. H., *et al.*, 1993. Soil redox and pH effects on methane production in a flooded rice soil. *Soil Science Society of America Journal 57*(2), 382–385. http://dx.doi.org/10.2136/sssaj1993.03615995005700020016x
25. Wang D., Zhang X., Jiang C C., *et al.*, 2012. Biochar research advances regarding soil improvement and crop response. *Chinese Journal of Eco-Agriculture 20*(8), 963–967. http://dx.doi.org/10.3724/SP.J.1011.2012.00963

Accumulation and Transfer of Heavy Metals in the Mangroves from Quanzhou Bay Wetland, SE Coast of China

YU RUI-LIAN*, HU GONG-REN, ZHANG WEI-FANG and LIU BING-XING
College of Chemical Engineering, Huaqiao University, Xiamen 361021, China

ABSTRACT: Levels of eight heavy metals in surface sediments and different tissues of *Aegiceras corniculatum* and *Kandelia candel* situated in Quanzhou Bay wetland were determined to assess the accumulation and transferability of heavy metals in the mangroves. Acid-extractable concentrations decrease in the sediments as Fe > Mn > Pb > Zn > Cu > Cr > Ni > Co. In both mangrove species, the distribution of metals occurs in the order of root > branch > leaf for Cu, leaf > root > branch for Ni, and root > leaf > branch for the other six metals. Bio-concentration factors of Ni, Cr, Cu, Zn, Fe and Mn are higher than those of Co and Pb in both species. *Kandelia candel* has a higher ability than *Aegiceras corniculatum* to accumulate Cu, Ni, Mn, Fe and Co, but weaker for Zn, Cr and Pb. Most of the metals are retained in the roots.

INTRODUCTION

MANGROVE forests are ligneous plant communities growing in the inter-tidal zones of tropical to subtropical coastal rivers, estuaries and inner-bays [1]. They are highly productive and play a vital role as a major primary producer within estuarine ecosystems [2–3]. As the last ecological barriers between terrestrial and marine ecosystems, mangrove forests can prevent coastal erosion and provide a good nursery ground for a number of commercially important aquatic organisms [4–5].

Heavy metals are considered as one of the most serious pollutants due to their toxicity, persistence and bioaccumulation [6], and their mobility and bioavailability in the environment are determined by their speciation. Two methods, named a single-step extraction procedure and a multiple-sequential extraction procedure, are commonly used to extract the bioavailable fractions of metals in soil/sediment. Dilute hydrochloric acid (HCl) is one of the more widely used extractants in single-step extraction procedures [7–8].

Mangroves play an important role in abating heavy metal pollution in offshore areas due to their absorbing and accumulating heavy metals through physiological and biochemical processes [9–10]. Quanzhou Bay (24°46′–24°58′N, 118°38′–118°47′E), once the famous jumping-off point of the silk route on the sea in ancient China (especially in Song and Yuan Dynasties), lies in the southeast of Fujian province, China, is a semi-enclosed bay with its mouth opening towards Taiwan Straits. There are nearly 400 ha of mangroves in Quanzhou Bay wetland, in which *Aegiceras corniculatum* and *Kandelia candel* are the dominant species. Quanzhou Bay has been threatened by heavy metal pollution due to the rapid urbanization and industrialization in the surrounding areas during the past few decades [11]. However, there are few reports on the in-situ remediation of heavy metal pollution using mangroves situated in Quanzhou Bay wetland. This study aims to determine the accumulation and transferability of eight heavy metals (Fe, Mn, Pb, Zn, Cu, Cr, Ni and Co) in the dominant mangrove species, *Aegiceras corniculatum* and *Kandelia candel*, found in Quanzhou Bay wetland. The results may then provide a scientific basis for assessing the in-situ remediation of heavy metal pollution using the mangroves situated in this area.

MATERIALS AND METHODS

In October 2009, field sampling was conducted in Quanzhou Bay mangrove wetland at low tide. There were five sampling sites each for *Aegiceras corniculatum* (A1 to A5) and *Kandelia candel* (K1 to K5) (Figure 1). At each sampling site, leaf, branch and root samples were separately collected from 5 representative mangrove trees with a height of > 2 m [4]. Five surface sediment samples (0–5 cm) were randomly collected

*Author to whom correspondence should be addressed.
E-mail: ruiliany@hqu.edu.cn

1544-8053/15/01 S075-05

doi:10.12783/issn.1544-8053/12/S1/12

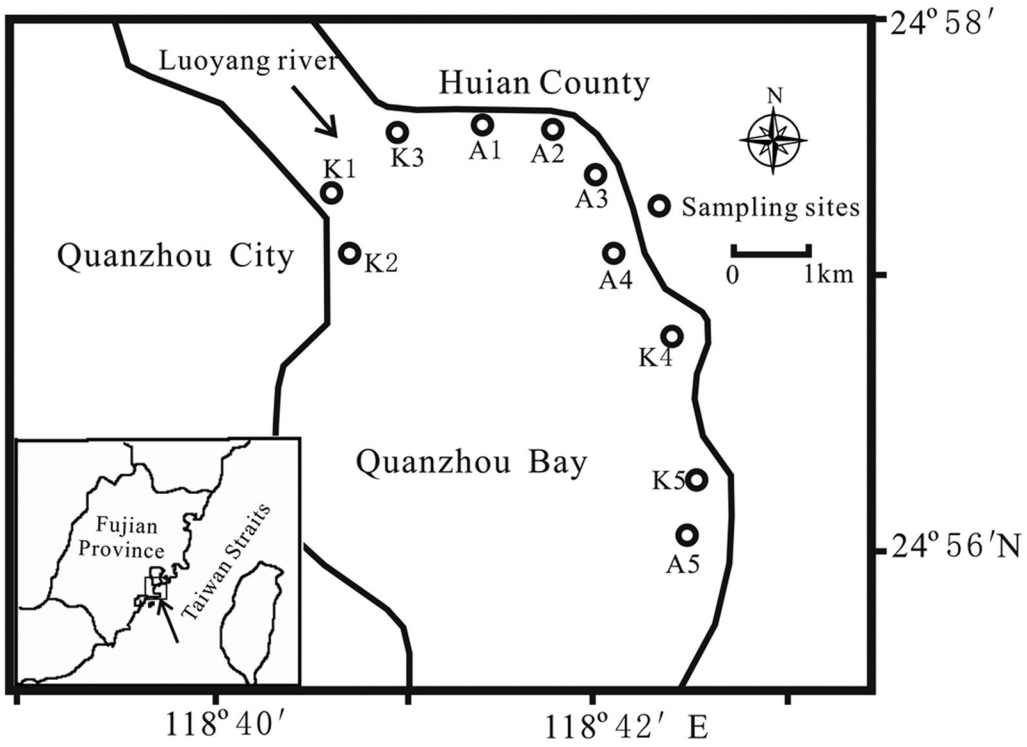

Figure 1. *Sampling location map of the study area.*

and then mixed to form one composite sample for each sampling site.

The plant samples (leaves, branches and roots) were first washed with tap water to remove the dirt, then washed with de-ionized water, oven-dried (60°C for 96 hours) to constant weight, and then ashed (450°C for 12 hours) and homogenized for further analysis [10]. For each plant sample, 0.2 g ash was digested with concentrated HNO_3 at 80°C in a water bath till dryness, then dissolved with 0.5 mol·L^{-1} HNO_3, and finally filtered into a 50-mL volumetric flask for further analysis. The pretreatment, preparation and metal extraction (using 0.5 mol·L^{-1} HCl) of sediment samples were following standard protocols [12]. Concentrations of heavy metals in the extracted solutions were determined using inductively coupled plasma atomic emission spectrometry. The background correction and matrix interference were monitored throughout the analyses. Analyses of the mixed standard solutions were done for every fifth sample to maintain the accuracy of analysis. Analyses of triplicates for all the samples showed the following coefficients of variation for elements: Fe ≤ 2.2%, Mn ≤ 1.7%, Zn ≤ 5.0%, Cr ≤ 3.4%, Cu ≤ 1.2%, Pb ≤ 3.6%, Ni ≤ 1.6% and Co ≤ 1.8%.

In this study, the bio-concentration factor (BCF; ratio of plant metal concentration to sediment metal concentration) and the transfer factor (TF; ratio of leaf metal concentration to root metal concentration) were respectively employed to evaluate the metals' accumulation ability from sediment to plant and their transfer ability from root to leaf within plants [2].

RESULTS AND DISCUSSION

Acid-extractable Concentrations of Heavy Metals in the Sediments

The acid-extractable concentrations of heavy metals in the surface sediments are listed in Table 1. Obvious variation for most elements is found at different sites. For example, Cu varies from 14.0 to 136 mg kg^{-1}, and Pb from 39.4 to 151 mg kg^{-1}. Sites of A1, A4, A5 and K5 show much higher concentrations of Cu than other sampling sites because there are domestic and aquaculture sewage outfalls near these 4 sites. Site K1 shows the highest level of Pb because it is near a national road, on which the traffic is very busy. The elemental sequence of average concentrations is Fe > Mn > Zn > Pb > Cu > Cr > Ni > Co, in which Cu and Pb are higher than the first-class limits (35 and 60 mg·kg^{-1} for Cu and Pb, respectively) of Chinese Marine Sediment Quality [13], indicating that Cu and Pb show a higher degree of contamination than other studied heavy metals.

Table 1. Acid-extractable Concentrations (mg·kg^{-1}) of Heavy Metals in Sediments.

Site	Cu	Zn	Ni	Cr	Mn	Co	Fe	Pb
A1	81.9	45.0	10.2	20.5	1122	5.18	9558	53.5
A2	23.0	76.6	6.30	18.7	892	4.00	6911	58.9
A3	27.0	87.5	8.10	21.3	1215	3.80	7020	62.2
A4	136	42.0	10.1	20.4	1052	5.19	7846	41.0
A5	70.1	45.2	10.7	21.5	859	5.71	8278	39.4
K1	14.0	56.0	5.40	41.8	708	3.90	7531	151
K2	23.6	76.9	6.39	18.8	892	4.10	6913	58.8
K3	18.0	82.5	6.10	16.2	777	3.80	6793	53.7
K4	25.0	70.8	7.70	18.0	1058	3.90	6830	57.1
K5	71.0	44.9	10.9	21.9	858	5.31	8277	39.8
Average	**49.0**	**62.7**	**8.19**	**21.9**	**943**	**4.49**	**7596**	**61.6**

A: *Aegiceras corniculatum*; K: *Kandelia candel*

Accumulation and Transfer of Heavy Metals in the Mangroves

The concentrations of heavy metals in different tissues of both mangrove species are listed in Table 2. There are obvious differences between metals in different tissues of the same species. On the whole, the elemental sequence of average concentrations in different tissues of both species is generally in the order of Fe, Mn > Cr, Zn > Cu > Pb > Co, with the exception of Ni, which is lower than Pb in branches and roots of *Aegiceras corniculatum* and roots of *Kandelia candel* but higher than Pb in branches of *Kandelia candel*, and higher than Cr and Zn in leaves of both species. Mn is obviously higher than Fe in branches and leaves, but significantly lower than Fe in roots of both mangroves. Cr is obviously higher than Zn in most tissues of both species with the exception of *Kandelia candel* roots. The concentrations of heavy metals in different tissues of both species show the order of: root > branch > leaf for Cu; leaf > root > branch for Ni; and root > leaf > branch for Fe, Mn, Cr, Zn, Pb and Co. Neither mangrove species can be considered as a potential hyperaccumulator, which should have the critical concentrations > 1000 mg·kg^{-1} in the aboveground tissues for Cu, Ni, Pb, Co and Cr, while > 10000 mg·kg^{-1} for Mn, Fe and Zn [14].

Average BCF values of the studied heavy metals in different tissues of both mangrove species are listed in Table 3. It is found that the elemental BCF values show different sequences in different tissues of both mangrove species. For *Aegiceras corniculatum*, the sequence is Cr > Zn > Mn > Cu > Ni > Co > Pb = Fe in branch, Ni > Cr > Mn > Zn > Cu > Pb = Co > Fe in leaf, Cr > Zn > Fe > Ni > Cu > Mn > Pb > Co in root, while Ni > Cr > Zn > Fe > Mn > Cu > Pb > Co for the whole plant. For *Kandelia candel*, the sequence is Cr > Cu = Mn > Ni > Zn > Co > Fe > Pb in branch, Ni > Cr > Mn > Zn > Cu > Co > Fe = Pb in leaf, Cr > Fe > Cu > Zn > Mn > Ni > Pb > Co in root, while Ni > Cr > Fe > Cu > Mn > Zn > Pb = Co for the whole plant. As a whole, the BCF values of Ni, Cr, Cu, Zn, Fe and Mn are much higher than those of Co and Pb in both mangrove species. The accumulating ability of *Kandelia candel* is relatively stronger than *Aegiceras corniculatum* for Cu, Ni, Mn, Fe and Co, but on the contrary for Zn, Cr and Pb.

Most studied elements show the highest BCF values in roots except for Ni, which presents the highest BCF in leaves. This indicates that most of the studied heavy metals are adsorbed and stored in the roots of both mangrove species so as to not be easily transported into adjacent water or sediment again. Simultaneously and crucially, the harm coming from the accumulation of most studied metals along the food chains is decreased. Except for Ni, when accumulated in the withered leaves, might be released into water and sediment again, may bring disadvantage in the mangrove's fixation and restoration for heavy metals. Most studied heavy metals present the lowest BCF values in branches, suggesting that a branch acts as a channel in the transport of heavy metals within the plant but only weakly retains the metals for both mangrove species.

Among the studied heavy metals, only Cr and Ni show the considerably high BCFs (>1) in the aboveground tissues of both mangrove species, suggesting

Table 2. Average Concentrations (mg·kg^{-1}) of Heavy Metals in the Tissues of Both Mangrove Species.

		Cu	Zn	Ni	Cr	Mn	Co	Fe	Pb
Aegiceras corniculatum	Branch	6.71	11.0	0.81	23.7	135	0.12	127	0.91
	Leaf	5.28	23.4	136	29.3	466	0.31	229	3.23
	Root	57.3	82.8	12.2	99.2	740	1.10	4619	18.2
Kandelia candel	Branch	7.42	10.1	1.12	23.7	275	0.14	132	0.53
	Leaf	5.33	16.0	131	25.0	684	0.24	237	1.66
	Root	41.3	95.0	6.80	89.6	874	1.28	20802	25.8

Table 3. Average BCF Values of Heavy Metals in the Tissues of Both Mangrove Species.

		Cu	Zn	Ni	Cr	Mn	Co	Fe	Pb
Aegiceras corniculatum	Branch	0.14	0.18	0.09	1.13	0.15	0.03	0.02	0.02
	Leaf	0.12	0.43	14.97	1.39	0.48	0.07	0.03	0.07
	Root	1.05	1.62	1.21	4.71	0.80	0.25	1.61	0.40
	whole	0.44	0.74	5.42	2.41	0.48	0.11	0.55	0.16
Kandelia candel	Branch	0.32	0.16	0.17	1.15	0.32	0.03	0.02	0.01
	Leaf	0.23	0.25	20.45	1.20	0.82	0.06	0.03	0.03
	Root	1.73	1.45	0.96	4.31	1.00	0.31	2.90	0.40
	whole	0.76	0.62	7.19	2.22	0.71	0.14	0.98	0.14

that both species may be classified as potential accumulators for Cr and Ni [15]. However, they still cannot be considered as potential hyper-accumulators, which should have the critical concentrations in the aboveground tissues > 1000 mg·kg^{-1} for Cr and Ni [14–15].

Average TF values of the studied heavy metals are listed in Table 4. The elemental sequence of transfer ability is Ni > Mn > Cr > Zn = Co > Pb > Cu > Fe in *Aegiceras corniculatum*, and Ni > Mn > Cr > Co > Zn > Cu > Pb > Fe in *Kandelia candel*. Generally, plant species with TF values > 1 can be classified as high-efficient plants for metal translocation from roots to leaves of plants [15]. The TF values of most studied metals are less than 1.0 except Ni (11.2 and 19.3 in *Aegiceras corniculatum* and *Kandelia candel*, respectively). This indicates that most studied metals are retained in the roots of both mangrove species, which results in the limited transfer of metals through leaves to the benthos in the mangrove ecosystems and thus reducing the transfer of these metals to aquatic food chains [2, 10]. Further work is required on the reason and mechanism of the high transfer ability of Ni from roots to leaves in both mangrove species.

CONCLUSIONS

The acid-extractable concentrations of heavy metals in the surface sediments in Quanzhou Bay mangrove wetland decrease in the order of Fe > Mn > Pb > Zn > Cu > Cr > V > Ni > Co. Only concentrations of Cu (4 sites) and Pb (2 sites) exceed the first-class limits of Chinese Marine Sediment Quality. Concentrations of the heavy metals in different tissues of both mangrove species show the accordant order of root > branch > leaf for Cu; leaf > root > branch for Ni; root > leaf > branch for Fe, Mn, Cr, Zn, Pb and Co. The BCF values of Ni, Cr, Cu, Zn, Fe and Mn are higher than those of Co and Pb in both mangrove species. Neither mangrove species could meet the requirements of a hyper-accumulator plant based on the accumulation capacity for the metals. *Kandelia candel* has a relatively higher ability than *Aegiceras corniculatum* to accumulate Cu, Ni, Mn, Fe and Co, but a weaker ability for Zn, Cr and Pb. Except Ni, the other metals show the highest BCF values in roots, indicating that most metals are adsorbed and stored in the roots of both mangrove species. The pattern of metal accumulation in plants depends on physical, chemical and biological processes of metals in the growing environment as well as the physiology of plants. Further work is required on the reason and mechanism of nickel's high transfer ability from roots to leaves in both mangrove species.

Table 4. Average TF Values of Heavy Metals in Both Mangrove Species.

	Cu	Zn	Ni	Cr	Mn	Co	Fe	Pb
Aegiceras corniculatum	0.09	0.28	11.2	0.30	0.63	0.28	0.05	0.18
Kandelia candel	0.13	0.17	1.3	0.28	0.78	0.19	0.01	0.06

ACKNOWLEDGEMENTS

The work was supported by National Natural Science Foundation of China (No.21077036) and and Natural Science Foundation of Fujian Province (2011J01273). We gratefully thank professor Richard Bindler for revising the English expression of this paper.

REFERENCES

1. Yim M. W. and Tam N. F. Y., "Effects of wastewater-borne heavy metals on mangrove plants and soil microbial activities", *Marine Pollut. Bull.,* 1999, 39: 179–186. http://dx.doi.org/10.1016/S0025-326X(99)00067-3
2. MacFarlane G. R., Koller C. E. and Blomberg S. P., "Accumulation and partitioning of heavy metals in mangroves: A synthesis of field-based studies", *Chemosphere*, 2007, 69: 1454–1464. http://dx.doi.org/10.1016/j.chemosphere.2007.04.059
3. Bayen, S., "Occurrence, bioavailability and toxic effects of trace metals

and organic contaminants in mangrove ecosystems: a review", *Environ. Int.*, 2012, 48: 84–101. http://dx.doi.org/10.1016/j.envint.2012.07.008

4. MacFarlane G. R., Pulkownik A. and Burchett M. D., "Accumulation and distribution of heavy metals in the grey mangrove, Avicennia marina (Fork.) Vierh: biological indication potential", *Environ. Pollut.*, 2003, 123: 139–151. http://dx.doi.org/10.1016/S0269-7491(02)00342-1
5. Nath B., Chaudhuri P. and Birch G., "Assessment of biotic response to heavy metal contamination in Avicennia marina mangrove ecosystems in Sydney Estuary, Australia", *Ecotox. Environ. Safe.*, 2014, 107: 284–290.http://dx.doi.org/10.1016/j.ecoenv.2014.06.019
6. Tam N. F. Y. and Wong Y. S., "Spatial variation of heavy metals in surface sediments of Hong Kong mangrove swamps", *Environ. Pollut.*, 2000, 110: 195–205.http://dx.doi.org/10.1016/S0269-7491(99)00310-3
7. Ayyamperumal T., Jonathan M. P., Srinivasalu S., Armstrong-Altrin J. S. and Ram-Mohan V., "Assessment of acid leachable trace metals in sediment cores from River Uppanar, Cuddalore, Southeast coast of India", *Environ. Pollut.*, 2006, 143: 34–45. http://dx.doi.org/10.1016/j.envpol.2005.11.019
8. Jayaprakash M., Jonathan M. P., Srinivasalu S., Muthuraj S., Ram-Mohan V. and Rajeshwara-Rao N., "Acid-leachable trace metals in sediments from an industrialized region (Ennore Creek) of Chennai City, SE coast of India: An approach towards regular monitoring", *Estuarine Coastal Shelf Sci.*, 2007, 22: 1–12.
9. Machado W., Silva-Filho E. V., Oliveira R. R. and Lacerda L. D., "Trace metal retention in mangrove ecosystems in Guanabara Bay, SE Brazil", *Marine Pollut. Bull.*, 2002, 44: 1277–1280. http://dx.doi.org/10.1016/S0025-326X(02)00232-1
10. Silva C. A. R., Silva A. P. and Oliveira S. R., "Concentration, stock and transport rate of heavy metals in a tropical red mangrove, Natal, Brazil", *Marine Chem.*, 2006, 99: 2–11. http://dx.doi.org/10.1016/j.marchem.2005.09.010
11. Yu R., Hu G., and Wang L, Speciation and ecological risk of heavy metals in intertidal sediments of Quanzhou Bay, China. *Environ. Monit. Assess.*, 2010, 163(1-4): 241–252. http://dx.doi.org/10.1007/s10661-009-0830-z
12. Hu G., Yu R., Zhao J. and Chen L., "Distribution and enrichment of acid-leachable heavy metals in the intertidal sediments from Quanzhou Bay, southeast coast of China", *Environ. Monit. Assess.*, 2011, 173(1-4): 107–116. http://dx.doi.org/10.1007/s10661-010-1374-y
13. China State Bureau of Quality and Technical Supervision, Chinese National Standards GB 18668-2002 Marine Sediment Quality, Beijing: Chinese Standards Press, 2002.
14. Wu Q. T. and Chen T. B. *Environment Bio-remediation technology*, Beijing: Chemical Industry Press, 2006: 86–87.
15. Usman A. R. A., Alkredaa R. S. and Al-Wabel M. I., "Heavy metal contamination in sediments and mangroves from the coast of Red Sea: Avicennia marina as potential metal bioaccumulator", *Ecotox. Environ. Safe.*, 2013, 97: 263–270. http://dx.doi.org/10.1016/j.ecoenv.2013.08.009

Feasibility Study of Individual Treatments of Desizing Wastewater

GUIHONG PEI[1], FENG YU[1] and JIANJUN LIU[2,*]
[1]*School of Civil Engineering and Architecture, Southwest Petroleum University, Chengdu 610500, China*
[2]*School of Geoscience and Technology, Southwest Petroleum University, Chengdu 610500, China*

ABSTRACT: The common treatment of printing and dyeing wastewater (PDW) is centralized processing the mix-wastewater generated by each printing and dyeing craft. On the basis of present process, this paper studies on individual treatment of desizing wastewater which contains less water and higher concentration of pollutants. Then takes 2000-tons per day PDW treatment plant as a case to estimate the cost of construction and operation. Compared with technical and economic of individual processing desizing wastewater and centralized processing PDW, it can be shown that individual processing desizing wastewater is more economical. The per cubic meter water can save 0.18 Yuan averagely, and the total of LCC will save 1,396,700 Yuan.

INTRODUCTION

PRINTING and dyeing wastewater (PDW) discharged from printing and dyeing industries is one of the main pollution sources of Chinese industrial system. According to statistics, the annual discharged PDW ranks the fifth in the total national industrial sectors [1]. At present, Chinese printing enterprises are mostly SMEs and scattered distribution. The discharged wastewater is difficult to centralize treatment, and most wastewater has not been effective governance which causes greatly environmental pollution because of directly discharged. So the treatment of PDW is important for China to improve the water environmental quality, especially, the technology of low-cost and practical is urgent need. This paper is aimed to explore an economically treatment method for PDW named "Individual Treatments of Desizing Wastewater". Then the cost of capital construction and operation are analyzed. The results will be useful and instructive to improve the treatment technology of PDW.

PDW is mainly discharged from the factories of cotton, fiber, chemical fiber and textile. Pretreatment unit of printing and dyeing process discharge desizing wastewater, scouring wastewater, bleaching effluent and mercerizing wastewater, dyeing process discharge the dyeing wastewater, printing process discharge printing wastewater and soap wastewater, finishing process discharge sorting wastewater [2–3]. In generally, the pH value of PDW is 6 to 10, the COD_{Cr} is 400 mg/L to 1000 mg/L, the BOD_5 is 100 mg/L to 400 mg/L, the SS is 100 mg/g to 200 mg/g, and the color is 100 times to 400 times [4–6]. The quantity of desizing wastewater is about 15% of total PDW while the pollutants is about 50% of the total emissions. The desizing wastewater is alkaline, and the pH value is 9 to 13. The starch desizing wastewater contains large amount of COD and BOD with better biodegradability. PVA desizing wastewater the value of COD can reach 8000 mg/L with poor biodegradability. The scouring wastewater with the character of large quantity, high-concentration organic, high alkaline and temperature, color is brownness and COD or BOD would reach several thousands of mg per liter. Bleaching wastewater is high quantity with low pollutants. Mercerizing wastewater is high alkali level, and the content of NaOH is about 3% to 5%. In general, many factories will recycle NaOH by the method of evaporation and concentration, so mercerizing wastewater is rarely discharged [7]. Dyeing wastewater with the character of great change in quality and quantity and pH is alkaline and reach more than 10. Dyeing wastewater has the following characteristics: high colorimeter, poor biodegradability, lower SS and high COD and BOD. Printing wastewater contains amount of slurry, BOD and COD. Finishing process wastewater mainly contains fiber tow, resin, formaldehyde, oiling agent and sizing agent with little quantity [8].

*Author to whom correspondence should be addressed.
E-mail: liujj0906@163.com

1544-8053/15/01 S085-07

doi:10.12783/issn.1544-8053/12/S1/13

Currently mainly treatment of PDW is centralized processing wastewater mixed by all processes of wastewater by using adsorption method, coagulation, gas flotation method, ultrasound technology, burning method and biooxidation process [9]. There also has some methods about pretreatment to remove COD and PVA of desizing wastewater at home and abroad, such as Fenton oxidation method, catalytic thermal treatment process [10], hybrid anaerobic baffled reactor (HABR) [11]. However, there is no study about individual treatment of desizing wastewater is the most refractory of all processes which has the character of less quantity, high-concentration organic contaminants, low BOD/COD value. In this paper, individual treatment of desizing wastewater is different from the treatment of remainder wastewater (mix-wastewater excepted for the desizing wastewater) in the process. In order to avoid the waste caused by over-treatment the easier degradable remainder wastewater, individual process is merely adopting special process for refractory desizing wastewater, but normal integrated process for the remainder wastewater. Finally, compared with the economy of two treatments mentioned above, it can be decided the feasibility of individual treatment of desizing wastewater.

TECHNICAL AND ECONOMIC FEASIBILITY STUDY OF INDIVIDUAL TREATMENTS OF DESIZING WASTEWATER

Due to small quantity, high-concentration organic contaminants, refractory and poor biochemical purification ability of desizing wastewater, it can be found that the change of quantity is less but the organic contaminants are significantly lower and the biodegradability is obviously improved by comparing originally wastewater with the remainder wastewater. On the basis of regular wastewater treatment, individual process of desizing wastewater is designed using two-stage anaerobic digestion to treat desizing wastewater which is smaller, extremely refractory and extending processing times, it usually uses the method of regular process to treat the remainder wastewater with large quantity, low pollutants and high biodegradability. When using centralized treatment of PDW, due to a large of contaminant with large quantity contained in the mix-wastewater, this process needs to increase the retention time of each unit and the size of each structure in order to achieve treatment efficiency.

Now take 2000-tons per day PDW treatment plant as an example to explore the feasibility of individual treatments of desizing wastewater. Quantity and quality of the water are shown in Table 1.

Table 1. Quantity and Pollutant of Wastewater.

No.	Pollutant	Mix-wastewater	Desizing Wastewater
1	Quantity	2000 m^3/d	300 m^3/d
2	COD_{Cr}	1100 mg/L	3600 mg/L
3	BOD_5	300 mg/L	1000 mg/L
4	SS	500 mg/L	1500 mg/L
5	Color	500 times	500 times
6	pH	9–11	12

The wastewater should reach the Integrated Pollutant Discharge Standard (GB8978-1996). The discharge standard of main pollutant is shown in Table 2 as follows.

The treatment technologies and processes are shown in Figure 1 and Figure 2 [12–13] respectively.

According to the quantity and quality of the water, it can be defined the design parameters of each structure, then calculate the size of structure and select equipment. The specific calculation can be seen as follows.

STRUCTURE CALCULATION AND EQUIPMENT AND EQUIPMENT SELETION OF COMPREHENSIVE TREATMENT OF PDW

Regulation and Aeration Pool

The main performance of regulation and aeration pool is to adjust the quantity of wastewater and uniform water quality. Pre-aeration would wipe off some air in wastewater and increase dissolved oxygen, then promote grease rise to the surface with flocculating activity on wastewater [14]. Regulation and aeration pool is reinforced concrete structure, the adjustment time is 8 h. The pool design size (L × W × H, the unit is meter) is $11 \times 11 \times 6 = 726$ m^3, and the superelevation of the pool is 0.5 m. There are some aerators and two submersible sewage pumps (type is 100WQ100-15-7.5, power is 7.5 kW, one-work-one-standby) in regulating reservoir, and the aeration intensity is 420 m^2/h.

Table 2. The Water Pollutant Discharge Standard.

No.	Pollutant	Discharge Standard
1	COD_{Cr}	≤ 100 mg/L
2	BOD_5	≤ 20 mg/L
3	SS	≤ 70 mg/L
4	Color	≤ 50
5	pH	6–9

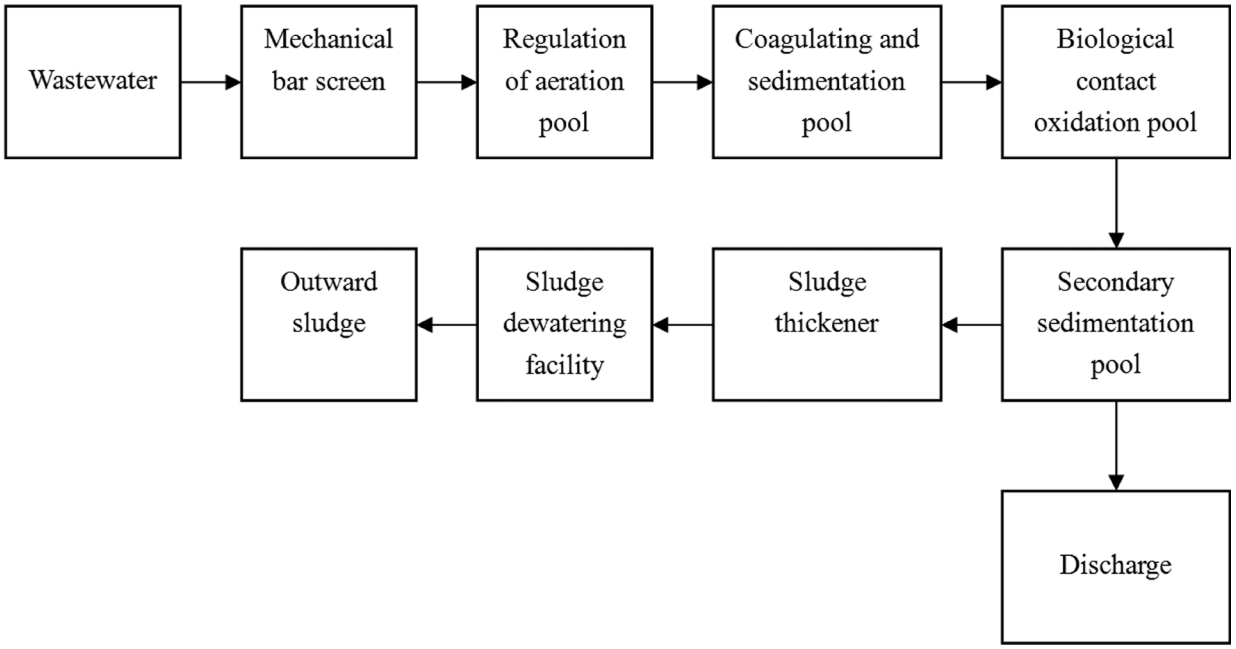

Figure 1. *Comprehensive treatment process of printing and dyeing wastewater.*

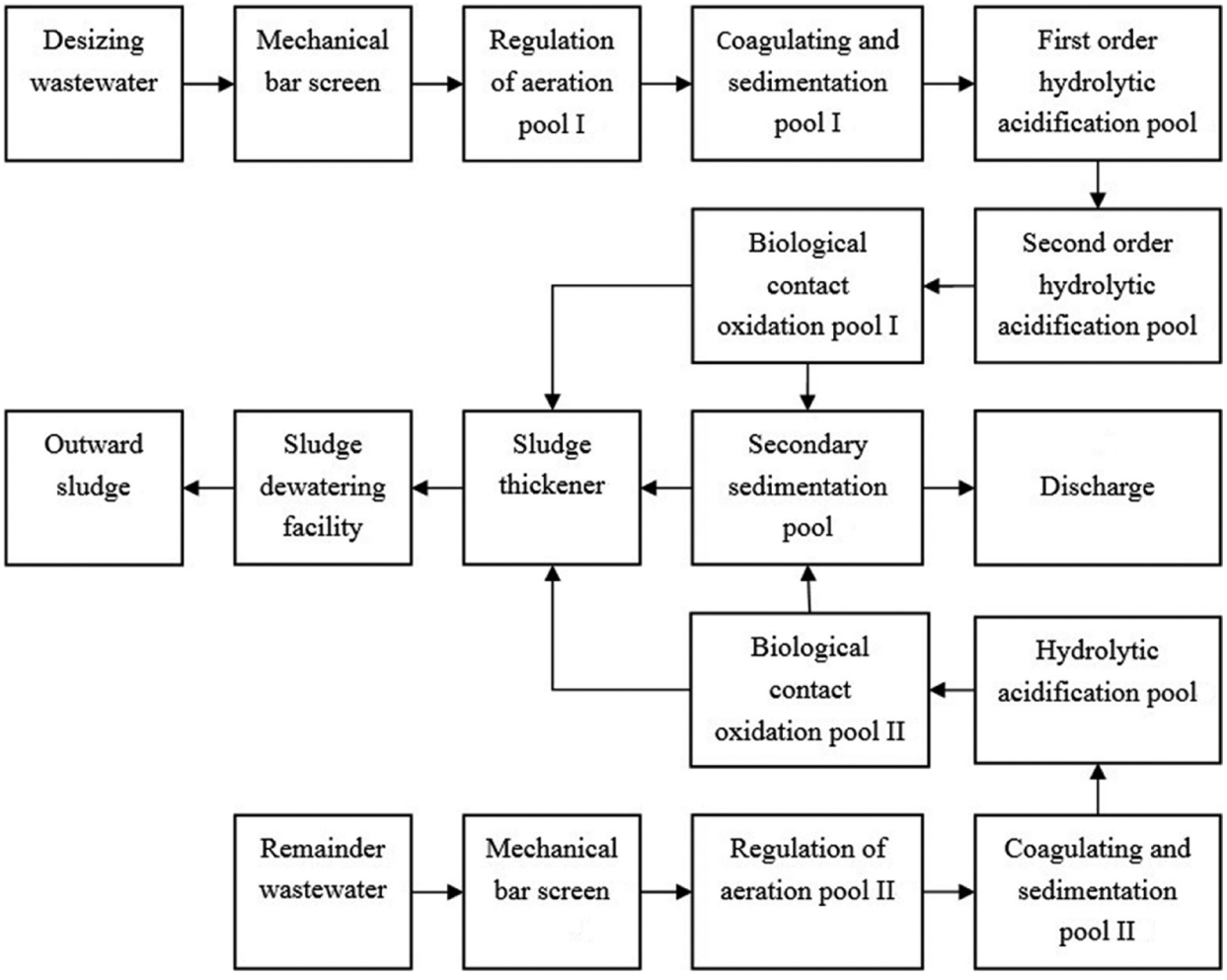

Figure 2. *Individual treatment process of desizing wastewater.*

Coagulating and Sedimentation Pool

The function of the coagulating and sedimentation pool is to remove the suspended material and colloid. Coagulating and sedimentation is not only to reduce the turbid degree of water, color and BOD_5, but also remove the microorganism, bacteria and virus. Coagulant select aluminum sulfate and response time is 30 min. Aluminum sulfate could combine suspended solids and colloid dye in wastewater to form larger flocculation and remove chromaticity by separation precipitation. The structure of the coagulating pool is reinforced concrete, and the design depth of water H is 3.5 m. The volume calculation formula is $V = Q \times 30/60 = 2000 \times 30/(60 \times 24)$, the size of the pool is $4 \times 3 \times 4 = 48$ m^3, and the superelevation is 0.5 m. Sedimentation pool is an inclined plate sedimentation pool. Surface loading of sedimentation pool is 3 m^3/m^2·h, and the size of the pool is $2 \times 2 \times 4 = 16$ m^3.

Hydrolysis Acidification Pool

The main function of hydrolysis acidification pool is to reduce the quantity of organic molecules which makes high molecular organic decompose into low molecular organic and improves the biodegradability. It is benefit for the subsequent aerobic period of treatment. When designing, retention time is 10 h, and the effective volume is 1000 m^3. The superelevation is 0.5 m, so the size of the pool body is $16 \times 13 \times 5.5$=1144 m^3.

Biological Contact Oxidation Pool

The function of biological contact oxidation pool is to make wastewater full contact with carrier. There are abundant microorganism in carrier which can degrade organic pollutant by adsorption, oxidation and generate new bio-film. Meanwhile, the wastewater gets purification. The structure is half ground type of reinforced concrete, retention time is 8 h, and volumetric loading is 2 kg BOD_5/(m^3·day). The gas-water ratio is 15:1, and the volume calculation formula is $V = Q(l_a - l_t)/M = 2000(300 - 20)/(2 \times 1000)$. So the size of the pool is $9 \times 7 \times 5 = 315$ m^3, and the superelevation is 0.5 m. Biological contact oxidation pool is filled with YCDT elastic space packing that is 3 m high and 189 m^3. There are two Roots Blowers (type is 2L52, one-work-one- standby), and the air quantity is 1250 m^3/h.

Secondary Sedimentation Pool

The main function of the secondary sedimentation pool is to remove the suspended solids from wastewater and separate mud with water. The type of secondary sedimentation is inclined plate sedimentation pool. Surface loading of sedimentation pool is 3 m^3/m^2·h, and the size of the pool is $5.5 \times 5.5 \times 4 = 121$ m^3.

Sludge Thickener

The goal of sludge thickener is to reduce the water content of sludge and decrease sludge volume. The structure of sludge thickener is reinforced concrete, the rate of water content of sludge is 99%. Sludge thicker concentration time is 12 h and the pool size is $4 \times 4 \times 5 = 80$ m^3. There are two sludge dewatering facilities (Type is DYQ-1000, power is 2.2 kW, one-work-one-standby) with the capacity is 5–10 m^3/h, and the runtime is 10 h/day.

STRUCTURE CALCULATION AND EQUIPMENT AND EQUIPMENT SELETION OF DESIZING WASTEWATER

Regulation and Aeration Pool I

The regulation time is 12 h, the pool body size is $6 \times 6 \times 4 = 144$ m^3, and the superelevation is 0.5 m. Aeration intensity is 62.5 m^3/h, and the regulating reservoir installation of 2 submersible sewage pumps (Type is 50WQ15-15-1.5, power is 1.5 kW, one-work-one-standby) [14].

Regulation of Aeration Pool II

The regulation time is 6 h, the pool body size is $12 \times 7 \times 5.5 = 462$ m^3, and the superelevation is 0.5 m. Aeration intensity is 354 m^3/h, and the regulating reservoir installation of 2 submersible sewage pumps (Type is 100WQ80-10-4, power is 4 kW, one-work-one-standby).

Coagulation and Sedimentation Pool I

The water depth H is 1.5 m and coagulant adopts aluminum sulfate. Reaction time is 30 min, and the volume formula is $V = Q \times 30/60 = 300 \times 30/(60 \times 24) = 6.25$ m^3. Pool body size is $2 \times 2 \times 2.5 = 10$ m^3, and the superelevation is 0.5 m. Sedimentation pool uses an inclined board setting basin, and the amount is one.

The surface loading is 3 $m^3/m^2 \cdot h$, and the size of sedimentation pool is $2 \times 2 \times 4 = 16$ m^3.

Coagulation and Sedimentation Pool II

The water depth H is 1.5 m and coagulant adopts aluminum sulfate. Reaction time is 30 min, and the volume formula is $V = Q \times 30/60 = 1700 \times 30/(60 \times 24) = 35$ m^3. Pool body size of coagulation is $4 \times 3 \times 4 = 48$ m^3, and the superelevation is 0.5 m. Sedimentation pool uses an inclined board setting basin, and the amount is one. The surface loading is 3 $m^3/m^2 \cdot h$, and the size of sedimentation pool is $4.5 \times 4.5 \times 4 = 81$ m^3.

First Order Hydrolytic Acidification Pool and Second Order Hydrolytic Acidification Pool

The residence time of each hydrolytic acidification pool is 8 h, and the effective volume of each pool is $300 \times 1.2 \times 8/24 = 120$ m^3. The size is $6 \times 5 \times 5 = 150$ m^3, and the superelevation is 0.5 m.

Hydrolytic Acidification Pool

Retention time is 6 h, and the effective volume is $1700 \times 1.2 \times 6/24 = 510$ m^3. The size of pool is $10 \times 10 \times 5.5 = 550$ m^3, and the superelevation is 0.5 m.

Contact Oxidation Pool I

Retention time is 8 h, volumetric loading is 2 kg $BOD_5/(m^3 \cdot day)$, the gas-water ratio is 15:1, the air quantity is 225 m^3/h, and the volume formula is $V = Q(l_a - l_t)/M = 300 \times (1000 - 20)/(2 \times 1000) = 147$ m^3. The size of pool is $6 \times 5 \times 5.5 = 165$ m^3, and the superelevation is 0.5 m. In the pool, it adopts YCDT elastic space packing, its height is 3 m and volume is 90 m^3.

Contact Oxidation Pool II

Residence time is 4 h, volumetric loading is 2 kg $BOD_5/(m^3 \cdot day)$, the gas-water ratio is 15:1, the air quantity is 530 m^3/h, and the volume formula is $V = Q(l_a - l_t)/M = 1700 \times (180 - 20)/(2 \times 1000) = 136$ m^3. The size of pool is $6 \times 5 \times 5.5 = 165$ m^3, and the superelevation is 0.5 m. In the pool, it adopts YCDT elastic space packing, its height is 3 m and volume is 82.5 m^3.

The total air quantity of pool I and Pool II is $255 + 530 = 755$ m^3/h, there are two Roots Blowers (Type is 3L44, one-work-one-standby).

Secondary Sedimentation Pool

The sedimentation pool type is inclined board setting basin, and the structure of pool is reinforced concrete. Its surface loading is 4 $m^3/m^2 \cdot h$, and the size is $5 \times 5 \times 4 = 100$ m^3.

Sludge Thickener

The operation mode of the thickener is intermittent operation, the concentration time is12 h, the water content of sludge is 99%, and the size of the sludge thickener is $4 \times 4 \times 5 = 80$ m^3. There are two sludge dewatering facilities (Type is DYQ-1000, power is 2.2 kW, one-work-one-standby). The machine runtime is 10 h/day, and the throughput of sludge is 5–10 m^3/day.

COST ANALYSIS

Construction Cost

Because of the construction of dyeing treatment plant is large in investment, so the structure and equipment cost account for larger proportion of the total investment of construction cost in the economic budget. Due to the limit of research condition, the construction cost can not be accurate calculated according to the actual construction situation, so its estimate is based on the volume of pool. In this paper, through a great deal of research and literature review, considering the factors of excavated volume and reinforcement, the cost of pool is 700 Yuan per cubic meter of pool volume. The cost of structures and equipments are shown in Table 3.

Operating and Processing Cost

Operating cost of wastewater treatment plant is composed of wage, power cost, maintenance cost, chemical cost and other cost [15]. Operating cost and depreciation cost contain processing cost. This paper points out that electricity price is 0.6 Yuan/(kW·h), the power consumption of comprehensive treatment of wastewater is about 1400 kW/day and individual treatment of desizing wastewater is 1300 kW/day. Employee wages is 20000 Yuan a year per person, each process employs 6 people. Water is 1 Yuan/m^3, water consumption of each process is 500 m^3/day. The paper points out that chemical cost is 0.4 Yuan per ton in the comprehensive treatment of PDW, the desizing wastewater treatment is 0.5 Yuan per ton and the remaining

Table 3. Cost of Structure and Equipment.

No.	Structures and Equipment Name of Comprehensive Treatment Process	Price (Yuan)	Structures and Equipment Name of Desizing Wastewater Individual Treatment Process	Price (Yuan)
1	Regulation of aeration pool	508,200	Regulation of aeration pool I	100,800
2	Coagulation sedimentation pool	44,800	Regulation of aeration pool II	323,400
3	Hydrolytic acidification pool	800,800	Coagulation sedimentation pool I	18,200
4	Contact oxidation pool	220,500	Coagulation sedimentation pool II	90,300
5	Secondary sedimentation pool	84,700	First order hydrolytic acidification pool	105,000
6	Sludge thickener	56,000	Second order hydrolytic acidification pool	105,000
7	Mechanical bar screen	20,000	Hydrolytic acidification pool	385,000
8	Submersible sewage pump	20,000	Contact oxidation pool I	115,500
9	Roots Blower (3L52)	316,000	Contact oxidation pool II	115,500
10	Dehydrator (DYQ-1000)	240,000	Secondary sedimentation pool	70,000
11	Elastic packing	47,000	Sludge thickener	56,000
12			Mechanical bar screen	25,000
13			Submersible sewage pump	12,000
14			Submersible sewage pump	16,000
15			Roots Blower (3L44)	256,000
16			Dehydrator (DYQ-1000)	240,000
17			Elastic packing	43,000
Total		**2,358,000**		**2,076,700**

part of wastewater treatment is 0.25 Yuan per ton in the individual treatment of desizing wastewater. In general, maintenance fee and instrument calibration fee is about 5% of the equipment cost, maintenance cost of equipment and pipeline is 1% of the equipment cost, so the total maintenance cost is about 6% of equipment cost. Depreciation cost is calculated by the depreciation period of 25 years, residuals rate is 5%. Other cost is about 15% of the sum of electricity, staff welfare, water, chemical cost, maintenance cost and depreciation cost [16]. Specific costs are shown in Table 4.

Through the analysis of construction cost, operation cost, processing cost, it can be found that operating cost and treatment cost of individual treatment of desizing wastewater are 970,700 Yuan per year and 1,049,600 Yuan per year, the unit treatment cost is 1.44 Yuan per cubic meter, and the operating cost and processing cost of comprehensive treatment of wastewater are 1,095,100 Yuan per year and 1,184,700 Yuan per year, the unit treatment cost is 1.62 Yuan per cubic meter.

Life Cycle Cost

Life cycle cost is the sum of construction cost and operation cost minus the net salvage value, the LCC analysis is mainly based on discount rate which is determined by the loan interest and the CPI values and would have wave motion in different age. according to figures released by the people's bank of China, in recent years, the average loan interest is 6.4% and the average CPI is 3.7% from 2006 to 2011, the discount rate is 10.3% (6.4% + 3.7% + 3.7% × 6.4%) [17]. The present discounted value of total operating cost of individual treatment desizing wastewater and comprehensive treatment wastewater is 8,790,500 Yuan and 9,920,000 Yuan, the construction cost is 2,076,700 Yuan and 2,358,000 Yuan and the net salvage value is 103,800 Yuan and 117,900 Yuan, respectively. So, the total of LCC is 10,763,400 Yuan and 12,160,100 Yuan respectively.

CONCLUSION

Compared individual treatment of desizing wastewater with comprehensive treatment of PDW in the

Table 4. Cost Analysis.

No.	Classification	Comprehensive Treatment of Wastewater (Yuan/year)	Individual Treatment of Desizing Wastewater (Yuan/year)
1	Electricity fee	307,000	285,000
2	Staff welfare	120,000	120,000
3	Water rates	183,000	183,000
4	Chemical cost	292,000	210,000
5	Maintenance cost	38,600	35,800
6	Depreciation cost	89,600	78,900
7	Other cost	154,500	136,900
8	Operating cost	1,095,100	970,700
9	Treatment cost	1,184,700	1,049,600

process, examples have shown that the craft of comprehensive treatment wastewater is simpler than that of individual treatment desizing wastewater, and the total number of pool is less while the total volume of pool is larger. At last, through calculated an real examples that 2000-tons per day PDW treatment plant and compared with the economic of individual treatment desizing wastewater and comprehensive treatment wastewater, it can be concluded that individual treatment of desizing wastewater will save 0.18 Yuan per ton than centralized treatment of dyeing wastewater. In this study, through the calculation of wastewater treatment plant with small water, it can be obtained that the total of LCC will save 1,396,700 Yuan. When using this treatment method in the plant with large water, as the base of construction cost increasing, life cycle cost would save much more. According to the result of calculation, individual treatment is more cost savings, so it can be considered that the method of individual treatment is feasible and it has a good potential applications in practice.

REFERENCE

1. Wang, J. F., Y. W. Zhao & Y. F. Mao. "Research progress of printing and dyeing wastewater treatment", *China Environmental Protection Industry*, 2012, No. 4, 30.
2. Sun, Z., "Characteristics of dyeing wastewater and the summary of biological treatment technology", *Coal Mine Modernization*, 2007, No. 1, 62.
3. Yu, Q. Y., "Advances in the treatment of printing and dyeing wastewater", *Industrial Safety and Environmental Protection*, 2011, Vol. 37, No. 8, 41.
4. Cao, F., "The quality characteristics and processing technology of printing and dyeing wastewater", *Science & Technology Information*, 2007, No. 19, 286.
5. Liang, J. & M. M. Cao. "Characterization of dyeing effluents and its treatment techniques", *Ground Water*, 2011, Vol. 33, No. 2, 67.
6. Wei, T. J., "The process selected of wastewater treatment of printing and dyeing industry", *Inner Mongolia Environmental Protection*, 2007, Vol. 19, No. 1, 54.
7. Z. B. He: "Characterization of dyeing effluents and their treatment techniques", *Dyeing & Finishing*, 2007, No. 17, 41.
8. Yu, Y., "Industrial printing and dyeing wastewater treatment technology", *Coastal Enterprises and Science & Technology*, 2009, No. 5, 33-35.
9. Wang, H., Y. Zhang & L. C. Li. "Present situation and development trend of printing and dyeing wastewater treatment technology", *Modern Business Trade Industry*, 2009, No. 10, 280.
10. Kumar, P., B. Prasad & S. Chand. "Treatment of desizing wastewater by catalytic thermal treatment and coagulation", *Journal of Hazardous Materials*, 2009, Vol. 163, No. 1, 433. http://dx.doi.org/10.1016/j.jhazmat.2008.06.114
11. Liu, R. R. *et al.* "The performance evaluation of hybrid anaerobic baffled reactor for treatment of PVA-containing desizing wastewater", *Desalination*, 2011, Vol. 271, No. 1-3, 287. http://dx.doi.org/10.1016/j.desal.2010.12.044
12. Li, J. Y., X. F. Ren & J. Y. Yang. "Hydrolytic acidification/delay aeration process for treatment of printing and dyeing wastewater", *Chemical Engineering and Equipment*, 2013, No. 7, 203.
13. Xu, Y. F. *et al.* "Anoxic/aerobic process for treatment of high strength PVA desizing wastewater", C*hina Water and Wastewater*, 2004, Vol. 20, No. 8, 80.
14. Du, F. & L. X. Ma. "The engineering desizing of the Treatment Process of Printing and Dyeing Wastewater", *Environmental Engineering*, 2009, Vol. 27, No. 2, 18.
15. Dai, S. M., X. W. Lu & X. N. Li. "Analysis on operating cost of waste water treatment infrastructure", *Journal of Nantong Vocational College*, 2005, Vol. 19, No. 4, 78.
16. Yuan, P. S., "The treatment cost analysis of sewage treatment plant", *Environmental Engineering*, 2008, Vol. 26, No. 2, 55–56.
17. Huang, H., Q. Zhang & B. Fu. "Comparison between investment programs of WWTP based on LCC theory", *China Water and Wastewater*, 2013, Vol. 29, No. 1,102–103.

Effects of Long-term Elevated CO_2 Fumigation on Microbial Communities in a Wetland Soil

X. SUI[1,2,3,4], R. T. ZHANG[1,2,3], L. B. YANG[1,2,3], H. X. ZHONG[1,2,3], J. F. WANG[1,2,3] and H. W. NI[1,*]

[1]*Institute of Natural Resource, Heilongjiang Academy of Sciences, Harbin 150040*

[2]*National and Provincial Joint Engineering Laboratory of Wetlands and Ecological Conservation, Harbin 150040*

[3]*Key Laboratory for Wetland and Restoration Ecology in Heilongjiang Province, Harbin 150040*

[4]*Northeast Forestry University, Harbin 150040*

ABSTRACT: In this study, we studied the effects of different Carbon dioxide concentrations on microbial community diversity in a wetland ecosystem in northern China. The open-top chamber (OTC) was situated in the boggy soil in which the dominant plant is *Deyeuxia angustifolia*. Between 2010 and 2013, we maintained the average Carbon dioxide concentration in OTC at 370 ppm, 550 ppm and 700 ppm. Soil samples were collected during the last year. Results show that soil fungal diversity indices in the 0–10 cm soil layer were significantly decreased by elevated concentration of CO_2 by 4.570 in ck. It was increased by 4.456, 4.373 and 4.13 by 350 ppm, 500 ppm and 700 ppm CO_2, respectively. Soil bacterial diversity indices in the 0–10 cm soil layer, however, were not significantly influenced by elevated CO_2 ($P > 0.05$). The results of principal component analysis (PCA) and Redundancy analysis (RDA) indicate that elevated CO_2 had no strict specificity with bacterial community diversity but strict specificity with fungal community, while environmental condition had great influence on fungal community diversity and soil nutrient. Organic carbon, nitrate nitrogen (NO-N), C/N, total nitrogen (N) and pH were the primary impact factors. These results suggest that the environmental conditions exhibit great influence on the community diversity of fungi and bacteria. It is also found that soil nutrient were indicative of the change of community diversity of fungi and bacteria.

INTRODUCTION

DUE to human activity, the CO_2 concentrations have been rising since the Industrial Revolution (IPCC, 2007; Vingarzan, 2004). CO_2 concentration is predicted to continue to increase at the level of 1.5 ppm per year, which may lead to a substantial increase of CO_2 level of 360 ppm to increase to 550 ppm by the mid-21st century (IPCC, 2007). The effects of global change on soil microbial communities are very important in that microbes can influence the ecosystems through their effects on carbon and nutrient cycling, yet there is little that has been reported. Soil microbial communities still have mysteries due to their extraordinary complexity (Chatinotas, 1998; Curtis, 2003). However, microbial ecology studies have developed because of the molecular techniques (Pace, 1997; Hugenholtz, 1998) with many complex phylogenetic techniques (Bohannan, 2003; Martin, 2002). This study investigated the effects of continuing elevated CO_2 concentration in a 4-year period on the microbial community in a wetland system in northern China. The system afforded an opportunity to study how elevated CO_2 interacts with a complex landscape in a natural ecosystem which is strongly impacted by water. The hypothesis that elevated CO_2 alters microbial community structure was tested by comparing microbial parameters in an open top chamber treatment ring and its surrounding landscape.

MATERIALS AND METHODS

Field Site and Soil Sampling

Soil samples were collected at Honghe nature reserve (E133°34′38″–133°46′29″, N47°42′18″–47°52′00″) wetland ecological system in Heilongjiang province, northeastern China. The soil is albic soil and marsh soil. The mean annual temperature is 1.9°C and annual average precipitation is 585 mm. The open-top chambers (each 4.2 m in diameter with hexagon and 2.8 m in height enclosed with a clear glass open-top chamber) were established in order to control CO_2 levels at the research station of Honghe nature reserve wetland

*Author to whom correspondence should be addressed.
E-mail: nihongwei2000@163.com; Telephone:+86-13503685999

1544-8053/15/01 S093-04

doi:10.12783/issn.1544-8053/12/S1/14

Ecosystems of Heilongjiang Academy of Sciences in the spring, 2009. *Deyeuxia angustifolia* were planted in May, 2009 and CO_2 began to increase after seeds germination. In each year, the exposure period was from the middle of April to the middle of October (the whole growing season). Three chambers were maintained at ambient atmospheric CO_2 concentrations (ca. 370 $\mu mol \cdot mol^{-1}$); the other six chambers were maintained at elevated levels (ca. 500 $\mu mol \cdot mol^{-1}$ and ca. 700 $\mu mol \cdot mol^{-1}$) by dispensing 100% CO_2 into the blower fans during the whole day. Flow rate of 100% CO_2 into the chambers was adjusted, if necessary, to maintained CO_2 concentrations. The CO_2 concentrations at OTC were monitored by an infrared gas analyzer (A-SENSE-D, Sense Air, Sweden). During July 2012, five soil samples for each site were randomly collected and immediately transported to the laboratory. The five soil samples mixed together and sieved to form a single soil sample, then stored at –20°C (Zheng, 2009).

The soil physical and chemical properties are described in Table 1.

DNA Extraction

Total DNA was extracted from 0.25 g soil using Power Max Soil DNA Isolation Kit (Mo Bio Laboratories Inc., Solana Beach, CA, USA), according to the manufacture's instructions. DNA extracts were stored at –20°C.

PCR Amplification

PCR amplification targeting the ITS rRNA gene of fungi was performed with the universal primers ITS1F (5′-(6-FAM)-CTTGGTCATTTAGAGGAAG-TAA-3′) labeled with 6-FAM fluorescence and ITS4 (5′-TCCTCCGCTTATTGATATGC-3′) and V3 region of the bacterial 16S rDNA with universal primers 27F (5′(6-FAM)-AGAGTTTGATCCTGGCTCAG-3′) and 1492R (5′-GGTTACCTTGTTACGACTT-3′). PCR reaction mixtures (25 µl) included 12.5 µl PCR mix (TaKaRa, Japan), 1.5 µl 10 µmol/L primers, 1 µl template DNA and were performed in triplicate for each sample. The PCR products were purified with the DNA Clean-up kit (Tiangen, China) PCR products were digested with the enzyme Hha I, the reaction programs was 37°C for 4 h. The DNA fragments were sent to Shanghai Sangon Co. for analysis using ABI 3730 system analyzer.

Data Analysis

To evaluate the effects of CO_2 concentration on soil microbial structure and function, Comparison of means was done using the one-way analysis of variance (ANOVA) and the least significant difference (LSD). When the results were significantly different ($P < 0.05$), Duncan post-hoc test was used to analyze multiple comparisons. Each terminal restriction fragment (T-RF) (Liu, 1997) in the profiles was considered as an operational taxonomic unit (OTU); Fluorescent fragments with peak height less than 50 were excluded from the analysis. Based on the number and abundance of OTU in the profiles, the Shannon diversity index (H), the Evenness index (E) and Simpson diversity index were measured using the Bio-dap software (Thomas, 2000). Statistical analysis was performed by Microsoft Excel (2003) and SPSS version 13.0.

Results

The Variation of Diversity of Fungi and Bacteria Under Different CO_2 Concentrations

The T-RFLP fingerprinting of fungi was performed using the restriction enzyme Hha I. According to the number of T-RFs and the relative peak heights, Shannon diversity index, Evenness index, and Simpson index were calculated (Table 2). The fungal community diversity indices revealed that fungal diversity differed greatly among the three CO_2 concentrations. The fungal diversity of different CO_2 elevation conditions is significant (see table 2), while the Shannon index of 370 ppm and 500 ppm does not show significant difference compared with ck, and the 700 ppm shows significant difference with ck ($p < 0.05$). The evenness

Table 1. The Physical and Chemical Properties of Soil.

Sites (ppm)	C (g/kg)	N (g/kg)	Ammonium Nitrogen (mg/kg)	Nitrate Nitrogen (mg/kg)	pH
370	206.22^{B}	5.20^{B}	15^{AB}	4.9^{BA}	5.01^{B}
550	189.50^{A}	5.61^{D}	17^{C}	4.5^{A}	5.11^{C}
700	196.41^{B}	5.54^{C}	14^{AB}	4.4^{A}	4.98^{B}
ck	191.46^{A}	4.42^{A}	13^{A}	4.3^{A}	4.76^{A}

Table 2. The Variation of Soil Fungi Diversity in Different CO_2 Elevation Conditions.

Fungi	Shannon Index	Evenness Index	Simpson Index
370 ppm	$4.456^{B} \pm 0.125$	$0.970^{A} \pm 0.000$	$0.013^{A} \pm 0.000$
500 ppm	$4.373^{AB} \pm 0.106$	$0.970^{C} \pm 0.000$	$0.014^{AB} \pm 0.001$
700 ppm	$4.130^{A} \pm 0.226$	$0.963^{B} \pm 0.001$	$0.005^{B} \pm 0.003$
ck	$4.570^{B} \pm 0.061$	$0.970^{C} \pm 0.000$	$0.011^{A} \pm 0.000$

Table 3. The Variation of Soil Bacteria Diversity in Different CO_2 Conditions.

Bacteria	Shannon Index	Evenness Index	Simpson Index
370 ppm	3.587 ± 0.275	0. 943 ± 0.057	0.327 ± 0.010
500 ppm	3.757 ± 0.275	0. 943 ± 0.057	0.273 ± 0.004
700 ppm	3.620 ± 0.173	0. 943 ± 0.057	0.032 ± 0.007
ck	3.680 ± 0.223	0. 943 ± 0.057	0.303 ± 0.007

of soil fungi is consistent in the three CO_2 elevation conditions.

For bacterial diversity, T-RFLP fingerprinting was performed also using the restriction enzyme Hha I. The Shannon index and Evenness index were lower than those of fungi. The Shannon index increased gradually from 350 ppm to ck, but the Shannon index, Evenness and Simpson index were not significantly ($p > 0.05$) different among different CO_2 conditions (Table 3).

Principal Component Analysis (PCA) of Soil Microorganism under Different CO_2 Concentrations

PCA was performed to analyze the microbial community in soils. Results of fungi [Figure 1(a)] showed that the total variance explained by the first principal component was 25.82% and twelve samples were divided into two groups, with samples ck in one group and the others in a second group. The percentage of variance explained by the second principal component was 10.99% and the two parts of that sample were further divided into three categories and distributed into three quadrants. PCA of bacteria [Figure 1(b)] showed that the contribution from the first principal component was 40.22%, and twelve samples were divided into two parts. Samples of 350 ppm resided in one group and the rest formed another group. The second principal component of the contribution rate was 9.6% and the two parts of the sample were further divided into three categories and distributed into three quadrants. These results indicate that CO_2 elevation had no specificity with bacterial community diversity, while the fungi community diversity showed regionalism. In figure 1A, in the second axis, the CK was divided into one group, and the others into one group, so the fungi diversity showed clearly.

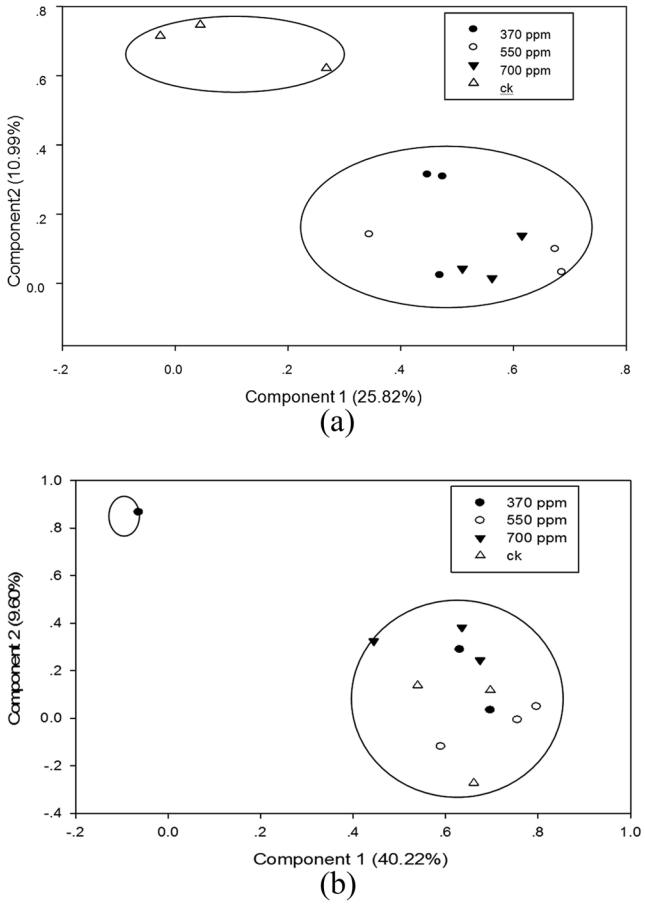

Figure 1. *Qualitative analysis of the main T-RFs of microorganism.*

Redundancy Analysis (RDA)

The relationship between environmental conditions and community diversity was analyzed (Figure 2). Results show that organic carbon (C) has the greatest influence on the community diversity followed by nitrate nitrogen (NO-N), C/N, total nitrogen (N) and ammonium nitrogen (NH-N). Organic carbon and nitrate nitrogen were positively correlated with the fungal and bacterial community diversity indices except evenness index of fungi. Total nitrogen, pH and C/N were positively correlated with three indices, including fungal Shannon diversity index (HF), bacterial species richness index (SB), species richness index of fungi (SF).

DISCUSSION

There were great differences of the fungal (not in bacteria, as stated below) community diversity between different treatments. Many studies in the litera-

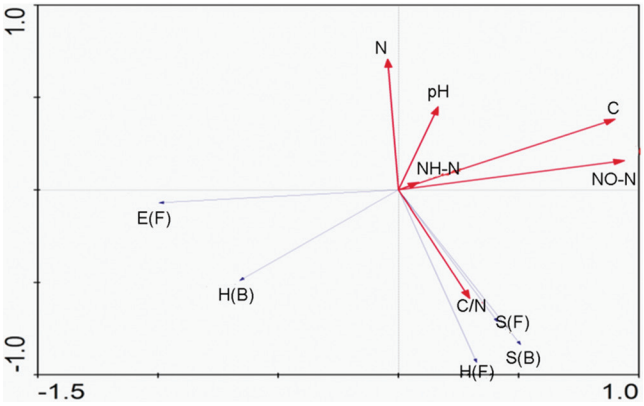

Figure 2. *RDA analysis of bacteria and fungi. The multi-axial figure of environmental conditions and community diversity. H(B), bacterial Shannon diversity index; S(B), bacterial species richness index; E(F), Evenness index of fungi; H(F), Shannon diversity index of fungi; S(F), species richness index of fungi; N, total nitrogen; NH-N, ammonium nitrogen; NO-N, nitrate nitrogen; C, organic carbon.*

ture show that high concentration CO_2 can significantly change the fungal structure and abundance (Morten *et al.*, 2002; Janus *et al.*, 2005), but some other studies found that the fungal structure did not change under increased CO_2 (Klamer *et al.*, 2002). In this study, the community diversity indices showed that CO_2 evaluation on the wetlands was effective. The Shannon diversity index of fungi in control (CK) was the highest followed by 370 ppm, 500 ppm and 700 ppm, indicating that the enhanced CO_2 concentration has changed the fungal structure significantly. However, little information on bacterial community to elevated CO_2 between OTC and control plots is primarily due to the fact that bacterial Shannon diversity did not change significantly. Soil organic carbon could significantly affect fungal structures, while its effect on bacterial diversity was minimal. PCA and RDA showed that bacterial community diversity had no strict specificity with increased CO_2 concentration and this is in line with the findings from David (2005). This study indicated that fungi, rather than bacteria, respond to elevated CO_2 concentration and that the respiratory properties of fungi and bacteria were significantly different. This result emphasizes the need to better understand the relationship between microbial community structure and CO_2 elevation.

ACKNOWLEDGEMENTS

This research was supported by the National Natural Science Foundation (NO.31470019, NO.31370426, NO.31170462), and Key Project of Youth Innovation Fund, Heilongjiang academy of sciences, Special project of subject team innovation ability enhancement, Heilongjiang academy of sciences (2014ST05).

REFERENCE

1. A. P. Martin: "Phylogenetic approaches for describing and comparing the diversity of microbial communities", *Appl Environ Microb* (AEM), 2002, 68, 3673–3682. http://dx.doi.org/10.1128/AEM.68.8.3673-3682.2002
2. A., R. A. Chatzinotas, W. Sandaa: "Analysis of broad-scale differences in microbial community composition of two pristine forest soils". *Syst. Appl. Microbiol*, 1998, 21, 579–587. http://dx.doi.org/10.1016/S0723-2020(98)80070-2
3. B. J. M. Bohannan and J. Hughes: "New approaches to analyzing microbial biodiversity data", *Curr. Opin. Microbiol*, 2003, 6, 282–287. http://dx.doi.org/10.1016/S1369-5274(03)00055-9
4. D. A. Lipson, M. Blair, G. Barron-Gafford: "Relationships between Microbial Community Structure and Soil Processes under Elevated Atmospheric Carbon Dioxide", *Microbial Ecol*, 2006, 51, 302–314. http://dx.doi.org/10.1007/s00248-006-9032-1
5. G. Thomas and D. Clay: "Bio-Dap, ecological diversity and its measurement." Alma, New Brunswick, Canada, Fundy National Park, Available at: http://nhsbig.inhs.uiuc.edu/wes/populations. Accessed 2000, 2006.
6. IPCC: "Climate Change 2007—the Physical Science Basis. Working Group I Contribution to the Fourth Assessment Report of the IPCC". 2007, Cambridge University Press, Cambridge, UK, 2009.
7. J. Q. Zheng, S. J. Han, F. R. Ren, Y. M. Zhou, X. B. Zheng, Y. Wang: "Effects of long-term CO_2 fumigation on fungal communities in a temperate forest soil", *Soil. Biol. Biochem*, 2009, 41, 2244–2247. http://dx.doi.org/10.1016/j.soilbio.2009.07.029
8. K. Morten, S. R. Michael, H. L. Lanfang, G. D. Bert, L. G. Jay: "Influence of Elevated CO2 on the Fungal Community in a Coastal Scrub Oak Forest Soil Investigated with Terminal-Restriction Fragment Length Polymorphism Analysis", *Appl. Environ. Microbiol*, 2002, 68: 4370-4376. http://dx.doi.org/10.1128/AEM.68.9.4370-4376.2002
9. L. R. Janus, N. L. Angeloni, J. McCormack: "Elevated atmospheric CO_2 alters soil microbial communities associated with trembling aspen (Populus tremuloides) roots", *Microbial Ecol*, 2005, 50, 102–109. http://dx.doi.org/10.1007/s00248-004-0120-9
10. W. Liu, T. Marsh, H. Cheng, L. Forney: "Characterization of microbial diversity by determining terminal restriction fragment length polymorphisms of genes encoding 16S rRNA", *Appl. Environ. Microbiol*, 1997, 63: 4516-4522.
11. M. Klamer, M. S. Roberts, L. H. Levine, D B. Grake and J. L. Garland: 'Influence of elevated CO_2 on the fungal community in a coastal scrub oak forest soil investigated with terminal-restriction fragment length polymorphism analysis", *Appl Envir Micro*, 2002, 68, 4370–4376. http://dx.doi.org/10.1128/AEM.68.9.4370-4376.2002
12. N. R. Pace: "A molecular view of microbial diversity and the biosphere", *Science*, 1997, 276, 734–740. http://dx.doi.org/10.1126/science.276.5313.734
13. P. Hugenholtz, B. M. Goebel, N. R. Pace: "Impact of culture-independent studies on the emerging phylogenetic view of bacterial diversity", *J. Bacteriol.*, 1998, 180, 4765–4774.
14. R. Vingarzan: "A review of surface ozone background levels and trends", *Atmos Environ*, 2004, 33, 3431–3442. http://dx.doi.org/10.1016/j.atmosenv.2004.03.030
15. T. P. Curtis, W. T. Sloan, and J. W. Scannall: "Estimating prokaryotic diversity and its limits", *Proc. Natl. Acad. Sci*, 2002, 99, 10494–10499. http://dx.doi.org/10.1073/pnas.142680199

Human Health Risk Assessment of Harmful Trace Elements in Coal Gasification Residues

JIANLI JIA*, YU WU, LE YANG, PEIJING WU, XIAOJUN LI and XUETING SUN
School of Chemical and Environmental Engineering, China University of Mining & Technology (Beijing), Beijing, 100083, China

ABSTRACT: On the basis of a pilot study, the present study established an efficient method for the assessment of human health risks caused by some harmful trace elements (e.g., arsenic, beryllium, mercury and fluorine) in coal gasification residues. The proposed assessment procedure was divided into five basic steps, namely, hazard identification, exposure assessment, toxicological evaluation, risk characterization and control value calculation. The results showed that the carcinogenic risks within sensitive areas could reach 2.31×10^{-4} and the total non-carcinogenic hazard quotient of these four harmful trace elements within sensitive areas was 12.13, which is much higher than the referencing risk level as 10^{-6} for carcinogenic risk and 1 for non-carcinogenic. In terms of risk management, it could be suggested that the concentration of Arsenic should be controlled under 7.29 $mg \cdot kg^{-1}$ within sensitive areas, meanwhile under 1.59×10^{-4} $mg \cdot kg^{-1}$ within insensitive areas.

INTRODUCTION

With the rapid growth of advanced large-scale coal gasification technology, recent years have witnessed the increasing discussion regarding human health risks caused by coal pollution. Since more and more residual waste, containing trace elements that are harmful to human health, has been released into the environment, such released contaminants would pose a serious threat to human life. Although the history of coal exploitation dates from the 18th century, the research on coal trace elements has lasted for only a century. In China, although scholars started to study coal pollution problems in 1970s, their focus was on the environmental impacts associated with coal combustion products (e.g., coal slag, ash and smoke dust). In recent years, researchers started to put emphasis on the impacts of coal trace elements on human health (Dai, 2012; Swaine, 2000). Meanwhile, numerous analytical approaches and models have been developed and implemented to address the assessed risks of coal organic and inorganic pollutants (Yu *et al.*, 2014). Peña-Fernández *et al.* (2014) established a model for the assessment of human health risks of metals and metalloids in urban environments, and the finding was that the content of contaminants in soils, such as arsenic or chromium, has exceeded the safe level for public. With the rapid development of the modern coal chemical industry, coal gasification process has produced significant coal waste. However, it is surprising that the studies on the impacts of coal gasification residues on underground water quality and human health has remained quite limited.

In this paper, an effective analytical/assessment method was established to evaluate potential risks to human health caused by harmful trace elements (Arsenic, Beryllium, Mercury and Fluorine) found in coal waste during the intake process. Chinese standard HJ25.3-2014 was used for reference since it provides guidance regarding the assessment of potential risks to human health at contaminated sites. Based on the obtained results and identified patterns, this paper provided human health risk assessment of harmful trace elements, and calculated safety control values as advised. Therefore, this current study is of significance to the maintenance of environmental safety as coal gasification and coal chemical industry keeps developing. It also provides instructive suggestions for environment capacity assessment, for effective advance warning, and for promoting clean coal processing, utilization and sustainable development.

*Author to whom correspondence should be addressed.
E-mail address: jiajianli77@126.com; Tel:+86-13810103722

1544-8053/15/01 S097-08

doi:10.12783/issn.1544-8053/12/S1/15

MATERIAL AND METHODS

Sample Collection and Analysis

The pilot coal gasification plant was located in Langfang (north latitude 39°34′83″ and east longitude 116°45′52.9″ in China PR), and the gasifying craftwork was carried out using a Surface gasifier. Cinder samples were randomly sampled from different distances (1.1 m, 1.8 m, 2.0 m, 2.5–3 m, and 3.5 m) to the gasification kindling point.

The coal underground gasification residue static leaching experiments were carried out to analyze the transfer characteristics of harmful trace elements to the groundwater environment using pure water as the extractant. Cinder samples (5g) were treated with 5 ml deionized water to obtain the leachate liquor by using horizontal vibration extraction procedure according to HJ557-2009 (Solid waste-Extraction procedure for leaching toxicity-Horizontal vibration method). The concentrations of Hg, F, and Be were analyzed by using inductively coupled plasma-mass spectrometry (ICP-MS, NexION 300D). The accuracy of the instrumental methods was checked by duplication of the samples, as well as by using control groups. All the following values are the average data of the three performed measurements. Concentrations of each trace element are provided in Table1.

Exposure Assessment

This study used two exposure scenarios, namely, sensitive areas and insensitive areas, to assess human health risks due to the lack of information about the test sites. The assessment of human exposure to a contaminant was generally estimated by measuring the daily intake and uptake of this contaminant. Since there is a total of nine exposure pathways, this paper only discusses the pathway of oral ingestion in underground water.

Exposure routes were considered for assessing non-carcinogenic and carcinogenic risks of trace elements.

Table 1. Trace Elements Concentrations in Simulating Ground Water Leaching Solution of Cinder Samples.

Sites (ppm)	1.1 m	1.8 m	2.0 m	2.5–3 m	3.5 m
As ($\mu g \cdot L^{-1}$)	0.97	3.72	3.44	4.19	16.80
Be ($\mu g \cdot L^{-1}$)	0.06	0.06	0.11	0.12	0.42
Hg ($\mu g \cdot L^{-1}$)	3.03	0.07	0.11	0.05	0.05
F ($\mu g \cdot L^{-1}$)	4.21	0.36	0.48	0.23	0.66

Usually, different exposure scenarios need to be evaluated separately. This paper considered the sensitive areas as the places where children and adults are exposed to a contaminant in a whole time manner, with expressions used to evaluate exposure through ingestion shown as following [Equations (1) and (2)]:

$$CGWER_{ca} = \frac{GWCR_c \times EF_c \times ED_c}{BW_c \times AT_{ca}} + \frac{GWCR_a \times EF_a \times ED_a}{BW_a \times AT_{CA}} \quad (1)$$

with $CGWER_{ca}$ representing the oral predicted exposure (carcinogenic) ($L \cdot kg^{-1} \cdot day^{-1}$); $GWCR_c$ was the water intake for a child ($L \cdot d^{-1}$); $GWCR_a$ was the water intake for an adult ($L \cdot d^{-1}$); ED_c was the exposure time (a) of a child; ED_a was the exposure time (a) of an adult; EF_c was the exposure rate ($d \cdot a^{-1}$) of a child; EF_a was the exposure rate ($d \cdot a^{-1}$) of an adult; BW_c was the weight (kg) of a child; BW_a was the weight (kg) of an adult; AT_{ca} was the average carcinogenic effect time.

$$CGWER_{nc} = \frac{GWCR_c \times EF_c \times ED_c}{BW_c \times AT_{nc}} \quad (2)$$

This paper considered the insensitive areas as places where children and adults are exposed to a contaminant in a whole time manner, with expressions used to evaluate exposure through ingestion shown as following [Equations (3) and (4)]:

$$CGWER_{ca} = \frac{GWCR_a \times EF_a \times ED_a}{BW_a \times AT_{ca}} \quad (3)$$

$$CGWER_{nc} = \frac{GWCR_a \times EF_a \times ED_a}{BW_a \times AT_{nc}} \quad (4)$$

with $CGWER_{ca}$ representing the oral predicted exposure (non-carcinogenic) ($L \cdot kg^{-1} \cdot day^{-1}$); AT_{nc} was the average non-carcinogenic effect time.

Toxicological Evaluation

It is well known that Be, Hg and F can cause arseniasis owing to the manifestation in drinking water. As a nonessential element of human bodies, the toxicity of elemental As is extremely low, although its compounds are highly toxic. The source of As includes not only the mineral, metallurgical, chemical, pharmaceutical and glass industry in decolorizing agents but also insecti-

cides, rodenticides, chemical fertilizers and pesticides. Farmers, housewives, and special occupational groups of workers are its major hazard groups. As can enter the body via the respiratory tract, digestive tract and skin contact. The latency of As in human bodies is up to several years or even decades, with symptoms of digestive and nervous system, as well as skin lesions of chronic poisoning. If the concentration of As in the blood of pregnant women exceeds the standard, fetal teratoma could be induced. At present, epidemiologists have sufficient evidence to prove that inorganic arsenic is an important predisposing factor for cancers. Since 2008, As pollution events have occurred in places such as Guizhou Dushan County, Hunan Chenxi County, Guangxi Hechi, Yunnan Yangzonghai, Henan Shahe, and Shandong Linyi.

Beryllium and its compounds are extremely toxic, and even trace amounts of it can be poisonous. The respiratory tract is the main route that beryllium invades human bodies. Long-term inhalation of small amounts of beryllium or beryllium oxide might cause pulmonary granuloma. Acute Be disease in the form of chemical pneumonitis was first reported in Europe in 1933 and in the United States in 1943. Metal beryllium has many excellent properties such as in manufacturing aircraft components, and its applications could not be replaced by other known materials.

Hg occurs inorganically as salts such as Hg (II) chloride. Hg salts primarily affect the gastrointestinal tract and kidney, and could cause acute kidney failure. Also, Hg can accumulate in people's brains. When the concentration of Hg reaches a high point, it would cause damage to brain tissues and hurt the central nervous system.

Hydrofluoric acid is a contact poison with greater hazards than many other strong acids such as sulfuric acid. It remains neutral in aqueous solution, and can quickly penetrate into tissues. It could invade human bodies through inhalation, ingestion or skin contact. At least nine U.S. workers died in such accidents between 1984 and 1994. F is a necessary trace element for human bodies, and a moderate amount of F is beneficial for human health. It has been known to prevent tooth decay and osteoporosis in the presence of low acceptable daily intake.

Risk Characterization

In order to understand the damage of such contaminants to human health, this study applied the risk assessment index known as the contamination risk (CR). Due to toxicity differences between carcinogenic and non-carcinogenic chemicals, one contaminant might have two risky characterizations. The parameters are shown in Table 2.

Table 2. Recommendation Values about Risky Characterization.

	Oral RfD_0 (mg/kg-d)	Oral SF_0	Skin RfD_d	Skin SF_d
Hg (inorganic)	3.00×10^{-4}	—	2.10×10^{-5}	—
As (inorganic)	3.00×10^{-4}	1.50	3.00×10^{-4}	1.50
F (fluoride)	6.00×10^{-4}	—	6.00×10^{-4}	—
Be	2.00×10^{-3}	—	1.40×10^{-5}	—

For each contaminant, the expressions used to evaluate contaminant risk through ingesting groundwater are as follows [Equation (5)]:

$$CR_{cgw} = CGWER_{ca} \times C_{gw} \times SF_0 \tag{5}$$

with CR_{cgw} representing the contaminant risk, C_{gw} is the concentration of underground water contaminant (mg L^{-1}).

For each contaminant, the expressions used to evaluate hazard quotient through ingesting groundwater are as follows [Equation (6)]:

$$HQ_{cgw} = \frac{CGWER_{nc} \times C_{gw}}{RfD_0 \times WAF} \tag{6}$$

with HQ_{cgw} representing hazard quotient.

Control Value Calculation

Control value of the assessed risks has a limiting value, since the concentration of a contaminant should be under control in case it produces harm to the environment and human health. According to government standard HJ25.3-2014, the control value of soil and underground water to avoid potential carcinogenic effects should be calculated based on the acceptable contaminant risk of a contaminant is 10^{-6}. When the control value of soil and underground water is calculated based on potential non-carcinogenic effects, the acceptable hazard quotient of a contaminant is 1.

Expressions used to evaluate exposure through ingestion were shown as following (for carcinogenic effect and non-carcinogenic effect respectively) [Equations (7) and (8)]:

$$RCVG_{cgw} = \frac{ACR}{CGWER_{ca} \times SF_0} \tag{7}$$

with $RCVG_{cgw}$ representing the control value of underground water based on potential carcinogenic effects, and ACR means the acceptable level of carcinogenic risks.

$$HCVG_{cgw} = \frac{RfD_0 \times WAF \times AHQ}{CGWER_{nc}} \quad (8)$$

with $HCVG_{cgw}$ representing the control value of underground water based on potential non-carcinogenic effects, and AHQ denotes the level of acceptable non-carcinogenic risks.

RESULTS AND DISCUSSION

Exposure Dose

To calculate the exposure dose, recommendation values were referred to HJ25.3-2014 in Table 3.

Within sensitive areas, human exposure to contaminants in drinking water was analyzed. For each contaminant, the exposure dose could be calculated using Equations (1) and (2) with the results shown in Table 4.

Within insensitive areas, human exposure to contaminants in drinking water was analyzed. For each contaminant, exposure dose could be calculated using Equations (3) and (4) with the results shown in Table 5.

Table 3. Recommendation Values about Exposure Dose.

Parameter	Unit	Sensitive Area	Insensitive Area
$GWCR_c$	$L \cdot d^{-1}$	0.7	0.7
$GWCR_a$	$L \cdot d^{-1}$	1.0	1.0
EF_c	$d \cdot a^{-1}$	350	—
EF_a	$d \cdot a^{-1}$	350	250
ED_c	a	6	—
ED_a	a	24	25
BW_c	Kg	15.9	15.9
BW_a	Kg	56.8	56.8
$ATca$	d	26280	26280
AT_{nc}	d	2190	9125
SAF	dimensionless	0.20	0.20
WAF	dimensionless	0.20	0.20

Risk Level

Sensitive Areas

Through the establishment of the mode, the risk characterization of four trace elements within sensitive areas could be obtained. This paper calculated the carcinogenic characterization risk of As in six samples, and non-carcinogenic hazard quotient of As, Hg, F and Be in all samples. The results were shown in Table 6.

Values of all six samples were above the standard of 10^{-6} and 3.5 m sampling had the highest risk level. Also, all sampling spots showed serious carcinogenic characterization risks.

First, the hazard quotients of Hg and F exceeded standard 1, and the total hazard quotient of 1.1 m sample exceeded the standard as well. Hg accounted for 48.62%, F accounted for 34.27%; the contribution ratio pie is shown in Figure 1(a). Secondly, for the 1.8 m sample, hazard quotient of As was 2.62, which was twice that of normal value. As accounted for 93.47%, with the contribution ratio pie shown in Figure 1(b). For the 2.0 m sample, hazard quotient of As was 2.42, which was twice that of the normal value. As accounted for 90.38%, with the contribution ratio pie shown in Figure 1(c). For the 2.5–3.0 m sample, hazard quotient of As was 2.95, which was almost three times that of the normal value. As accounted for 95.66%, with the contribution ratio pie shown in Figure 1(d). Finally, for the 3.5 m sample, the hazard quotient of As was 11.82, which was almost 12 times that of normal value. As accounted for 97.42%, with the contribution ratio pie shown in Figure 1(e).

To conclude, all samplings were above the standard, and 3.5 m sampling spot displayed severe non-carcinogenic risks. With an increase in distance, the non-carcinogenic hazard quotient of underground water kept growing, so did the proportion of As in the contribution ratio pie. However, the total hazard quotient did not increase. For the 3.5 m sampling spot, there was a sharp increase, and the concentration of As was above the standard. According to the government standard, the corresponding water quality belonged to level IV.

Insensitive area

Through the establishment of the mode, the risky

Table 4. Exposure Dose within Sensitive Areas.

	1.1 m	1.8 m	2.0 m	2.5–3 m	3.5 m
$CGWER_{ca}$ ($L \cdot kg^{-1} \cdot d^{-1}$)	9.15×10^{-3}	9.15×10^{-3}	9.15×10^{-3}	9.15×10^{-3}	9.15×10^{-3}
$CGWER_{nc}$ ($L \cdot kg^{-1} \cdot d^{-1}$)	4.22×10^{-2}	4.22×10^{-2}	4.22×10^{-2}	4.22×10^{-2}	4.22×10^{-2}

Table 5. Exposure Dose under Insensitive Areas.

	1.1 m	1.8 m	2.0 m	2.5–3 m	3.5 m
$CGWER_{ca}$ ($L \cdot kg^{-1} \cdot d^{-1}$)	4.19×10^{-3}	4.19×10^{-3}	4.19×10^{-3}	4.19×10^{-3}	4.19×10^{-3}
$CGWER_{nc}$ ($L \cdot kg^{-1} \cdot d^{-1}$)	1.21×10^{-2}	1.21×10^{-2}	1.21×10^{-2}	1.21×10^{-2}	1.21×10^{-2}

characterization of four trace elements within insensitive areas could be obtained. This study calculated the carcinogenic characterization risk of As in six samples, and non-carcinogenic hazard quotient of As, Hg, F and Be in all samples. The results are shown in Table 7.

Values of all six samples were above the standard value of 10^{-6} and 3.5 m sampling had the highest risk level. Also, all the sampling spots showed serious carcinogenic characterization risks.

No trace elements in 1.1 m, 1.8 m, 2.0 m, 2.5 m or 3 m samples exceeded the standard value. However, the total hazard risks in 1.1m sample went beyond the standard value. For the 3.5 m sample, hazard quotient of As was 3.39, which was three times that of normal value. As accounted for 97.42%, with the contribution ratio pie shown in Figure 2(b).

Control Value

For sensitive areas, several conclusions could be drawn based on the results presented in the previous section. Contaminant risks of As in all samples were above the standard value, and thus control value needed to be calculated. Hazard quotients of As in 1.8 m, 2 m, 2.5–3 m and 3.5 m samples and hazard quotients of Hg and F in 1.8 m exceeded the standard value, and all of those samples needed to calculate the control value. The rest of samples were under control.

For insensitive areas, several conclusions could be drawn based on the results presented in the previous section. Contaminant risks of As in all samples were above the standard value, and they need to be calculated. Hazard quotient of As in 3.5 m sample exceeded the standard value, and thus the control value needed to be calculated.

Sensitive Area

Using Equation (7), *RCVG* of As could be calculated.

$$RCVG_{cgw} = \frac{10^{-6}}{9.15 \times 10^{-3} \times 1.5} = 7.29 \times 10^{-5}\,\mathrm{mg \cdot kg}$$

Using Equation (8), *HCVG* of As could be calculated.

$$HCVG_{cgw}2 = \frac{3 \times 10^{-4} \times 0.2 \times 1}{4.22 \times 10^{-2}} = 1.42 \times 10^{-3}\,\mathrm{mg \cdot kg^{-1}}$$

with a comparison of available data, the lowest value was chosen as the control value so that the concentration of As could be controlled under 7.29E-05 $mg \cdot kg^{-1}$.

Using Equation (8), *HCVG* of Hg could be calculated.

$$HCVG_{cgw}2 = \frac{3 \times 10^{-4} \times 0.2 \times 1}{4.22 \times 10^{-2}} = 1.42 \times 10^{-3}\,\mathrm{mg \cdot kg^{-1}}$$

Using Equation (8), *HCVG* of F could be calculated.

$$HCVG_{cgw}2 = \frac{6 \times 10^{-4} \times 0.2 \times 1}{4.22 \times 10^{-2}} = 2.84 \times 10^{-3}\,\mathrm{mg \cdot kg^{-1}}$$

Insensitive Area

Using Equation (7), *RCVG* of As could be calculated.

$$RCVG_{cgw} = \frac{10^{-6}}{4.19 \times 10^{-3} \times 1.5} = 1.59 \times 10^{-4}\,\mathrm{mg \cdot kg^{-1}}$$

Table 6. Carcinogenic Characterization Risk and Non-carcinogenic Hazard Quotient.

	Contaminant	1.1 m	1.8 m	2.0 m	2.5–3 m	3.5 m
Carcinogenic characterization risk of groundwater	As	1.34×10^{-5}	5.11×10^{-5}	4.72×10^{-5}	5.75×10^{-5}	2.31×10^{-5}
Non-carcinogenic hazard quotient of groundwater	As	0.68	2.62	2.42	2.95	11.82
	Be	0.06	0.01	0.01	0.01	0.044
	Hg	2.10	0.05	0.08	0.04	0.035
	F	1.48	0.13	0.17	0.08	0.234
	Total	**4.32**	**2.80**	**2.68**	**3.08**	**12.13**

Table 7. Carcinogenic Characterization Risk and Non-carcinogenic Hazard Quotient.

	Contaminant	1.1 m	1.8 m	2.0 m	2.5–3 m	3.5 m
Carcinogenic characterization risk of groundwater	As	6.1×10^{-6}	2.3×10^{-5}	2.16×10^{-5}	2.6×10^{-5}	1.06×10^{-5}
Non-carcinogenic hazard quotient of groundwater	As	0.20	0.75	0.70	0.85	3.39
	Be	1.7×10^{-2}	2.0×10^{-3}	3.0×10^{-3}	4.0×10^{-3}	1.3×10^{-2}
	Hg	0.61	0.02	0.02	0.01	0.01
	F	0.42	0.04	0.05	0.02	0.07
	Total	**1.24**	**0.80**	**0.77**	**0.88**	**3.48**

Using Equation (8), *HCVG* of As could be calculated.

$$HCVG_{cgw} = \frac{3\times10^{-4}\times0.2\times1}{1.21\times10^{-2}} = 4.96\times10^{-3}\,\mathrm{mg\cdot kg^{-1}}$$

with a comparison of available data, the lowest value was chosen as the control value so that concentration of As could be controlled under 1.59×10^{-4}mg·kg^{-1}.

Using Equation (8), *HCVG* of Hg could be calculated.

$$HCVG_{cgw} = \frac{3\times10^{-4}\times0.2\times1}{1.21\times10^{-2}} = 4.96\times10^{-3}\,\mathrm{mg\cdot kg^{-1}}$$

Using Equation (8), *HCVG* of F could be calculated.

$$HCVG_{cgw} = \frac{6\times10^{-4}\times0.2\times1}{1.21\times10^{-2}} = 9.92\times10^{-3}\,\mathrm{mg\cdot kg^{-1}}$$

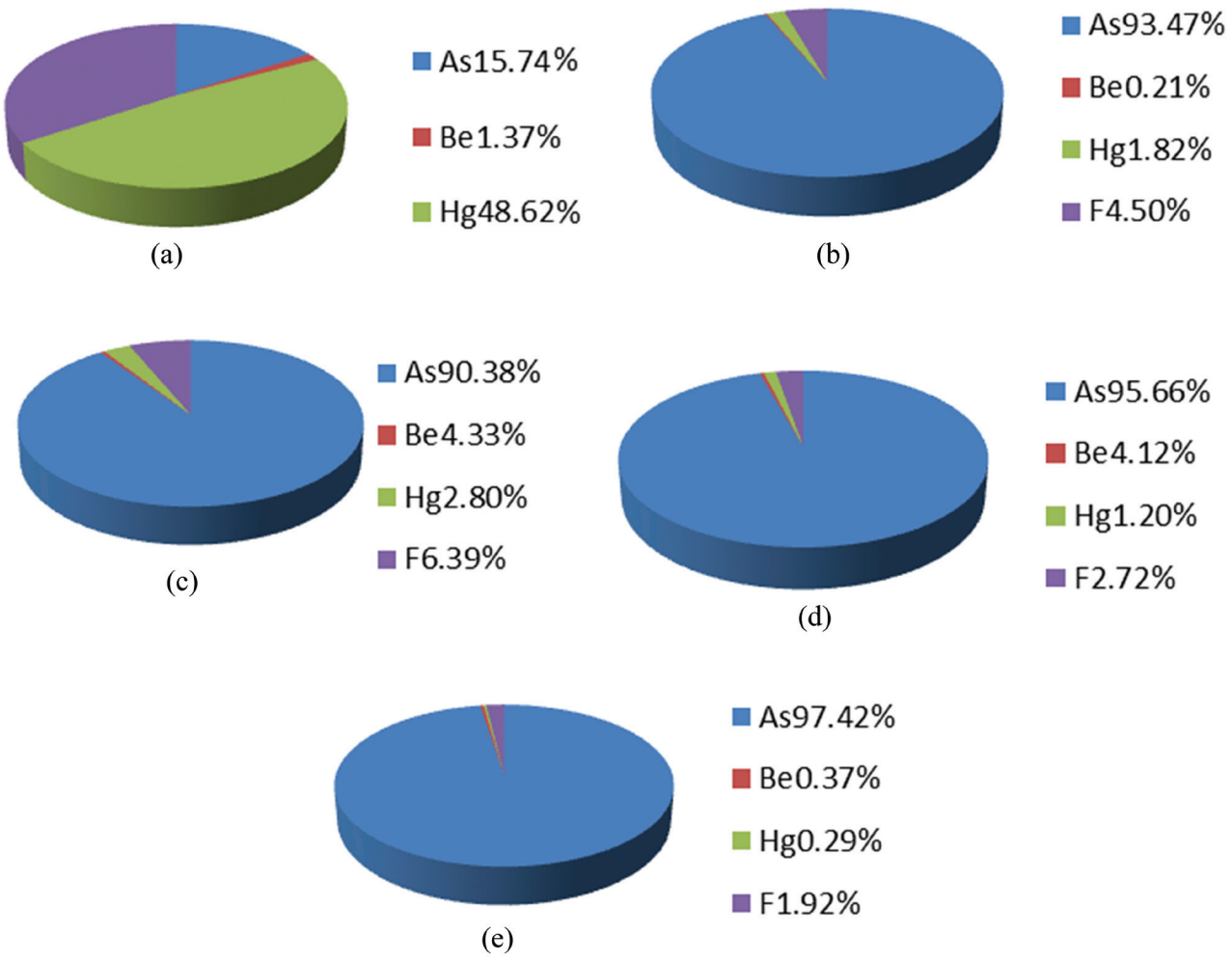

Figure 1. *The contribution of non-carcinogenic hazard quotient in different distance to the kindling point: (a) 1.1 m sample; (b) 1.8 m sample; (c) 2.0 m sample; (d) 2.5–3 m sample; and (e) 3.5 m sample.*

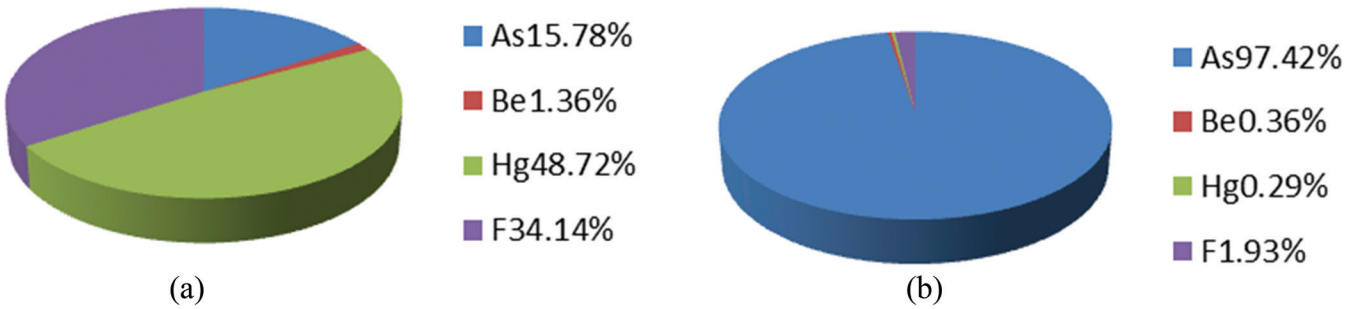

Figure 2. *The contribution of non-carcinogenic hazard quotient with different distance to the kindling point: (a) 1.1 m sample; and (b) 3.5 m sample.*

CONCLUSIONS

The difference between technical documents of USEPA (USEPA, 2005) and this assessment system was that the latter explicitly distinguished the sensitive areas from insensitive areas. On the one hand, the present study provided a comprehensive assessment of risks in both childhood and adulthood. On the other hand, the factor of pollutant concentrations was included into the model to calculate contaminant risks, and the process of assessing each contaminant's exposure level was simplified. Therefore, the established system could effectively reduce the computational complexity and measurement uncertainties.

During the assessment process of human health risks caused by underground gasification practice, sampling spots from 1.1m to 3.5m in residual landfill had both carcinogenic and non-carcinogenic risks. Also, hazard quotient in drinking water was tested in both sensitive and insensitive areas. Computational results showed that the carcinogenic characterization risks of five samples collected from different sites within sensitive areas were 1.34×10^{-5}, 5.11×10^{-5}, 4.72×10^{-5}, 5.75×10^{-5} and 2.31×10^{-4}, respectively. The non-carcinogenic hazard quotients of samples were 4.32, 2.80, 2.68, 3.08 and 12.13, respectively. All of the values exceeded the standard value and the concentration of As, F and Hg negatively affected human health. For insensitive areas, the carcinogenic characterization risks of five samples collected from different sites within sensitive areas were $6.10E \times 10^{-6}$, 2.30×10^{-5}, 2.16×10^{-5}, 2.60×10^{-5} and 1.06×10^{-4}, respectively. The non- carcinogenic hazard quotients of samples were 1.24, 0.80, 0.77, 0.88 and 3.48, respectively. All sites had displayed carcinogenic characterization risks, and only As found in 1.1 m and 3.5 m sites had caused severe damage on human health.

The control value was obtained through the established model, with the value of As as 7.29 $mg \cdot kg^{-1}$, the value of F as 2.84×10^{-3} $mg \cdot kg^{-1}$, and the value of Hg as 1.42×10^{-3} $mg \cdot kg^{-1}$ within sensitive areas. Also, sampling spots between residuals landfill 1.1 m and 3.5 m showed carcinogenic contaminant risks, whereas sampling spots between residuals landfill 1.1 m and 3.5 m displayed non-carcinogenic hazard quotient. The control values of As, Hg and F were 1.59×10^{-4} $mg \cdot kg^{-1}$, 4.96×10^{-3} $mg \cdot kg^{-1}$, and 9.92×10^{-3} $mg \cdot kg^{-1}$, respectively.

ACKNOWLEDGEMENTS

This study was supported by the National Basic Research Program of China (973 Program) (No. 2014CB238906) and National Science Foundation of China (21107041). We also thank Professor Shuqin Liu for providing coal residual samples.

REFERENCES

1. Yang Duoguiand Gao Feipeng, "Quantitative Evaluation and Analysis on Human Health Risk", *China Population, Resources and Environment*, 2007.
2. A. Pe-a-Fernández, M.J. González-Mu-oz, M.C. Lobo-Bedmar, "Establishing the importance of human health risk assessment for metals and metalloids in urban environments", *Environment International, 72* (2014) 176–185. http://dx.doi.org/10.1016/j.envint.2014.04.007
3. Yingxin Yu and Xinxin Wang, "Evaluation of human health risks posed by carcinogenic and non-carcinogenic multiple contaminants associated with consumption of fish from Taihu Lake, China", *Food and Chemical Toxicology, 69*(2014) 86–93. http://dx.doi.org/10.1016/j.fct.2014.04.001
4. Ljiljana Medic Pejic and Javier García Torrent, "A new simple methodology for evaluation of explosion risk in underground coal mines", *Journal of Loss Prevention in the Process Industries, 26*(2013) 1524e1529.
5. Qihong Zhao and Ying Wang, "Potential health risks of heavy metals in cultivated topsoil and grain, including correlations with human primary liver, lung and gastric cancer", *Anhui province, Eastern China, in Science of the Total Environment 470–471*(2014) 340–347. http://dx.doi.org/10.1016/j.scitotenv.2013.09.086
6. Peimiao Li and Xuelu Gao, "Trace elements in major marketed marine bivalves from six northern coastal cities of China: Concentrations and risk assessment for human health", *Ecotoxicology and Environmental Safety, 109*(2014)1–9. http://dx.doi.org/10.1016/j.ecoenv.2014.07.023
7. D. Cicchella and S. Albanese, "Trace elements and ions in Italian bottled mineral waters: Identification of anomalous values and human

health related effects", *Journal of Geochemical Exploration, 107* (2010) 336–349. http://dx.doi.org/10.1016/j.gexplo.2010.04.004

8. Shifeng Dai and Deyi Ren, "Geochemistry of trace elements in Chinese coals: A review of abundances, genetic types, impacts on human health, and industrial utilization", *International Journal of Coal Geology 94* (2012) 3–21. http://dx.doi.org/10.1016/j.coal.2011.02.003
9. Shifeng Dai, "Factors controlling geochemical and mineralogical compositions of coals preserved within marine carbonate successions: A case study from the Heshan Coalfield, southern China", *International Journal of Coal Geology, 109–110* (2013) 77–100. http://dx.doi.org/10.1016/j.coal.2013.02.003
10. Vladimir V. Seredin, "Coal deposits as potential alternative sources for lanthanides and yttrium", *International Journal of Coal Geology, 94* (2012) 67–93. http://dx.doi.org/10.1016/j.coal.2011.11.001
11. Irena Kostova and Christina Vassileva, "Influence of surface area properties on mercury capture behaviour of coal fly ashes from some Bulgarian power plants", *International Journal of Coal Geology, 116–117* (2013) 227–235. http://dx.doi.org/10.1016/j.coal.2013.03.008
12. Shifeng Dai, "Enrichment of arsenic, antimony, mercury, and thallium in a Late Permian anthracite from Xingren, Guizhou, Southwest China", International Journal of Coal Geology 66, (2006) 217–226. http://dx.doi.org/10.1016/j.coal.2005.09.001
13. Eskenazy Greta and Shifeng Dai, "Fluorine in Bulgarian coals", *International Journal of Coal Geology, 105* (2013) 16–23. http://dx.doi.org/10.1016/j.coal.2012.11.011
14. Marcio A. Kronbauer and Maria Izquierdo, "Geochemistry of ultra-fine and nano-compounds in coal gasification ashes: A synoptic view", *Science of the Total Environment, 456–457* (2013) 95–103. http://dx.doi.org/10.1016/j.scitotenv.2013.02.066
15. Shifeng Dai and Dan Li, "Mineralogy and geochemistry of boehmite-rich coals: New insights from the Haerwusu Surface Mine, Jungar Coalfield, Inner Mongolia, China", *International Journal of Coal Geology 74* (2008) 185–202. http://dx.doi.org/10.1016/j.coal.2008.01.001
16. Ya. E. Yudovich and M.P. Ketris, "Mercury in coal: a review Part 2. Coal use and environmental problems", *International Journal of Coal Geology, 62* (2005) 135–165. http://dx.doi.org/10.1016/j.coal.2004.11.003
17. Shifeng Dai, "Abundances and distribution of minerals and elements in high-alumina coal fly ash from the Jungar Power Plant, Inner Mongolia, China", *International Journal of Coal Geology, 81* (2010) 320–332. http://dx.doi.org/10.1016/j.coal.2009.03.005
18. Shifeng Dai, "Mineralogical and compositional characteristics of Late Permian coals from an area of high lung cancer rate in Xuan Wei, Yunnan, China: Occurrence and origin of quartz and chamosite", *International Journal of Coal Geology, 76* (2008) 318–327. http://dx.doi.org/10.1016/j.coal.2008.09.001
19. Robert A. Creelman, "Use of Geological Science for Improved Understanding of Pf Furnace Deposition", *10th Australian Coal Science Conference*, Nov18–19, 2013, Brisbane, Queensland.
20. A.H. Clemensa, "Abundances and distribution of minerals and elements in high-alumina coal fly ash from the Jungar Power Plant, Inner Mongolia, China", *International Journal of Coal Geology, 81* (2010) 320–332. http://dx.doi.org/10.1016/j.coal.2009.03.005
21. USEPA. Guidelines for Carcinogen Risk Assessment, EPA/630/P-03/001F. Risk Assessment Forum, Washington, DC. 2005.

Improvement of Heavy Metal Resistant Bacteria on Phytoremediation of Reclaimed Land using Coal Gangue

YAN YU, YUXIU ZHANG*, QIAN ZHANG, XIAOQING ZHANG, XIAOJUN MENG and ZHAOHUA LU
School of Chemical and Environmental Engineering, China University of Mining & Technology (Beijing), Beijing, 100083,China

ABSTRACT: Pot experiments were conducted to evaluate the effect of a heavy metal resistant bacteria strain *Pseudomonas aeruginosa* (LB5Z) on phytoremediation of reclaimed land using coal gangue. Two sets of treatments were conducted. Planting *Amorpha fruticosa* L. was used in one set of experiment, while the other used planting and inoculation with the strain LB5Z at the same time. Both treatments involve four kinds of soils (coal gangue; coal gangue: loess = 1:1; coal gangue: loess = 1:2; and loess). The result showed that *Amorpha fruticosa* L. was suitable for the remediation of coal gangue-polluted land, and further revealed that inoculation of *Pseudomonas aeruginosa* was a feasible means for promoting plant growth and improving tolerance of the plant to heavy metals. Particularly, the ratio of coal gangue to loess is recommended as 1:2.

INTRODUCTION

A large amount of coal gangue is formed during the processes of coal mining and coal wash. In China, the total amount of produced coal is about 3.7 billion tons in 2013, in which coal gangue accounts for 10%~15% [1]. There are currently nearly 2000 coal gangue dumps in China, and the total stock of coal gangue keeps an increasing trend with a rate of about 0.15–0.2 billion tons per year [2]. Treatment and utilization of coal gangue has become an important issue in reducing environmental pollution from coal mining.

There are a number of ways to use coal gangue, including synthesized utilization and reuse since coal gangue contains different elements. Utilization of coal gangue for land reclamation can not only promote recovery the of ecological environment of the nearby mining areas, but also bring significant economic benefits [3,4,5]. The crucial issue for land reclamation using coal gangue as the main substrate is the optimal depth of top soil to meet the requirements of crop growth and reduce the possibility of soil pollution at the same time [6].

Phytoremediation is a commonly used method to reclaim coal gangue-polluted soil. It uses plants with high tolerance to remove pollutants from the environment. Through in-situ rhizospheric processes, the toxic heavy metals can be bioconcentrated (phytoextraction) and bioimmobilized or inactivated (phytostabilization) by plants. However, an elevated level of heavy metals generally displays high toxicity to most plants, which can impair the metabolism of plants and further inhibit their normal growth. As a result, the potential for metal phytoextraction by plants may be weakened to some extent, which in turn restricts the application of this technology. In view of this, it is necessary to develop proper phytoremediation strategies for heavy metal-contaminated soils [7]. It is noticed that the phytoaccumulation efficiency may be influenced by not only the plant itself but also the interaction between the plant roots and surrounding soil environment. Therefore, as the important aspects of phytoremediation technology, the biomass production and the tolerance of the plants to heavy metals may be enhanced by strengthening the interactions between plants and beneficial microbes [8]. As is reported, plant growth-promoting bacteria (PGPB) can reduce heavy metal stress and meanwhile promote phytoremediation and biomass production in heavy metal polluted soils. There are different growth-promoting mechanisms: the siderophores, production of indole-3-acetic acid (IAA), the fixation of atmospheric nitrogen, and the enzyme 1-aminocyclopropane-1-carboxylate (ACC) deaminase [9]. Heavy metal resistant bacteria have a significant effect on the mobility of trace metals and availability to the plant. Through producing siderophores, they can ensure iron availability, reduce soil pH and solubilize phosphates [10].

*Author to whom correspondence should be addressed.
E-mail: yxzhang@sina.com; Tel: +86-101-62339207

1544-8053/15/01 S105-09

doi:10.12783/issn.1544-8053/12/S1/16

There were many environmental problems in the coal mining areas of Shanxi Province, China, such as destruction of vegetation, decrease of biodiversity, and degradation of the whole ecosystem. Such problems are particularly severe in the coal gangue surrounding land. Thus the reclamation of the contaminated land nearby the gangue dump is crucial for ecological restoration and reconstruction of this coal mining area. Studies were carried out to choose a suitable phytoremediation technology.

The main purposes of this paper are: (1) to determine the feasibility of coal gangue mixed with the surrounding soil used for phytoremediation; (2) to assess the ecological potential risk of different mixed rations; (3) to analyze the resistance to heavy metals of the strain isolated from coal gangue; and (4) to investigate the effects of the heavy metal resistant bacteria on promotion of plant growth. Based on these results, it will be possible to elucidate the feasibility of application of coal gangue in land reclamation and the phytoremediation by heavy metal resistant bacteria.

EXPERIMENTAL PROCEDURE

Experimental Materials

Acid coal gangues were obtained from the mining waste dump area in Shanxi Province, China. The main chemical characteristics of the experimental coal gangue were as follows: pH value was 3.69, organic matter and available phosphorus was 18.02 $g \cdot kg^{-1}$ and 31.83 $mg \cdot kg^{-1}$, respectively. The element contents of Cd, Cr, Cu, Ni and Zn in coal gangue were 33.21, 41.55, 38.12, 27.34 and 249.50 $mg \cdot kg^{-1}$, respectively. Among them, the content of Cd was 33 times larger than that in the Environmental Quality Standard III for Soils in China, which seriously inhibited plant growth. Organic matter and available phosphorus were determined according to the methods [11]. The content of heavy metal was determined by ICP-AES after digested by the method [12].

The used loess was native soil around the experimental area, which was deficient in nutrients. The organic matter and available phosphorus was 2.56 $g \cdot kg^{-1}$ and 5.55 $mg \cdot kg^{-1}$, respectively. To dispose of and utilize coal gangue safely, pot experiments were designed. The experimental soils were obtained by mixing coal gangue and loess soil, i.e. single coal gangue; coal gangue: loess 1:1 (Ratio I); coal gangue: loess 1:2 (Ratio II) and single loess.

Seeds were collected from *Amorpha fruticosa* L., a common woody plant found surrounding the mining area.

Coal Gangue Leaching Toxicity

Coal gangue was first ground and sieved, and then 5 g of the sample was added to a flask that contained 50 mL deionized water, which was placed on a shaking table. The contents of heavy metals in leachate were measured at day 0, day 1, day 3, day 5 and day 7 in triplicate, respectively. The concentration of heavy metals in leachate was measured by ICP-AES.

To investigate the relationship between 7-day release ratio of heavy metal and the ratio of available heavy metal in coal gangue, existing forms of heavy metal in coal gangue were determined. Changes in the fraction of heavy metals were determined by sequential extraction, as described by Tessier *et al.* [13]. In this study, a two step-extraction was used to determine the available part of heavy metal. Briefly, the exchangeable part (EXE) was obtained by extraction with 1 M NH_4OAc at pH = 7, and then the carbonate part (CAR) was obtained by extraction with 1 M NH_4OAc at pH = 5. Then, the total amount of EXE and CAR could be used to characterize the availability of heavy metal.

Resistant Strain

A coal gangue sample of 5 g was added to 45 mL liquid beef-protein medium and cultured at 30°C and 200 rpm for 24 h. Then 2 mL of the suspension was added to another liquid beef-protein medium containing 100 $mg \cdot L^{-1}$ of Cd^{2+}. The suspension was incubated with a series of liquid beef-protein mediums containing Cd^{2+} at a concentration up to 1000 $mg \cdot L^{-1}$. After incubation, 0.2 mL of suspension was transferred into a solid medium with Cd^{2+} of 1000 $mg \cdot L^{-1}$. It was then cultured at 30°C for 72 h. After repeated isolation and purification, a Cd-resistant strain (LB5Z) was obtained. On the basis of analysis of the sequence of 16S rRNA, the strain LB5Z was identified as Pseudomonas aeruginosa, which was published by Zhang *et al.* [14].

The strain LB5Z was incubated in nitrogen culture medium with tryptophane for 3 days [15]. Afterwards, 1 mL of cell suspension was shifted to a tube and subjected to a vigorous mixing with 2 ml of Salkowski's reagent. Then, the mixture was placed for 20 min at room temperature. A pink color indicated the production of IAA. The phosphate solubilization capacity of the strain was determined by dissolving phosphate circle after culturing in both organic phosphate medium

and inorganic phosphate medium. The capacities of nitrogen fixation and production of biosurfactant were determined by the methods of Wang [16].

Effect of Heavy Metals on the Growth of Cd-resistant Bacteria Strain

Supplemented with different concentrations of heavy metals, 100 mL LB broth was inoculated in the culture flask of 250 mL with bacterial isolate in the logarithmic phase. All the cultures were cultured at 37°C for 20 h, and the optical density was measured at 600 nm (in triplicate).

The logarithmic growth phase strain was inoculated in an amount of 5% to a 0~250 $g \cdot L^{-1}$ coal gangue suspension (pH = 7.2). Another liquid medium with the same coal gangue content but without inoculation was used as the control. All the liquid mediums were cultured at 37°C for 20 h, and the optical density at 600 nm and pH value of suspensions were determined.

Effect of Cd-resistant Bacteria on the Growth of Plants

To investigate the effect of the bacterial strain LB5Z on plant growth, the pot experiments were carried out. Four kinds of soils (Coal gangue; Ratio I; Ratio II and Loess) were used. For the first set of treatments, seeds of *Amorpha fruticosa* L. were planted (plant control, PC). For the second set of treatments, besides planting, inoculation with LB5Z at the same time was also carried out (inoculated LB5Z, LB5Z). Each treatment was performed in triplicate, thus totally 36 pots were used.

In all the experiments, 20 surface-sterilized seeds of *Amorpha fruticosa* L. were placed at a depth of 1.0 cm in a plastic pot containing 400 g of soil.

During the inoculation process, the strain LB5Z was cultured in the LB broth medium, and the cells in the exponential phase could be collected through the method of centrifugation at 12,000 rpm for 10 min. Afterwards, the cells were rinsed by sterile distilled water and centrifuged again. By resuspending cell pellet in sterile distilled water, bacterial inoculant with an inoculant density of 10^8 cell ml^{-1} was prepared. Bacterial suspensions (10 mL per pot) were sprayed on the soil surface every 10 days. At the same time, the control group treatments were watered with 10 mL distilled water. All pots were placed indoor at a temperature ranging from 18 to 31°C After 75 days, the plants were removed from the pots carefully for cleaning their root surface with distilled water. Through washing several times, the root surface was clean, and plant fresh weight, plant height, root length and stem length could be measured.

Ecological Risk Assessment of Coal Gangue-mixed Soils

Evaluation of heavy metal pollution of different treatments was carried out before and after inoculation. Potential ecological risk index (RI) was calculated by a commonly used formula, which could be used to assess the ecological risk of heavy metals in soil or sediments [17]. The value of RI can be calculated by a formula as follows:

$$RI = \sum_{i=1}^{m} E_r^i = \sum_{i=1}^{m} \left(T_r^i \times \frac{C_s^i}{C_n^i} \right)$$

where RI is calculated as the potential ecological risk index of all heavy metals in mixed soils of different treatments; E_r^i denotes the potential ecological risk of individual heavy metal; C_s^i denotes the concentration of heavy metal in mixed soils; C_n^i denotes the reference value of heavy metal in soils (based on standard level III in China used in agriculture and forestry production and the normal growth of plants, wherein Cu, Cd, Cr, Ni and Zn are 400, 1, 300, 200 and 500 $mg \cdot kg^{-1}$, respectively); and T_r^i denotes the toxic-response factor of given heavy metal (based on the HAKANSON approach, wherein Cu, Cd, Cr, Ni and Zn are 5, 30, 2, 5 and 1 $mg \cdot kg^{-1}$, respectively). According to the HAKANSON approach, five categories of E_r^i and four categories of RI could be defined as shown in Table 1. This category method was the premise of the following discussion.

Statistical Analysis

The statistical analysis in this study was all carried

Table 1. Indices and Grades of Potential Ecological Metal Contamination.

E_r^i	Grade of Ecological Risk of Single Metal	RI Value	Grade of Potential Ecological Risk of Environment
$E_r^i < 40$	Low risk	RI < 150	Low risk
$40 \le E_r^i < 80$	Moderate risk	150 ≤ RI < 300	Moderate risk
$80 \le E_r^i < 160$	Considerable risk	300 ≤ RI < 600	Considerable risk
$160 \le E_r^i < 320$	High risk	RI ≥ 600	High risk
$E_r^i \le 320$	Very high risk	0.23	

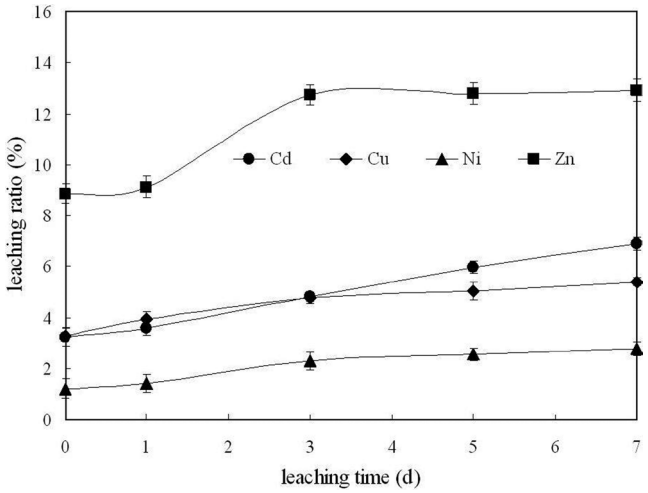

Figure 1. *Leaching ratio of heavy metal in coal gangue.*

out in SPSS 10.0. Differences between groups in plant growth were assessed by analysis of variance (ANOVA) followed by Fisher LSD test ($p < 0.05$).

RESULTS AND DISCUSSION

Coal Gangue Leaching Toxicity

The potential environmental harm of coal gangues has drawn the attention of different research groups due to their toxicity, bioavailability and geochemical behavior [4,18]. In the stacking process, leaching and weathering may occur, resulting in pollution of soil and groundwater. To investigate the toxicity of coal gangue used in this study, a 7-day leaching experiment was carried out. After the 7-day leaching experiment, the concentration of heavy metal in leachate reached a stable state (Figure 1). The results showed that heavy metal pollution of coal gangue mainly occurred in the early stage of leaching and weathering. Similarly, Yue [19] also found a rapid leaching of coal gangue which reached a stable state in only 24 h. In this study, the concentration of Cd increased at a nearly constant rate during the whole process, while the concentrations of both Ni and Zn could reach a stable state quickly on day 3.

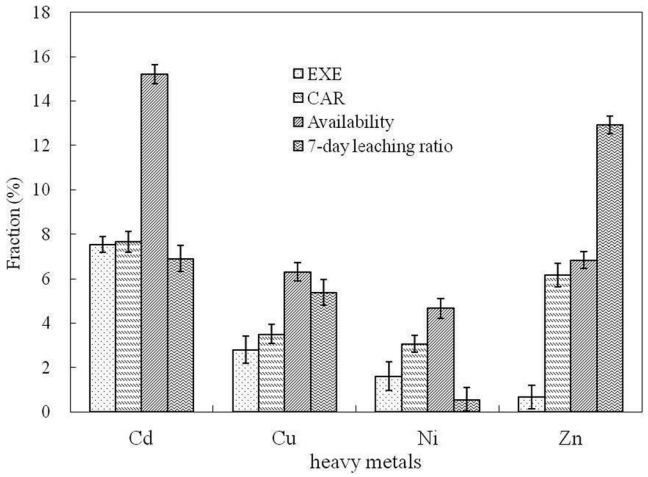

Figure 2. *7-day leaching ratio and ratio of different forms of heavy metal in coal gangue.*

The release rates of different heavy metals are not identical. After 7 days of leaching, most of the exchangeable Cd was released from coal gangue, while the percentage of released Cu was close to the ratio of available form of Cu in coal gangue. This indicated that the available form of Cu in coal gangue was substantively released during 7 days of leaching (Figure 2). Only 0.57 % of Ni was released from coal gangue, which was much lower than the exchangeable ratio. The release ratio of Zn was 12.93%, but the ratio of available form of Zn was only 6.85%. It can be deduced that some of the Zn was associated with Fe-Mn oxides released from coal gangue under leaching condition. The same results were also reported by other researches [20,21] that leaching coal gangue could enhance the availability of heavy metal due to low pH and low oxidation-reduction potential. The concentration of metal dissolved out and the release rate from coal gangue were not only related to the pH value of leachate, but also related to the element concentration in coal gangues [18].

Characteristics of the Bacteria

Biological characteristics studies showed that the strain LB5Z possess the ability of solubilizing phosphate, nitrogen fixation and producing IAA (Figure 3). The results also showed that the strain LB5Z possesses the ability of nitrogen fixation. The strain of *Pseudomonas aeruginosa* LB5Z was also reported as an indicator of increased uptake of nutrients and enhanced production of plant biomass in Zn stress [22,23]. Other studies showed that it could induce production of ACC deaminase, siderophore, antibiotics, hydrogen cyanide and volatile compounds [24].

Effect of Heavy Metals on the Growth of Cd-resistant Bacteria Strain

LB5Z was inoculated by using different concentrations of heavy metals (Figure 4) in order to simulate their toxicity to plants when there were heavy metals

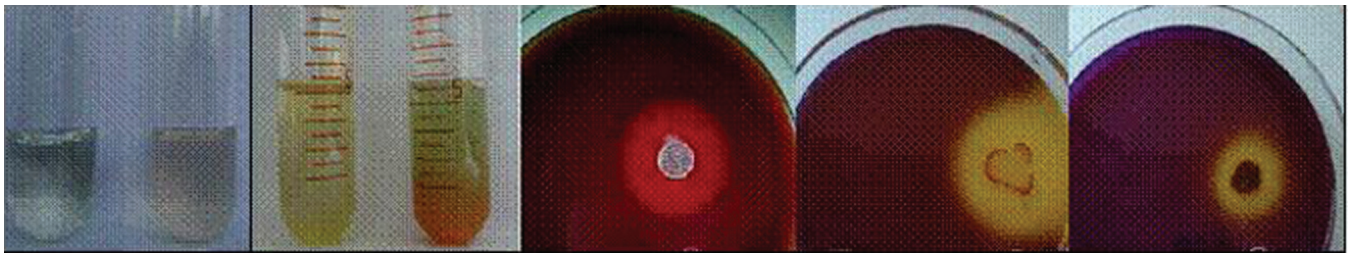

Figure 3. *The production of IAA, NH_3, biosurfactant, organic and inorganic phosphate by LB5Z (from left to right).*

in coal gangue. The strain LB5Z was tolerant to Cd at 450 mg·L^{-1}. When the concentration of Ni, Cu and Zn was close to 100 mg·L^{-1}, the optical density of strain LB5Z decreased by half. Based on the screening result from coal gangue and verification in solution gradient, the strain LB5Z was proved to be more adaptive at high concentration of Cd. In order to understand the adaptation of strain LB5Z to combined contamination of heavy metals, the effects of coal gangue content on LB5Z growth were examined in liquid medium (Figure 4). LB5Z, as a Cd-resistant strain, can grow and reproduce under the presence of enough nutrients and trace elements contained in coal gangue. A similar finding was also reported by Wang *et al.* [25]. When the content of coal gangue was up to 250 g·L^{-1}, the bacterial growth generally displayed a declining trend due to the toxicity of heavy metals, which altered the metabolic and physiological properties of bacteria [26]. According to the growth response of LB5Z under coal gangue stress, its tolerance to higher coal gangue content was evident.

There was a general slight decline trend of pH with the increase of concentration of coal gangue, both for inoculation and non-inoculation (Figure 4). One possible reason is that coal gangue *per se* is acidic. Another possible reason may be that some bacteria can release acidic substances, resulting in the pH decrease and rendering undissolved phosphate converted into dissolved phosphate [27]. For the inoculation treatment group, pH was significantly higher than that of the control group (non-inoculation). Regarding the mechanism of pH increase by inoculation of bacteria, further studies will be carried out. Previously, Ma *et al.* reported that the bacteria that were isolated from a heavy metal-polluted environment could increase the pH of soil, resulting in the decrease of solubility of heavy metal, which is beneficial for phytoremediation [28].

Influence of Cd-resistant Bacteria Strain on the Growth of Plants

The PGPB used in place of synthetic chemicals is known as beneficial microorganisms. It is capable of improving plant growth by supplying the plant with nutrients. This could be beneficial for sustaining environmental health and improving soil productivity. *Pseudomonas aeruginosa* LB5Z shows high resistance to heavy metals and improves the growth of plants. In

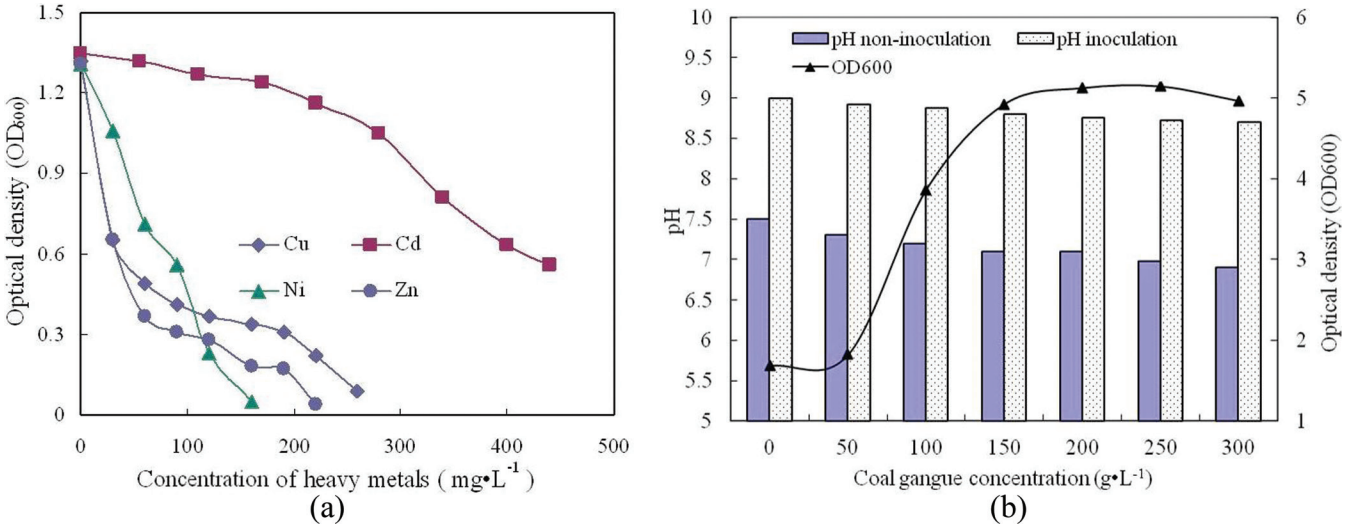

Figure 4. *Tolerance of LB5Z to different kinds and content of heavy metals in coal gangue.*

view of this, the promoting efficiency of *Pseudomonas aeruginosa* for plant growth was examined on Amorpha fruticosa L. with different coal gangue contents in pot experiments (Figure 5).

Amorpha fruticosa L. showed some visible evidences when grown in soils mixed with coal gangue in different ratios. Seeds in single coal gangue did not sprout. The greatest budding ratio was found in the group Ratio I, while the single loess group presented lower bud ratio. The plant height, root length and fresh weight of loess treatment were found relatively low. The concentrations of Cd^{2+} in coal gangue, Ratio I, and Ratio II groups were 32.15, 13.19 and 10.22 mg·kg^{-1}, respectively. The high Cd^{2+} concentration in coal gangue restrained seed germination. As seeds in Ratio I and Ratio II sprout normally, this suggests that a concentration of Cd^{2+} at 13.19 mg·kg^{-1} can be tolerated. However, in the growth stage, the inhibition effect of a high concentration of Cd^{2+} on seedlings began to appear, leading to slow growth in Ratio I. In this experiment, the relatively low concentration 10.22 mg·kg^{-1} did not show significant adverse effects on seedlings.

Generally, the strain LB5Z treatments resulted in a significant increase in budding and growth of plants. Even for Ratio I, the plant germination and growth were still significantly higher in inoculated treatment than those without inoculation treatment. However, there was no stimulative effect on germination even for the group with Cd-resistant bacteria inoculation, due to a high concentration of heavy metals in single coal gangue treatment. As reported by Russel *et al.* [29], plants that grew on Cd medium from seeds presoaked by heavy metal resistant bacteria exhibited longer and heavier roots, higher biomass and lower Cd accumula-

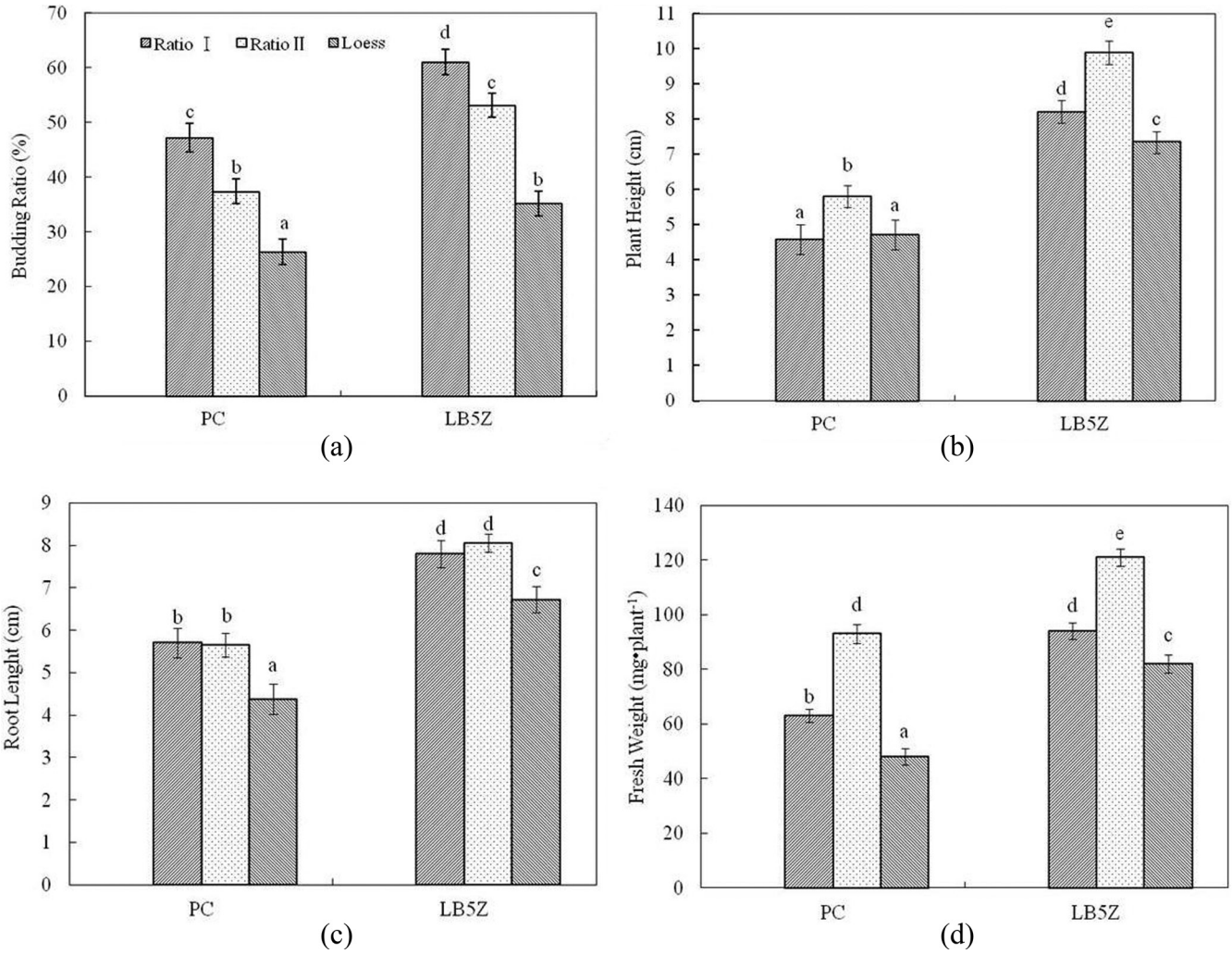

Figure 5. *Budding ratio, plant height, root length and fresh weight of Amorpha fruticosa L. in mixed soils with different ratios of coal gangue 75 days after seeding (Error bars represent ±SD of three replicates and different letters a, b, c and d above columns indicate significant differences among treatments at the 5% level).*

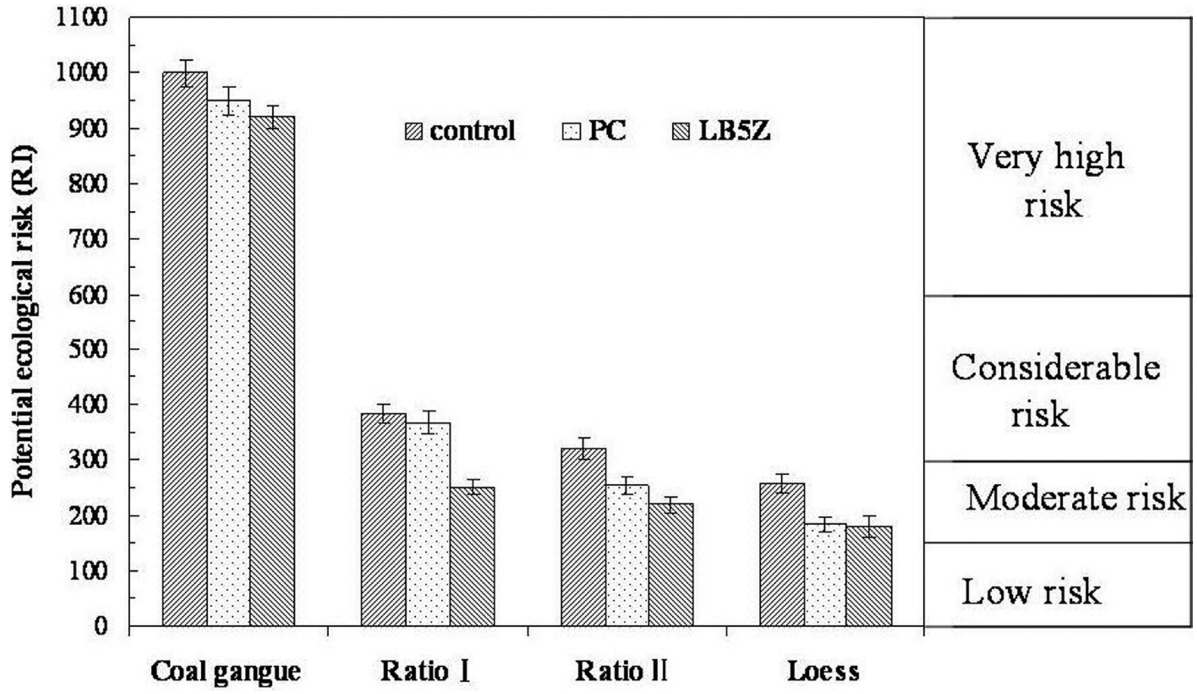

Figure 6. *Potential ecological risk index of different treatments.*

tion of 50 ppm. But when the concentration of Cd was up to 100 ppm, there was no significant difference between heavy metal resistant bacteria with association and those without association. Thus, it is important to choose optimal tolerance range of heavy metal resistant bacteria in phytoremediation promoted by PGPB. The positive effects of PGPB on the yield and growth of plants can be explained by the promoting effects of these bacteria on auxin and cytokinin production, phosphate solubilization, N_2-fixation and antimicrobial substance production [26]. Similarly, the yield and plant growth enhancement effects could be attributed to the bacteria used in this study on *Amorpha fruticosa* L.

Toxicity Assessment of Soils

Table 2 summarizes the ecological risk assessment results of toxic heavy metals in different treatment soils. As can be seen, the toxic index of Cd was significantly higher than that of other metals, because of its larger percentage in exchangeable and carbonate fraction. Cd might bring a relatively higher risk to local ecosystem, while other heavy metals were all in low ecological risk. This phenomenon indicated that toxic indexes probably had a close relation with the chemical speciation of heavy metals [30]. The high risk of Cd to local environment should receive more attention in the future study.

Figure 6 shows the values of RI, which can be used to quantify the overall potential ecological risk of different treatments. Coal gangue as a mining residue has a very high potential ecological risk. Plant and inoculation have no evident effect on amelioration of coal gangue, suggesting that coal gangue should be treated before reclamation. Due to the location near the coal mine area, the loess is affected by coal mining residues to some extent. Therefore, the potential ecological risk was at the moderate level. Such situation, however, can be improved by inoculation of strain LB5Z. Both Ratio I and Ratio II were in the considerable risk grades.

Table 2. E_r^i of Each Heavy Metal in Different Treatments.

Sample	Cd	Cr	Cu	Ni	Zn
Coal gangue	996/946/918	0.23/0.12/0.11	0.10/0.11/0.10	0.19/0.16/0.15	0.52/0.54/0.56
Ratio I	382/367/349	0.22/0.20/0.17	0.43/0.37/0.33	0.67/0.60/0.49	0.39/0.34/0.30
Ratio II	318/252/218	0.15/0.14/0.13	0.32/0.27/0.34	0.51/0.46/0.41	0.27/0.30/0.25
Loess	256/183/180	0.13/0.11/0.11	0.23/0.22/0.21	0.30/0.26/0.21	0.20/0.23/0.20

Note: Values separated by a slash in one column are the E_r^i of heavy metal in control, PC and LB5Z, respectively.

Planting is useful in decreasing the risk grade especially for Ratio II. For instance, the potential ecological risk of Ratio II becomes moderate after planting. Inoculation could further decrease the ecological risk, especially for Ratio I. It could be concluded based on these results that planting and inoculation are very advantageous to ecological restoration.

Taking RI and growth of *Amorpha fruticosa* L. into account, treatment Ratio II was recommended for the reclamation of coal gangue and soil surrounded by coal mining by using phytoremediation combined with microorganisms.

Other studies have investigated the adverse effect of long-term reclamation of soil with coal gangue [18,31]. The results show that for the reclaimed soil by coal gangue, with the increase of covering soil, the contents of Ni, Pb, Cu, Cd and Hg are all higher than those in the background soil, except for Mn and As. There is a certain degree of heavy metal accumulation. To further confirm the long-term effects of coal gangue, a long-term experimental study is needed.

CONCLUSIONS

Coal gangue is a waste residual during coal mining production processes, which results in high concentration of heavy metals, especially Cd, in coal gangue-polluted land. The strain *Pseudomonas aeruginosa* LB5Z isolated from coal gangue has a high tolerance to Cd and coal gangue. At the same time, strain LB5Z could promote *Amorpha fruticosa* L. growth and improve its tolerance to heavy metals.

The experimental results suggested that native woody plant *Amorpha fruticosa* L. is suitable for the reclamation of coal gangue-polluted land. *Amorpha fruticosa* L. could grow normally at the ratio 1:1 and 1:2 of coal gangue with the loess. This study also demonstrates that the introduction of *Pseudomonas aeruginosa* LB5Z is a promising method for improving plant growth as well as the plants' tolerance to heavy metals. Planting and inoculation could decrease potential ecological risk of soil mixed with coal gangue and loess, and the preferable ratio is 1:2.

REFERENCES

1. Sun, C.S., Guo, J.L., "Review and outlook on China coal industry development in 2013", *Coal Economic Research*, Vol. 34, No. 2, 2014, pp. 5–10.
2. Liu, K., Ma, Y.D., Hou, X.K., "Environmental hazards and comprehensive utilization of coal gangue in our country", *Coal*, Vol. 22, No. 5, 2013, pp. 26–28.
3. Cao, D.W., Ji, J., Liu, Q.Q., He, Z.Y., Wang, H.N., You, Z.P., "Coal gangue applied to low-volume roads in China", *J. Trans. Res. Board,* No. 2204, 2011, pp. 258–266. http://dx.doi.org/10.3141/2204-32
4. Qian, K.M., Zhang, L., Wang, L.P., "An environmentally sound usage of both coal mining residue and sludge", *Advanced Materials Research,* 2011, Vol. (183–185), pp. 595–599.
5. Hao, G., Yun, F., Zhan, Y.L., Sen, Y., Song, Z., "Study on the property and reuse of coal gangue in Liupanshui, Guizhou province, China", *Int. Journal of Mining, Reclamation and Environment*, Vol. 27, 2012, pp. 366–373.
6. Xu, L.J., Huang, C., Zhang, R.Q., Liu, H.P., Yan, J.P., Meuser, H., Makowsky, L., "Physical and chemical properties and distribution characteristics of heavy metals in reclaimed land filled with coal gangue", *Transactions of the Chinese Society of Agricultural Engineering*, Vol.30, No.5, 2014, pp. 211–219.
7. Ma, Y., Rajkumar, M., Freitas, H., "Improvement of plant growth and nickel uptake by nickel resistant-plant-growth promoting bacteria", *Journal of Hazardous Materials*, Vol. 166, 2009, pp. 1154–1161. http://dx.doi.org/10.1016/j.jhazmat.2008.12.018
8. Nie, L., Shah, K.K.V., Patra, D.D., "Effects of Metal-Resistant Plant Growth Promoting Bacteria on Growth and Cadmium Accumulation of Corn", *Int. J. Phytoremediation,* Vol. 15, 2013, pp. 743–55. http://dx.doi.org/10.1080/15226514.2012.735287
9. Marta, N.S., Mucha, P., Rocha, A.C., Gomes, C.R., Almeida, C.M.R., "A strategy to potentiate Cd phytoremediation by saltmarsh plants-Autochthonous bioaugmentation", *Journal of Environmental Management,* Vol. 134, No. 1, 2014, pp. 136–144.
10. Rajkumar, M., Ma, Y., Freitas, H., "Improvement of Ni phytostabilization by inoculation of Ni resistant Bacillus megaterium SR28C", *J. Env. Man.*, Vol. 128, 2013, pp. 973–980. http://dx.doi.org/10.1016/j.jenvman.2013.07.001
11. Lu R.K., "Physical Chemical Analysis of soils", Chinese agricultural science and Technology Press, 2000.
12. Chen, H.H., Bao, H.J., Fu, R.R., Ying, H.S., Lu, C.M., Jin, X.Z., Xiao, D.H., "Determination of Cr, As, Cd, Hg and Pb in iron ores using inductively coupled plasma-Mass spectrometry with microwave digestion", *Rock and Mineral analysis,* Vol. 31, No. 2, 2012, pp. 231–240.
13. Tessier, A., Campbell, P.G.C., Bisson, M., "Sequential extraction procedure for the speciation of particulate trace metals", *Anal. Chem.*, Vol. 51, No. 7, 1979, pp. 844–851. http://dx.doi.org/10.1021/ac50043a017
14. Zhang, Y.X., Song, X.Q., Huang, L., Hu, Z.Q., Chai, T.Y., "Isolation of a cadmium-resistant bacterium from coal mining and heavy metal tolerance", *Journal of China Coal Society*, Vol. 35, No. 10, 2010, pp. 1735–1741.
15. Bric, M., Bostock, R.M., Silversone, S.E., "Rapid in situ assay for indole acetic acid production by bacteria immobilization on a nitrocellulose membrane", *Appl. Environ. Microbiol.*, Vol. 57, No. 2, 1991, pp. 535–538.
16. Wang, L., "Experimental method and technology of Environmental Microbiology", Chemical Industry Press, 2009.
17. Maanana, M., Saddik, M., Maananc, M., Chaibi, M. Assobhei, O. Zourarah, B., "Environmental and ecological risk assessment of heavy metals in sediments of Nador lagoon, Morocco", *Ecological Indicators,* Vol. 48, 2014, pp. 616–626. http://dx.doi.org/10.1016/j.ecolind.2014.09.034
18. Zhang, H.J., Ouyang, S.L., "Release characteristics of heavy metals from coal gangue under simulation leaching conditions", *Energy Exploration & Exploitation*, Vol. 32, No. 2, 2014, pp. 413–422. http://dx.doi.org/10.1260/0144-5987.32.2.413
19. Yue, J., "Studies on forms of heavy metals in coal gangue and leaching experiment", Master degree thesis, Shanxi University, China, 2010, pp. 27–49.
20. Lv, X.W., Chen, C.Y., Huang, R., Dang, Z., "Speciation analysis and transfer of heavy metals in atmospheric particulates", *Journal of South China University of Technology (Natural Science Edition)*, Vol. 33, No. 1, 2005, pp. 75–79.
21. Wang, H., Hao, Q.W., Yin, E.Q., "A study on water pollution from eluvating and immersing gangue", *Coal Geology of China*, Vol. 18, No. 2, 2006, pp. 43–45.
22. Islam, F., Yasmeen, T., Ali, Q., Ali, S., Arif, M.S., Hussain, S., Rizvi,

H., ″Influence of Pseudomonas aeruginosa as PGPR on oxidative stress tolerance in wheat under Zn stress", *Ecotoxicology and Environmental Safety*, Vol. 104, No. 3, 2014, pp. 285–293. http://dx.doi.org/10.1016/j.ecoenv.2014.03.008

23. Adesemoye, A.O. and Kloepper, J.W., ″Plant-microbes interactions in enhanced fertilizer-use efficiency", Applied Microbiology and Biotechnology, Vol. 85, No. 1, 2009, pp. 1–12. http://dx.doi.org/10.1007/s00253-009-2196-0
24. Adesemoye, A.O., Obini, M., Ugoji, E.O., ″Comparison of plant growth-promotion with *Pseudomonas aeruginosa* and *Bacillus subtilis* in three vegetables", *Braz. J. Microbiol.*, Vol. 39, 2008, pp. 423–428. http://dx.doi.org/10.1590/S1517-83822008000300003
25. Wang, T., Wang, Y., Wang, J., ″Research on potential fertilization of coal gangue in the Weibei Coal field, China", *Act. Geo. Sin.*, Vol. 82, 2008, pp. 717–725.
26. Rajkumar, M. and Freitas, H., ″Influence of metal resistant-plant growth-promoting bacteria on the growth of *Ricinus communis* in soil contaminated with heavy metals", *Chemosphere*, Vol. 71, No. 5, 2008, pp. 834–842. http://dx.doi.org/10.1016/j.chemosphere.2007.11.038
27. Ali, S., Hamid, N., Nagina, N., ″Screening of phosphate solubilizing microorganisms using different original and modified culture media", *Biologia Plantarum*, Vol. 44, 1998, pp. 110–122.
28. Ma, Y., Prasad, M. N.V., Rajkumar, M., Freitas, H., ″Plant growth promoting rhizobacteria and endophytes accelerate phytoremediation of metalliferous soil", *Biotechnol Adv.*, 2011, Vol. 29, pp. 248–58. http://dx.doi.org/10.1016/j.biotechadv.2010.12.001
29. Russel, S., Saifone, C., Enzo, A.P., Francois, M., Mrinal, B., ″Heavy metal phytoremediation potential of heavy metal resistant soil bacterial isolate, Achromobacter sp. Strain AO22", APCBEE Procedia, Vol. 5, 2013, pp. 502–207. http://dx.doi.org/10.1016/j.apcbee.2013.05.085
30. Zhu, H.N., Yuan, X.Z., Zeng, G.M., Jiang, M., Liang, J., Zhang, C., Yin, J., Huang, H.J., Liu, Z.F., Zhi, F., Jiang, H.W., ″Ecological risk assessment of heavy metals in sediments of Xiawan Port based on modified potential ecological risk index", *Trans. Nonferrous Met. Soc. China*, Vol. 22, No. 6, 2012, pp. 1470–1477. http://dx.doi.org/10.1016/S1003-6326(11)61343-5
31. Zheng, Y.G., Zhang, Z.G. Yao, D.X., Chen X.Y., ″Characteristics of temporal spatial distribution and enrichment of heavy metals in coal mine reclaimed soil", *J. China Coal Society*, Vol. 38, No. 8, 2013, pp. 1476–1483.

Characteristics of Sulfate Reduction–Ammonia Oxidation under Anaerobic Conditions

YI YUAN[1,2], YONG HUANG[1,2,*], XIANG LI[1,2], CHUN-LEI ZHANG[1,2], LI ZHANG[1,2], YANG PAN[1,2] and FU-XIN LIU[1,2]
[1]*School of Environmental Science and Engineering, Suzhou university of Science and technology, Suzhou, 215011, China*
[2]*Jiangsu Collaborative Innovation Center of Technology and Material of Water Treatment, Suzhou, 215009, China*

ABSTRACT: The sulfate reduction–ammonia oxidation reaction with ANAMMOX sludge at autotrophic condition was investigated. It was found that the pH level decreased, and elemental sulfur and dinitrogen were produced at the end of this process, while NO_3^--N was a byproduct. A lower ratio of n(N) to n(S) can improve SO_4^{2-}-S conversion ratio where a larger portion of NH_4^+-N was oxidized into NO_3^--N, resulting in a decreased removal ratio of n(TN)/n(TS). This indicates that ammonia can be oxidized into NO_2^--N or NO_3^--N by sulfate, then the residual NH_4^+-N and the produced NO_2^--N would be removed via ANAMMOX.

INTRODUCTION

THE excess amount of ammonium usually leads to the eutrophication which poses threats to water quality and human health [1]. The balance of natural sulfur cycle could be interfered by high sulfate concentrations resulting in the release of toxic sulfides [2,3]. At the same time, sulfides bring potential damage to the environment, such as odor, corrosion [4,5]. Wastewater from various industry departments, e.g., pharmacy, food and paper making industry, often contains ammonium and sulfate. It is, therefore, necessary to develop an effective method to remove ammonium and sulfate simultaneously. Biological technologies are commonly used in nutrient removal for lower energy consumption and operation cost. Unfortunately, ammonium and sulfate in wastewater are usually treated separately at present. Recently, treatment procedures have been proposed for ammonium. For instance, the procedure of anaerobic ammonium oxidation (ANAMMOX), as shown in Equation (1), uses nitrite as an electron acceptor to oxide ammonia into dinitrogen under anaerobic autotrophic condition [6]. The maximum nitrogen removal capability of ANAMMOX reaches 70 $kg\cdot(m^3\cdot d)^{-1}$ [7], it is therefore used to treat wastewater with high ammonia concentration. In the presence of sulfate-reducing bacteria (SRB), sulfate can be converted to sulfide with organics as electron donor under anaerobic conditions. Sulfide oxidizing bacteria (SOB) can oxide sulfide into elemental sulfur which can be recycled [8]. Biological desulfurization process, however, is only suitable for sulfur removal. As the same time, it has its own limitations, e.g., long treatment procedure, oxygen supply needed and relatively high cost for sulfate treatment.

$$1NH_4^+ + 1.32NO_2^- + 0.066HCO_3^- + 0.13H^+ \rightarrow 1.02N_2 + 0.26NO_3^- + 0.066CH_2O_{0.5}N_{0.15} + 2.03H_2O \quad (1)$$

Recent studies have found that the conversion of sulfur might be related to nitrate or ammonia [9,10], which brings new ideas for simultaneous removal of nitrogen and sulfur. Sulfide and nitrate can be removed simultaneously with dinitrogen and elemental sulfur as the product at anoxic condition, defined as a denitrifying sulfide removal (DSR) process. As for wastewater in high concentration of ammonia and sulfate, sulfate should be converted to sulfide with SRB at anaerobic condition, and ammonia could be oxidized to nitrite or nitrate at aerobic condition. Sulfide and nitrite or nitrate could then be removed simultaneously through the DSR process [11]. Several representative treatment processes are listed in the following: denitrifying ammonium oxidation (DEAMOX) [12], sulfate reduction, autotrophic denitrification and nitrification integrated (SANI) [13], and simultaneous desulfurization/denitrification (SDD) [14]. Each of these has its own limitations, e.g., oxygen supply is needed during nitrifica-

*Author to whom correspondence should be addressed.
E-mail: yhuang@mail.usts.edu.cn

1544-8053/15/01 S115-07

doi:10.12783/issn.1544-8053/12/S1/17

tion and organism could be consumed during sulfate reduction. Additionally, the anaerobic-aerobic-anoxic conditions potentially increase the financial budget and operation complexity.

Fdz-Polanco *et al.* [10,15] reported that ammonia and sulfate could be removed synchronously in an anaerobic fluidized bed reactor (AFBR) filled with granular activated carbon (GAC) when treating industrial wastewater that was rich in organic matter, nitrogen and sulfate. Such a procedure was named sulfate reduction and ammonia oxidation (SURAMOX), main chemical reaction of which is shown in Equation (2):

$$2NH_4^+ + SO_4^{2-} \rightarrow N_2 + S + 4H_2O \qquad \Delta G^{\cdot} = -44.3\ kJ\cdot mol^{-1} \tag{2}$$

The $\Delta G^{\cdot}$ of this reaction is too small to be reproduced until Yang *et al.* [16] demonstrated that the process requires involvement of microorganisms. Liu *et al.* [17] proves that SURAMOX process shows a great biotechnological potential for completely autotrophic reaction using ANAMMOX bacteria. It is attractive that ammonia and sulfate could be removed synchronously in an anaerobic treatment plant using sulfate reduction–ammonia oxidation. But there are many unanswered questions related to the characteristics of this reaction. For instance, some researchers considered that S^{2-} should be the intermediate product [10,18–19] due to S^{2-} detection in heterotrophic environment. While other researchers considered S^{2-} should not be the intermediate product [17] due to no S^{2-} observed in autotrophic environment. pH value increased in autotrophic environment [17] but decreased in heterotrophic environment [19,20]. Only Samubon [20] and Rikmann *et al.* [19] reported NO_3^--N was produced obviously in heterotrophic environment. In summary, sulfate reduction-ammonia oxidation reaction would be changed if organic matter presented or not. Sulfate reduction–ammonia oxidation reaction is autotrophic reaction, the research in autotrophic environment, therefore, could explain the mechanism of it. The aim of this research is to study all possible transformation pathways for both nitrogen and sulfur during sulfate reduction–ammonia oxidation reaction in autotrophic environment.

MATERIALS AND METHODS

Experimental Setup

Total volume of the batch reactor is 0.55 L and the effective volume is 0.45 L. A thick cylindrical woven carrier in the three dimensions of 12 cm (length) by 7 cm (height) by 0.2 cm (thickness) was used as the supports for micro-organism growth. Water filling ratio is 1. All of the connections were sealed with silicone, and water hoses were sealed with clip. The reactor was covered with shielding cloth. After filling, pure nitrogen was stripped into reactor for 30 min in order to displace the oxygen. The reaction was then proceeded in an oscillator under the temperature of (32 ± 2)°C.

Inoculums and Synthetic Water

Activated sludge used in this study was obtained from ANAMMOX sludge [21]. The initial biomass concentration in the reactor was about 0.518 $g\cdot L^{-1}$ and MLVSS/MLSS was 0.465.

NH_4Cl and $(NH_4)_2SO_4$ were used for providing ammonium and sulfate during sulfate reduction–ammonia oxidation reaction. The amounts of these chemical components varied depending on the ratio of n(N)/n(S). Na_2S was used to provide S^{2-}/HS^- and $NaNO_2$ or $NaNO_3$ was used to provide NO_2^- or NO_3^- during autotrophic denitrification.

The mineral medium composition used throughout this study was ($g\cdot L^{-1}$): $KHCO_3$, 0.9; $NaHCO_3$, 0.9; KH_2PO_4, 0.027; $CaCl_2\cdot 2H_2O$, 0.136; $MgCl_2$, 0.2. The composition of trace element I and II were based on van de Graff *et al.* [22]. 1 mL of trace element I and 1.25 mL of trace element II were added to a liter of raw water.

Experimental Procedure

For sulfate reduction–ammonia oxidation reaction, the pH was about 7.6–7.8 in the influent and the duration for reaction was 3d. The SO_4^{2-}-S concentration in influent was controlled at 68.6$mg\cdot L^{-1}$. The NH_4^+-N concentration in influent was 120 $mg\cdot L^{-1}$ and the ratio of n(N)/n(S) was 4 during the period 1 ~ 126d. The NH_4^+-N concentration in influent was 60 $mg\cdot L^{-1}$ and the ratio of n(N)/n(S) ratio was 2 during the period 128d ~185d.

For autotrophic denitrification batch experiments after 185d, the NO_3^--N concentration in influent was 30 $mg\cdot L^{-1}$ and S^{2-} was 28 $mg\cdot L^{-1}$ in experiment 1. And the NO_2^--N concentration in influent was 30 $mg\cdot L^{-1}$ and S^{2-} was 28 $mg\cdot L^{-1}$ in experiment 2. Each experiment was implemented 7 times and reaction duration was 1 day.

Analytical Methods

The concentrations of nitrogen compounds and sulfate were measured using standard methods according to American Publish Health Association [23]. The sample was filtered by a fiber paper with the hole diameter of 0.45 μm. NH_4^+-N, NO_2^--N, SO_4^{2-}-S and S^{2-} were measured colorimetrically, while NO_3^--N was measured spectro-photometrically. The pH value was recorded using a digital, portable pH meter.

RESULTS AND DISCUSSION

Transformation of Sulfate during Sulfate Reduction–Ammonia Oxidation Reaction

The conversion ratio of SO_4^{2-}-S was about 20% when n(N)/n(S) ratio was 4. The ratio reached to 60% when the ratio of n(N)/n(S) was 2, as shown in Figure 1. S^{2-}/HS^- was not detected in the whole experiment. The color of ANAMMOX sludge became brown with pale yellow solid gradually attached, as shown in Figure 2. After 90d, the sludge turned yellow and some pale yellow solids were washed out of the reactor. The solids filtered through fiber paper with the hole diameter of 0.45 μm hole were placed in water and alcohol, respectively. It was found that the solid could be dissolved in alcohol. Janssen *et al.* [24] found that elemental sulfur generated through the biological process was covered with a layer of similar protein polymers, which could be unsinkable colloidal solids. Some of the elemental sulfur was generated in this experiment attached to the wall of reactor [seen in Figure 2(c)], others were washed out. Further study should be examined whether HS^-/S^{2-} degraded quickly as an intermediate which was shown in Results from Autotrophic Denitrification of S^{2-} section.

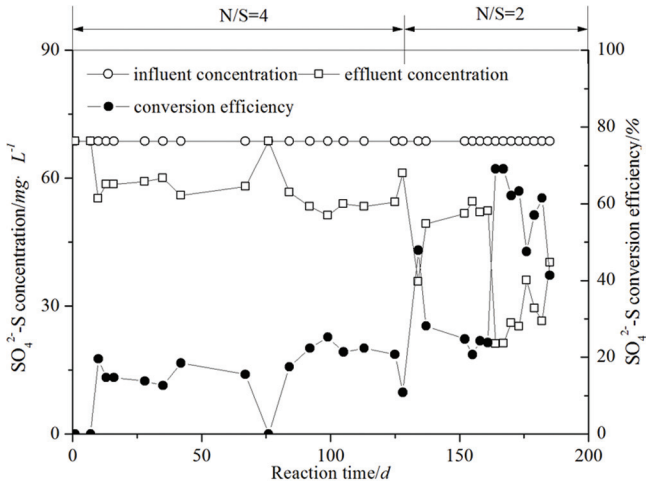

Figure 1. *Variety of sulfate in the process of sulfate reduction–ammonia oxidation.*

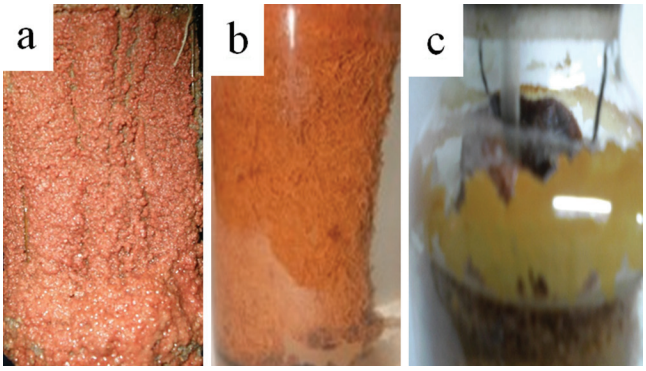

Figure 2. *Change of sludge color for sulfate reduction- ammonia oxidation: (a) Before incubate; (b) Incubate for 90d; and (c) Elemental sulfur attached to the wall of reactor.*

Transformation of Nitrogen during Sulfate Reduction—Ammonia Oxidation Reaction

As shown in Figure 3, ammonia conversion efficiency increased from 60% to 100% gradually when n(N)/n(S) ratio was 4. The conversion efficiency of ammonia was also 100 % when n(N)/n(S) ratio was 2.

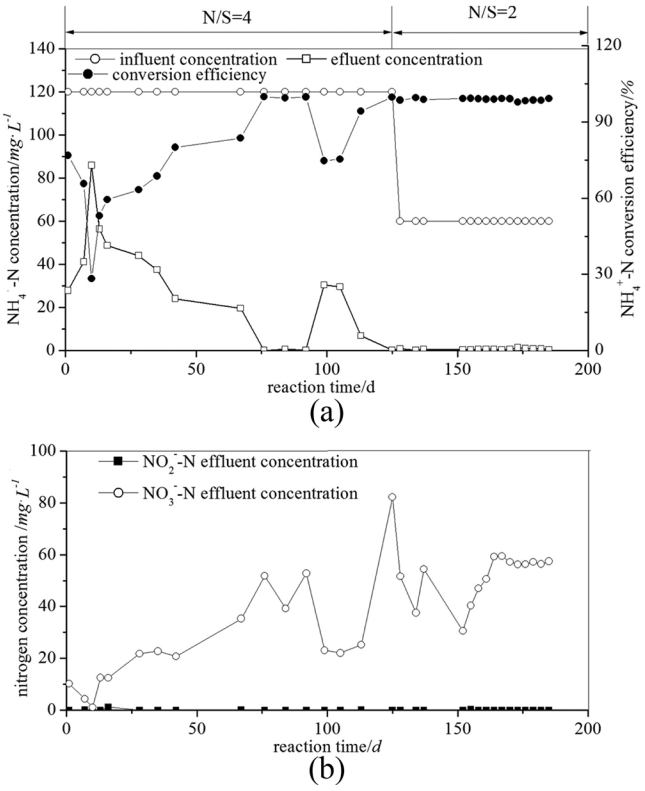

Figure 3. *Variety of nitrogen in the process of sulfate reduction- ammonia oxidation.*

NO_2^--N was not detected in the whole experiment. By contrast, a larger amount of NO_3^--N was detected and the maximum concentration was 82 mg·L^{-1}. It showed that the lower n(N)/n(S) ratio was, the more NO_3^--N would be produced. That whether NO_3^--N could be produced during the process of sulfate reduction - ammonia oxidation has received little attention. NO_3^--N was even not mentioned as a product in the paper of Zhang *et al.* [25]. However, NO_3^--N was found as a product in this study. NO_3^--N could be produced in the ANAMMOX process according to Equation (1). The amount of NO_3^--N detected in this study was larger than that produced, as shown in Table 2.

pH Change in Sulfate Reduction–Ammonia Oxidation Reaction

The pH value could be increased in conventional ANAMMOX process due to the consumption of H^+ [26,27]. Sulfate reduction–ammonia oxidation is found to be a new type of biological process similar to ANAMMOX. It, however, can be seen from Figure 4 that pH in effluent was lower than that in the influent which was similar to the findings from Samubon [20] and Rikmann *et al.* [19].

The Effect of n(N)/n(S) on Sulfate Reduction–Ammonia Oxidation

As shown in Figure 5, when n(N)/n(S) ratio was 4, the average conversion rate of NH_4^+-N and SO_4^{2-}-S was 3.8 mmol·L^{-1}·d^{-1} and 0.24 mmol·L^{-1}·d^{-1}, respectively. The average generation rate of NO_3^--N was 1.47 mmol·L^{-1}·d^{-1}.When n(N)/n(S) ratio was 2, the average conversion rate of NH_4^+-N and SO_4^{2-}-S was 1.41 mmol·L^{-1}·d^{-1} and 0.42 mmol·L^{-1}·d^{-1}, respectively. Average generation rate of NO_3^--N was at 1.37 mmol·L^{-1}·d^{-1}. It could be concluded that SO_4^{2-}-S conversion rate increased with n(N)/n(S) ratio decreasing

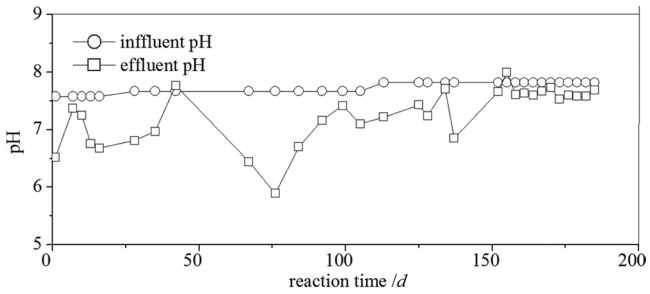

Figure 4. *pH change in the process of sulfate reduction–ammonia oxidation.*

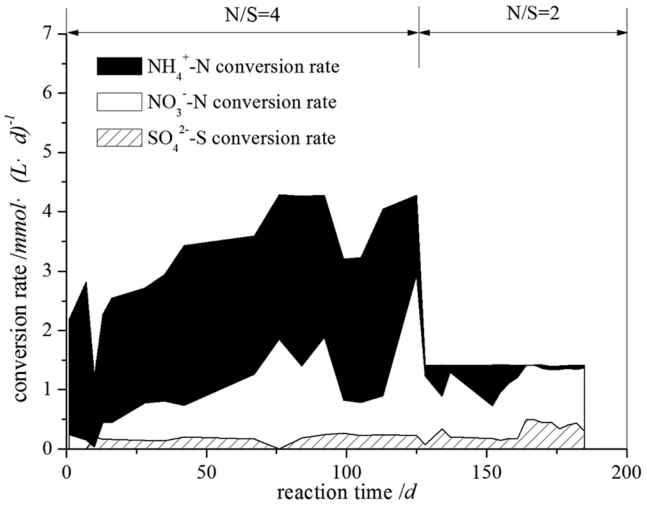

Figure 5. *Variety of materials conversion rates in the process of sulfate reduction–ammonia oxidation.*

while SO_4^{2-}-S concentration in influent was constant. However, little change of NO_3^--N generation rate was observed. NO_2^--N was not detected in effluent and nitrogen loss was observed under different n(N)/n(S) ratios.

As shown in Figure 6, it can be seen that NH_4^+-N/SO_4^{2-}-S conversion ratio and n(TN)/n(TS) removal ratio were positively correlated with n(N)/n(S) of raw water. When n(N)/n(S) was 2, NH_4^+-N/SO_4^{2-}-S conversion ratio was 3.45±0.5 which was close to 2. n(TN)/n(TS) removal ratio was only 0.11±0.05. The 97.2% of the converted NH_4^+-N was oxidized to

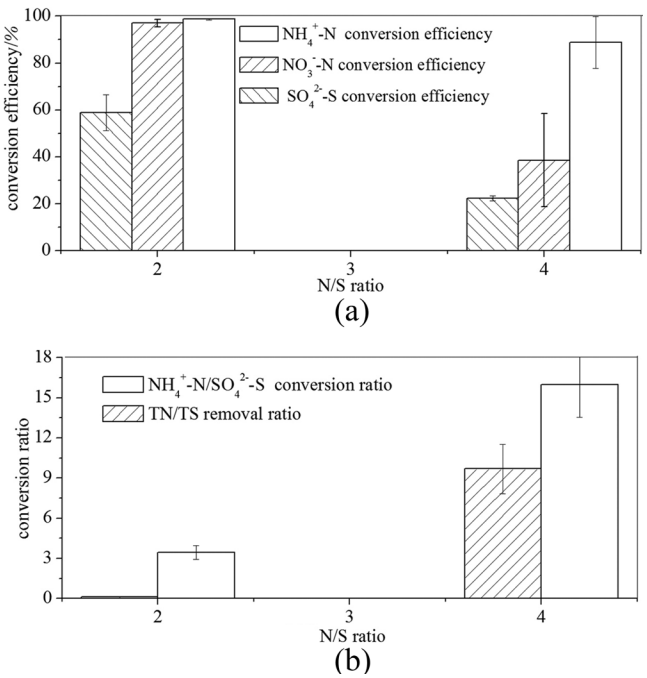

Figure 6. *Effect of n(N)/n(S) ratio on substrates conversation.*

NO_3^--N with 2.8% of nitrogen loss. This was not in line with the findings from Liu *et al.* [17]. Both NH_4^+-N/SO_4^{2-}-S conversion ratio (at 15.96 ± 2.41) and n(TN)/n(TS) removal ratio (at 9.69±1.84) were far away from the theoretical value [10,17] when n(N)/n(S) was 4. At the same time, 38.7% of the converted NH_4^+-N was oxidized to NO_3^--N. Therefore, it is concluded that n(N)/n(S) had little effect on NH_4^+-N conversion efficiency. However, lower n(N)/n(S) ratio could lead to higher SO_4^{2-}-S conversion rate. Portion of NH_4^+-N converted into NO_3^--N which has led to smaller nitrogen losses. All of these have demonstrated that sulfate reduction–ammonia oxidation reaction is not an elementary reaction but a number of reactions.

Results from Autotrophic Denitrification of S^{2-}

To examine whether autotrophic denitrification depended on S^{2-} occurred during the process, additional experiments were conducted after 185d. Results from this analysis are list in Table 1. The concentrations of NO_3^--N/NO_2^--N and S^{2-} barely changed in the influent and effluent. This denotes that micro-organisms in the reactor cannot degrade S^{2-}. It also demonstrates that S^{2-} is not an intermediate product during the process of sulfate reduction–ammonia oxidation reaction.

The Material Balance during Sulfate Reduction–Ammonia Oxidation

The above-listed results show that sulfate reduction -ammonia oxidation might be composed of a series of reactions. According to the detected HS^-/S^{2-}, Fdz-Polanco *et al.* [10] speculated the equations might be that as follows:

$$3SO_4^{2-} + 4NH_4^+ \rightarrow 3S^{2-} + 4NO_2^- + 4H_2O + 8H^+ \quad (3)$$

$$3S^{2-} + 2NO_2^- + 8H^+ \rightarrow N_2 + 3S + 4H_2O \quad (4)$$

$$2NO_2^- + 2NH_4^+ \rightarrow 2N_2 + 4H_2O \quad (5)$$

Some researchers tend to support this assumption because HS^-/S^{2-} was detected in their heterotrophic experiments [18,19]. It could be analyzed that sulfate- reducing bacteria (SRB) might reduce sulfate into HS^-/S^{2-} using organic or hydrogen as electron donor under organic anaerobic conditions. At the same time, HS^-/S^{2-} could further facilitate autotrophic denitrification.

In this experiment, ANAMMOX sludge was inoculated and cultured in inorganic nutrient environment. Therefore, no organic substrates were available for SRB to produce HS^-/S^{2-}. This can partially explain the fact that HS^-/S^{2-} was not detected in this study. According to autotrophic denitrification experiments, the reduction product of SO_4^{2-}-S is S^0 instead of S^{2-}. HS^-/S^{2-} also were not detected in the experiment of Liu *et al.* [17], which was implemented in an inorganic environment too. Liu *et al.* [17] speculated the reactions of sulfate reduction–ammonia oxidation in Equations (5) and (6):

$$NH_4^+ + SO_4^{2-} \rightarrow NO_2^- + S^0 + 2H_2O \quad (6)$$

$$2NH_4^+ + 2NO_2^- \rightarrow 2N_2 + 4H_2O \quad (5)$$

Although this speculation can explain that elemental sulfur is produced directly from SO_4^{2-}-S with NH_4^+-N oxidation in this experiment, it cannot explain the phenomena of the production of large quantity of NO_3^--N and the drop of pH value. NO_3^--N can only be produced via ANAMMOX [seen Equations (1) and (5)] in both sub-step reactions supposed by Fdz-Polanco *et al.* [10] or Liu *et al.* [17]. In ANAMMOX reaction, NH_4^+-

Table 1. The Transformation Rule of Substrates in Autotrophic Denitrification Experiments.

	Experiment 1				Experiment 2			
Time	NO_3^--N in Influent, (mg/L)	NO_3^--N in Effluent, (mg/L)	S^{2-} in Influent, (mg/L)	S^{2-} in Effluent, (mg/L)	NO_2^--N in Influent, (mg/L)	NO_2^--N in Effluent, (mg/L)	S^{2-} in Influent, (mg/L)	S^{2-} in Effluent, (mg/L)
1	30.0	30.0	28	28	30.1	30.0	28	28
2	29.9	29.8	28	28	30.1	29.9	28	28
3	29.9	29.9	28	28	30.0	29.9	28	28
4	30.0	30.0	28	28	30.0	30.0	28	28
5	30.0	30.0	28	28	29.8	29.7	28	28
6	30.0	30.0	28	28	29.8	29.8	28	28
7	30.0	30.0	28	28	30.0	30.0	28	28

Table 2. The Material Balance during Sulfate Reduction–Ammonia Oxidation.

Operation Time, d	n(N)/n(S)	Converted NH_4^+-N, mg·L^{-1}	Converted SO_4^{2-}-S, mg·L^{-1}	NO_3^--N Production, /mg·L^{-1}	NO_3^--N Production in Theory, mg·L^{-1}
1~126	4	106	15.4	41.1	11.9
128d~185	2	59	40.44	57. 5	6.6

N/NO_2^--N conversion ratio is 1.00:1.32, with portion of NO_2^--N converted to NO_3^--N to provide electron for the reduction of CO_2 [28]. It is, commonly, considered that the production of NO_3^--N is due to ANAMMOX in sulfate reduction–ammonia oxidation [10,15–18,29].

According to the speculation by Liu *et al.* [17], 0.26 mmol NO_3^--N could be generated due to 2.32 mmol consumption of NH_4^+-N can generate during sulfate reduction–ammonia oxidation. The amount of NO_3^--N generated according to the amount of NH_4^+-N conversion can be calculated at different reaction stages in this experiment, which are far less than the actual production (listed in Table 2). In addition, the pH value of the reaction system should increase due to acid consumption in the ANAMMOX reaction. However, the pH of this reaction system was actually decreased. This is partly due to the fact that the majority of NO_3^--N was not produced via ANAMMOX pathways but via other pathways. The only electron acceptor in the reaction system was SO_4^{2-}-S. Therefore, it can be inferred that SO_4^{2-}-S could oxide portion of NH_4^+-N into NO_3^--N according to Equation (7):

$$4SO_4^{2-} + 3NH_4^+ + 2HCO_3^- \rightarrow 4S^0 + 3NO_3^- + 2H_2O + 2CO_3^{2-} \quad (7)$$

The total alkalinity of the reaction is consumed in the process and leads to the drop of pH value, which is consistent with the experimental phenomena. Thus sulfate reduction–ammonia oxidation system could be presumed as follows:

$$NH_4^+ + SO_4^{2-} \rightarrow NO_2^- + S^0 + 2H_2O \quad (6)$$

$$2NO_2^- + 2NH_4^+ \rightarrow 2N_2 + 4H_2O \quad (5)$$

The n(N)/n(S) ratio is a key parameter for the oxidation of NH_4^+-N into NO_2^--N or NO_3^--N by SO_4^{2-}-S. When n(N)/n(S) is low, NH_4^+-N should be excessively oxidized into NO_3^--N to provide enough electrons to reduce SO_4^{2-}-S. Therefore, when SO_4^{2-}-S concentration was constant, NO_3^--N generation efficiency at n(N)/n(S) ratio of 2 was much higher than that when n(N)/n(S) ratio was 4 (see Figure 6).

CONCLUSION

The products of sulfate reduction–ammonia oxidation with ANAMMOX bacteria are elemental sulfur and dinitrogen. Such a process leads to the decrease of pH. It is not a simple continual reaction but a series of complex reactions resulting in the instability of NH_4^+-N and SO_4^{2-}-S molar conversion ratio. Ammonia may be oxidized to NO_2^--N or NO_3^--N by sulfate. Generated NO_2^--N and the residual ammonia can then be removed via ANAMMOX.

ACKNOWLEDGEMENTS

This research was funded by National Natural Science Foundation of China (51008202, 51478284), the major projects of the Environmental Protection Department of Jiangsu Province (201104) and the Natural Science Foundation of Jiangsu province university (12kjb610005). Thanks to the support from the Priority Academic Program Development of Jiangsu Higher Education Institutions and the Jiangsu focus professional class of environmental science and engineering.

REFERENCES

1. Miladinovic, N., and Weatherley, L.R., "Intersification of ammonia removal in a combined ion-exchange and nitrification column", *Chem. Eng. J.*, Vol. 135, 2008, pp.15–24.
2. Silva, A. J., Varesche, M. B., Foresti, E., Zaiat, M. "Sulfate removal from industrial wastewater using a packed-bed anaerobic reactor", *Process Biochemistry*, Vol. 37, No. 9, 2002, pp. 927–935.
3. Kioussis, D. R. and Kofinas, P., "Characterization of anion diffusion in polymer hydrogels used for wastewater remediation", *Polymer*, Vol. 46, No. 22, 2005, pp. 9342– 9347.
4. Ghigliazza, R., Lodi, A. and Rovatti, M., "Kinetic and process considerations on biological reduction of soluble and scarcely soluble sulfates", *Resources, Conservation and Recycling*, Vol. 29, No. 3, 2000, pp. 181–194.
5. Gonzalias, A. E., Kuschk, P., Wiessner, A., Jank, M., Jastner, M., Koser, M., "Treatment of an artificial sulphide containing wastewater in subsurface horizontal flow laboratory-scale constructed wetlands", *Ecological Engineering*, Vol. 31, No. 4, 2007, pp. 259–268.
6. Jetten, M. S. M., Strous, M., van de Pas-Schoonen, K. T., Schalk, J., van Dongen, U.G.J.M., van de Graaf, A. A., Logemann, S., Muyzer, G., van Loosdrecht, M.C.M, Kuenen, J.G., "The anaerobic oxidation of ammonium", *FEMS Microbiology Reviews*, Vol. 22, No. 6, 1998, pp. 421–437.
7. Tang, C. J., Zheng, P., Wang, C. H., Mahmood, Q., Zhang, J.Q., Chen, X.G., Zhang, L., Chen J.W., "Performance of high-loaded ANAMMOX

UASB reactors containing granular sludge", Water Research, Vol. 45, No. 1, 2011, pp. 135–144.

8. Khanal, S. K. and Huang, J. C., "ORP - based oxygenation for sulfide control in anaerobic treatment of high—sulfate wastewater", *Water Research*, Vol. 37, No. 9, 2003, pp. 2053–2065.
9. Widdel, F., Microbiology and ecology of sulphate and sulphur reducing bacteria. *Biology of Anaerobic Microorganisms*. New York, 1998, pp. 469–586.
10. Fdz-Polanco, F. M., Fernandez, N., Uruena, M. A., Uruena, M. A.,Garcia, P. A., and Villaverde, S., "New process for simultaneous removal of nitrogen and sulpfur under anaeriobic condition", *Water Research*, Vol. 35, No. 4, 2011a, pp. 1111–1114.
11. Jesús, R. A., Elias, R. F., Gomez, J., "Simultaneous biological removal of nitrogen, carbon and sulfur by denitrification", *Water Research*, Vol. 38, No. 14–15, 2004, pp. 3313–3321.
12. Kalyuzhnyi, S., Gladchenko, M., Mulder, A., Versprille, B., "DEAMOX—New biological nitrogen removal process based on anaerobic ammonia oxidation coupled to sulphide-driven conversion of nitrate into nitrite", *Water Research*, Vol. 40, No. 19, 2006, pp. 3637–3645.
13. Wang, J., Lu, H., Chen, G. H., Lau, G.N., Tsang, W.L., van Loosdrecht, M.C.M., "A novel sulfate reduction, autotrophic denitrification, nitrification integrated (SANI) process for saline wastewater treatment", *Water Research*, Vol. 43, No. 9, 2009, pp. 2363–2372.
14. Chen, C., Wang, A. J., Ren, N. Q., Lee, D. J., Lai, J. Y., "High-rate denitrifying sulfide removal process in expanded granular sludge bed reactor", *Bioresource Technology,* Vol. 100, No. 7, 2009, pp. 2316–2319.
15. Fdz-polanco, F., Fdz-polanco, M., Fernandez, N., Uruena, M. A., García, P.A., Villaverde, S., "Simultaneous organic nitrogen and sulfate removal in an anaerobic GAC fluidized bed reactor", *Water Science and Technology*, Vol. 44, No. 4, 2001b, pp. 15–22.
16. Yang, Z. Q. and Zhou, S. Q., "Simultaneous removal of ammonium and sulfate from synthetic wastewater by anaerobic biodegradation", *Ecological Science*, Vol. 27, No. 5, 2008, pp. 427–428.
17. Liu, S. T., Yang, F. L., Gong, Z., Meng, F.G., Chen, H. H., Xue, Y., Furukawa, K., "Application of anaerobic ammonium oxidizing consortium to achieve completely autotrophic ammonium and sulfate removal", *Bioresource Technology*, Vol. 99, No. 15, 2008, pp. 6817–6825.
18. Zhao, Q. L., Li, W., You, S. J., Simultaneous removal of ammonium-nitrogen and sulphate from wastewaters with an anaerobic attached-growth bioreactor. *Water Science and Technology*, Vol. 54, No. 8, 2006, pp. 27–35.
19. Rikmann, E., Zekker, I., Tomingas, M., Tenno, T., Menert, A., Loorits, L., Tenno, T., "Sulfate- reducing anaerobic ammonium oxidation as a potential treatment method for high nitrogen-content wastewater", *Biodegradation*, Vol. 23, 2012, pp. 509–524.
20. Samubon, P.C., "Anaerobic ammonia removal in presence of organic matter: a novel route", *Journal of Hazardous Materials*, Vol. 149, 2007, pp. 49–59.
21. Li, X., Huang, Y., Zhou, C., Yuan, Y., Li, D.P., Liu, F.X., "Nitrogen removal increased in anammox reactor by effluent recirculation", *Transactions of the Chinese Society of Agricultural Engineering*, Vol. 29, No. 9, 2013, 178–183.
22. van de Graaf, A. A., Bruijn, D. P., Robertson, L. A., Jetten, M.S.M., Kuenen, J.G., "Autotrophic growth of anaerobic ammonium-oxidizing micro- organisms in a fluidized bed reactor", *Microbiology,* Vol. 142, No. 8, 1996, pp. 2187–2196.
23. APHA, 1998, *Standard Methods for the Examination of Water and Wastewater*, 20th ed. United Book Press, USA.
24. Janssen, A., de Keizer, A., van Aelst, A., Fokkink, R., Yangling H.,Lettinga, G., "Surface characteristics and aggregation of microbiologically produced sulphur particles in relation to the process conditions", *Colliods and Surfaces B: Biointerfaces,* Vol. 6, No. 2, 1996, pp. 115–129.
25. Zhang, L., Zheng, P., He, Y. H., Jin, R.C., "Performance of sulfate-dependent anaerobic ammonium Oxidation", *Science in China Series B: Chemistry*, Vol. 52, No. 1, 2009, pp. 86–92.
26. Soetaert, K., Hofmann, A. F., Middelburg, J. J., Meysman, F. J. R., Greenwood, J., "The effect of biogeochemical processes on pH", *Marine Chemistry*, Vol. 105, 2007, pp. 30–51.
27. Chen, J. W., Zheng, P., Tang, C. J., Yu, Y., "Effect of Low pH on the performance of high-loaded ANAMMOX reactor", *Journal of Chemical Engineering of Chinese Universities*, Vol. 24, No. 2, 2010, pp. 320–325.
28. Strous, M., Heijnen, J. J., Kuenen, J. G., Jetten, M.S.M., "The sequencing batch reactor as a powerful tool for the study of slowly growing anaerobic ammonium-oxidizing microorganisms", *Applied Microbiology and Biotechnology*, Vol. 50, No. 5, 1998, pp. 589–596.
29. Yang, Z. Q., Zhou, S.Q. and Sun, Y. B., "Start-up of simultaneous removal of ammonium and sulfate from an anaerobic ammonium oxidation (anammox) process in an anaerobic up-flow bioreactor", *Journal of Hazardous Materials*, Vol. 169, No. 1–3, 2009, pp. 113–118.

Heavy Metal Pollution Characteristics in the Kaili Coal Mining Region, Guizhou Province, China

Y. CHEN[1,2], H. X. ZHAO[2], Z. H. XIE[2], H. Y. HUANG[2], S. Y. ZANG[3] and B. LIAN[1,4,*]

[1]*State Key Laboratory of Environmental Geochemistry, Institute of Geochemistry, Chinese Academy of Sciences, Guiyang 550002, China*

[2]*Key Laboratory of Karst Environment and Geohazard Prevention, Ministry of Education, Chemistry Engineering College, Guizhou University, Guiyang 550003, China*

[3]*Shenyang University of Chemical Technology, Shenyang 110142, China*

[4]*College of Life Science, Nanjing Normal University, Nanjing 210023, China*

ABSTRACT: The exploitation of coal resources has resulted in a series of ecological and environmental problems. The aim of this study was to determine the pollution characteristics of the river-soil-vegetation system in the Kaili coal mining region. By analysing the heavy metal content of samples from water, soil, and plants along a section of the Chongan River channel downstream from the coal mining region, this research shows that a number of wastewater quality indices have already exceeded the Secondary Chinese Discharge Standards. The soil in the mining region has been slightly polluted by Zn and seriously polluted by Hg. Moreover, it is shown that all plant samples such as *Pteris vittata* L., rice seedlings, and vegetables, such as capsicum, cucumber, kidney bean, tomato, and eggplant, have been affected by coal mine wastewater. These results demonstrated that the upper reaches of the Chongan River have been seriously polluted by coal mine wastewater, and as such need imminent environmental management.

INTRODUCTION

ALTHOUGH coal is an important energy resource, the exploitation and utilisation thereof has gone on for thousands of years, resulting in a series of ecological and environmental problems, locally and globally [1,2]. In the process of coal production, acid drainage from mines, coal washing, tailings dumps, and abandoned mine pits have endangered the peripheral ecosystems of mining areas [3,4]. For example, due to the influence of acid coal mine wastewater, heavy metal and chloride contents exceeded limits [5]; the heavy metal content of soil in Donezk Coal Field in the former Soviet Union exceeded all limits, and 90% of soil in the city was polluted by mercury with a maximum mercury content of 19 mg/kg [6]; acid coal mine wastewater changed over the seasons, and the river ecosystem was also influenced in Hocking River Basin, Ohio, USA [7]. In Wangaloa Coal Mine, Otago, New Zealand, the acid coal mine wastewater produced through the open-air storage of mass gangues resulted in increasing the heavy metal contents in the nearby rivers, and a decrease in pH in some rivers to as low as 2 to 4 [8]. Some research has been aimed at problems caused by coal mining such as geological hazards, water resource destruction, environmental pollution, and land resource destruction, as well as their corresponding consequences [9–11]. However, less attention was paid to the changes to overground vegetation features and soil quality in mining areas [12,13]. Long-term pollution has resulted in localised ecological crises.

Coal reserves are abundant in Guizhou Province with many coal mines distributed across the province. Kaili lies in the southeast of the province. There are three major rivers in this area: the Qingshui, the Chongan, and the Bala, in addition to 35 tributary streams. Collectively, the river system acts as an important ecological screen for the upper reaches of the Changjiang River. The district from Yudong to Jiangkou is one of the coal mining centres of Kaili, where there are seven villages and 30 to 40 active coal mines. Much acid mine drainage and leachate from tailing piles is directly discharged into the upper reaches of the Chongan River, without treatment: this causes the river to be polluted by coal mine wastewater as far as its mouth. This study aimed to determine the pollution characteristics of the river-soil-vegetation system in the Kaili coal mining region.

*Author to whom correspondence should be addressed.
E-mail: bin2368@vip.163.com or lianbin@njnu.edu.cn Tel: +86 025-85891050

1544-8053/15/01 S123-09

doi:10.12783/issn.1544-8053/12/S1/18

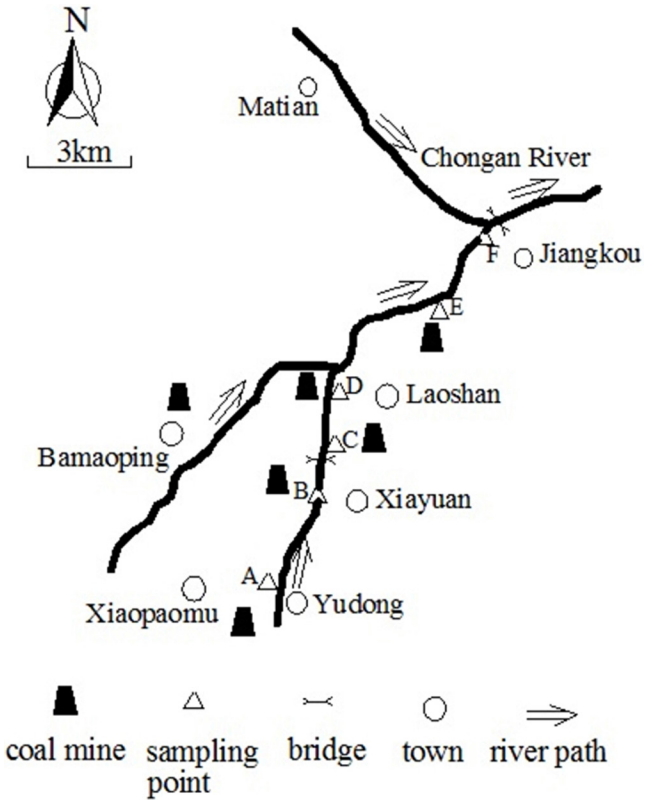

Figure 1. *Map of the sampling sites.*

Introduction of Sampling Sites

Water samples were collected from Yudong to Jiangkou at Kaili, Guizhou Province. The total length of the river under study was 15 km. Along the river channel, water samples were collected at six different locations in the upper, middle, and lower reaches, marked by A to F in Figure 1.

The water samples and sampling spots were: A. from the upper reaches of the river near Yudong; B. from the river near the abandoned Qiaotou coal mine; C. from the pithead of the Qiaotou coal mine; D. from the river near the tailings pile of the Laoshan coal mine; E. from the source of black coal washing waste water, and F. from the river under the Jiangkou Bridge.

MATERIALS AND METHODS

The pH, suspended solids (SS), and chromaticity were measured according to Chinese National Standards [14–16].

Both regular and banded-layout methods [17] were adopted for sampling agriculturally cultivated soils along the course of the polluted river, throughout the entire investigation region, by collection of samples at five points a, b, d, e, and f (corresponding respectively to water sampling points A, B, D, E, and F). Water sampling point C was at the pithead, so no soil sample could be collected there. The soil sample points are located, in turn, at: a, on the bank near Yudong; b, on the bank near the abandoned Qiaotou coal mine; d, on the bank near the tailing dump of the Laoshan coal mine; e, on the bank from soil near the coal washing drainage water; f, on the bank under the Jiangkou Bridge. Two sampling locations (1) (0–20 m) and (2) (20–40 m) from the water were investigated separately at each soil sampling point. By using quartering [17], one kilogramme of soil sample was recovered.

The soil samples were spread onto a sheet of clean plastic, impurities were removed, the soil was air-dried at 30°C, and then the soil samples were ground, initially to pass through a 2 mm sieve, and then to pass through a 0.15 mm sieve. Finally, they were sub-packed for further use at 4°C [17].

The soil samples (sieved to 2 mm) were used to determine the pH according to the method given in GB15618-1995 [18].

The soil sample solution was prepared in accordance with the HCl-HNO_3 treatment method in HJ/T166-2004[17], for determining the contents of total iron, total zinc and total lead. The soil sample solution was prepared for determining total mercury content following the leaching method [19].

Pteris vittata L was chosen as a typical indicator plant collected from a range of plants near the edge of the polluted river; samples were collected according to both regular and banded-layout methods and the plum blossom-layout method [17]. The position of sampling sites and the number of samples were the same as the soil sampling sites. Finally, the samples were cleaned with distilled water immediately after collection, labelled, and stored in sample bags [17].

Rice seedlings (the complete stem was collected) and various vegetables (edible parts only) were collected from the soil lying up to 20 m away from the polluted river. Then, the samples were cleaned with distilled water immediately after collection, labelled, and put into sample bags. Plant samples were washed repeatedly with deionised water, and water in the plant samples was removed. Then, the samples were oven-dried at 105°C for 30 min, and baked for 24h at 338.15°C to 70°C. Finally, the samples were powdered, and sieved through a 100-mesh sieve. The screen underflow was prepared for subsequent use. The sample solution for the analysis of total iron, total zinc, and total lead was prepared following the dry cinefaction method [20].

The sample solution for total mercury determination was prepared following the mixed-acid leaching method [19]. The methods of measuring the contents of total iron, total zinc, and total lead are given by David [21] and Jarvis and Kym [22], while Li *et al.* [19] and Jarvis and Kym [22] describe the methods of measuring the total mercury content and the total aluminium content, respectively. The ICP-OES (Varian, Vista MPX) was used to measure the contents of total iron, total zinc, total mercury and total lead.

RESULTS AND DISCUSSION

Water quality and major metal contents of the polluted river samples at the six sampling points are given in Table 1.

The results presented in Table 1 indicate that the pH at B, C, D, and E was between 2.6 and 3.0, which was far below the discharge standard (6-9), and the pH of A and F was within the scope of the relevant discharge standard. The SS at C and E was 16000 and 12600, respectively, which was far over the discharge standard (80), and the concentrations of Fe, Hg, Pb, and Zn far exceeded the discharge standard. Moreover, except for total lead content, water quality indices at C and E (only 10m away from the pollution source) were over the Secondary Chinese Wastewater Discharge Standard. Therefore, it represented Grade V (according to water area environment of surface water and protecting objects in surface water environmental quality standards, surface water can be classified as Grade I, II, III, IV, or V successively, where Grade V water is seriously polluted). Sampling points A, B, and D were about 100 to 300m away from the nearest pollution sources, and at these locations the concentrations of various pollutants were lower because of the diluting effect of the river water and precipitation. Furthermore, there were local flora and crops such as rice and corn near the river bank, which may absorb contaminants from the river. As a result, water quality will be partially improved as it flows downstream. For Point F downstream, the nearest pollution source was about 2 km away. As a consequence, the river water was diluted because of abouchement of new rivers, and many heavy metals in the water were deposited and absorbed by soils and plants along the bank as the pH increased; this let the water quality indices at sampling point F conform to the Secondary Chinese Wastewater Discharge Standard.

A river polluted by coal mines will result in negative effects on the soil and vegetation along the river bank. For instance, some heavy metals entered the soil with accumulation thereof in the river, which resulted in their enrichment in soils and absorption by soil and vegetation. This has led to deterioration of the soil ecological environment and agricultural product quality. Long-term consumption of these polluted agricultural products harms human health [24,25].

The heavy metals present in various chemical states in acid coal mine wastewater would be gradually enriched in the soil by accumulation and migration. The enrichment factor (EF) was adopted [26–29] to analyse the degree of enrichment of total iron, mercury, zinc, and lead in the soils. During the analytical process, a soil reference element (such as Si, Al, etc.) was selected, whose content was less affected by wastewater from coal mines. During the analytical process, Al was selected as a soil reference element, whose content was less affected by wastewater in soil because of its big buffer capacity, even though some other reports showed Al is sensitive to pH changes [30,31]. Al was chosen for this purpose and its EF calculated as follows:

$$EF = \frac{[Me]_a / [Al]_a}{[Me]_b / [Al]_b}$$

Table 1. Water Quality Analysis: All Sampling Points.

Water Sample	pH	SS (mg L^{-1})	Chromaticity (description/extension rate)	Total Iron (mg L^{-1})	Total Mercury (μg L^{-1})	Total Zinc (mg L^{-1})	Total Lead (mg L^{-1})
A	6.73	39	Light yellow, transparent / 8	—	0.06	0.06	—
B	2.78	91	Light yellow, transparent / 3200	337.7	0.09	2.5	—
C	2.67	319	Deep yellow, transparent / 16000	1651.2	0.27	6.1	0.2
D	2.85	281	Light yellow, transparent / 32	75.2	0.02	1.3	0.09
E	2.69	761	Deep yellow, transparent / 12600	1532.5	0.10	6.1	0.3
F	5.98	68	Light yellow, transparent / 16	4.4	—	0.1	—
Discharge Standard II* [23]	6–9	300	80	—	0.05	5.0	1.0

Note: the data of Table 1 are the average of three samples in the same sampling points.

*The Secondary Chinese Wastewater Discharge Standard is the wastewater discharge standard stated in GB8978-1996 Integrated wastewater discharge standard.

Where, $[Me]_a$ is the mass fraction of Fe, Hg, Zn, or Pb in the sample, $[Al]_a$ is the mass fraction of Al in the sample, [Me]b is the mass fraction of Fe, Hg, Zn, or Pb with respect to their background values, and $[Al]_b$ is the mass fraction of Al with respect to its background value (background values for soil in China, 1990). The results are shown in Table 2.

From the EF values, one can deduce whether the enrichment of heavy metals elements in soil is normal. If EF > 1, it is shown that the relative enrichment of elements have been affected by human activities.

It can be seen from Table 2 that Fe, Hg, Zn, and Pb were enriched in soils due to human activities. In particular, the EF of total soil iron was greater than 40, and all soils from the sampled region were extremely enriched in Fe. The EF of mercury was generally in the range 20–40, and the mercury contents reached an ultra-enriched status. The main reason for this enrichment was change in pH of the sampled river water, which caused corresponding changes in the total iron content of the river water. Fe^{3+} can stably present in aqueous solutions at pH < 3.0: as the pH increased, however, Fe^{3+} will be hydrolysed to produce $Fe(OH)_3$ in the river [32], and the precipitates will settle out as the river flows. Meanwhile, $Fe(OH)_3$ in the precipitates is able to adsorb and retain Hg, Zn, and Pb. Therefore, the total mercury, total zinc, and total lead contents will also increase in the soils sampled in the township. This indicated that the exploitation of coal mines and the discharge of coal mine wastewater may potentially cause both local river pollution and heavy metal enrichment of soils in the mining area.

It is also shown from Table 2 that the enrichment in heavy metals caused by coal mine waste water occurs not only in the vicinity of abandoned coal mine B and the tailings pile D, but also in operational coal mines. Moreover, it demonstrated that the influence of coal mines on the surrounding environment is on-going.

To further determine whether heavy metal enrichment can cause the problems associated with heavy metal pollution, the soil samples were analysed by using the individual pollution index [33] and Nemerow integrated pollution index [34].

The individual pollution index is calculated as follows:

$$I_i = \frac{C_i}{S_i}$$

Where C_i is the measured heavy metals concentration; S_i is the permissible value of the heavy metal under evaluation. The results are given in Table 3.

To evaluate overall environmental quality, we have used the Nemerow index [34], which reflects both maximum and average values of pollutant concentrations relative to their objective levels:

$$P_N = \sqrt{\frac{MaxI_i^2 + AvgI_i^2}{2}}$$

Table 2. Metal Element Contents in the Soils.

Sampling Point	Number of Soil Samples	Total Aluminium[a] (mg kg^{-1})	Total Iron		Total Mercury		Total Zinc		Total Lead	
			Content (mg kg^{-1})	EF[c]	Content (mg kg^{-1})	EF	Content (mg kg^{-1})	EF	Content (mg kg^{-1})	EF
A	(1)	49.34	47389.20	2162.67	1.790	36.95	143.02	2.59	48.12	2.48
	(2)	37.21	12831.31	776.47	1.312	35.91	18.34	0.44	26.89	1.84
B	(1)	36.53	20059.23	1236.45	1.658	46.23	90.82	2.22	34.57	2.41
	(2)	32.76	13864.24	952.93	0.786	24.44	48.04	1.31	25.62	1.99
D	(1)	50.62	54317.12	2416.16	1.155	23.24	150.01	2.64	46.25	2.33
	(2)	42.35	27258.43	1449.30	0.622	14.96	120.83	2.55	43.61	2.62
E	(1)	28.47	21312.95	1685.65	0.792	28.33	41.53	1.30	36.54	3.27
	(2)	22.84	7854.18	774.31	1.398	62.34	22.01	0.86	26.93	3.00
F	(1)	53.51	85843.41	3612.29	1.696	32.28	253.72	4.23	46.84	2.23
	(2)	29.48	8665.37	661.87	0.514	17.76	29.36	0.89	26.31	2.27
Background value for China's soils[b]		66.20	29.40		0.065		74.20		26.00	

Note: The data of Table 2 are the average of three-time repeated analysis.

[a]As the reference element for the analysis of EF, total aluminium EF need not be considered.

[b]All the background values of soil in China are from "Background values of soils in China" (1990).

[c]EF < 2, deficiency to minimal enrichment; EF = 2–5, moderate enrichment; EF = 5–20, significant enrichment; EF = 20–40, very high enrichment; EF > 40, extremely high enrichment [27].

Table 3. Permissible Values for Soil Environment Quality Assessment.

Mass Term		Soil pH		
		< 6.5	6.5 to 7.5	> 7.5
Total Mercury*	Aquatic plant, dry farming, fruit tree, etc.	0.30	0.50	1.0
	Vegetable	0.25	0.30	0.35
Total Zinc		200	250	300
Total Lead*	Aquatic plant, dry farming, fruit tree, etc.	80	80	80
	Vegetable	50	50	50

*Note: Soil in the sampling area was usually used to grow vegetables and paddy rice. In Table 3, mercury and lead have two kinds of permissible values in soil: one for vegetables and one for dry farming, fruit trees, and aquatic plants. When assessing soil pollution, vegetable soil permissible values are widely utilised as the evaluation criterion.

Where P_N is an integrated pollution index, Max I_i is the maximum value of all the individual indices, and Avg I_i is the average of all individual indices. The evaluated performance indices of heavy metal pollution combined with I_i and P_N are given in Table 4.

In comparison to soil pollution standards [17], it was shown that the level of total mercury in soils reached the status of serious pollution, and the maximum individual pollution index was 7.16 at point A. Over the whole sampling area, the degree of mercury pollution decreased in order: A, B, F, D, and E. The maximum individual pollution index for total zinc was 1.27 at point F, indicating that the soil from sampling point F was also slightly polluted. The extent of zinc pollution over the whole area, in decreasing order was sampling point F, D, A, B, and E. The degree of zinc pollution in the area 20 to 40 m from the bank was lower than that in the area up to 20 m away. The maximum individual pollution index for total lead was 0.96 at point A, and the enrichment of lead approached the upper danger limit at point A. Moreover, across the whole area, the degree of lead pollution was, in descending order, sampling point A, D, F, E, and B.

According to the Nemerow integrated pollution index, $P_N \geq 3.0$ for different sampling points indicated serious pollution by heavy metals. The extent of this pollution, in decreasing order was: sampling point A, B, F, E, and D, which indicated that the heavy metal pollutants in coal mine wastewater had already migrated to points F, A and B by transportation and deposition of river water and migration and conversion of soil. This could have potentially negative effects on the health of local residents.

As a result, soils over the whole area showed various levels of heavy metal enrichment, and the soil at some individual sampling sites was significantly polluted by heavy metals. To determine whether the heavy metal pollutants can be transferred and transformed in plant tissues, thus affecting their growth, *Pteris vittata* L. was used as an indicator species, as shown in Figure 2.

It was shown in Figure 2 that the four heavy metal elements Fe, Hg, Zn, and Pb moved from the soil into the tissues of *Pteris vittata* L. with varying degrees of enrichment. *Pteris vittata* L. can still continue growing under these difficult conditions. The closer the polluted river was, the more luxuriant its growth, indicating that soil polluted by heavy metals could not impair the growth of *Pteris vittata* L.

The roots, stems, and leaves of *Pteris vittata* L were assayed to better understand its ability to accumulate heavy metals and reveal whether it can be regarded as the indicator plant with potential for phytoremediation of soils seriously polluted by heavy metals. The results are shown in Figure 3.

Figure 3 showed that the heavy metal concentrations in *Pteris vittata* L. decreased in the following order: roots, stems, and then leaves. This indicated that the heavy metals came mainly from the soil. The extent of the enrichment in underground parts was far greater than that above ground. That was to say, the heavy metallic elements tended to decrease with ascending tissues in *Pteris vittata* L. When they arrived at the leaves,

Table 4. Evaluation Indices of Heavy Metal Pollution in the Surface Soil Layer of the Sampling Region.

Soil Sample		A		B		D		E		F	
Item		(1)	(2)	(1)	(2)	(1)	(2)	(1)	(2)	(1)	(2)
Individual Pollution Index[a]	Total Mercury	7.16	5.25	47389.20	2.62	4.62	2.07	3.17	4.66	5.65	1.71
	Total Zinc	0.72	0.09	12831.31	0.19	0.75	0.48	0.21	0.09	1.27	0.12
	Total Lead	0. 96	0.54	13864.24	0.51	0.93	0.87	0.73	0.54	0.94	0.53
Nemerow Integrated Pollution Index[b]		5.35		4.87		3.46		3.48		4.17	

Note: The data of Table 4 are the average of three-time repeated analysis.

[a]The individual pollution index is graded: $I_i \leq 0.7$, clean (safe); $0.7 < I_i \leq 1.0$, still clean (limit); $1.0 < I_i \leq 2.0$, slight pollution; $2.0 < I_i \leq 3.0$, moderate pollution; $I_i \geq 3.0$, serious pollution [17].

[b]The grading standards of the Nemerow integrated pollution index P_N are the same as those of the individual pollution index.

the contents of total lead and total mercury were only 0.020 and 0.033 mg kg^{-1}, respectively.

Usually the extent of the transformation of heavy metals in plant tissues is expressed by *S/R* [35], the ratio of heavy metal contents in the above ground parts to those in the roots. The higher the ratio is, the stronger the ability of the plant to transport heavy metals will be. When *S/R* exceeds 0.5, the plant is deemed to possess the ability to phytoremediate soils polluted by heavy metals. In the sampled township the *S/R* ratios in *Pteris vittata* L. for the heavy metals Fe, Zn, Pb, and Hg were 0.05, 0.62, 0.39, and 0.12, respectively. This showed that *Pteris vittata* L. was suitable for the remediation of soils polluted by zinc.

It can be seen from the assessments above that the water body, soil, and vegetation over the whole sampling area were affected by heavy metal pollution caused by coal mine wastewaters. It was noted that paddy rice in the mining area was seriously polluted, which was because the crops grew near the river and they were directly irrigated with polluted river water.

Thus, it is necessary to further study agricultural products from the mining area and analyse how toxic the heavy metals elements could be to agriculture and humans. Heavy metal pollution of soil in the planting area is likely to affect the normal growth of rice [36]. For example, rice has a strong capacity to absorb Pb in the soil and store it in each part of the plant. By determining the contents of heavy metals in rice seedlings, the ability of agricultural goods to enrich lead was analysed in terms of the enrichment factor [37]. The formula is presented as follows:

$$f = \frac{C_1}{C_2}$$

Where, f is the enrichment factor of agricultural products to a soil element, C_1 is the concentration of

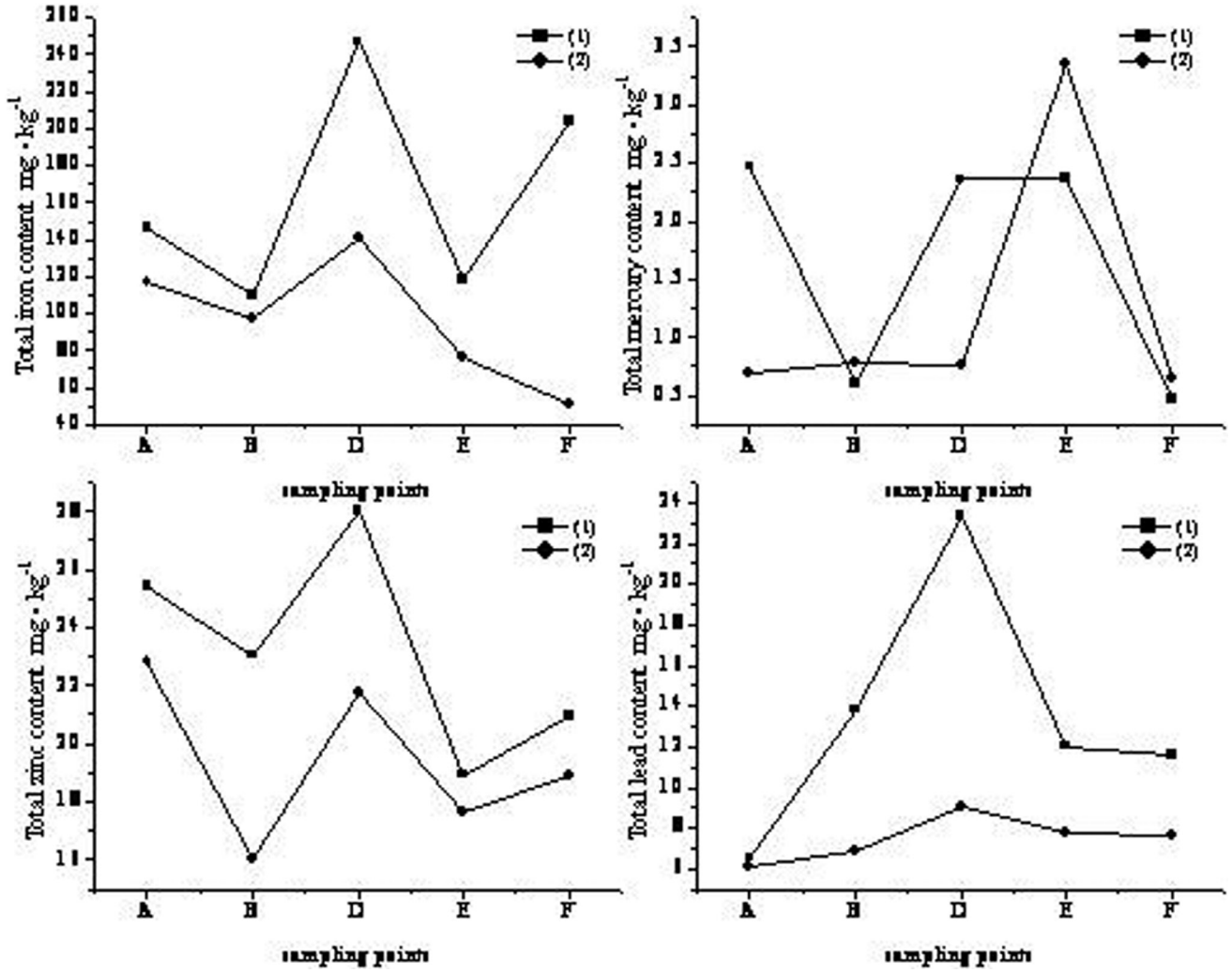

Figure 2. *Heavy metal contents of Pteris vittata L.*

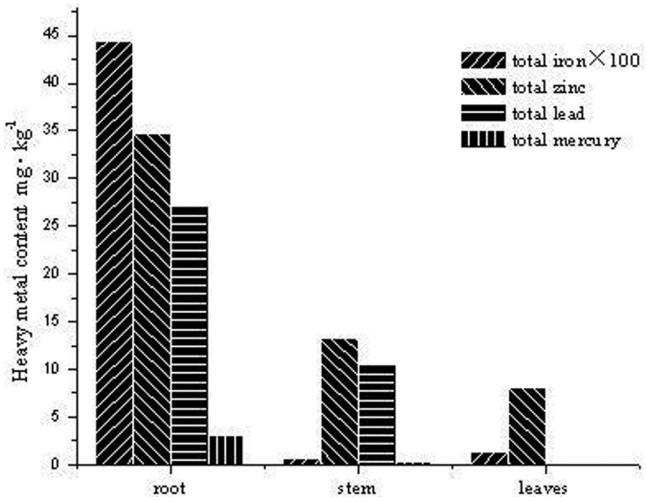

Figure 3. *Accumulation characteristics of heavy metals in different parts of Pteris vittata L.*

this element in agricultural products, and C_2 is its concentration in the soil. The larger the enrichment factor, the stronger the enrichment capacity for heavy metals in soil. The results are given in Table 5.

Table 5 showed that rice roots had a greater capacity to enrich heavy metals than the above-ground tissues at both sampling sites. High heavy metal contents would have a negative effect on rice growth. The toxic elements, Pb and Hg, which were not essential for the growth of rice, displayed varying degrees of enrichment.

The study mainly analysed samples of capsicum, cucumber, kidney bean, tomato, and eggplant grown within the mining area and made further evaluations of heavy metal pollution in vegetables and described the potential effects on humans according to the single pollution index method [33] and hazard quotient to human health (*HQ*) [29]. The hazard quotient to human health is calculated as follows:

$$HQ = \frac{[W_{plant}] \times [M_{plant}]}{R_f D \times B}$$

Where *HQ* is the evaluated performance index of potential hazard; $[W_{plant}]$ is the consumptive amount of a certain polluted vegetable required in a day, kg d^{-1}, calculated in accordance with 0.301 kg d^{-1} *per capita*, $[M_{plant}]$ is the heavy metal content in the vegetable, R_fD mg kg^{-1}, is the reference quantity of heavy metals in the food material, mg $(kg\ d)^{-1}$, R_fD for Zn is 0.30 mg $(kg\ d)^{-1}$, for Pb it is 0.0035 mg $(kg\ d)^{-1}$, and for Hg it is 0.0003 mg $(kg\ d)^{-1}$ [38], and is the average mass of an adult (60 kg). More detailed data are reported in Table 6.

It was found from Table 6 that capsicum, cucumber, kidney bean, tomato, and eggplant had all been polluted by heavy metals to various degrees. Specifically, according to the grading standards of individual pollution index, capsicum, cucumber, tomato, and eggplant were slightly polluted by zinc, and kidney bean was moderately polluted by zinc. Capsicum and cucumber were slightly polluted by lead. However, tomato, eggplant, and kidney bean were all seriously polluted by lead. In addition, capsicum, cucumber, kidney bean, tomato, and eggplant were all seriously polluted by mercury. Of these five vegetables, kidney bean was most seriously polluted overall. Meanwhile, the higher the HQ, the greater the potential harm to human health. From Table 6, the potential damaging effect from lead and mercury was the most serious to local residents.

CONCLUSIONS

Coal mining can cause serious degradation of ecosystems. It is shown that wastewater from coal mines caused heavy metal pollution and associated potential environmental hazards through research on the regional river-soil-vegetation system of Kaili, Guizhou Province. The following conclusions can be drawn:

- Firstly, the river under study is very acidic with high contents of solid suspended substances, high chromaticity, and high contents of heavy metals.

Table 5. Heavy Metal Concentrations and EF of Paddy Rice Crops at the Sampling Points.

Sampling Point	Vegetation Types	Total Zinc		Total Lead		Total Iron		Total Mercury	
		mg kg^{-1}	*f*	mg kg^{-1}	*f*	mg kg^{-1}	*f*	mg kg^{-1}	*f*
Yudong Vicinity	Paddy Rice (above-ground part)	76.29	0.53	3.00	0.06	994.17	0.02	0.239	0.13
	Paddy Rice (root)	168.24	1.18	1.50	0.03	38971.41	0.82	1.043	0.58
Laoshan Coal Mine Vicinity	Paddy Rice (above-ground part)	31.27	0.21	7.54	0.16	974.14	0.02	0.272	0.24
	Paddy Rice (root)	101.53	0.68	13.64	0.29	40533.87	0.75	0.337	0.29

Note: The data of Table 5 are the average of three three-time repeated of each analysis.

Table 6. Heavy Metal Contents of Vegetables in the Sampling Region.

Vegetable Type	Total Zinc			Total Lead			Total Mercury		
	mg kg^{-1}	I_i	*HQ*	mg kg^{-1}	I_i	*HQ*	mg kg^{-1}	I_i	*HQ*
Capsicum	24.87	1.24	0.42	Trace amount	-	-	0.490	49.00	8.19
Cucumber	38.73	1.94	0.65	Trace amount	/-	-	0.335	33.50	5.60
Kidney bean	55.13	2.76	0.92	10.60	53.00	15.19	0.617	61.70	10.32
Tomato	22.83	1.14	0.38	6.07	30.35	8.70	0.883	88.30	14.77
Eggplant	23.23	1.16	0.39	3.04	15.20	4.36	0.607	60.70	10.15
National Hygienic Standard of Food [39]	20			0.2			0.01		

Note: The data of Table 6 are the average of three-time repeated analysis.

- Secondly, total mercury and iron in the soil reached ultra-enriched status. It is shown that the soil was slightly polluted by Zn and seriously polluted by Hg. The integrated pollution level of several pollutants continues ecosystem deterioration across the whole mining area.
- Finally, plant samples (*Pteris vittata* L., rice seedlings, and vegetables) were polluted by heavy metals from coal mine wastewater, and the plant pollution was more serious than soil pollution, especially in vegetable crops. Lead contents of kidney beans, tomato, and eggplant were above the permissible contents by 53.00, 30.35, and 15.20 times (Chinese Food Hygiene Standards), respectively. Mercury contents of capsicum, cucumber, kidney beans, tomato, and eggplant exceeded the recommended levels by 49.00, 33.50, 61.70, 88.30, and 60.70 times (Chinese Food Hygiene Standards), respectively.

ACKNOWLEDGEMENTS

This work was jointly supported by the National Science Fund for Creative Research Groups (Grant No. 41021062), National Key Basic Research Program of China (Grant No. 2013CB956702), National Natural Science Foundation of China (Grant No. 40803037), and knowledge innovational program of Chinese Academy of Sciences (kzcx2-yw-135-2).

REFERENCES

1. Sun, J., Tang, C. Y., Wu, P., Liu, C. Q., Zhang, R. X., ″Migration of Cu, Zn, Cd and As in epikarst water affected by acid mine drainage at a coalfield basin, Xingren, Southwest China", *Environmental Earth Sciences,* Vol. 69, No. 8, 2013, pp. 2623–2632. http://dx.doi.org/10.1007/s12665-012-2083-3
2. Lupton, M. K., Rojas, C., Drohan, P., Bruns, M. A., ″Vegetation and Soil Development in Compost-Amended Iron Oxide Precipitates at a 50-Year-Old Acid Mine Drainage Barrens", *Restoration Ecology,* Vol. 21, No. 3, 2013, pp. 320-328. http://dx.doi.org/10.1111/j.1526-100X.2012.00902.x
3. Younger, P. L., ″Mine water pollution in Scotland: nature, extent and preventative strategies", *The Science of the Total Environment*, Vol. 265, 2001, pp. 309–326. http://dx.doi.org/10.1016/S0048-9697(00)00673-2
4. Yao, D. X., Meng, J., Zhang, Z. G., ″Heavy metal pollution and potential ecological risk in reclaimed soils in Huainan mining area", *Journal of Coal Science and Engineering*, Vol. 16, 2010, pp. 316–319 (In Chinese). http://dx.doi.org/10.1007/s12404-010-0319-y
5. Edeltrauda, H. R., ″Impact of mining and metallurgical industries on the environment in Poland", *Applied Geochemistry*, Vol. 11, No. 1-2, 1996, pp. 3–9. http://dx.doi.org/10.1016/0883-2927(95)00083-6
6. Panov, B. S., Dudik, A. M., Shevchenko, O. A., ″On pollution of the biosphere in industrial areas: the example of the Donets coal Basin", *International Journal of Coal Geology*, Vol. 40, No. 2-3, 1999, pp. 199–210. http://dx.doi.org/10.1016/S0166-5162(98)00069-X
7. Robert, G. V. and Morgan, L. V., ″Macroalgal communities from an acid mine drainage impacted watershed", *Aquatic Botany*, Vol. 71, 2001, pp. 93–107. http://dx.doi.org/10.1016/S0304-3770(01)00184-X
8. Amanda, B. and Dave, C., ″Arsenic, copper and zinc occurrence at the Wangaloa coal mine, southeast Otago, New Zealand", *International Journal of Coal Geology*, Vol. 45, 2000, pp. 181-193.
9. Shi, H., ″Study on the Bio-environment Issues and Strategy in Coal Mine in Shanxi", *Chongqing Environmental Science*, Vol. 24, No. 2, 2002, pp. 11–12 (in Chinese).
10. Bell, F. G., Stacey, T. R. D., Genske, D., ″Mining Subsidence and Its Effect on the Environment: Some Differing Examples", *Environmental Geology*, Vol. 40, No. 2, 2000, pp. 135–152. http://dx.doi.org/10.1007/s002540000140
11. Sidle, R. C., Kamil, I., Sharma, A., Yamashita, S., ″Stream Response to Subsidence from Underground Coal Mining in Central Utah", *Environmental Geology*, Vol. 40, 2000, pp. 279–291. http://dx.doi.org/10.1007/s002540050007
12. Gorokhovich, Y., Voros, A., Reid, M., Mignone, E., ″Prioritizing Abandoned Coal Mine Reclamation Projects within the Contiguous United States Using Geographic Information System Extrapolation", *Environmental Management*, Vol. 32, No. 4, 2003, pp. 527–534. http://dx.doi.org/10.1007/s00267-003-3043-1
13. Guo, D. G., Bai, Zh. K., Shangguan, T. L., Shao, H. B., Qiu, W., ″Impacts of Coal Mining on the Aboveground Vegetation and Soil Quality: A Case Study of Qinxin Coal Mine in Shanxi Province, China", *Clean Soil, Air, Water*, Vol. 39, No. 3, 2011, pp. 219–225. http://dx.doi.org/10.1002/clen.201000236
14. GB6920-1986. 1986. Water quality; Determination of pH value; Glass electrode method, the national standard in the People's Republic of China.
15. GB11901-1989. 1989. Water quality-Determination of suspended substance-Gravimetric method, the national standard in the People's Republic of China.
16. GB11903-1989. 1989. Water quality-Determination of colority, the national standard in the People's Republic of China.
17. HJ/T166-2004. 2004. Technical specification for soil environmental monitoring, the environmental protection trade standard in the People's Republic of China.
18. GB15618-1995. 1995. Environmental Quality Standard for Soils, the national standard in the People's Republic of China.
19. Li, Z. G., Feng, X. B., He, T. R., Yan, H. Y., Lian, L., ″Determination

of Total Mercury in Soil Sediment by Aquaregia Digestion in the Water Bath Coupled with Cold Vapor Atom Fluorescence Spectrometry Bulletin of Mineralogy", *Petrology and Geochemistry*, Vol. 24, 2005, pp. 140–143 (in Chinese).

20. GB12283-1990. 1990. Fruits, vegetables and derived products-Decomposition method of organic matter, the national standard in the People's Republic of China.
21. David, K. J., "A geochemical study of a breccia body in the central Tennessee zinc district", *Journal of Geochemical Exploration*, Vol. 30, No. 1-3, 1988, pp. 197–207. http://dx.doi.org/10.1016/0375-6742(88)90059-3
22. Jarvis, I. and Kym, E. J., "Inductively coupled plasma-atomic emission spectrometry in exploration geochemistry", *Journal of Geochemical Exploration*, Vol. 44, No. 1-3, 1992, pp. 139–200. http://dx.doi.org/10.1016/0375-6742(92)90050-I
23. GB8978-1996. 1996. Integrated wastewater discharge standard, the national standard in the People's Republic of China.
24. Chinh, L. D., Gheewala, S. H., Bonnet, S., "Integrated environmental assessment and pollution prevention in Vietnam: the case of anthracite production", *Journal of Cleaner Production*, Vol. 15, No. 18, 2007, pp. 1768–1777. http://dx.doi.org/10.1016/j.jclepro.2006.03.006
25. Massas, I., Kalivas, D., Ehaliotis, C., Gasparatos, D., "Total and available heavy metal concentrations in soils of the Thriassio plain (Greece) and assessment of soil pollution indexes", *Environmental Monitoring and Assessment,* Vol. 185, No. 8, 2013, pp. 6751–6766. http://dx.doi.org/10.1007/s10661-013-3062-1
26. Singh, M., Ansari, A. A., Muller, G., "Heavy metals in fresh deposited sediments of the Gomati River (a tributary of the Ganga River): Effects of human activities", *Environmental Geology*, Vol. 29, No. 3-4, 1997, pp. 246–252. http://dx.doi.org/10.1007/s002540050123
27. Loska, K., Wiechula, D., Korus, I., "Metal contamination of farming soils affected by industry", *Environment International*, Vol. 30, No. 2, 2004, pp. 159–165. http://dx.doi.org/10.1016/S0160-4120(03)00157-0
28. Donkor, A. K., Bonzongo, J. C., Nartey, V. K., Adotey, D. K., "Mercury in different environmental compartments of the Pra River Basin, Ghana", *Science of the Total Environment*, Vol. 368, No. 1, 2006, pp. 164–176. http://dx.doi.org/10.1016/j.scitotenv.2005.09.046
29. Chary, N. S., Kamala, C. T. D., Raj, S. S., "Assessing risk of heavy metals from consuming food grown on sewage irrigated soils and food chain transfer", *Ecotoxicology and Environmental Safety*, Vol. 69, No. 3, 2008, pp. 513–524. http://dx.doi.org/10.1016/j.ecoenv.2007.04.013
30. Keskin, T. E., "Mineral-water interaction and hydrogeochemistry of groundwater around Bartın coal mine. Turkey", Fresenius Environmental Bulletin, Vol. 22, No. 9a, 2013, pp. 2750–2762.
31. Keskin, T. E. and Toptaş, S., "Heavy metal pollution in the surrounding ore deposits and mining activity: a case study from Koyulhisar (Sivas-Turkey)", Environmental Earth Sciences, Vol. 67, 2012, pp. 859–866. http://dx.doi.org/10.1007/s12665-012-1541-2
32. Li, G. B. and Liu, C. 1989. Deferrization and demanganization of ground water, PA: Chinese construction industry publishing company (in Chinese).
33. Yao, C. X., Chen, Z. L., Zhang, J., Hou, J., "Heavy Metal Pollution Assessment of Vegetables in Pudong Zone of Shanghai", *Journal of Agro-Environment Science*, Vol. 24, 2005, pp. 761–765.
34. Nemerow, N. L. 1985. Stream, Lake, Estuary, and Ocean Pollution (2nd ed.), PA: New York, Van Nostrand Reinhold.
35. Fujimori, T. and Takigami, H., "Pollution distribution of heavy metals in surface soil at an informal electronic-waste recycling site", *Environmental Geochemistry and Health*, Vol. 36, No. 1, 2014, pp. 159–168. http://dx.doi.org/10.1007/s10653-013-9526-y
36. Muchuweti, M., Birkett, J. W., Chinyanga, E., Zvauya, R., Scrimshaw, M. D., Lester, J. N., "Heavy metal content of vegetables irrigated with mixtures of wastewater and sewage sludge in Zimbabwe: Implications for human health", *Agriculture Ecosystems & Environment,* Vol. 112, No. 1, 2005, pp. 41–48. http://dx.doi.org/10.1016/j.agee.2005.04.028
37. Sutapa, B. and Bhattacharyya, A. K., "Heavy metal accumulation in wheat plant grown in soil amended with industrial sludge", *Chemosphere*, Vol. 70, No. 7, 2008, pp. 1264–1272. http://dx.doi.org/10.1016/j.chemosphere.2007.07.062
38. GB5749-2006. 2006. Standards for drinking water quality, the national standard in the People's Republic of China.
39. GB2762-2012. 2012. Maximum levels of contaminants in foods, the national standard in the People's Republic of China.

Risk Evaluation of Water Pollution in the Middle Catchments of Weihe River

YINGE LIU[1,*], YIXUAN YANG[2] and CHUNDI XU[1]

[1]*Key Laboratory of Disaster Monitoring and Mechanism Simulating in Shaanxi Province, College of Geography and Environment, Baoji College of Arts and Science, Baoji 721013, China*

[2]*College of Materials and Chemical Engineering, Hainan University, Haikou 570228, China*

ABSTRACT: A risk assessment model, including risk evaluation indexes, for river water pollution was established using the fuzzy theory and the variation coefficient was used to weight the indexes and the five levels of water pollution risk was defined. The proposed approach is demonstrated for risk evaluation of water pollution in the Weihe River, located in northern China. The risk of water quality parameters and interval of water pollution were analyzed. The results showed that 79% of the river is in high risk and mainly located in lower reaches. The BOD_5, COD and permanganate index are the greatest source of risk. Moreover, compared with different methods of the river water quality and risk assessment, the proposed method has its own advantage in risk evaluation of river water pollution.

INTRODUCTION

THE purpose of risk assessment of water pollution is to evaluate the possibility of adverse events and their influences on water environment, aiming to provide basis for decision-making of government agencies. Water resource shortage and water pollution have become two major problems for the sustainable utilization of water resources and have been focused on in numerous studies [1–2]. At present, there are many approaches for water risk studies, including statistical analysis method, the comprehensive index method, BP neural network and fuzzy recognition model used for groundwater pollution, environmental health of city and water supply risk assessment [3–7]. These methods have different advantages depending on study objectives. This paper combines fuzzy mathematics and coefficient of variation to quantitatively assess water pollution risk, aiming to provide basis for river water quality control.

DATA AND METHODS

Data

Water samplings were obtained from six monitored sections in middle basin of the Weihe River mainstream. These six monitoring sections were selected based on hydrological characteristics of the Weihe River and current pollution situation. The monitored sections scattered from upper reaches to downstream in middle basin of Weihe River mainstream were Sq1, Sq2, Sq3, Sq4, Sq5 and Sq6 in Figure 1. The layout of monitoring sections represents spatial distribution of water pollution in the river. The six parameters, including BOD_5, COD, Potassium permanganate index, ammonia nitrogen, petroleum, and nitrite nitrogen, were used as risk evaluation indexes.

Assessment model

Risk assessment of water pollution could be challenging as it often involves many water quality parameters. In this study, since water quality parameters are of different dimensions and their magnitudes vary a lot, all water quality data have been standardized. Based on fuzzy mathematics and coefficient of variation, a fuzzy evaluation model (FEM) for river water quality risk assessment has been established. The following 5 steps are involved in model building.

1. Identify water quality parameters. In this study, we have identified five water quality parameters including potassium permanganate index, BOD_5, COD, ammonia nitrogen, petroleum and nitrite

*Author to whom correspondence should be addressed.
E-mail: yingeliu@163.com Tel: 0917-3566337

1544-8053/15/01 S133-04

doi:10.12783/issn.1544-8053/12/S1/19

nitrogen, which represent the overall situation of water pollution of the Weihe River. The risk evaluation index set M is established [Equation (1)].

$$X = \{x_i\}, i = 1, 2, ..., l \quad (1)$$

where l is the number of selected assessment parameters, x_i is the ith water risk evaluation parameter, and in this study, $l = 6$.

2. A risk evaluation criteria set is determined [Equation (2)].

$$D = \{d_i\}, j = 1, 2, ..., m \quad (2)$$

where m is the number of risk class, d_j is the ith water risk class, and $m = 5$.

Risk is a fuzzy concept and currently there is no uniform standard risk classification. Considering water quality criterion of the Chinese standard (GB3838, 2002) and actual conditions of the Weihe River, water pollution risk level is divided into five classes and the five levels are listed as the following: no risk, smaller risk, small risk, high risk and particularly high risk (Table 1).

3. The membership matrix Z between M and D is established [Equation (3)].

$$Z_{ij} = \begin{bmatrix} z_{11} & W & z_{1m} \\ A & C & T \\ z_{n1} & E & Z_{nm} \end{bmatrix} \quad (3)$$

Table 1. Water Pollution Risk Assessment Grade Standard.

Risk Class	1	2	3	4	5
Risk Degree	No risk	Smaller risk	Small risk	High risk	Particularly high risk
Risk Standard	< 0.25	0.25–0.5	0.25–0.4	0.45–0.5	> 0.5

Where Z_{ij} is the risk assessment degree of the ith parameter in the jth water risk criteria.

4. The coefficient of variation is used to determine the indexes weight V_i [Equation (4)].

$$V_i = \frac{\sqrt{\frac{1}{l}\sum_{i=1}^{l}\left(x_i - \frac{1}{l}\sum_{i=1}^{l} x_i\right)}}{\frac{1}{l}\sum_{i=1}^{n} x_i} \quad (4)$$

where $0 \le V_i \le 1$

5. A risk evaluation matrix F is established [Equation (5)]. At the same time, risk assessment index RI is calculated [Equation (6).

$$F = V \cdot Z = (f_1 \ldots f_2 \cdots, \ldots f_m) \quad (5)$$

$$I = \frac{\sum_{j=1}^{l} f_i \times j}{\sum_{j=1}^{l} f_i} \quad (6)$$

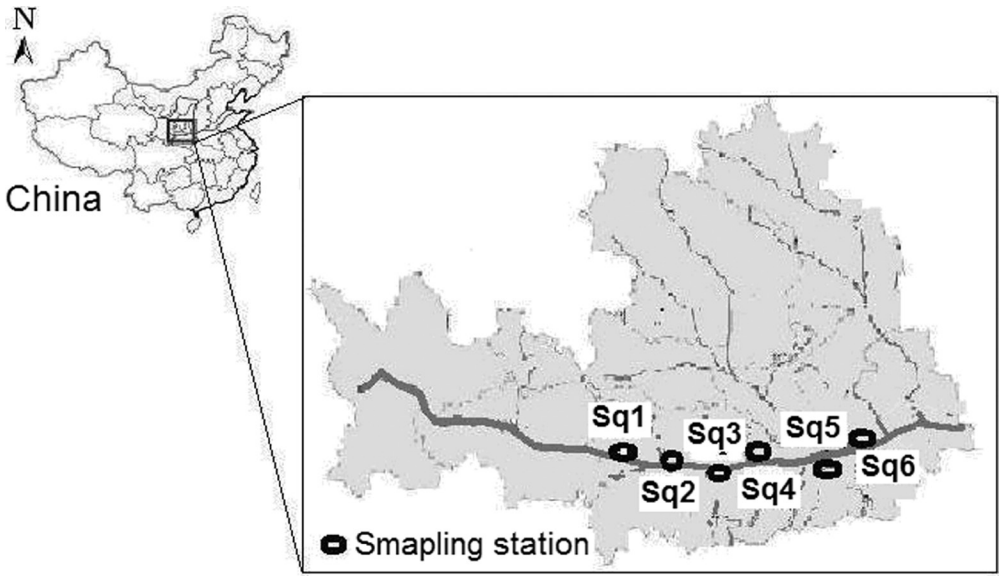

Figure 1. *Distribution of monitored stations in the middle catchment of Weihe River.*

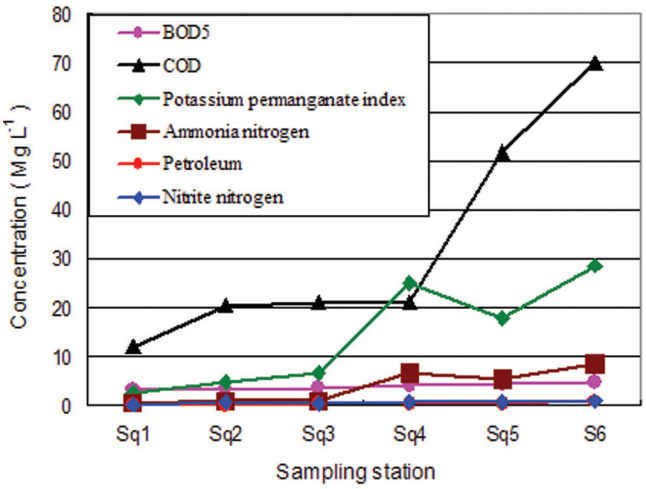

Figure 2. *The water pollutant concentration in each monitored section.*

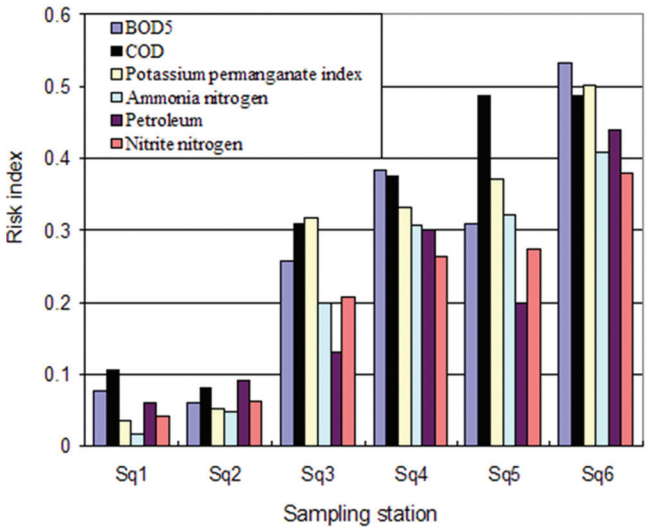

Figure 3. *Risk index of each pollutant in each monitored section.*

RESULTS AND DISCUSSION

In the study, selection of water quality parameters is important, which represents typical contaminant of Weihe River. In accordance with the requirements of the national standard GB17378-1998, water quality samples were collected while all pollutants were monitored six times a year, ensuring reliability of water quality control. Spatial distribution of water pollutant concentration in the middle basin of the Weihe River is presented in Figure 2. The river reach with most serious pollution is the downstream region, where concentrations of COD and Potassium Permanganate are greater. The index weights are calculated and listed in Table 2. Note that the weight of COD and Potassium Permanganate weight is relatively large, which indicates that these two kinds of pollutants have a greater impact on water quality. The second is BOD_5 and ammonia nitrogen pollution parameters and the other is the smallest. The risk index of each section of pollutants can be seen from Figure 3. Most water pollution risk index is relatively high, and mainly located in lower reaches of the river basin. The largest risk is in the Sq6 (Tianjingrendu). According to the risk grading standards in Table 1, comprehensive risk classes are shown in Figure 4. It was found that risk of water pollution at reach level 3 accounts for 79% of the entire river. Such water quality pollution is highly related to regional river carrying capacity and industrial emission sources [8–9].

To verify the model, we checked evaluation results with other methods, including the comprehensive index method (CIM) [10], the traditional fuzzy model (FM) [11] and Environment report data (ERD). Comparison results are shown in Figure 5. Note that in the risk assessment for upstream, our method denotes lower risk compared to other methods, while for the downstream section, risk evaluation from our method and other methods are consistent, especially in high risk areas. This clearly shows that the FEM model is practical and can be applied to a wide range of river water quality risk assessment. However, when the sampling size is unusually large, water quality risk assessment by FEM model may be less than the actual risk. This is due to the fact that unusually small sampling risk assessment value from FEM may be larger than actual risk. Hence, the output from FEM should be corrected in water quality risk assessment.

CONCLUSIONS

Through the above analyses, examples show that fuzzy evaluation model is a good method for water quality risk assessment; simultaneously, the river water quality risk assessment model has obvious advantages so that the river water quality can be accurately judged, while it is a better tool for evaluation of water pollution management. Moreover, water pollution risk

Table 2. The Weight of Water Pollution Parameters in Each Section.

Index	BOD_5	COD	Potassium Permanganate	Ammonia Nitrogen	Petroleum	Nitrite Nitrogen
Weight	0.167	0.181	0.158	0.125	0.196	0.172

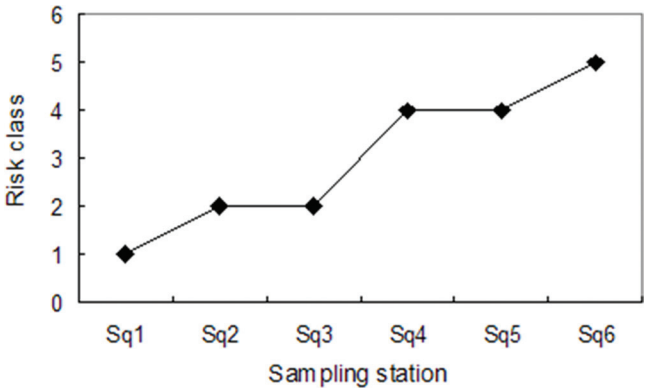

Figure 4. *Comprehensive assessment risk class of water pollutant.*

assessment results show that the risk of river water pollution is relatively high in Weihe River, while most of the river water quality is in high risk, especially in the downstream. In addition, risk assessment shows that the BOD_5 and COD are greater sources of river pollution, and degree of water pollution risk is related to water discharge and environmental vulnerability of the city. Therefore, in high-risk areas, wastewater treatment and management should strengthen.

ACKNOWLEDGEMENTS

The study was supported by the Key Laboratory Project of Shaanxi Province of China (13JS010), the Key Research Foundation of Baoji College of Arts and Science (ZK11159) and Shaanxi Province Geography Key Discipline Project.

REFERENCES

1. Landis, W. G. and J. F. Thomas, Regional risk assessment as a part of the long-term receiving water study, *Integrated Environmental Assessment and Management*, Vol. 5, No. 2, 2009, pp. 234–247. http://dx.doi.org/10.1897/IEAM_2008-062.1
2. Aouissi, J., S. Benabdallah, Z. L. Chabaâne and C. Cudennec, Modeling Water Quality to Improve Agricultural Practices and Land Management in a Tunisian Catchment Using the Soil and Water Assessment Tool, *Journal of Environmental Quality*, Vol. 43, 2014, pp. 18–25. http://dx.doi.org/10.2134/jeq2011.0375
3. Luo, P. P., B. He, P. L. B. Chaffe, D. Nover, K. Takara and M. R. R. Maz, Statistical analysis and estimation of annual suspended sediment of major rivers in Japan, *Environmental Science, Processes & Impacts*, Vol. 15, 2013, pp. 1052–1061. http://dx.doi.org/10.1039/c3em30777h
4. Kazi, T. G., M. B. Arain, M. K. Jamali, N. Jalbani, H. I. Afridi, R. A. Sarfraz, J. A. Baiga, and Q. Abdul, Assessment of water quality of polluted lake using multivariate statistical techniques: A case study. *Ecotox Environ Safe*, Vol. 72, 2009, pp. 301–309. http://dx.doi.org/10.1016/j.ecoenv.2008.02.024
5. Li, J. B., G. H. Huang and G. M. Zeng, An integrated fuzzy stochastic modeling approach for risk assessment of groundwater contamination, *Journal of Environmental Management*, Vol. 82, 2007, pp. 173–188. http://dx.doi.org/10.1016/j.jenvman.2005.12.018
6. Singh, K. P., A. Basant, A. Malik and G. Jain, Artificial neural network modeling of the river water quality—A case study, *Ecological Modeling*, Vol. 220, No. 6, 2009, pp. 888–895. http://dx.doi.org/10.1016/j.ecolmodel.2009.01.004
7. Guo, Q. C., Z. F. He, L. Li and L. Q. Kou, Application of BP Neural Network on Water Environmental Quality Evaluation of Weihe River, *Bulletin of Soil and Water Conservation*, Vol. 31, No. 4, 2011, pp. 112–115.
8. Li, J. K., H. E. Li,B. Shen and W. Deng, Monitoring and estimating non-point source pollution on typical sections along the Weihe River, *Advances in Water Science*, Vol. 22, No. 6, 2011, PP. 818–828.
9. Wang, T. R., G. N. Sun and S. Y. Liu, Relationship between Spatiotemporal Variation of Water Pollution and Runoff Volume of Mainstream Section of the Weihe River in Shaanxi Province, *Arid Zone Research*, Vol. 28, No. 4, 2011, pp. 599–615.
10. Liu, Y. G., N. L. Wang, Y. Q. Zhao and X. B. Wu, Application of GIS in regional ecological risk assessment of water resources, *Environmental Engineering and Management Journal*, Vol. 12, No. 7, 2013, pp. 1465–1474.
11. Geng, Y. N., J. Zhang, Q. Zhou, C. D. Xu and Y. Q. Zhao, Fuzzy synthetic evaluation of Weihe water quality, *Environmental Engineering and Management Journal*, Vol. 10, No. 10, 2011, pp. 1477–1484.

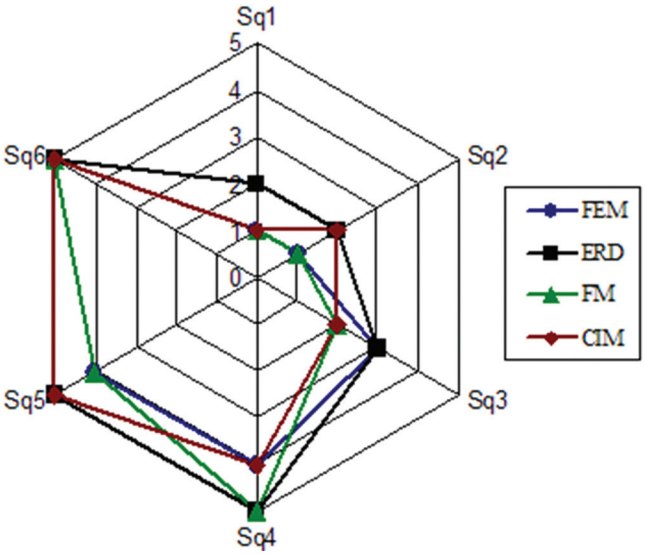

Figure 5. *Water pollution risk class in different methods.*

Nitrogen Conversion Characteristics of ANAMMOX Sludge for Long-term Preservation

YI YUAN[1,2,3], YONG HUANG[2,3,*], XIANG LI[2,3], HUIPING DENG[1], YUHUII ZHENG[2,3] and YANG PAN[2,3]

[1]*School of Environmental Science and Engineering, Tongji University, Shanghai, 200092, China*

[2]*School of Environmental Science and Engineering, Suzhou university of Science and technology, Suzhou, 215009, China*

[3]*Jiangsu Collaborative Innovation Center of Technology and Material of Water Treatment, Suzhou, 215009, China*

ABSTRACT: Since inoculated sludge with ANAMMOX could efficiently reduce the start-up time of the ANAMMOX reactor, it is important to develop a cost-effective technology for preservation. In the present study, the flocculent ANAMMOX sludge was preserved under either –20°C, 5°C, natural environment or 30°C for 15d, 30d, 45d, 150d and 365d, respectively. The preserved ANAMMOX sludge under all these conditions displayed different levels of nitrification. Specifically, freezing conditions (–20°C) led to a loss of ANAMMOX activity, whereas ANAMMOX activity was the highest in natural environment, which showed a positive linear relationship with the relative amount of substrates. Moreover, a short-term anoxic (≤ 45d) preservation in a dark yet natural environment (0 ~ 15°C) is a highly economical and effective approach.

INTRODUCTION

ANAEROBIC ammonia oxidation (ANAMMOX, Equation 1) is the pathway of biological oxidation of ammonium (NH_4^+) under anoxic conditions when nitrite (NO_2^-) is used as an electron acceptor, with dinitrogen gas (N_2) as a reaction product. This pathway has some obvious advantages. For example, extra carbon resources is not needed, nitrogen removal efficiency could be up to 61.4 $kgN \cdot m^{-3} \cdot d^{-1}$ [1], less sludge is produced, and the operation cost is relatively cheap (0.75 € $(kgN)^{-1}$) compared to the cost when traditional nitrogen removal technique is undertaken (2~5 € $\cdot (kgN)^{-1}$) [2]. Therefore, the technology based on ANAMMOX pathway has been recognized as one of the most sustainable approaches to removing nitrogen from wastewater with high concentration of NH_4^+-N.

$$1NH_4^+ + 1.32NO_2^- + 0.066HCO_3^- + 0.13H^+ \rightarrow$$
$$1.02N_2 + 0.26NO_3^- + 0.066CH_2O_{0.5}N_{0.15} + 2.03H_2O \quad (1)$$

However, ANAMMOX has been proved difficult to be integrated into common wastewater treatment practices, primarily due to the growth rate of ANAMMOX bacteria, with the doubling time ranging between 1.8 and 11 days [3]. This often slows down the start-up time of the treatment processes [4,5]. However, inoculated sludge with ANAMMOX sludge could help decreasing the start-up time of the reactor [6]. Usually, sludge is stored in a starved state of wastewater treatment. Vlaeminck *et al.* preserved starved ANAMMOX sludge with or without nitrate when three different temperatures were used (i.e., 20°C, 4°C and –20°C) [6]. They found that ANAMMOX activity was the highest when sludge was preserved at 4°C without nitrate added, whereas the frozen culture did not show any ANAMMOX activities [6]. Nevertheless, Rothrock *et al.* found that frozen ANAMMOX sludge preserved with skim milk could still display some ANAMMOX activities [7]. Although the refrigerated ANAMMOX sludge could maintain some high levels of activities, the downside is that it needs a high level of energy. Therefore, the goal of this study is to develop a simple and cost-effective method for the storage of ANAMMOX sludge.

MATERIALS AND METHODS

Synthetic medium

A synthetic medium was used with concentrations of different components shown as following (per liter): NH_4Cl, 382 mg; $NaNO_2$, 641 mg; $KHCO_3$, 1000 mg;

*Author to whom correspondence should be addressed.
E-mail: yhuang@mail.usts.edu.cn

1544-8053/15/01 S137-07

doi:10.12783/issn.1544-8053/12/S1/20

KH_2PO_4, 27 mg; $MgCl_2$, 200 mg; $CaCl_2 \cdot 2H_2O$, 136 mg. The trace element solution I (including 5 $g \cdot L^{-1}$ EDTA and 5 $g \cdot L^{-1}$ $FeSO_4$) was 1mL per liter, and trace element solution II was 1.25 mL per liter [8]. The pH was adjusted to 7.2 ± 0.2 with HCl.

Inoculums Sludge

The activated culture used in this study was obtained from ANAMMOX reactors. The ANAMMOX granular sludge was ground and washed with deionized water for three times. Flocculent sludge (5.1 mL~5.3 mL) was then drawn into a conical flask with an effective volume of 50 mL. The ratio of MLVSS/MLSS was 0.465.

Preservative Test

50 mL synthetic medium was drawn into each flask filled with sludge. The flasks were sparged with dinitrogen gas for 0.5 h, sealed up with aluminum foil, and then preserved under five different temperature conditions with varying time as shown in Table 1. All experiments were set parallel samples.

Determination the Nitrogen Removal Rate

To determine nitrogen removal rate, 100 mL of synthetic medium was added to ANAMMOX sludge. It was sparged with dinitrogen gas for 5 min, then sealed in a bottle, and then oscillated at the speed of 110 $r \cdot min^{-1}$ in an incubator covered with black cloth (the inner temperature was (32±1)°C). The nitrogen removal rate of ANAMMOX sludge was measured after 24 hours, and the total nitrogen removal rate of sludge before storage was 0.107 $kgN \cdot m^{-3} \cdot d^{-1}$.

Table 1. Preservation Temperature and Time for ANAMMOX Sludge.

Time, d	Mesophilic Temperature, 30°C	Natural Environment, 0~30°C	Refrigeration, 5°C	Freezing, –20°C
15	A1	B1[a]	C1	D1
30	A2	B2[a]	C2	D2
45	A3	B3[b]	C3	D3
150	A4	B4[c]	C4	D4
365	A5	B5[d]	C5	D5

[a]Ambient temperature from 15°C down to 5°C.
[b]Ambient temperature from 15°C down to 0°C.
[c]Ambient temperature from 15°C down to 0°C, and gradually heated to 33°C.
[d]Ambient temperature from 15°C down to 0°C, and gradually heated to 33°C, but then decreased to 5°C.

Chemical Analysis

The concentrations of nitrogen compounds were measured according to standard methods, as set out by American Public Health Association [9]. NH_4^+-N or NO_2^--N concentration was measured calorimetrically, whereas NO_3^--N concentration was measured spectrophotometrically. The measurement of pH was done using a portable digital pH meter.

Calculation Formula

Metabolic types of stored sludge could be ANAMMOX, partial nitrification, nitrification, endogenous denitrification and/or endogenous digestion. The half equations of endogenous denitrification and endogenous digestion are shown in Equations (2)–(4) [10]:

$$\frac{1}{2}NO_3^- + \frac{1}{2}H^+ + e^- \rightarrow \frac{1}{2}NO_2^- + \frac{1}{2}OH^-, \quad \Delta G^\theta = -41.45\ KJ \cdot mol^{-1} \tag{2}$$

$$\frac{1}{3}NO_2^- + \frac{2}{3}H^+ + e^- \rightarrow \frac{1}{6}N_2 + \frac{2}{3}OH^-, \quad \Delta G^\theta = -30.75\ KJ \cdot mol^{-1} \tag{3}$$

$$\frac{1}{20}C_5H_7O_2N + \frac{9}{20}H_2O \rightarrow \frac{1}{5}CO_2 + \frac{1}{20}HCO_3^- + \frac{1}{20}NH_4^+ + H^+ + e^- \tag{4}$$

In these equations, ΔG^θ is the free energy released at the standard state when pH = 7.

Equation (5) is established according to the coefficient of the mass balance described in Table 2.

$$\begin{gathered} a + b - 0.1d - 0.05e - 0.15f = C_{NH_4^+\text{-}N_{in}} - C_{NH_4^+\text{-}N_{eff}} \\ 1.32a - b + c - d + f = C_{NO_2^-\text{-}N_{in}} - C_{NO_2^-\text{-}N_{eff}} \\ 0.26a + c - d = C_{NO_3^-\text{-}N_{eff}} - C_{NO_3^-\text{-}N_{in}} \\ 2.04a - 0.1d - 0.05e + 0.85f = \\ \left(\begin{array}{l} C_{NH_4^+\text{-}N_{in}} + C_{NO_2^-\text{-}N_{in}} + C_{NO_3^-\text{-}N_{in}} \\ -C_{NH_4^+\text{-}N_{eff}} - C_{NO_2^-\text{-}N_{eff}} - C_{NO_3^-\text{-}N_{eff}} \end{array} \right) \end{gathered} \tag{5}$$

It can be seen from Equations (2) and (3), that ni-

Table 2. Coefficients by the Material Balance (Unit: mg·L^{-1}).

	Conversed via ANAMMOX	Conversed via Partial Nitrification	Conversed via Nitrification	Conversed via Endogenous Denitrification for NO_3^--N	Conversed via Endogenous Denitrification for NO_2^--N	Conversed via Endogenous Digestion
NH_4^+-N	a	b	0	–0.1d	–0.15f	–0.05e
NO_2^--N	1.32a	–b	c	–d	f	0
NO_3^--N	–0.26a	0	–c	d	0	0
ΔN	2.04a*	0	0	–0.1d	0.85f	–0.05e

The amount reduced is +, the amount increased is –.
*It is considered the cell production according to Equation (1).

trate reduction releases more free energy than that of nitrite reduction for each 1 mol electron. Under the same conditions, a nitrate reduction pathway is easier to accomplish. Moreover, similar studies suggested that *Paracocus denitrificans* and *Psuedomonas fluorescens* gave priority to use nitrate as the electron acceptor when the electron donor was limited [11,12]. Since there were limited organic carbon sources in the reaction system, nitrate reduction [Equation (2)] was the preferential endogenous denitrification pathway. Nitrogen loss in such system might only be caused by ANAMMOX pathway or endogenous denitrification pathway of nitrite.

If ammonia and nitrite are degraded synchronously when nitrate is produced as a product, nitrogen loss could be caused by ANAMMOX pathway without the occurrence of nitrite-denitrification (i.e. $f = 0$) or endogenous digestion pathway(i.e. $e = 0$).

If ammonia and nitrite are degraded synchronously without nitrate produced, nitrogen loss could be caused by ANAMMOX pathway and endogenous denitrification pathway, without the occurrence of partial nitrification (i.e. $b = 0$), nitrification (i.e. $c = 0$) or endogenous digestion (i.e. $f = 0$).

If nitrogen loss occurs in the system, but ammonia and nitrite nitrogen are not degraded synchronously, and the concentration of the effluent ammonia nitrogen is higher than that of raw water, no ANAMMOX reaction, partial nitrification or nitrate reduction pathway (i.e. $a = 0$, $b = 0$, $d = 0$) would happen.

If nitrogen loss does not occur in the system, then there is no ANAMMOX reaction or no endogenous denitrification pathway (i.e. $a = 0$, $d = 0$, $f = 0$).

The amount of substrate could be calculated based on Equation (6).

$$\text{the relative amount of substrate} = \frac{C_{preserve} \times V_{preserve}}{M_{sludge} \times NRRs \times PT \times 1000} = \frac{C_{preserve} \times V_{preserve}}{M_s \times \frac{C_{activity}}{HRT \times M_s} \times PT \times 1000} = \frac{C_{preserve} \times V_{preserve}}{NRRv \times PT \times 1000} \quad (6)$$

In this equation, $C_{preserve}$ is the concentration of nitrogen in preservative fluid, $(C_{NH_4^+\text{-}N} + C_{NO_2^-\text{-}N})$ mg·L^{-1}. $V_{preserve}$ is the volume of preservative fluid, L. M_s is the quantity of sludge stored, g. NRR_s is the nitrogen removal rate of sludge, kg·kg^{-1}·d^{-1}. PT is the preservation time of sludge, d. $C_{activity}$ is the concentration of nitrogen in the activity determination solution, $(C_{NH_4^+\text{-}N} + C_{NO_2^-\text{-}N})$, mg·L^{-1}. NRR_v is the nitrogen removal rate of sludge, kg·m^{-3}·d^{-1}.

Table 3. The Results of Nitrogen Conversion of ANAMMOX Sludge After Preserved under Different Duration and Temperature.

Preservation Time, d	Mesophilic Temperature			Natural Environment			Refrigeration			Freezing		
	NH_4^+-N	NO_2^--N	NO_3^--N	NH_4^+-N	NO_2^--N	NO_3^--N	NH_4^+-N	NO_2^--N	NO_3^--N	NH_4^+-N	NO_2^--N	NO_3^--N
	mg·L^{-1}											
15	95.4	113	0	58.9	84.5	0	83.8	99.5	0	105.8	111	0
30	95	120.5	1	53.1	106	7.1	85.9	109	0	91.8	119	0
45	98	122.5	1.4	78.6	104.5	0	92.7	122	3.6	106.3	98	0
150	95	120	15	84	118	0	97	121	15	107.8	105	8
365	123	129	0	120.8	125	0.5	108.5	119	0	134.8	73.75	0

Table 4. The Characteristics of Nitrogen Conversion of ANAMMOX Sludge after Preserved under Different Conditions.

	Mesophilic Temperature	Natural Environment	Refrigeration	Freezing
Preservation Time, d	NH_4^+-N degradation:NO_2^--N degradation:NO_3^--N production			
15	1:17: 0	1:1.11:0	1:1.88:0	–1:3.28:0
30	1:1.9:0.2	1:0.51:0.15	1:1.49:0	1:1.34:0
45	1: 3.75:0	1:1.19:0	1:1.1:0.49	–1:5.08:0
150	1:2:3	1:0.75: 0	1:3:5	–1:3.21:1.03
365	–1:0.04:0	–1:0.24: 0.02	–1:1.29:0	–1:1.62:0

RESULT AND DISCUSSIONS

Results of Activities of ANAMMOX Sludge under Different Temperature and Storage Duration

The nitrogen conversion results of preserved ANAMMOX sludge are shown in Table 3.

A small amount of ammonia nitrogen could be converted if sludge was stored at 30°C. With an increase of storage duration, the color of the sludge turned black, accompanied with a pungent odor. During the preservation process, supplied nutritional substrates could not enable bacteria to sustain on themselves, and thus they gradually disintegrated, decayed and began to release H_2S, resulting in black appearance and smelly odor.

Sludge preserved under natural environment for 150 days or stored in refrigeration for 45 days could convert ammonia and nitrite in a similar way. By contrast, frozen sludge could not convert ammonia, even when the color remained bright red with the red effluent. One possible explanation is that the cells of ANAMMOX bacteria might have been broken, with hemachrome C released into the water [13].

Table 4 shows that the substrate conversion stoichiometric ratios of all preserved ANAMMOX sludge mixture were out of the range of a typical ANAMMOX stoichiometry (degradation of NH_4^+-N: degradation of NO_2^--N: production of NO_3^--N= 1:1.32:0.26). Obviously, there were other reactions.

Nitrogen transition characteristics of sludge after preservation

Figure 1 is based on nitrogen balance. The ANAMMOX sludge stored under different temperature or duration conditions all exhibited nitrification capability. Because some aerobic ammonia oxidizing bacteria often co-exist with ANAMMOX sludge [13], their abundance declined during the preservation period. Aerobic ammonia oxidizing bacteria, however, could survive in a starvation state or fluctuating environment with low mortality or energy requirements [14,15] when the concentrations of substrate are low. Therefore, the preserved ANAMMOX sludge could still display nitrification capability.

The proportion of the ANAMMOX pathway as ANR (ANAMMOX ratio); the proportion of aerobic ammonia oxidation pathway as AOR (ammonia oxidation ratio); the proportion of nitrite oxidation as NOR (nitrite oxidation ratio); the proportion of endogenous denitrification for nitrate as NaDR (nitrate- denitrification ratio); the proportion of endogenous denitrification for nitrite as NiDR (nitrite-denitrification ratio); the endogenous digestive pathway as DR (digesting ratio).

It was found that nitrogen loss was completed by ANAMMOX and endogenous denitrification pathway when sludge was preserved in refrigeration, mesophilic temperature or natural environment preservation for less than 45d. However, the frozen ANAMMOX sludge showed no ANAMMOX conversion capacity, and the nitrogen loss was caused by endogenous denitrification pathway.

Nitrogen Removal Capacities of ANAMMOX Sludge with Different Preservation Strategies

Table 5 shows that ANAMMOX sludge could maintain 20.2% of nitrogen removal capacity after 15 days of mesophilic preservation, and retain 43.6% of nitrogen removal capacity after 15 days of refrigerated preservation. This indicates that sludge stored in refrigeration was better than that kept at mesophilic temperature, at least for the short term. However, the removal activity declined rapidly for both cases when the storage time increased until it became 0 after 150 days of storage.

After 15d, 30d, 45d and 150d of preservation under natural environment, the nitrogen removal capac-

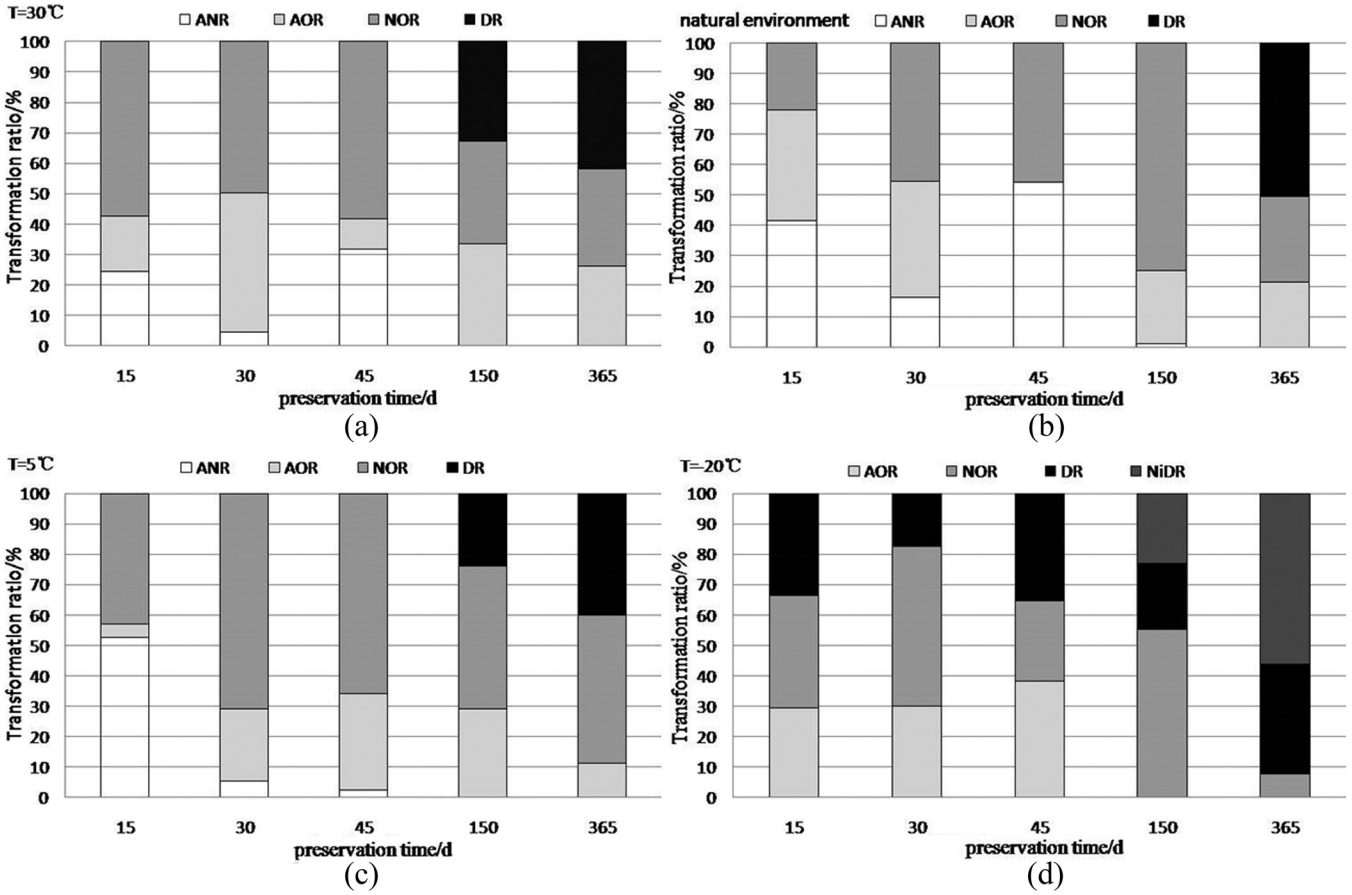

Figure 1. *Percentages of different pathways in ANAMMOX sludge after preservation under different conditions.*

ity of ANAMMOX sludge remained as 80.9%, 59.6%, 43.8% and 26.2%, respectively. Dosta *et al.* showed that ANAMMOX sludge still retained strong ANAMMOX activity at 15°C, because the reduction of related enzymes activities at low temperature could disable the metabolism of bacteria [17]. By contrast, 365 days of preservation under natural environment (0~33°C) caused the nitrogen removal capacity of ANAMMOX sludge to reduce to zero. Since high temperatures during the summer season might help accelerate the endogenous digestion of ANAMMOX sludge, the storage of ANAMMOX sludge is considered suitable under natural environment (0~15°C) for a short time (≤ 45d) instead of a long term preservation.

As for frozen preservation, ANAMMOX sludge still displayed nitrogen removal capacity, although it was caused by endogenous denitrification. Vlaeminck *et al.* suggested that the preserved ANAMMOX sludge mix-

Table 5. The Nitrogen Removal Capacities of ANAMMOX Sludge after Preservation.

	Mesophilic Temperature		Natural Environment		Refrigeration		Freezing	
Preservation Time, d	Nitrogen Removal Rate, $kg \cdot m^{-3} \cdot d^{-1}$	Nitrogen Removal Capacity Reserved, %	Nitrogen Removal Rate, $kg \cdot m^{-3} \cdot d^{-1}$	Nitrogen Removal Capacity Reserved, %	Nitrogen Removal Rate, $kg \cdot m^{-3} \cdot d^{-1}$	Nitrogen Removal Capacity Reserved, %	Nitrogen Removal Rate, $kg \cdot m^{-3} \cdot d^{-1}$	Nitrogen Removal Capacity Reserved, %
15	0.0216	20.2	0.0866	80.9	0.0467	43.6	0.0132	12.3
30	0.0135	12.6	0.0638	59.6	0.0351	32.8	0.0192	17.9
45	0.0095	8.9	0.0469	43.8	0.0117	10.9	0.0257	24.0
150	0	0	0.028	26.2	–	–	0.0092	8.6
365	–	–	–	–	0.0025	2.3	0.02145	20.0

"–": value was negative.

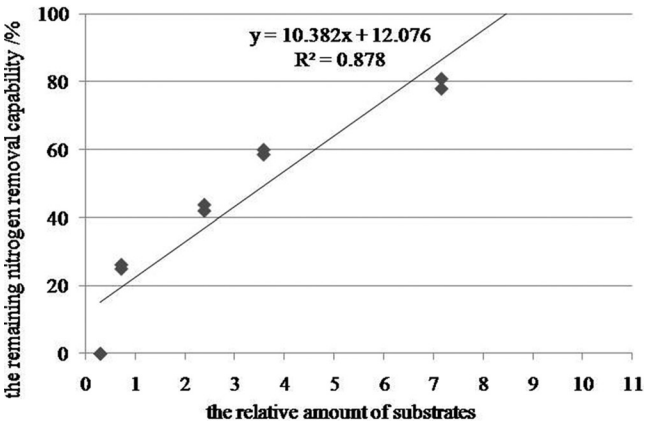

Figure 2. *Effect of relative materials quantity on ANAMMOX sludge activity after preservation.*

ture could only degrade nitrate [6]. This also indicates that the preserved ANAMMOX sludge might have denitrification capability, and frozen preservation would lead to nitrogen loss with endogenous denitrification.

Effects of Relative Substrate on Nitrogen Removal Performance of Sludge under Natural Environment Preservation

Not only preservation temperature or duration has imposed important impacts on nitrogen removal capability of ANAMMOX sludge, but also the relative amount of substrate is the key for sludge preservation.

Nitrogen removal capability of ANAMMOX sludge increased with an increase in the relative amount of substrates under natural environment preservation (as shown in Figure 2). This indicates that the shorter the preservation time is, and the more preservative fluid substrates are, the stronger the activity of sludge is after the preservation process.

5 g ANAMMOX sludge was stored at either 0~15°C or 30°C for 25 days. For both cases, nitrogen removal capacity was around 40% (see Table 6), which was close to the predicted value (the maximum deviation was only 11.27%). This suggested that nitrogen removal capacity of sludge under natural environment preservation could be predicted by the relative amount of substrates. Also, the activity of sludge after the preservation process could remain at around 80% if the relative amount of substrates is above seven as shown in Figure 2.

CONCLUSION

The stored ANAMMOX sludge had displayed nitrification capacity. Freezing (–20°C) not only contributed to high operating costs, but also led to the rupture of microbial cells and the reduction of ANAMMOX activity.

Sludge stored under natural environment (0~15°C) could remain the highest ANAMMOX activity. Meanwhile, there was a positive linear relationship between the remaining nitrogen removal capability of ANAMMOX sludge and the relative amount of substrates. When the relative amount of substrates was above seven, approximately 80% of nitrogen removal capability remained. Therefore, under natural environment, it could be a cost-effective approach to preserving ANAMMOX sludge from light and oxygen conditions when ambient temperature was between 0 and 15°C, at least in the short term (≤ 45 d).

ACKNOWLEDGMENT

This research was funded by National Natural Science Foundation of China (51008202, 51478284) , and the major projects of the Environmental Protection Department of Jiangsu Province (201104). Thanks to the support from the Priority Academic Program Development of Jiangsu Higher Education Institutions and the Jiangsu focus professional class of environmental science and engineering.

REFERENCES

1. Tang, C.J., Zheng, P., Wang, C. H., "Performance of high-loaded ANAMMOX UASB reactors containing granular sludge", *Water Research*, Vol. 45, No. 1, 2011, pp. 135–144. http://dx.doi.org/10.1016/j.watres.2010.08.018
2. Jetten, M.S.M., Wagner, M., Fuerst, J., "Microbiology and application

Table 6. Verification Results for Model.

Batch	Temperature, °C	Nitrogen Nemoval Rate Before Preservation, $kg \cdot m^{-3} \cdot d^{-1}$	Relative Amount of Substrates	Nitrogen Removal Rate After Preservation, $kg \cdot m^{-3} \cdot d^{-1}$	Nitrogen Removal Capacity Reserved		Deviation, %
					Actual, %	Predicted, %	
1	0~15	0.500	3.68	0.227	45.4	51.06	5.66
2	30	0.499	3.69	0.199	39.9	51.17	11.27

of the anaerobic ammonium oxidation (‘ANAMMOX’) process”, *Current Opinion in Biotechnology*, Vol. 12, No. 3, 2001, pp. 283–8. http://dx.doi.org/10.1016/S0958-1669(00)00211-1

3. Isaka, K., Date, Y., Sumino, T., ″Growth characteristic of anaerobic ammonium-oxidizing bacteria in an anaerobic biological filtrated reactor”, *Appl. Microbiol. Biotechnol.*, Vol. 70, 2006, pp. 47–52. http://dx.doi.org/10.1007/s00253-005-0046-2
4. Schmid, M.C., Maas, B., Dapenda, A., ″Biomarkers for in site detection of anaerobic ammonium- oxidizing (anammox) bacteria”, *Appl. Environ. Microbiol.*, Vol. 71, No. 4, 2005, pp. 1677–84. http://dx.doi.org/10.1128/AEM.71.4.1677-1684.2005
5. Strous, M., Heijnen, J.J., Kuenen, J.G., ″The sequencing batch reactor as a powerful tool for the study of slowly growing anaerobic ammonium-oxidizing microorganisms”, *Appl. Microbiol. Biotechnol.*, Vol. 50, 1998, pp. 589–96. http://dx.doi.org/10.1007/s002530051340
6. Vlaeminck, S.E., Geets, J., Vervaeren, H., ″Reactivation of aerobic and anaerobic ammonium oxiders in OLAND biomass after long-term storage”, *Appl. Microbiol. Biotechnol.*, Vol. 74, No. 1, 2007, pp.1376–84. http://dx.doi.org/10.1007/s00253-006-0770-2
7. Rothrock, Jr., M.J., Vanotti, M.B., Szogi, A.A., ″Long-term preservation of ANAMMOX bacterial”, *Appl. Microbiol. Biotechnol.*, Vol. 92, No. 5, 2011, pp. 147–157. http://dx.doi.org/10.1007/s00253-011-3316-1
8. van de Graff, A.A., De Bruijin, P., Robertron, L.A., ″Autotrophic growth of anaerobic ammonium- oxidizing micro-Organisms in a fluidized bed reactor”, *Microbiology*, Vol. 142, No. 8, 1996, pp. 2187–2196. http://dx.doi.org/10.1099/13500872-142-8-2187
9. APHA, 1998, Standard Methods for the Examination of Water and Wastewater, 20th ed. United Book Press, USA.
10. Rittmann, B.E. and McCarty, P.L., 2002, Environmental Biotechnology: Principles and Applications, Beijing: Tsinghua University Press, 59–135.
11. Thomsen, J.K., Geest, T., Raymond, P.C., ″Mass spectrometric studies of the effect of pH on the accumulation of intermediates in denitrification by Paracoccus denitrificans”, *Applied and Environmental Microbiology*, Vol. 60, No. 2, 1994, pp. 536–541.
12. Almeida, J.S., Reis,M.A., Carrondo, M.J., ″Competition between nitrate and nitrite reduction in denitrification by Pseudomonas flourescens”, *Biotechnology and Bioengineering*, Vol. 46, No.5, 1995, pp. 476–484. http://dx.doi.org/10.1002/bit.260460512
13. Schmidt, I., Slieker, O., Schmid, M., ″Aerobic and anaerobic ammonia oxidizing bacteria— competitors or natural partners?”, *FEMS Microbiology Ecology*, Vol. 39, No. 3, 2002, pp.175–181.
14. Vogelsang, C., Gollembiewski, K., Ostgaard, K., ″Effect of preservation techniques on the regeneration of gel entrapped nitrifying sludge”, *Water Research*, Vol. 33, No. 1,1999, pp. 164–168. http://dx.doi.org/10.1016/S0043-1354(98)00200-0
15. Geets,J., Boon,N., and Verstraete, W., ″Strategies of aerobic ammonia oxidizing bacteria for coping with nutrient and oxygen fluctuations”, *FEMS Microbiology Ecology*, Vol. 58, No. 1, 2006, pp. 1–13. http://dx.doi.org/10.1111/j.1574-6941.2006.00170.x
16. Van Niftrik, L., Geerts, W.J.C., Van Donselaar, E.G., ″Combined structural and chemical analysis of the ANAMMOXosome: A membrane-bounded intracytoplasmic compartment in ANAMMOX bacteria”, *Journal of Structural Biology*, Vol. 161, No. 3, 2008, pp. 401–410. http://dx.doi.org/10.1016/j.jsb.2007.05.005
17. Dosta, J., Fernández, I., Vázquez-Padín, J.R., ″Short-and long term effects of temperature on the ANAMMOX process", Journal of Hazardous Materials, Vol.154, No.1-3, 2008, pp.688-693. http://dx.doi.org/10.1016/j.jhazmat.2007.10.082

Basic Characteristics and Effective Control of Gangue Piles in Mining Areas: A Case Study

JIXIONG ZHANG, RUI GAO, MENG LI*, SHENGGEN CAO and SHIWEI LIU
[1]*State Key Laboratory of coal Resources and Mine Safety, China University of Mining & Technology, Xuzhou 221116, China*
[2]*School of Mines, Key Laboratory of Deep Coal Resource Mining, Ministry of Education of China, China University of Mining and Technology, Xuzhou, 221116, China*

ABSTRACT: Discharged gangues are stockpiled on the surface and are characteristic of mining areas. The rejected materials are an environmental risk. The definition of effective methods to control and prevent pollution caused by gangue piles has become a relevant research topic. The present research will characterise gangue pile origins and their physico-chemical features. According to their physico-chemical characteristics, the effect of gangue piles on the environment in a mining area was analysed. Thereafter, the method of backfill mining was proposed as an effective method for gangue pile control and prevention. The backfill and control effects were investigated and results showed that gangue backfill mining bestowed significant economic and environmental benefits. Using this method, 160,000 t of gangues have been dealt resulting in a reduction of land occupied by 5,200 ha and land degradation covering some 29,600 ha. Gangue piles and their associated pollution have been effectively controlled with ensuing environmental benefits in mining areas.

INTRODUCTION

COAL gangue, as a solid waste generated by coal mining and processing, represents the industrial solid waste with the largest amount of annual discharge and accumulation in China [1–3]. In coal mining, gangues piles are characteristic of mining areas and associated with surface accumulation. Mining areas are usually affected by heavy metal contamination [4–5], and continuous coal mining activities increase gangue discharges to the environment. Stockpiled gangues in China have accumulated to 5.5 billion tonnes according to as yet incomplete statistics. There are 1,600 large-scale gangue piles, occupying approximately 20,000 ha of land. In addition, the pile volume is increasing at a rate of between 200 and 500 million tonnes p.a., increasing environmental risks associated with mining activities and also occupying a large land area [6–8]. In particular, the pollution produced by gangues affects coal production and nearby residents. It is essential that coal mine managers effectively control the pollution from gangue piles. Many scholars have conducted research into pollution control around gangue piles, and proposed land reclamation or gangue-based power generation as solutions [9–11]. However, these methods have limited applicability and effects.

The main subjects of this research are the physico-chemical characterisation of gangues in a gangue pile, to be analysed with regard to its influence on the environment and to propose gangue backfill mining as a method of controlling pollution in mining areas. Using this method could prevent the pollution, and its associated effects, from accumulated gangues and protect the environment. The research provided guidance on the disposal of gangue piles and other solid wastes in mining areas.

ORIGIN OF GANGUES IN GANGUE PILES

Gangue is a kind of rock with a low carbon content which is harder than coal. It is produced by the association with coal seam excavation during coal mining and washing operations. Gangue piles are mainly composed of excavation gangue and washed gangue. Excavation gangue is a rock generated in the process of developing coal seams or preparing tunnel excavation while washed gangue refers to the parting or a small amount of rock on the roof and floor generated during mining activities, such as rock materials discharged by wash-separation of coal in above-ground preparation plants [12]. These two types of gangues are accumu-

*Author to whom correspondence should be addressed.
E-mail: limeng77521@126.com

1544-8053/15/01 S145-10

doi:10.12783/issn.1544-8053/12/S1/21

Figure 1. *Gangue pile.*

lated in gangue piles by piling up on the surface (Figure 1).

PHYSICO-CHEMICAL FEATURES OF GANGUE

Mineral Compounds

Ten representative gangue samples were selected from Pingdingshan gangue piles to analyse their mineral composition by D/Max-3B X-ray diffractometer. Excavation gangue was mainly lifted from underground to accumulate in the Pingdingshan gangue piles. Qualitative analysis was conducted on the basis of the standard powder diffraction files (PDF) for various minerals, provided by the International Centre for Diffraction Data of The Joint Committee on Powder Diffraction Standards (JCPDS-ICDD). Afterwards, standard methods were used to conduct comparative analyses. The X-ray diffraction spectra of the gangue samples are basically the same. One example of typical test results is shown in Figure 2.

Quantitative analysis was performed using the K-value method of Chinese Standard GB5225–86. The mineral compositions of those gangue samples tested are listed in Table 1.

Quantitative analysis was performed using the K-value method of Chinese Standard GB5225-86. The mineral compositions of the gangue samples are listed in Table 1.

Figure 2 and Table 1 show that the gangue consisted of more quartz and kaolinite, as well as a small amount of illite, andreattite, chlorite, siderite, pyrite, etc. Among which, quartz and kaolinite accounted for more than 50% by mass, and were the main components used in gangue backfill mining to confer adequate stiffness upon placement and compaction.

Chemical Composition

The chemical composition of collected gangue samples (Table 2) suggested that the gangue samples contained more SiO_2 and Al_2O_3, a small amount of Na_2O, MgO, K_2O, CaO, Fe_2O_3, P, S, Mn, etc., as well as trace

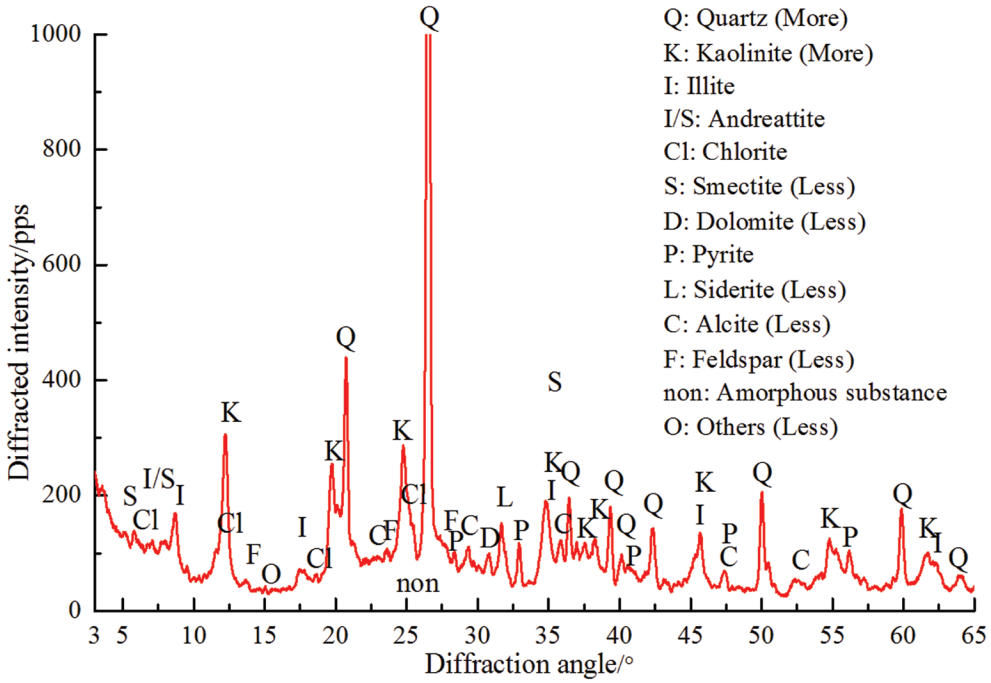

Figure 2. *X-ray diffraction spectrum of gangue samples.*

Table 1. Mineral Composition of Gangue Samples (%).

Quartz	Kaolinite	Illite	Andreattite	Smectite	Chlorite	Feldspar	Dolomite	Calcite	Siderite	Pyrite	Coal
20	33	10	11	2	2	0.5	0.5	0.5	1.3	2.6	15

amounts of Ba, Cu, Pb, F, Cl, etc. Owing to the minerals containing carbon, aluminium, and CaO, gangues were likely to be hydrolysed and weathered.

Compactness and Pore Structure

The compactness of gangues was assessed by scanning electron microscope (SEM) with different resolutions (Figure 3). The gangue samples contain coarse cavities, poorly-developed fractures and a compact structure. Besides, the characteristic distribution of clay minerals was not apparent; micro-voids and fractures between coarse grained minerals and fine grained clays were widely developed; moreover the cementation was found between coarse grained minerals and the clay fraction. Moderate fractures in partially coarse grained minerals were widely developed with good interconnectivity, while the partial fine grained clay was layered and compact.

Mercury intrusion porosimetry was employed to measure the pore structure of the gangue samples. The pore volume was obtained by measuring the amount of mercury forced into the pore spaces under different external pressures. Meanwhile, the proportion of different sized pores in the gangue was determined. The relationship between the total mercury influx and the pore size distribution of the gangue samples is shown in Figure 4. If the pore size was greater than 100,000 nm, the amount of mercury influx was less than 0.001 mL/g; for pore sizes between 1,000 and 100,000 nm, the mercury influx increased to 0.005 mL/g at a pore size of 1,000 nm; the mercury influx increased to 0.013 mg/Lat a pore size of 200 nm; when pore size was less than 200 nm, the mercury influx increased until reaching its maximum value of 0.016 mL/g.

Tables 3 and 4 show pore characteristics and their size distribution in gangues tested with mercury intrusion porosimetry. The porosity of the gangue was 5.64% and pore size ranged from 100 to 1,000 nm (48.6% of the total pore size distribution). Since the average pore size was 46.13 nm, they were classified as meso-microporous materials, and the pore edges were well cemented to the surrounding rock particles lending the material a high permeability which favoured oxidation of, and leaching from, the gangues.

INFLUENCE OF GANGUE PILES ON THE ENVIRONMENT

Land Occupation

In coal mining areas, a large amount of solid waste, such as gangues, is discharged. In China, production of piled gangues has reached some 5.5 billion tonnes, occupying a land area of about 20,000 ha. In addition, the pile volume is increasing at a rate of 200 to 500 million tonnes p.a. Gangue is mainly dealt with surface deposition. The number of gangue piles has also been increasing; lots of arable land and natural vegetation have been lost, causing a waste of land resources [13]. The environment around mining areas is therefore degraded [14]. The annual output and rate of increase of gangue generation are shown in Figure 5. In addition, long-term gangue accumulation leads to its being weathered. Then the powdery residual soil thus formed floats off such stockpiles and modifies the pH of the native, underlying, and surrounding soils. Subsequently, the previous natural and biogeochemical balance in these soils is destroyed.

Water Pollution

The weathering and leaching of precipitates from gangue piles induces physico-chemical changes and the precipitation of toxic heavy metals. The gangue releases pollutants such as: SO_4^{-2}, F^-, Mn, Zn, etc., under rainfall-induced leaching and its effects. Material weathering increases pollutant concentrations. Those pollutants infiltrate and percolate to underground water sources, representing a hazard to human health. Moreover, higher sulphur contents in the gangue promotes

Table 2. Chemical Composition of Gangue Samples (%).

Na_2O	MgO	Al_2O_3	SiO_2	K_2O	CaO	Fe_2O_3	P	S	Ba	Mn	Cu	Pb	Zn	Ti	F	Cl
0.41	1.4	207	53.7	2.0	1.3	6.7	0.05	1.53	≤ 0/002	0.043	0.0005	< 0.0002	0.005	0.42	< 0.045	0.009

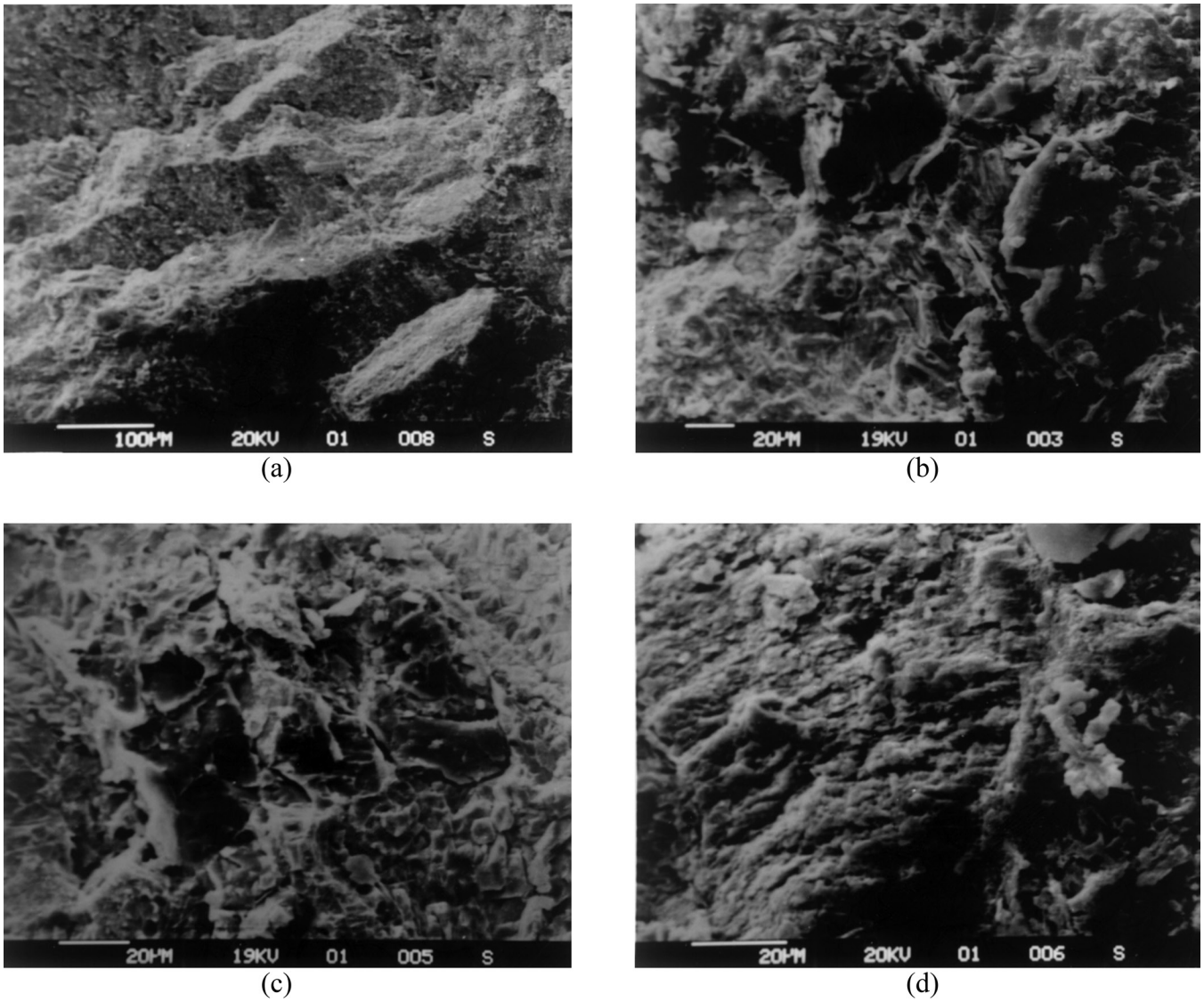

Figure 3. *SEM pictures of gangue samples: (a) Magnification; 150×; (b) Magnification: 400×; (c) Magnification: 600×; and (d) Magnification: 800×.*

sulphuric acid formation during weathering and rainfall-induced leaching and causes water acidification with consequent surface and groundwater pollution. Consequently, fish and other freshwater organisms could die and the environment is further degraded as a result [15].

Atmospheric Pollution

The long-term accumulated gangues are likely to form fine grained particles by weathering and erosion. Toxic heavy metals such as Pb, Zn, etc. contained in the particles are taken-up by the surrounding atmosphere under wind action. The increase in suspended particle load promotes a decrease in air quality, further harming the health of workers in the area. Due to the high permeability of gangues, spontaneous combustion occurs and temperature increases in gangue piles after the oxidation of their reactive chemical components. As the internal temperature of gangue piles increases to 800 to 1200°C after spontaneous combustion, a large amount of harmful gases including CO, CO_2, SO_2,

Table 3. Gangue Pore Characteristics.

Mass, g	Density, g·cm^{-3}	PermeAbility, mdarcy	Porosity, %	Average Pore Size, nm	Total Area of Hole, m^2/g
70.87	2.38	4.41	5.64	46.13	2.17

Table 4. Gangue Pore Characteristics.

Mass, g	Density, g·cm^{-3}	PermeAbility, mdarcy	Porosity, %	Average Pore Size, nm	Total Area of Hole, m^2/g
70.87	2.38	4.41	5.64	46.13	2.17

H_2S, and NO_x are released [16]. These gases reduce local air quality and also affect human health of residents in mining areas. Besides, the vegetation around mining areas tends to die-back. These spontaneous combustion events can last as long as 10 years or more, causing acute deterioration of the environment in mining areas [17].

Geological Hazards

Gangue piles are composed of particles with different sizes and shapes [11]. The larger internal pores and loose internal structure lead to poor stability in the piles. The tested angles of repose ranged from 33° to 37° in the selected gangue samples (Figure 6). Rainfall or manual excavation produced hazards such as landslides and debris flows associated with slope changes. Meanwhile, the higher gangue porosity was likely to react with oxygen, resulting in an increase in the internal temperature of the stockpile. Consequently, a series of related hazards such as explosions and collapse are more likely.

GANGUE BACKFILL MINING METHOD

Basic Principles

The gangue backfill mining method refers to the application of solid waste in mining areas, such as gangue, to backfill mined-out areas. In addition, to solve problems related to land subsidence and collapse, this method increases solid wastes recycling, protects land resources, and stabilises existing construction works. Backfilling has been an effective method for the treatment of environmental problems caused by coal mining [18].

In gangue backfill mining, crushed gangues were transported underground using a backfill material vertical feed system [19]. The material transported to the backfill conveyor, which was hung on the back of the top beam of the backfill mining hydraulic support and used as backfill for mined-out areas, was deposited through the dumping hole in the backfill conveyor. Furthermore, a tamping device fixed to the back of the backfill mining hydraulic support was used to compact the backfill (Figure 7).

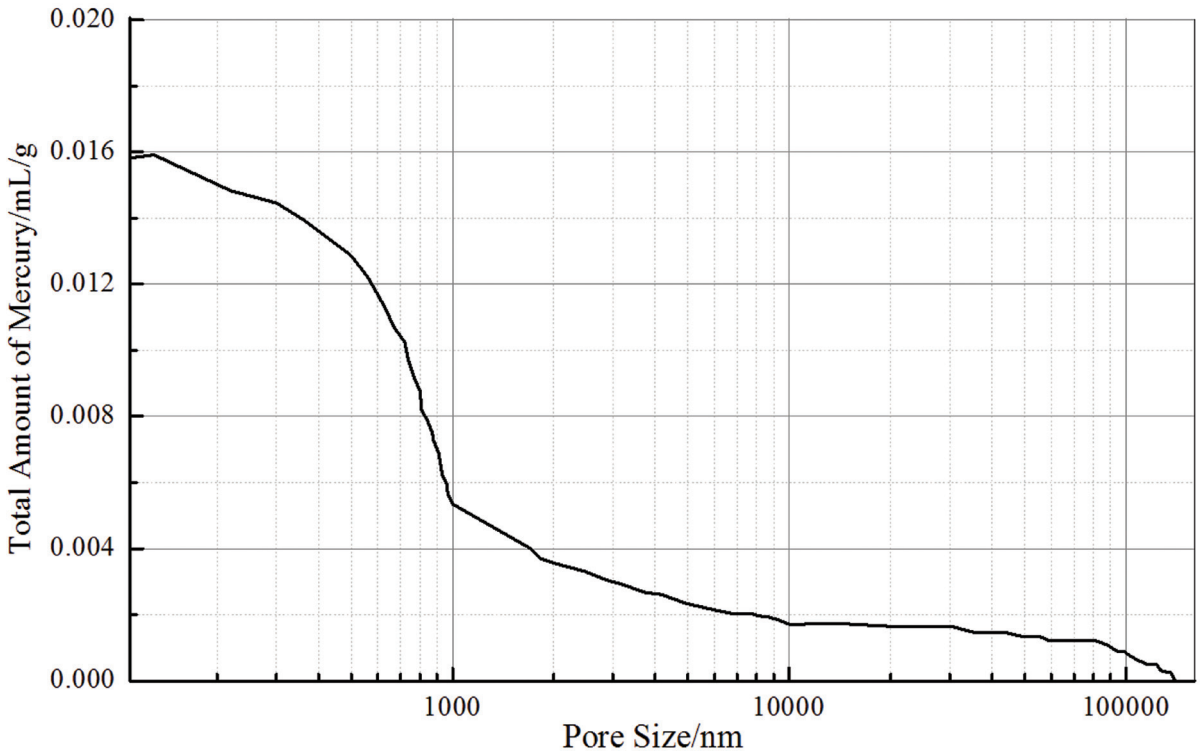

Figure 4. Relationship between total amount of mercury and pore size.

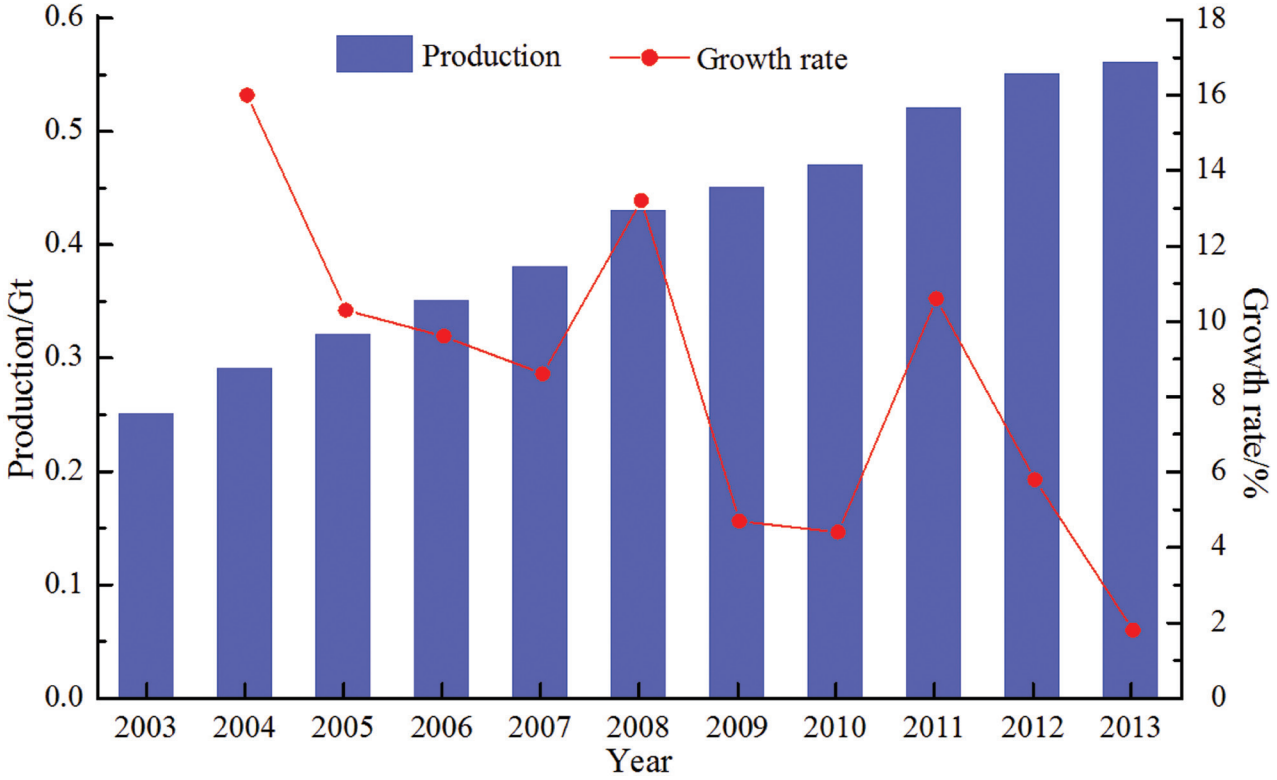

Figure 5. *Production and growth rate of gangue from 2003 to 2013.*

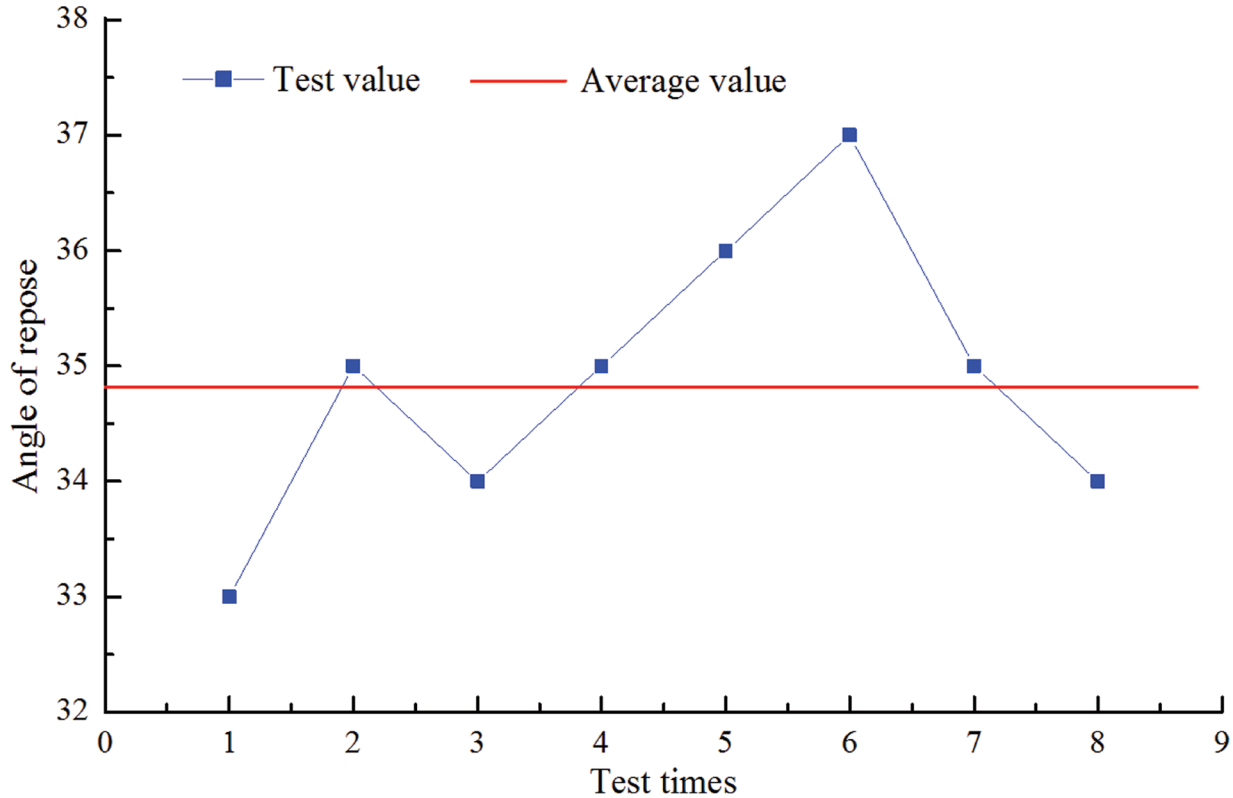

Figure 6. *Test results: angle of repose.*

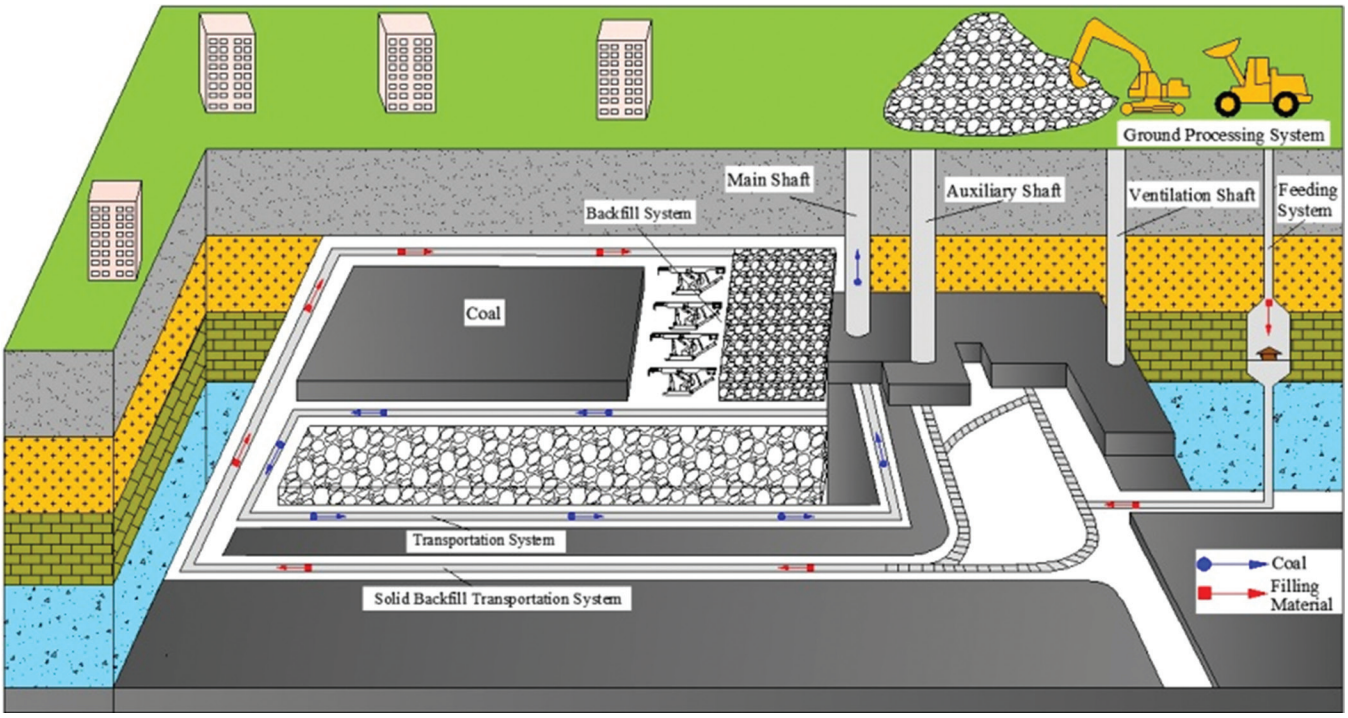

Figure 7. *Basic principle of gangue backfill mining.*

Backfill Technique

The gangue backfill technique is developed from the basic concepts of mechanical coal mining [20]. It is able to mine and backfill simultaneously with a hydraulic support and may be compared with traditional coal mining techniques and, as such, is both a mining, and a backfilling, technology. The mining technology used is a traditional one and the layout of a typical gangue backfill mining panel is shown in Figure 8.

The gangues are transported to the backfill conveyor which was hung on the back of the top beam of the backfill mining hydraulic support from the panel entry using the gangue belt conveyor by passing through a self-advancing transfer conveyor. Then, they are unloaded to the backfill area through its dumping hole. Afterwards, backfilled gangues which were unloaded as backfill are compacted using a tamping device fixed on the back of the support. In this way, the initially loose, piled, backfill materials are vibro-compacted. The bearing strength of the backfilled gangues increased, controlling future movement/settlement of the overburden. Simultaneous backfill and mining operations in any given panel were possible.

Equipment Used

The main devices for gangue backfill mining consisted mainly of a backfill mining hydraulic support, a backfill conveyor, and a self-advancing transfer conveyor.

Backfill Mining Hydraulic Support

The function of the backfill mining hydraulic support was to prop the roof as it was exposed by coal mining and to allow space for later placement and compaction of backfill. The dumping structure on the back was used to compact the loose materials in the backfill space. Generally, the support comprises a top beam, column, base, four-bar mechanism, the back of the top beam, and additional dumping devices. The back of the top beam was supported by two inclined columns to increase its strength and stability.

Backfill Conveyor

The backfill conveyor was hung off the lower part of the back of the top beam of the backfill mining hydraulic support. Its function was to unload material into the backfill space.

Self-advancing Transfer Conveyor

In gangue backfill mining, the self-advancing transfer conveyor and gangue belt conveyor were combined

Table 5. Comprehensive Analysis of Governance Effect.

	Economic Benefits				Environmental Benefits			
Panel	Newly Added Output Value, Million ¥	Newly Added Tax, Million ¥	Reducing Land Compensation, Million ¥	Prolonging Service Time, Years	Disposal of Gangue, Tonnes	Reducing Land Occupation, Hectares	Reducing Land Destruction, Hectares	Others
13080	87	23.7	2.52	10	160,000	5,200	29,600	1. Reducing hazards of gangue piles 2. Lessening air pollution 3. Reducing water pollution 4. Eliminating radiation

to satisfy the gradual advance in the gangue backfill mining panel. Backfilled gangues are transported to the backfill conveyor which was hung from the lower part of the back of the top beam of the backfill mining hydraulic support using a belt conveyor. This arrangement could self-advance the working panel.

PROJECT CASE STUDY

Project Overview

The case study analysed Panel 13080 in the Pingdingshan coal mine. The panel was 100 m long and had been advanced about 350 m at a mined height of 3.3 m, at an average inclination angle of 8° and an average burial depth of 360 m. The immediate roof was composed of a 5.3 m thick shale layer, whereas the basic roof consisted of a 31.5 m thickness of sandstone and the floor was composed of a 15.9 m thickness of sandy mudstone. There were various brick-concrete constructions such as buildings in a nearby village. To deal with gangue piles on the surface and protect the local environment, the operators of the Pingdingshan coal mine selected gangues from the locally available gangue piles as backfill material for mined-out areas. The layout of Panel 13080 is shown in Figure 9.

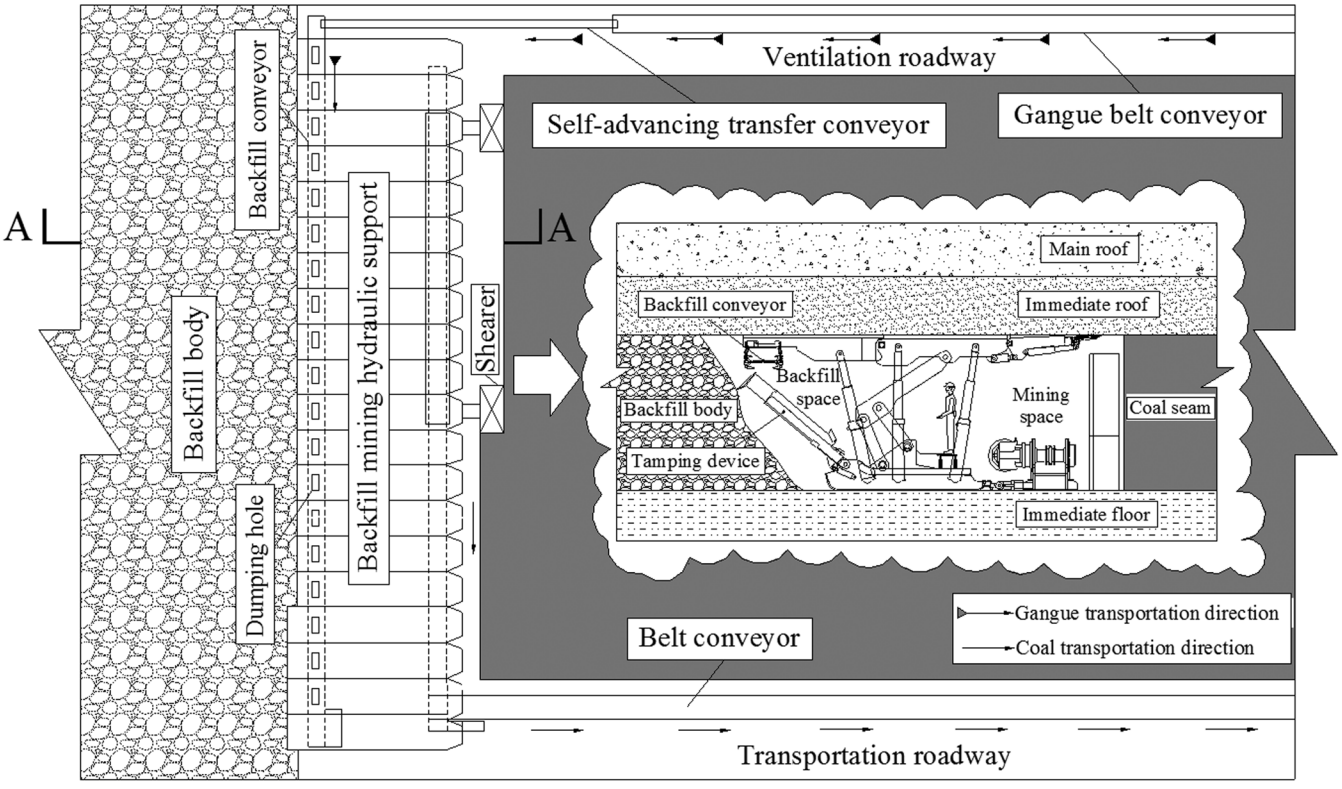

Figure 8. Panel layout of gangue backfill mining.

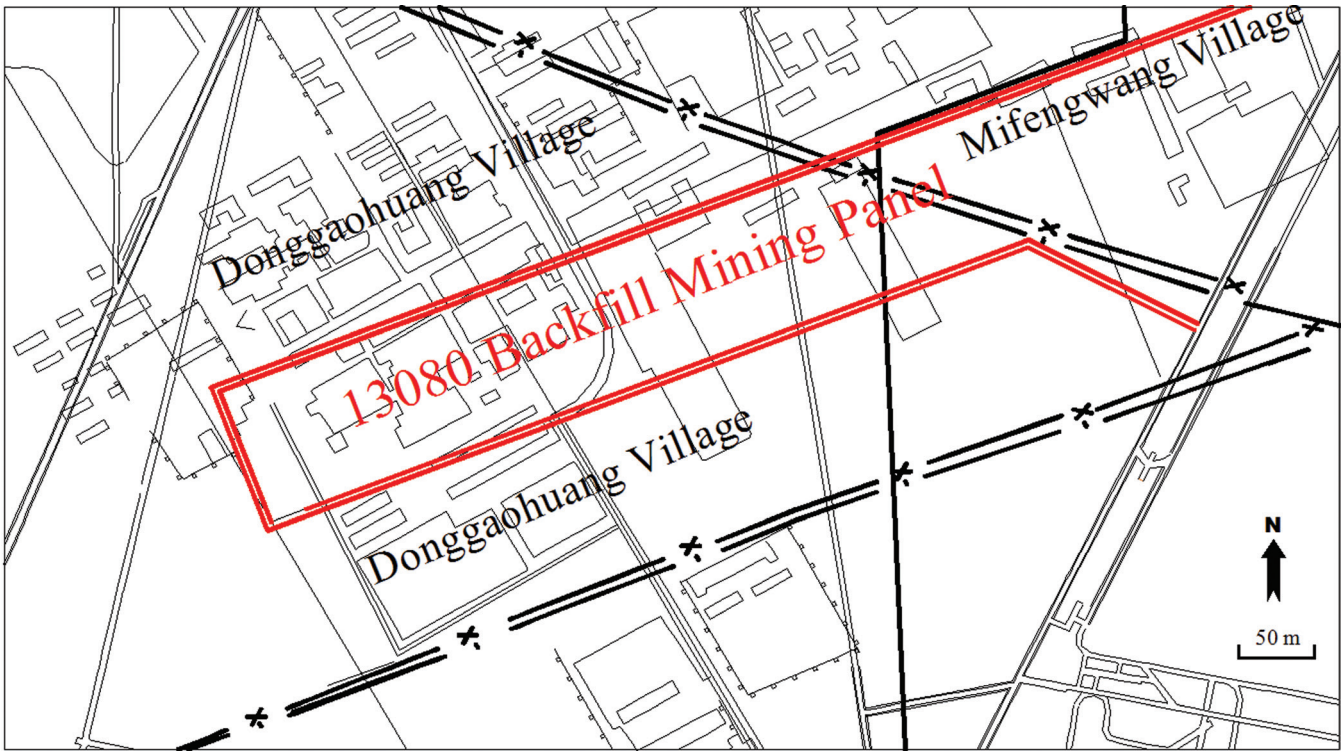

Figure 9. *Layout of Panel 13080.*

Pollution Controlling Effect

Gangue backfill mining has yielded economic benefits for the Pingdingshan coal mine. It dealt with a large amount of gangues which was environmentally favourable towards the local mining area (Table 5).

Table 5 indicates that this technique reaped a greater economic benefit for Panel 13080: output increased by ¥87 million, while the tax on such an increased output rose by ¥23.7 million, and the land compensation bill fell by ¥2.52 million. In addition, effectively, the technique controlled pollution from the local gangue piles by removing and reburying 160,000 t of gangue material, which decreased the demand for land by 5,200 ha and prevented the destruction of a further 29,600 ha. The gangue backfill mining could prevent pollution resulting from solid mine waste and protect the local environment.

CONCLUSIONS

The physico-chemical features of gangues from local stockpiles were obtained experimentally. The influence of gangue piles on the local environment was analysed. In addition, a method of controlling pollution from gangue piles was proposed, by combining the tests with a project case study and ensuring pollution-control effects were investigated. The main conclusions could be summarised as:

1. The authors analysed the origin of the gangue materials from gangue piles. The physico-chemical features measured included: mineral composition, chemical constituents, and pore structure. This work laid a foundation for analysing the influence of gangue piles on the local environment.
2. The impact of gangue piles on the environment in the local mining area was studied in terms of land occupation, water pollution, atmospheric pollution, and geo-hazards.
3. A method of controlling the pollution from gangue piles based on basic mining principles and backfill technology was proposed to mitigate the aforementioned influences.
4. The integration of experimental data with a project case study indicates that backfill effects, and the quality of this method, introduce economic and environmental benefits. The results showed that the method could prevent the pollution, and its associated effects, from accumulated gangues and protect the environment.

ACKNOWLEDGMENT

This paper was supported by State Key Laboratory of Coal Resources and Safe Mining (No. SKLCRSM12X01) (CUMT), Qing Lan Project (Jiangsu Province) and Fundamental Research Funds for the Central Universities (No.2014YC02) (CUMT).

REFERENCES

1. Y.Z. Sun, J.S. Fan, P. Qin, H.Y. Niu. Pollution extents of organic substances from a coal gangue dump of Jiulong Coal Mine, China. *Environmental and Geochemistry Health,* 2009, 31(1): 81–89. http://dx.doi.org/10.1007/s10653-008-9158-9
2. X. Querol, M. Izquierdo, E. Monfort *et al.* Environmental characterization of burnt coal gangue banks at Yangquan, Shanxi Province, China. *International Journal of Coal Geology*, 2008, 75(2): 93–104. http://dx.doi.org/10.1016/j.coal.2008.04.003
3. Q. Xue, H.J. Lu, Y. Zhao, L. Liu. The metal ions release and microstructure of coal gangue corroded by acid-based chemical solution. *Environmental Earth Sciences*, 2014, 71(7): 3235–3244. http://dx.doi.org/10.1007/s12665-013-2743-y
4. C. Wang, D. Harbottle, Q.X. Liu, Z.H. Xu. Current state of fine mineral tailings treatment: A critical review on theory and practice. *Minerals Engineering*, 2014, 58: 113–131. http://dx.doi.org/10.1016/j.mineng.2014.01.018
5. H.B. Liu, Z.L. Liu. Recycling utilization patterns of coal mining waste in China. *Resources, Conservation and Recycling*, 2010, 54: 1331–1340. http://dx.doi.org/10.1016/j.resconrec.2010.05.005
6. G.W. Fan, D.S. Zhang, X.F. Wang. Reduction and utilization of coal mine waste rock in China: A case study in Tiefa coalfield. *Resources, Conservation and Recycling*, 2014, 83: 24–33. http://dx.doi.org/10.1016/j.resconrec.2013.12.001
7. V. Lucile, A. Lena, Ö. Björn. The effects of back?lling and sealing the waste rock on water quality at the Kimheden open-pit mine, northern Sweden. *Journal of Geochemical Exploration*, 2013, 134: 99–110. http://dx.doi.org/10.1016/j.gexplo.2013.08.003
8. D. Servida, S. Comero, M.D. Santo *et al.* Waste rock dump investigation at Rosia Montana gold mine (Romania): a geostatistical approach. *Environmental Earth Sciences*, 2013, 70(1): 13–31. http://dx.doi.org/10.1007/s12665-012-2100-6
9. Y.J. Lu, "Compaction treatment affected to moisture content of coal reject backfilling reclaimed land. *Coal Science and Technology*, 2010, 38(11): 125–128.
10. J.H. Dong, Z.F. Bian, H.F. Wang. Comparison of heavy metal contents between different reclaimed soils and the control soil. *Journal of China University of Mining & Technology*, 2007, 36(4): 531–536.
11. K. Liu, Y.D. Ma, X.K. Hou. Environmental hazards of coal gangue and comprehensive utilization. *Coal*, 2013, 22(5): 59–61.
12. X.X. Miao, J.X. Zhang, G.L. Guo. *Method and technology of full-mechanized coal mining with solid waste filling*. China University of Mining & Technology Press, Xuzhou, 2010.
13. A. Lena, A. Elin, M. M. Seth. Neutralization/prevention of acid rock drainage using mixtures of alkaline by-products and sulfidic mine wastes. *Environmental Science and Pollution Research*, 2013, 20(11): 7907–7916. http://dx.doi.org/10.1007/s11356-013-1838-z
14. H. Zhang, X. Zhang, Y.S. Deng. Experimental research on coal gangue reclamation in collapse area of coal-mines and its pollution control. *Environmental Sanitation Engineering*, 2008, 16(5): 4–6.
15. Z.F. Bian, D. Jin, J.H. Dong *et al.* Discussion on rational ways for coal gangue treatment and utilization. *Journal of Mining & Safety Engineering*, 2007, 24(2): 132–136.
16. H.J. Wu, F.Y. Zeng, H.F. Yao *et al.* Danger evaluation and control technology of coal mine gangue spontaneous combustion. *Coal Science and Technology*, 2013, 41(4): 119–123.
17. Y.L. Duan, X.Q. Zhou, M.G. Yu *et al.* The relations between spontaneous combustion degree and explosions of gangue dump. *Journal of China Coal Sciety*, 2009, 34(4): 514–519.
18. Q. Zhang, J.-X. Zhang, Y.-L. Huang *et al.* Backfilling technology and strata behaviors in fully mechanized coal mining working face. *International Journal of Mining Science and Technology*, 2012, 22(2): 151–157. http://dx.doi.org/10.1016/j.ijmst.2011.08.003
19. J.M. Xu, J.X. Zhang, Y.L. Huang *et al.* Experimental research on the compress deformation characteristic of waste-fly ash and its application in backfilling fully mechanized coal mining technology. *Journal of Mining and Safety Engineering*, 2011, 28(1): 158–162.
20. J. Li, D.S. Wang, Z.P. Wang *et al.* Application of solid backfill mining under dams avoiding raising waste rock. *China Mining Magazine,* 2013, 22(6): 66–69.

Adsorption of Heavy Metals by Adsorbents from Food Waste Residue

X.D. FAN[1,2,*] and X.K. ZHANG[1]

[1]*Environmental and Municipal Engineering School of Tianjin Cheng Jian University, Tianjin 300384, China*

[2]*Tianjin Key Laboratory of Aquatic Science and Technology, Tianjin 300384, China*

ABSTRACT: Food waste residue is an intractable problem worldwide. The current study discussed the potential of adsorbents prepared from food waste residue (AFWR) for heavy metal removal from wastewater. The microstructure of AFWR was characterized, and kinetic studies on the simultaneous adsorption of Pb^{2+}, Cu^{2+}, Zn^{2+} and Cd^{2+} ions from aqueous solutions by AFWR were carried out. It was found that the adsorption of all heavy metals followed a pseudo-second-order kinetics, so that there was a competitive adsorption for Pb^{2+}, Cu^{2+}, Zn^{2+} and Cd^{2+}. According to the experimental results, the adsorption in competition beads with the heavy metals presented an order of Cu^{2+} > Pb^{2+} > Zn^{2+} > Cd^{2+}.

INTRODUCTION

RECENTLY, numerous approaches have been studied for developing more effective technologies, not only to reduce the amount of heavy metal wastewater but also to improve the quality of the treated effluent [1,2]. Among these approaches, adsorption is the most versatile and the most widely used method by far, in which activated carbon is the most commonly used adsorbent. However, the cost of activated carbon is too high [3,4], which limits its wide applications in practical industries. In view of this, inexpensive adsorbents have attracted extensive attention around the world in the past decades [5,6].

Sewage sludge is carbonaceous in nature and has volatile components in its matrix, so that it can be used as an adsorbent for metal ions [7,8]. As a matter of fact, the use of activated carbon from sewage sludge has presented a strong potential as an adsorbent material due to its functional groups [9,10]. In our preliminary investigation, we also reported the preparation of activated carbon from sewage sludge, and further examined its adsorption property for dye removal from aqueous solutions [11].

Household and municipal food waste is a tough issue worldwide, especially in the rapidly growing cities and super-cities [12,13]. An important mitigation option is the diversion of reusable materials through sorting out food waste. Accordingly, different approaches have been proposed to support the sorting and reduction of food waste, such as legislation, top-down policy, community involvement and recycling [14,15]. In recent years, the recycling of food waste gradually has become a mainstream method, and more and more attention has been paid to the reuse of food waste for environmental protection, such as fermentation of food waste mixture for cell protein, prevention of volatile fatty acids and H_2 production [16,17]. Similar to sewage sludge, food waste is also carbonaceous in nature and has volatile components in its matrix [18,19]. As a result, it is probably suitable for preparing adsorbents.

The aim of this study is to investigate the feasibility of using unique adsorbents from food waste residue to achieve simultaneous removal of heavy metals produced by industrial activities. It is believed that the study is useful for low-cost industrial wastewater treatment, in which the simultaneous removal of several heavy metals is required.

EXPERIMENTAL PROCEDURE

Preparation of Adsorbents from Food Waste Residue

The food waste residue collected from Tianjin food waste Treatment Works of China was anaerobically digested and dewatered. The sample of food waste resi-

*Author to whom correspondence should be addressed.
E-mail: fanxiaodan.kai@163.com; Tel: 086-022-23085117

1544-8053/15/01 S155-04

doi:10.12783/issn.1544-8053/12/S1/22

due was first dried at 105°C for 2h, and then crushed and sieved through a sieve with a uniform size of 0.05–0.1 mm. 20 g of the dried sample was heated at 500°C for 0.5 h with a heating rate of 15°C/min in the nitrogen atmosphere. Thus, the adsorbents prepared by food waste residue (AFWR) were obtained.

Chemicals

All chemicals used in this work were of analytical purity. The stock solution of Cu^{2+}, Pb^{2+}, Cd^{2+} and Zn^{2+} with a concentration of $1.0 g \cdot L^{-1}$ were prepared using $CuSO_4$, $Pb(NO_3)_2$, $3CdSO_4 \cdot 8H_2O$ and $(CH_3COO)_2Zn \cdot 2H_2O$, respectively.

Adsorption Experiments

Adsorption experiments were conducted at 25°C. 0.50 g of AFWR and 25 mL heavy metal ion solution with desired concentration were added into a conical flask of 100 mL, and then the mixture was stirred by a shaking thermostat machine at a speed of 120 rpm for 2h (the contact time excluded). In kinetic experiments, Pb^{2+}, Cd^{2+} and Ni^{2+} ion solutions of 10 $mg \cdot L^{-1}$ were used, and the adsorption time varied between 0 and 400 min. The filter liquor was analyzed for the concentration of residual heavy metal ion by using Agilent 3510 atomic absorption spectrophotometer. The amount of adsorption (q) was calculated according to the following equation:

$$q = \frac{(C_0 - C_e)V}{m} \tag{1}$$

Where C_0 and C_e are the initial and equilibrium heavy metal ion concentrations ($mg \cdot L^{-1}$), respectively; V is the volume of the solution (L); and m is the amount of adsorbent used (g). All the adsorption experiments were conducted in duplicate, and the mean values were adopted.

Scanning Electron Microscope (SEM)

SEM images were recorded to visualize the sample morphology. Pore structure and structural changes could be observed by SEM.

RESULTS AND DISCUSSION

A field emission scanning electron microscope was used to observe the surface morphology of AFWR (Figure 1). As can be seen, there are some fibrous structures and sheet structures, and those fibrous structures cover on or intersperse in the sheet structures. Since fiber bundles can form a larger number of macropores or micropores, the fibrous structures are relatively loose compared with the sheet structures, thus improving the adsorption performance of AFWR. Notably, the sheet structures also play an important role in the adsorption; namely, they can provide the support for the fiber structures.

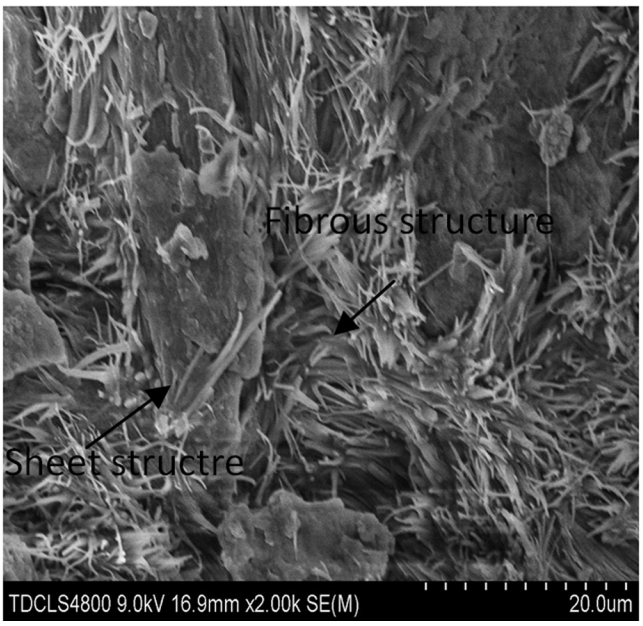

Figure 1. *SEM images of AFWR.*

Competitive Adsorption

In general, the competitive ability of heavy metals can be represented by competitive adsorption coefficients. For example, the coefficient of Cu^{2+} can be expressed as follows together with Pb^{2+}, Zn^{2+} and Cd^{2+} [20]:

$$a_{(Cu^{2+})} = \frac{q_e / C_{0(Cu^{2+})}}{q_e / C_{0(Cu^{2+})} + q_e / C_{0(Pb^{2+})} + q_e / C_{0(Zn^{2+})} + q_e / C_{0(Cd^{2+})}} \tag{2}$$

Where q_e is the adsorbed amount ($mg \cdot g^{-1}$) at equilibrium state, and C_0 is the initial concentration. According to the above expression, the bigger the competitive adsorption coefficient, the higher the competitive ability of heavy metals.

$$a_{(Cu^{2+})} + a_{(Pb^{2+})} + a_{(Zn^{2+})} + a_{(Cd^{2+})} = 1 \tag{3}$$

Table 1. The Competitive Adsorption Coefficients of Different Heavy Metal Ions.

Ion	Competitive Adsorption Coefficient			
	Pb^{2+}	Cu^{2+}	Zn^{2+}	Cd^{2+}
Cu^{2+}-Zn^{2+}		0.50	0.50	
Cu^{2+}-Pb^{2+}	0.49	0.51		
Cu^{2+}-Cd^{2+}		0.52		0.48
Pb^{2+}-Zn^{2+}	0.54		0.46	
Pb^{2+}-Cd^{2+}	0.53			0.47
Zn^{2+}-Cd^{2+}			0.50	0.50
Cu^{2+}-Pb^{2+}-Zn^{2+}	0.33	0.37	0.31	
Cu^{2+}-Pb^{2+}-Cd^{2+}	0.33	0.35		0.32
Cu^{2+}-Zn^{2+}-Cd^{2+}		0.34	0.33	0.33
Pb^{2+}-Zn^{2+}-Cd^{2+}	0.35		0.33	0.32
Cu^{2+}- Zn^{2+}-Cd^{2+}-Pb^{2+}	0.26	0.28	0.24	0.22

Table 1 showed that the competitive adsorption coefficients with an individual heavy metal are larger than those with multi-metals. For example, the coefficients with two metals are about 0.50, whereas those with four kinds of heavy metals are below 0.30. Although the adsorption of Cd^{2+} is the lowest in this study, its competitive adsorption coefficient still exceeds 0.23, indicating the feasibility of simultaneous adsorption of heavy metals from aqueous solutions by AFWR.

The competitive adsorption characteristics of Pb^{2+}, Cu^{2+}, Zn^{2+} and Cd^{2+} are studied. Table 2 shows the metal removal from multi-metal solution (10 and 20 $mg{\cdot}L^{-1}$) and individual heavy metal solutions (10 $mg{\cdot}L^{-1}$), respectively. As can be seen, the heavy metal adsorption performance in individual heavy metal solutions is better than that in multi-metal solution. For individual heavy metal solutions, Cu^{2+} and Cd^{2+} can be removed by AFWR more efficiently, of which the removal of Cu^{2+} is the highest in competitive adsorption. In contrast, the removal of Zn^{2+} is remarkably reduced since most active sites are occupied by other heavy metal ions. That is to say, the adsorption in competition beads with the following heavy metals presents an order of $Cu^{2+} > Pb^{2+} > Zn^{2+} > Cd^{2+}$. This result suggests that the presence of Cd^{2+} and Zn^{2+} has little impact on the adsorption of other heavy metal ions. It is noticed that although the adsorption of Cd^{2+} is the minimum in this study, its removal still exceeds 5.0 mg/L^{-1}, which further confirms the feasibility of simultaneous adsorption of heavy metals from aqueous solutions by AFWR.

Table 2. The Concentrations of Pb^{2+}, Cu^{2+}, Zn^{2+} and Cd^{2+} Ions Removed from Water.

	Multi-metal 10 $mg{\cdot}L^{-1}$	Multi-metal 20 $mg{\cdot}L^{-1}$	Individual Metal 10 $mg{\cdot}L^{-1}$
Cu^{2+}	6.12	5.81	6.26
Zn^{2+}	6.04	4.64	8.17
Pb^{2+}	6.53	4.44	7.37
Cd^{2+}	5.13	4.61	5.89

Adsorption kinetics

Adsorption kinetics of Pb^{2+}, Cu^{2+}, Zn^{2+} and Cd^{2+} are analyzed using the Elovich pseudo-first-order rate equation [21]:

$$a\log(q_e - q_t) = \log q_e - \frac{K_1}{2.303t} \tag{4}$$

Where q_e is the adsorbed amount ($mg{\cdot}g^{-1}$) at equilibrium state, q_t is the adsorbed amount ($mg.g^{-1}$) at time t and K_1 is the rate constant of pseudo-first-order adsorption (min^{-1}). q_e and K_1 can be calculated from the slope and intercept of the plot of log ($q_e - q_t$), respectively (Figure not shown here). In fact, the calculated equilibrium adsorption capacity, q_e (Cal.), should be in accordance with the experimental value q_e (exp.) [22]. However, in this study, although the correlation coefficient values (R^2) are high, the experimental q_e values do not agree with the calculated ones (Table 3).

The adsorption kinetics can also be described by pseudo-second-order equation [21]:

$$\frac{t}{q_t} = \frac{1}{K_2 q_e^2} + \frac{t}{q_e} \tag{5}$$

Where K_2 is the rate constant of pseudo-second-order adsorption ($g{\cdot}mg^{-1}{\cdot}min^{-1}$). K_2 and q_e can be calculated from the slope and intercept of the plot of t/q_t, respectively. It is found that the calculated q_e agrees well with the experimental q_e (Table 3). The large correlation coefficient of the pseudo-second-order model and the consistency between the calculated q_e and the experimental data both demonstrate that the adsorption of heavy metal ions (Pb^{2+}, Cu^{2+}, Zn^{2+} and Cd^{2+}) onto AFWR can be approximated by the pseudo-second-order model more favorably than by the pseudo-first-order model. This result suggests that the adsorption mechanism for heavy metal ions is the pseudo-second-order kinetic model based on the adsorption rather than the mass transfer from the solution to the adsorbent surface [22]. Hence, the rate-limiting step may be the chemical adsorption involving valance forces by sharing or exchanging electrons between heavy metal ions and the adsorbent.

Table 1. The Fitting Kinetics Parameters for Adsorption.

	Pseudo-first-order				Pseudo-second-order			
	$q_{e\ exp}$ mg·g^{-1})	R^2	$q_{e\ cal}$ (mg·g^{-1})	K_1 g·(mg·min)$^{-1}$	$q_{e\ exp}$ (mg·g^{-1})	R^2	$q_{e\ cal}$ (mg·g^{-1})	K_2 g·(mg·min)$^{-1}$
Cu^{2+}	5.10	0.816	4.61	0.046	5.13	0.999	5.03	0.045
Pb^{2+}	2.97	0.735	3.11	0.074	2.98	0.998	3.04	0.198
Zn^{2+}	3.01	0.789	3.18	0.081	3.12	0.999	3.19	0.076
Cd^{2+}	2.99	0.793	3.29	0.067	3.00	0.999	3.05	0.241

CONCLUSIONS

AFWR can be used as an effective adsorbent with a high removal percentage for the simultaneous adsorption of all heavy metals (Pb^{2+}, Cu^{2+}, Zn^{2+} and Cd^{2+}) from aqueous solutions, and the adsorption kinetics follow the pseudo-second-order equation. The competitive adsorption results show that the presence of competitive ions can reduce the removal percentage of each heavy metal ion. During competitive adsorption, the adsorption beads with the heavy metals presents an order of $Cu^{2+} > Pb^{2+} > Zn^{2+} > Cd^{2+}$.

ACKNOWLEDGEMENTS

The authors are grateful for the financial support from the Tianjin City Application Basis and Advanced project, and the Young and Middle-aged Talents Plan provided by Tianjin of China.

REFERENCES

1. Patricia, M., Andrea, S., Alicia, F. C., "Simultaneous heavy metal removal mechanism by dead macrophytes", *Chemosphere*, Vol. 62, 2006, pp. 247–254. http://dx.doi.org/10.1016/j.chemosphere.2005.05.010
2. Ng, J., Cheung, W., McKay, G., "Equilibrium studies for the sorption of lead from effluents using chitosan", Chemosphere, Vol. 52, 2003, pp. 1021–1030. http://dx.doi.org/10.1016/S0045-6535(03)00223-6
3. Barakt, M. A., "New trends in removing heavy metals from industrial wastewater", *Arabian Journal of Chemistry*, Vol. 43, 2011, pp. 61–77.
4. Baccar, R., Blanquez, P., Bouzid, J., *et al.*, "Equilibrium, thermodynamic and kinetic studies on adsorption of commercial dye by activated carbon derived from olive-waste cakes", *Chemical Engineering Journal*, Vol. 165, 2010, pp. 457–464.http://dx.doi.org/10.1016/j.cej.2010.09.033
5. Juliana, Q. Albarelli, Rodringo, B., Rabelo, Diego, T., Stantos, *et al.*, "Effects of supercritical carbon dioxide on waste banana peels for heavy metal removal", *The Journal of Supercritical Fluids*, Vol. 58, 2011, pp. 343–351. http://dx.doi.org/10.1016/j.supflu.2011.07.014
6. Wang, X. J., Xu, X. M., Liang, X., *et al.*, "Adsorption of copper(II) onto sewage sludge–derived materials via microwave irradiation", *J. Hazar. Mater.* Vol. 192, 2011, pp. 1126–1133. http://dx.doi.org/10.1016/j.jhazmat.2011.06.030
7. Kazi, T. G., Jamali M. K., Siddiqui, A., *et al.*, "An ultrasonic assisted extraction method to release heavy metals from untreated sewage sludge samples", *Chemosphere*, Vol. 63, No. 3, 2006, pp. 411–420. http://dx.doi.org/10.1016/j.chemosphere.2005.08.056
8. Zhou, S. Q., Lu, W. D., Zhou, X., "Effects of heavy metals on plant-ing watercress in kailyard soil amended by adding compost of sewage sludge", *Process Safety and Environmental Protection*, Vol. 8, No. 4, 2010, pp. 263–268. http://dx.doi.org/10.1016/j.psep.2010.03.005
9. Hydari, S. H., Sharififard, H., Nabavinia, M., *et al.*, "A comparative investigation on removal performance of commercial activated carbon chitosan biosorbent and chitosan/activated carbon composite for cadmium", *Chemical Engineering Journal*, Vol. 193–194, No. 6, 2012, pp. 276–282. http://dx.doi.org/10.1016/j.cej.2012.04.057
10. Kargi, F., Ozmihc, I. S., "Comparison of adsorption performances of powdered activated sludge and powdered activated carbon for removal of turquoise blue dyestuff", *Process Biochemistry*, Vol. 40, 2005, pp. 2539–2544. http://dx.doi.org/10.1016/j.procbio.2004.11.003
11. Fan, X. D., Zhang, X. K., "Adsorption properties of activated carbon from sewage sludge to alkaline-black", Materials letter, Vol. 62, 2008, pp. 1704–1706. http://dx.doi.org/10.1016/j.matlet.2007.09.085
12. Li, Z. T., Lu, H. W., Ren, L. X., *et al.* "Experimental and modeling approaches for food waste composting: A review", *Chemosphere*, Vol. 93, 2013, pp.1247-1257. http://dx.doi.org/10.1016/j.chemosphere.2013.06.064
13. Jiang, J. G., Zhang, Y. J., Li, K. M., *et al.*, "Volatile fatty acids production from food waste: Effects of pH, temperature, and organic loading rate", *Bioresour. Technol.*, Vol. 143, 2013, pp. 525–530. http://dx.doi.org/10.1016/j.biortech.2013.06.025
14. Dai, X. H., Duan, N., Dong, B., *et al.*, "High-solid anaerobic co-digestion of sewage sludge and food waste in comparison with mono digestions: Stability and performance", Waste Management, Vol. 33, 2013, pp. 308–316. http://dx.doi.org/10.1016/j.wasman.2012.10.018
15. Tampio, E., Ervasti, S., Paavola, T., *et al.*, "Anaerobic digestion of autoclaved and untreated food waste", *Waste Management*, Vol. 34, 2014, pp. 370–377. http://dx.doi.org/10.1016/j.wasman.2013.10.024
16. Chen, X., Yan, W., Sheng K. C., *et al.*, "Comparison of high-solids to liquid co-digestion of food waste and green waste". *Bioresour. Technol.*, Vol. 154, 2014, pp. 215–221. http://dx.doi.org/10.1016/j.biortech.2013.12.054
17. Liu, X. Y., Li, R. Y., Ji, M., *et al.*, "Hydrogen and methane production by co-digestion of waste activated sludge and food waste in the two-stage fermentation process: Substrate conversion and energy yield", *Bioresour. Technol.*, Vol. 146, 2013, pp. 317–323. http://dx.doi.org/10.1016/j.biortech.2013.07.096
18. Boni, M. R., Sbaffoni, S., Tuccinardi, L., "The influence of slaughterhouse waste on fermentative H_2 production from food waste: Preliminary results", Waste Management, Vol. 33, 2013, pp. 1362–1371. http://dx.doi.org/10.1016/j.wasman.2013.02.024
19. Quested, T. E., Marsh, E., Stunell, D., *et al.*, "Spaghetti soup: The complex world of food waste behaviours", Resource Conservation and Recycling, Vol. 79, 2013, pp. 43–51. http://dx.doi.org/10.1016/j.resconrec.2013.04.011
20. Wu, F. C., Tseng, R. L., Juand, R. S., "Kinetic modeling of liquid-phase adsorption of reactive dyes and metal ions on chitosan", *Water Res.*, Vol. 35, 2001, pp. 613–618. http://dx.doi.org/10.1016/S0043-1354(00)00307-9
21. Ho, Y. S., McKay, G., "The kinetics of sorption of divalent metal ions onto sphagnum moss peat", *Water Res.*, Vol. 34, 2000, pp. 735–742. http://dx.doi.org/10.1016/S0043-1354(99)00232-8
22. Mckay, G., Ho, Y. S., "Pseudo-second-order model for sorption processes", *Process Biochem.*, Vol. 34, 1999, pp. 451–465. http://dx.doi.org/10.1016/S0032-9592(98)00112-5

Uranium Mobility in Waste Materials Generated by Uranium Mining and Hydrometallurgy: Implications for its In-Situ Immobilization

Z. G. FENG[1,*], B. ZHANG[1,2], X. Z. DUAN[1], R. CHEN[1,2], X. L. WANG[1,2], Q. MA[1] and S. L. HAN[1]

[1]*School of Nuclear Resource Engineering, University of South China, Hengyang 421001, China*

[2]*Key Discipline Laboratory for National Defense for Biotechnology in Uranium and Hydrometallurgy, University of South China, Hengyang 421001, China*

ABSTRACT: Six uranium tailings samples from the shallow depth of two large-scale uranium tailings ponds in South China, which were affected by pedogenesis, were analyzed to determine the occurrence modes of uranium. The results demonstrated that an average of nearly 80% of the uranium in the samples was mobile and potentially mobile, indicating that this type of uranium tailings could significantly threaten their ambient environment when their contents of uranium were relatively high. In this sense, the possibility of the in-situ immobilization of active uranium in the uranium tailings was discussed. The experimental data indicated that the active uranium could be immobilized through its reaction with phosphate, which was theoretically feasible and promising in curbing uranium pollution.

INTRODUCTION

URANIUM tailings and waste rocks are solid waste materials generated by uranium mining and hydrometallurgy, except in-situ leaching uranium. Being generally open-air stacked, they cause potential radioactive risk to their ambient environment [1–2], which is often pronounced for tailings that are remnants of uranium ores after being crushed, milled and leached out by acidic solution, and contain a fine texture and residual acid. This feature can facilitate the decomposition of residual uranium-bearing components in the tailings, thereby resulting in the mobilization of uranium in aerated environment. In China, uranium tailings are mainly produced from hydrothermal-type uranium mines in the southern provinces [3]. Despite the percolation-proof treatment for most tailings ponds, the absolute environmental security cannot be ensured. For example, the surrounding soils could become polluted by mobile uranium leached from the tailings ponds by surface runoff originated from rainfall [4–5].

Due to the current passive percolation-proof precaution against the environmental uranium pollution produced by uranium migration, and the substantial consumption of material and financial resources caused by the traditional remediation technologies of uranium-contaminated soils [2], it is essential to seek an economical and effective method to curb uranium pollution. Some researchers [6–7] have found that phosphate can in-situ immobilize soluble uranium in supergene geo-media. In this regard, we propose a concept that active uranium could be immobilized in-situ by chemical process (e.g., phosphate added to the tailings). Such an additive would need to be stable over long durations under local environmental conditions, thereby prohibiting the activation of uranium. The main prerequisite for conducting a study on uranium immobilization is to clarify the occurrence modes of uranium in the pollution sources, which determine the adopted uranium immobilization techniques. However, such characterization of the uranium occurrence mode in the tailings is still lacking.

In this study the uranium occurrence modes by sequential chemical extraction procedures were determined for six samples from the shallow depth of two large-scale uranium tailings ponds in South China, and the mobility and release potentials of the uranium were quantitatively estimated. On this basis, the possibility of the in-situ immobilization of active uranium was preliminarily discussed. This study provided a scientific reference for studies on curbing uranium pollution that should be considered in the future work.

*Author to whom correspondence should be addressed.
E-mail: feng_zg@sina.com

1544-8053/15/01 S159-05

doi:10.12783/issn.1544-8053/12/S1/23

SAMPLING AND EXPERIMENTAL METHODOLOGY

Sampling

The samples were collected from two large-scale uranium tailings ponds (labeled as A and B ponds in this study) in South China, which store waste materials after acidic heap leaching and agitated tank leaching of granite-type uranium ores. This work only referred to the shallow part of the uranium tailings piles affected by pedogenesis. The tailings located in the depths and those not influenced by pedogenesis will be discussed in another paper. The tailings, from which the samples were collected, were located at a sub-surface horizon with a depth of 10 cm from the surface of a beach face where weeds have grown, and the distance between the sampling spots was more than 10 m. Six samples were selected, which were labeled as a1, a2 and a3 from pond A, and b1, b2 and b3 from pond B, respectively.

Experiments

Based on the previous occurrence mode analysis schemes of the radionuclides in soils and sediments [8–10], an improved sequential chemical extraction procedure was adopted in this study (Table 1). Samples were analyzed for pH, which ranged from 3.84 to 4.92. In the uranium immobilization experiments, the active uranium extracted from the sample b3 was used as the test solution (following the Fraction II method shown in Table 1), and then reacted with the ammonium phosphate and calcium chloride at room temperature under pH conditions of 3.5, 4.0, 4.5 and 5.0, respectively. Then the immobilization rates of the active uranium were calculated through measuring the contents of residual uranium in test solution.

The concentrations of uranium in bulk samples were analyzed using ELAN DRC-e quadrupole inductively coupled plasma mass spectrometer (Q-ICP-MS) (PerkinElmer Ltd., Canada) at the Institute of Geochemistry, Chinese Academy of Sciences. The analytical accuracy controlled by two soil standards (GSS-4 and GSS-6) showed that the relative deviation of uranium was below 10%. Uranium in solutions by sequential chemical extraction was measured using a WGJ-III type trace uranium analyzer (Hangzhou Daji Photoelectric Instrument Ltd., China), with detection limit of 0.02 ppb, and relative deviation < 5% controlled by uranium standard solution. All the reagents used in this study were analytical grade.

RESULTS AND DISCUSSION

Chemical Forms of Uranium

The occurrence modes of uranium were shown in

Table 1. The Sequential Chemical Extraction Procedure of Uranium.

Fraction	Phase	Extraction Method
I	Exchangeable (including water-soluble)	2 g of sample was extracted with 20 mL of 1 M magnesium chloride solution (pH = 7.0). After 2 h of shaking at room temperature, it was centrifuged for 10 min at 8000 rpm. The supernate was reserved for analysis.
II	Associated with carbonates	To the residue of Fraction I, 50 mL of 1 M sodium acetate was added, and the pH was adjusted to 5.0 with acetic acid. After 7 h of shaking at room temperature, it was centrifuged for 10 min at 8000 rpm. The supernate was reserved for analysis.
III	Co-precipitated with amorphous ferromanganese oxyhydroxides	The residue from Fraction II was extracted with 20 mL Tamm's solution (10.9 g/L oxalic acid + 16.1 g/L ammonium oxalate, pH = 3.0). After 5 h of shaking at room temperature, it was centrifuged for 10 min at 8000 rpm. The supernate was reserved for analysis.
IV	Associated with crystalline ferromanganese oxyhydroxides	To the residue of Fraction III, 20 mL of CDB solution (sodium dithionite–trisodium citrate–sodium bicarbonate, pH = 7.0) was added. After 5 h of shaking at room temperature, it was centrifuged for 10 min at 8000 rpm. The supernate was reserved for analysis.
V	Organic matter-bound	To the residue of Fraction IV, 20 mL of 30% H_2O_2 was added. After 1 h of digestion at room temperature, it was transferred into a water bath to continue digestion for 1 h at 85 °C and allowed to evaporate down to near dryness. This step was repeated. Then 50 mL of 1 M ammonium acetate was added and adjusted to pH = 2.0 by nitric acid. After 2 h of shaking at room temperature, it was centrifuged for 10 min at 8000 rpm. The supernate was reserved for analysis.
VI	Associated with residue phases	The residue from Fraction V was totally dissolved with 15 mL aqua regia and 8 mL HF using microwave digestion after preheating. The sample solution was diluted to 50 mL with ultra pure water and reserved for analysis.

Table 2. The deviations between total uranium concentrations of various chemical forms and bulk sample were less than 10%, indicating the results were reliable. The concentrations of uranium were 13.2~91.3 ppm in the samples a1~a3 and b1~b2, and with a maximum of 1800 ppm in the sample b3, which was much higher than that of the typical crustal granitoids (3.5 ppm) [11] and the background value of Chinese soil (3.03 ppm) [12]. Therefore, the risk of uranium tailings as a major source of uranium pollution was not exaggerated.

The uranium of various occurrence modes in each sample demonstrated similar distribution features (Figure 1). As a whole, uranium preferentially occurred in carbonate (Fraction II) and organic matter-bound phases (Fraction V), and in the residual phase (Fraction VI), while its concentrations in amorphous ferromanganese oxyhydroxide (Fraction IV) and exchangeable phases (Fraction I) were relatively lower, and even cannot be detected in the Fraction I of a2 and the Fraction IV of a3. As there are no organic substances in the tailings produced during the hydrometallurgy of granite-type uranium ores, the preferential occurrence in the Fraction V (*Note:* the organic matter contents of the six samples ranged from 0.55% to 1.95%, shown in our unpublished data) must be the result of pedogenetic transformation. The occurrence modes of uranium might be different in uranium tailings that were not affected by pedogenesis. These results demonstrated that uranium in tailings might have experienced redistribution.

Mobility and Release Potential of Uranium

Previous works [9–10,13], which have conducted substantial ecological availability evaluation for radionuclides in supergene solid media, generally considered the following points: (1) Fractions I and II have relatively strong mobility, and therefore belong to the part that is easily released into the environment, whereas Fractions III and V commonly exhibit certain degree of mobility during the change of redox condition of the media, and thus are the part that is potentially released into the environment; (2) Fractions IV and VI are inert as their minerals are stable in structures and cannot be decomposed on short time scales. The percentages of uranium in Fractions I+II and Fractions III+V of the six samples were 27%~59% (with the average value of 42%), and 33%~46% (with 38% on average), respectively. In addition, the percentages of uranium in Fractions I+II+III+V were 62%–96%, with 79% on average. In this sense, over 40% of uranium was active, about 38% was potentially active, and the sum of these two types of uranium was close to 80% (Figure 2). Therefore, the tailings would produce a significant threat to the ecological environment when they contain high contents of residual uranium.

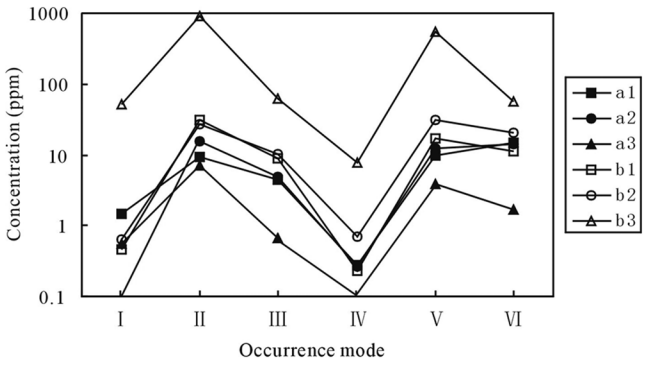

Figure 1. *Distribution patterns of various uranium chemical forms in the six samples. Note: a1~a3 and b1~b3 stand for sample No., shown in Table 2.*

Implications for in-situ Immobilization of Mobile Uranium

Uranium in nature usually occurs as U^{4+} oxidation state (insoluble) under reducing conditions, but in the U^{6+} oxidation state (soluble) under oxidizing conditions [14]. As uranium mainly exists as U^{6+} oxidation state in the supergene environment, the effective immobilization of active uranium would be achieved through the precipitation of U^{6+} by a chemical reaction that can maintain long-term stability under the local environmental conditions. As free uranyl ion (UO_2^{2+}) is the main occurrence mode of soluble U^{6+} in aqueous media of pH < 5 [15], it may be the dominant form of active uranium in the above six samples.

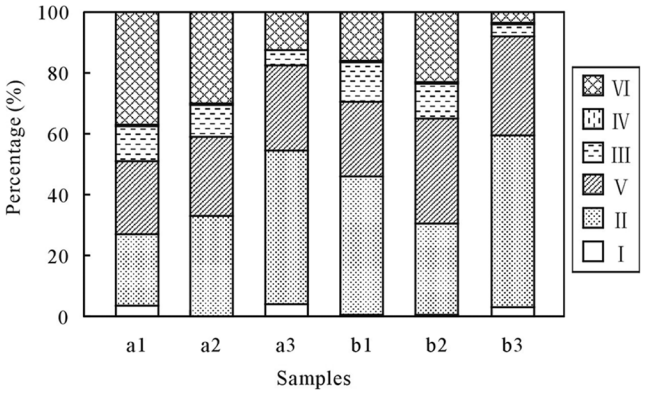

Figure 2. *Different occurrence mode percentages of the total uranium in the six samples. I, exchangeable; II, associated with carbonates; III, co-precipitated with amorphous ferromanganese oxyhydroxides; IV, associated with crystalline ferromanganese oxyhydroxides; V, organic matter-bound; VI, associated with residue phases.*

Table 2. Concentrations of Uranium in Various Chemical Forms in the Uranium Tailings Samples and Their Deviations to the Analytical Results of Bulk Samples.

	Concentration/ppm								
Sample No.	**I**	**II**	**III**	**IV**	**V**	**VI**	**Sum of I to VI**	**Bulk Sample**	**Deviation*, %**
a1	1.49	9.4	4.49	0.28	9.55	14.82	40.03	36.4	9.97
a2	0	15.59	4.79	0.26	12.55	14.31	47.5	45.2	5.09
a3	0.55	6.96	0.68	0	3.9	1.72	13.81	13.2	4.62
b1	0.46	31.04	8.79	0.23	17.13	11.12	68.77	68.7	0.1
b2	0.63	26.62	10.09	0.69	31.18	20.41	89.62	91.3	–1.84
b3	52.85	914.85	62.57	7.78	537.19	57.23	1632.47	1800	–9.31

Note: *Deviation = [(Sum of I to VI)-(bulk sample)] / (bulk sample)*100%

The experimental results of uranium immobilization showed that the immobilization rates of soluble uranium were 86.5%, 93.6%, 96.0% and 99.3% under pH conditions of 3.5, 4.0, 4.5 and 5.0, respectively, and increased along with the solution pH. In this reaction, the uranium immobilization was actually generated by the precipitation of a calcium uranyl phosphate compound. This indicated that the in-situ immobilization of active uranium using phosphate under an appropriate pH condition was theoretically feasible. However, there are numerous factors that affect uranium mobility in solid media including temperature, medium texture, organic/inorganic complexes, humidity and microbial activities besides the redox potential and pH [2], and further studies are still needed on the process of in-situ immobilization. Therefore, although several challenges in-situ immobilization remain unsolved, the concept of using this method to curb uranium pollution is promising.

CONCLUSIONS

1. Generally, uranium preferentially occurs in carbonate and organic matter-bound phases, regardless of the uranium contents of the tailings, whereas the proportions of uranium in exchangeable (including water-soluble) and amorphous ferromanganese oxyhydroxide phases are much lower.
2. In the samples studied, the proportions of active and potentially active uranium are close to 80%. Therefore, uranium tailings would produce a significant threat to the ecological environment when they contain high contents of residual uranium.
3. The immobilization of active uranium in the uranium tailings using phosphate is theoretically feasible, and the concept of in-situ uranium immobilization to curb uranium pollutions is thus promising.

ACKNOWLEDGEMENTS

This work was supported by the National Natural Science Foundation of China (NSFC, Grant no. 41373115, 40973070), and Zhengxiang Scholar Program of the University of South China.

REFERENCES

1. Carvalho, I. G., Cidu, R., Fanfani, L., *et al.*, "Environmental impact of uranium mining and ore processing in the Lagoa Real District, Bahia, Brazil", *Environ. Sci. Technol.*, 2005, 39, 8646–8652. http://dx.doi.org/10.1021/es0505494
2. Gavrilescu, M., Pavel, L. V., and Cretescu, I., "Characterization and remediation of soils contaminated with uranium", *J Hazard Mater*, 2009, 163, 475–510. http://dx.doi.org/10.1016/j.jhazmat.2008.07.103
3. Suo, M. X., Liu, F., Wang X. G., *et al.*, "Study on microbial distribution rule and nuclide curing of uranium waste dumps", *Resource Development & Market*, 2013, 29(7), 679–682.
4. Wang, L. C., Luo, X. G., Peng, F. F., *et al.*, "Changes of microbial activity and functional diversity of contaminated soil microbes community in uranium tailings", *Environmental Science & Technology*, 2014, 37(3), 25–31.
5. Du, Y., Zhu, X. J., Gao, B., *et al.*, "Distribution characteristics of uranium in typical sites of tailings pond in uranium mine", *Nonferrous Metals (Mine Section)*, 2014, 66(1), 5–9.
6. Salome, K. R., Green, S. J., Beazley, M. J., *et al.*, "The role of anaerobic respiration in the immobilization of uranium through biomineralization of phosphate minerals", *Geochim Cosmochim Ac*, 2013, 106, 344–363. http://dx.doi.org/10.1016/j.gca.2012.12.037
7. Jerden, J. J. L., Sinha, A. K., and Zelazny, L., "Natural immobilization of uranium by phosphate mineralization in an oxidizing saprolite–soil profile: chemical weathering of the Coles Hill uranium deposit, Virginia", *Chem Geol*, 2003, 199, 129–157. http://dx.doi.org/10.1016/S0009-2541(03)00080-9
8. Crespo, M. T., Villar, L. P. D., Jiménez, A., *et al.*, "Uranium isotopic distribution in the mineral phases of granitic fracture fillings by a sequential extraction procedure", *Appl Radiat Isotopes*, 1996, 47, 927–931. http://dx.doi.org/10.1016/S0969-8043(96)00089-9
9. Guo, P., Duan, T., Song, X., *et al.*, "Evaluation of a sequential extraction for the speciation of thorium in soils from Baotou area, Inner Mongolia", *Talanta,* 2007, 71, 778–783. http://dx.doi.org/10.1016/j.talanta.2006.05.038
10. Martínez-Aguirre, A., Garcia-León, M., and Ivanovich, M., "U and Th speciation in river sediments", *Sci Total Environ*, 1995, 173/174, 203–209. http://dx.doi.org/10.1016/0048-9697(95)04759-X

11. Mou, B. L., "Elemental geochemistry", 1st edn, 122–128; 1999, Peking University Press, Beijing.
12. Environmental Monitoring Head Station of China, "Elemental background values of Chinese soils", 1st edn, 89; 1990, Chinese Environmental Science Press, Beijing.
13. Song, Z. L., Zhu, Z. Z., and Yang, C., "Speciation of elements (e.g., uranium) and mobility of uranium in calcareous soils from Wujiang river catchments", *Resources and Environment in the Yangtze Basin*, 2009, 18(5), 471–476.
14. Langmuir, D., "Uranium solution-mineral equilibria at low temperature with applications to sedimentary ore-deposits", *Geochim Cosmochim Ac*, 1978, 42, 547–569. http://dx.doi.org/10.1016/0016-7037(78)90001-7
15. Langmuir, D., "Aqueous environmental geochemistry", 1st edn, 109–122; 1997, Prentice Hall, Upper Saddle River, New Jersey.

Grafting Diethylene Triamine onto Bagasse with Ammonium Ceric Nitrate as an Initiator

HONGXIANG ZHU[1], QIAOPING KONG[1], XUEJUAN CAO[1], NANNAN XIA[2] and JIN WANG[3,*]
[1]*College of Light Industry and Food Engineering, Guangxi University, Nanning, 530004, China*
[2]*PCFM Lab, School of Chemistry and Chemical Engineering, Sun Yat-Sen University, Guangzhou 510275, China*
[3]*College of Agriculture and Biology, Shanghai Jiao Tong University, Shanghai, 200240, China*

ABSTRACT: Bagasse cellulose was grafted with diethylenetriamine to prepare a copolymer. Ammonium ceric nitrate was chosen as the initiator. Considering the optimum zeta potential, conditions including initiator concentration, the mass ratio of monomer to cellulose, preparation temperature and time are discussed. In addition, the graft copolymers were characterized by scanning electron microscopy (SEM), Fourier transform infrared spectra (FT-IR), and X-ray diffraction analysis (XRD). The grafting bagasse cellulose has the advantage of being biodegradable and has low cost of raw materials. Its absorbent properties are an attractive alternative for wastewater treatment and avoids environmental pollution.

INTRODUCTION

As a cheap and abundant resource, cellulose is a renewable and biodegradable natural polymer [1]. In recent years, oil resources have been decreasing while the price of oil and its products are rising. The interest in the production of polymer materials from cellulose, a highly important polymer, is growing steadily [2].

Cellulose is a polysaccharide polymer, and there are three reactive hydroxyl groups at the C-2, C-3 and C-6 atoms of the anhydroglucose unit (AGU), which grants cellulose with the possibility to carry out various chemical reactions [1], such as esterification [3], etherification [4], oxidation [5], and polymer grafting [6,7]. With these methods, the grafted polymer not only retains the cellulose's valuable features, such as low electrifiability, high hydrophilicity, and considerable thermal stability, and also possessing new properties. From this standpoint, cellulose modification via grafting is exceptionally promising [8]. Recently, grafting has become a popular method of modifying cellulose to adsorption materials, such as moisture adsorption, heavy metal ion adsorption, organic solvent adsorption, and poison gas adsorption materials [9].

The parameter Zeta potential was adopted here to illustrate the electric potential in the solid/liquid interfacial layer of a material, and it is also a crucial and helpful feedback of surface charges [10]. Because of the existing carboxyl and hydroxyl groups in cellulose, the original cellulose had a negative potential of –17.5 ± 0.8 mV [11]. The amino group bears a positive charge, and the zeta potential would be reversed by grafting diethylenetriamine onto celluloses. The zeta potential is related to the content of nitrogen in cellulose. Determination of the zeta potential is a good way to value chemical reactions at surface through surface charge changes [12]. However, there is little information about the zeta potential value as a factor for cellulose modification. The main objective of this paper is to graft diethylenetriamine onto bagasse celluloses directly to get the surface-modified celluloses. Grafting's effect on modified celluloses is determined by the zeta potential. The chemical structure of the grafted cellulose was characterized by FT-IR and XRD. The surface morphology of the grafted cellulose was studied by SEM. The results showed that bagasse celluloses could be grafted with diethylenetriamine in aqueous medium.

MATERIALS AND METHODS

Materials

Natural cellulose (bleached bagasse pulp), is a commercial product, that was supplied by Nanning Sugar Industry, P.R. China. The other chemicals in the experiments were diethylenetriamine (reagent grade, Cheng-

*Author to whom correspondence should be addressed.
E-mail: wangjin100@sjtu.edu.cn

1544-8053/15/01 S165-06

doi:10.12783/issn.1544-8053/12/S1/24

du Kelon, P.R. China), ammonium ceric nitrate, absolute ethyl alcohol (reagent grade, Shanghai Miura, P.R. China), and acetone (reagent grade, Chengdu Kelon, P.R. China).

Instruments

The zeta potentials of the grafted cellulose were determined using a Zetasizer Nano with a Malvern PSS0012-17 Instrument. The natural cellulose and grafted cellulose were analyzed via scanning electron microscopy (SEM) with a Hitachi S-3400N Instrument, Fourier transform infrared spectroscopy (FT-IR) with a Pekin Elmer Spectrum BX Instrument, and X-ray diffraction (XRD) with a Rioch 4153B172 Instrument.

Graft Copolymerization

To obtain the product necessary to the experiment, we take 10g of the bleached bagasse pulp board which was pretreated as the following: first defibered with a fluffer for 5 min, washed thoroughly with distilled water and absolute ethyl alcohol to remove impurities, and then dried. 2 g of pretreated bagasse cellulose and 100 mL distilled water were added into a three-necked round bottom flask. With an electrical stirrer, the flask was continuously purged with gaseous N_2 in a water bath at stable set temperature. After defibering for 20 minutes, a certain amount of initiator with the concentration of 40mmol/L was added to the flask and initiated cellulose surface to produce free radicals within a given period. The initiator is known to give rise to a significant amount of free radicals at the cellulose surface. The graft copolymerization was initiated when 2 g of diethylenetriamine was added. The reaction last for 2.5 h at 60°C.

Finally, when the grafting reaction was terminated, the reaction mixture was dried under vacuum at 50°C for 12 h after it was cooled to room temperature. In order to remove the diethylenetriamine homopolymer, the dried product was extracted with acetone in a soxhlet apparatus for 24 h, and the extracted product was dried and weighed.

Zeta Potential Measurement

Zeta Potential charges on the surface of grafted cellulose in pure water were measured with a Malvern PSS0012-17 Zetasizer. The modified celluloses were dispersed in water to form 3% consistency cellulose suspension, and the grafted cellulose suspensions were analyzed to determine the zeta potential [13].

RESULTS AND DISCUSSION

The Structure of Cellulose: Changes Before and After Modification

A mechanism to explain graft copolymerization of diethylenetriamine onto bagasse celluloses with ammonium ceric nitrate as an initiator in an aqueous medium is shown in Scheme 1:

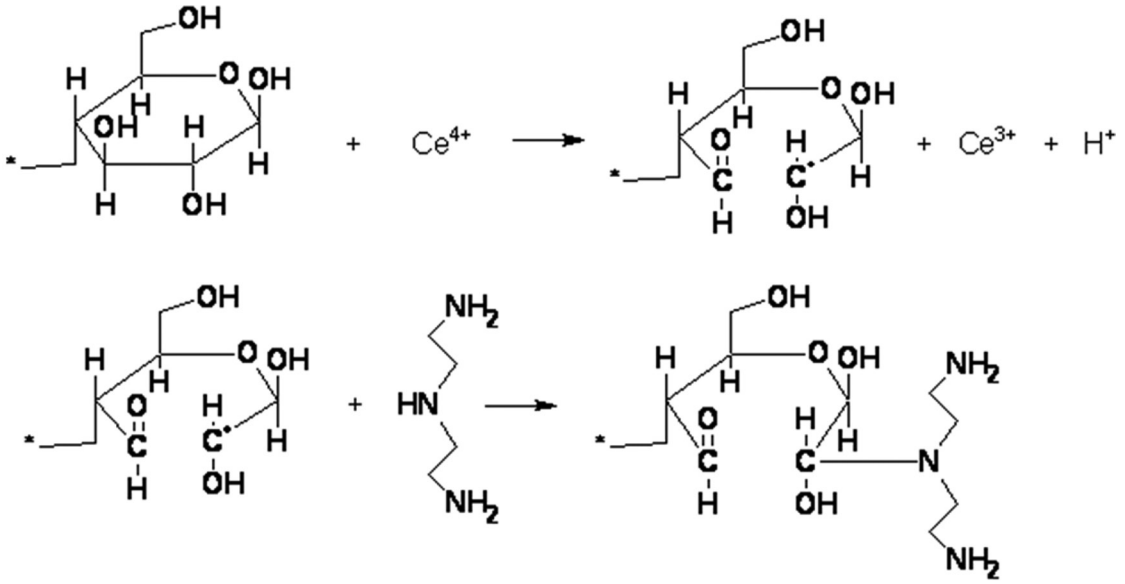

Scheme 1. *The mechanism of graft polymerization of diethylenetriamine on bagasse celluloses by ceric (IV) ion is shown. Ceric (IV) ion initiates ring opening of C_2 and C_3 hydroxyl groups of anhydro-D-glucose of cellulose, resulting in free radicals that promote the grafting of diethylenetriamine monomer on cellulose support.*

As a redox initiator for grafting of a variety of vinyl monomers onto biopolymers, ceric ammonium nitrate (CAN) has been used extensively [14]. The main mechanism is that a Ce(IV) ion initially forms a Ce(IV)–cellulose complex. As shown in Scheme 1 [15], the complex is reduced to a Ce(III) ion with the formation of a free radical at either C_2 or C_3 on the cellulose backbone. The free radical then reacts with the diethylenetriamine monomer, which is used to initiate graft copolymerization [16].

Effect of Initiator Concentration

With other parameters unchanged, different initiator concentrations were adopted as in Figure 1. As can be seen, the zeta potential increased with the concentration of initiator from 10 to 40 mmol/L, but decreased at 40 mmol/L and higher. While the initiator concentration was in the range of 10 to 30 mmol/L, the zeta potential rose from –15 to –7 mV, below zero, which indicated that more sites were activated by ceric ions and the diethylenetriamine was grafted onto the cellulose. Though the amino groups would make the zeta potential rise, a large amount of hydroxyl groups was dominant. When the initiator concentrations was between 40 to 50 mmol/L, the zeta potential reached a high point above zero. It was implied that more amino groups were grafted onto the cellulose. However, with the increasing initiator concentration, the zeta potential of modified cellulose did not increase; conversely, it decreased below zero. This may be due to the active sites on the cellulose being cross-linked or reacted with other groups at the initiating stage [17].

Effect of the Mass Ratio of Monomer: Cellulose

With other parameters unchanged, different mass ratio of monomer to cellulose were adopted as Figure 2. The zeta potential increases with the mass ratio of monomer: cellulose from 0.5:1 to 1:1, but decreases at 1:1 and higher. While the mass ratio of monomer:cellulose was in the range of 0.5:1 to 1:1, the zeta potential rose from –10.7 to –9.9 mV. This behavior would be attributed to accumulation of monomer molecules in close proximity to the cellulose backbones. However, upon further increasing the mass ratio of monomer:cellulose from 1:1 to 3:1, the grafted cellulose zeta potential decreased. This could be due to viscosity increase of the medium hindering the movement of free radicals [18]. Therefore, the grafted cellulosic zeta potential reduced with the decline in efficiency of the cellulosic grafting reaction. The optimal ratio of the monomer to cellulose was 1:1.

Effect of Reaction Temperature

With other parameters unchanged, different reaction temperatures were adopted as in Figure 3. The zeta potential increases with the reaction temperature from 40°C to 70°C, but decreases at 70°C and higher. While the temperature was in the range of 40°C to 70°C, the zeta potential rose from –17.5 to –8.5 mV, which indicated that although diethylenetriamine was grafted onto the cellulose, a large amount of hydroxyl groups was dominant. The increase of zeta potential up to 70°C would be attributed to the formation of active sites on cellulose, which was improved by the generation of more free radicals with rising tempera-

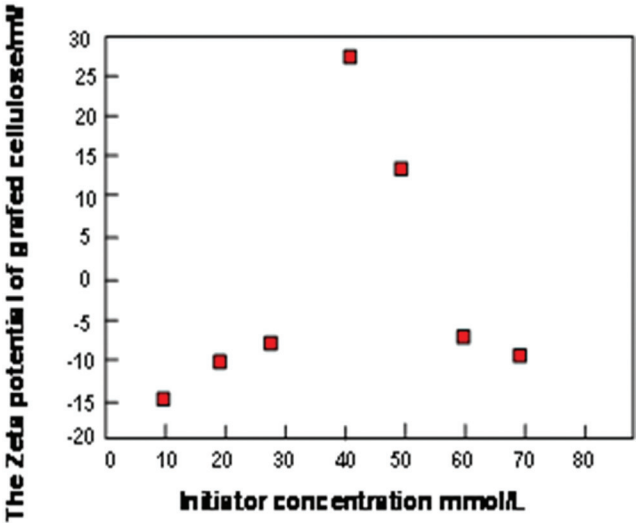

Figure 1. *Effect of initiator concentration.*

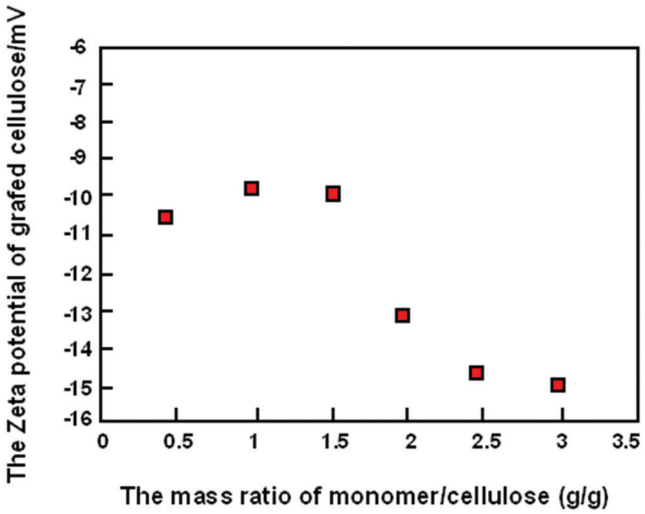

Figure 2. *Effect of the mass ratio of monomer/cellulose (g/g).*

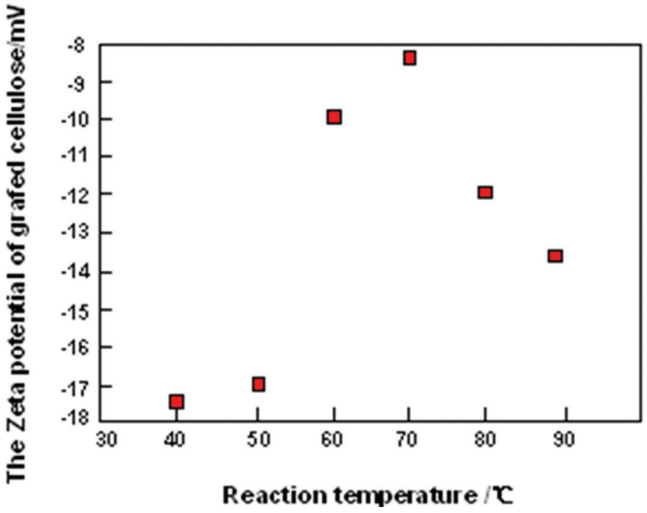

Figure 3. *Effect of reaction temperature.*

tures. However, with the temperature increase from 70 to 90°C, the free radicals reacted and led to an increase of homopolymerization, which may decrease the efficiency of grafting. So, the optimum temperature for the grafting reaction was 70°C.

Effect of Reaction Time

With other parameters unchanged, different reaction time were adopted as Figure 4, the zeta potential increases with the reaction time from 1 to 3 h, but decreases at 3 h and higher. Initially, from 1 h to 2 h, there were relatively few free radicals produced at the cellulose surface, so there was relatively little grafting of amino groups. The zeta potential was below –15 mV, which was mainly caused by hydroxyl and carboxyl groups on the surface of the cellulose. At 3 h, the zeta

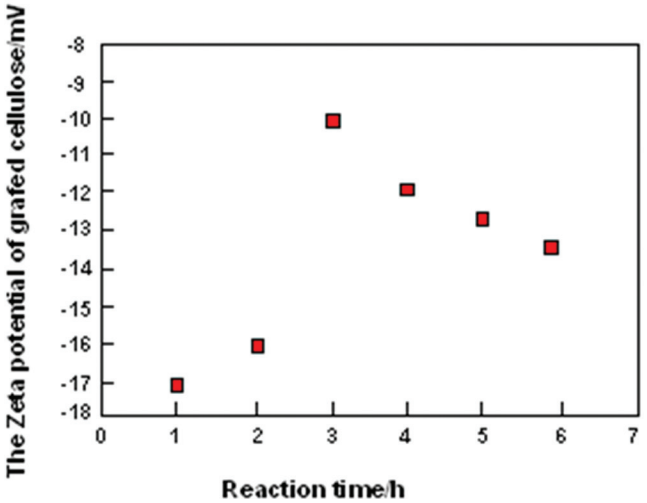

Figure 4. *Effect of reaction time.*

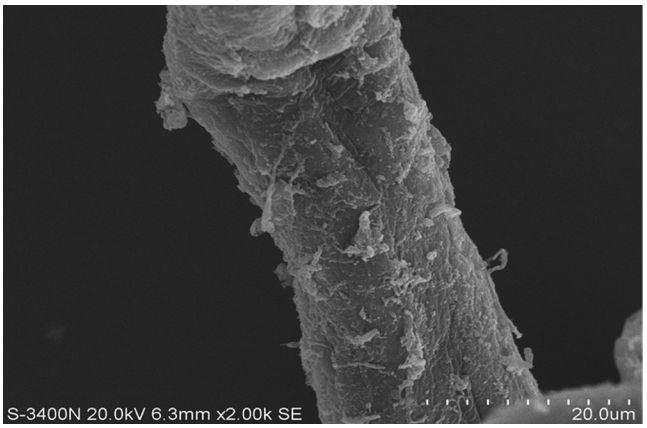

Figure 5. *SEM photographs of natural cellulose.*

potential reached a top point of –10 mV. This would be attributed to propagation of grafting chains that took the place caused by availability of more active species. On further increasing the reaction time beyond 3 h, all the active sites were exhausted as the mutual annihilation of growing grafted chains occurred, so the zeta potential decreased.

Scanning Electron Microscopy (SEM) Analysis

The study of surface topology of polymers using SEM gained much interest due to a wide range of morphological information provided by this technique. Figure 5 and Figure 6 show the micro-morphology changes of the smooth surface for natural cellulose and rough surface with branches for grafted cellulose, respectively.

Because of the existence of hydrogen bonds between the celluloses and the structures of cellulose, the

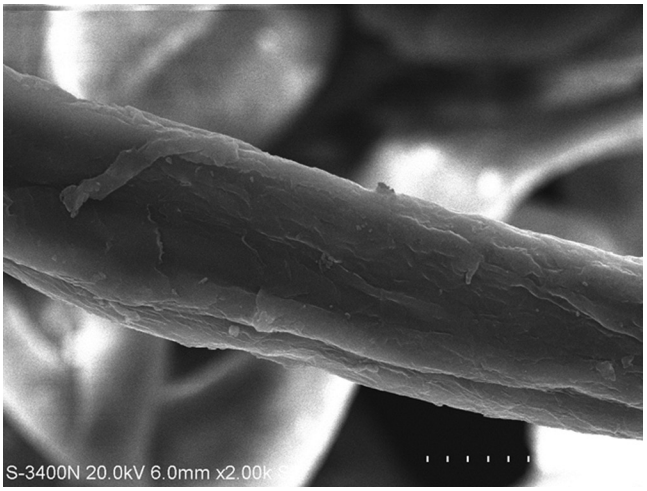

Figure 6. *SEM photographs of grafted cellulose.*

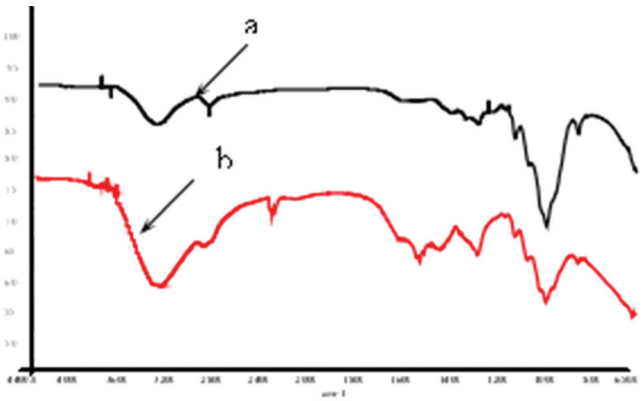

Figure 7. *FT-IR spectra of natural cellulose (a) and grafted cellulose (b).*

surface was seldom destroyed in the pulping process. However, the surface of graft copolymer presented fines with some floccules. This possibly occurred because cells on the surface of the cellulose reacted with ceric ions led to the cleave of chemical structure and the change of morphology. The floccules of grafted cellulose was cross-linked when the products were dried.

Fourier Transform Infrared Spectrum Analysis

FT-IR spectra of natural cellulose and grafted cellulose are shown in Figure 7. Assignment of the main bonds in all samples are shown in Table. 1.

Between the spectra of natural cellulose and grafted cellulose, the significant changes are the peaks at 2928 cm^{-1}, 1648 cm^{-1}, 1558 cm^{-1}, and 1473 cm^{-1}. Absorption peaks at 2928 cm^{-1}, 1648 cm^{-1}, 1558 cm^{-1}, and 1473 cm^{-1} are due to the diethylenetriamine monomer molecule, and they are not present in the spectrum of natural cellulose. After grafting, broadening bond at 3337 cm^{-1} corresponding to –OH adsorption was shifted to 3301 cm^{-1}, which would be influenced by N-H stretching vibration. Additionally, after modification, the –CO adsorption bond at 1198 cm^{-1} in natural cellulose shifted to 1169 cm^{-1}, which could be considered to be the result of the C-N stretching vibration leading to stretching vibration of the –CO– bond.

Table 1. Assignment of the Main Bonds in All Samples [19].

Peak Shift/cm^{-1}	Assignment
3700–3200	$V_{(–OH)}$
3500–3300	$V_{(–NH2–, –NH–)}$
2936–2916	$V_{(-CH-)}$
1650–1550	$\delta_{(–NH–)}$
1485–1445	$\delta_{(–CH)}$
1410–1260	$\delta_{(–OH)}$
1250–1000	$V_{(–CO–)}$
1220–1020	$V_{(–CN–)}$

X-ray Diffraction Analysis

The X-ray diffraction patterns of natural cellulose and grafted cellulose at room temperature from 2θ = 10° to 70° are shown in Figure 8. The XRD pattern of natural cellulose [Figure 8(c)] shows that it, as well as all other native polymeric substances [20], has a partial crystalline structure. There were two obvious sharp peaks at 16.03° and 22.36°, and two minor sharp peaks at 29.36° and 34.94°. These XRD results indicated the crystalline and amorphous structure of native cellulose, respectively. The XRD pattern of grafted cellulose [Figure 8(d)], compared with natural cellulose, underwent enormous changes. The sharp peaks were weakened at 16.03° and 22.36°, strengthened at 29.36°, and disappeared at 34.94°. However, two smaller sharp peaks appeared at 22.5° and 28.5°. This proved that the crystalline structure of the natural cellulose extensively changed, and the grafting reaction process would not only occur in the amorphous regions, but also in crystalline regions.

CONCLUSIONS

1. Based on the zeta potential value, optimum conditions were an initiator concentration of 40 mmol/L, mass ratio of monomer to bagasse celluloses 1:1, reaction temperature of 70°C, and a reaction time of 3 h.

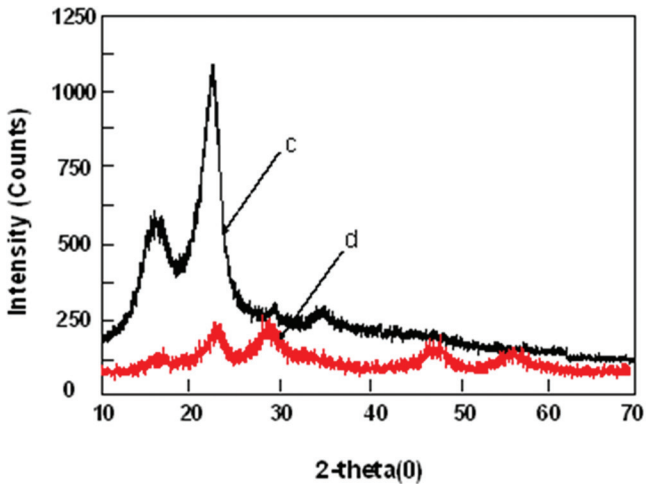

Figure 8. *X-ray diffraction pattern of natural cellulose (c) and grafted cellulose (d).*

2. The structure and properties of the grafted product were characterized by SEM, FT-IR, and XRD. The experiment showed that structure of grafted cellulose greatly changed, compared with natural cellulose.

ACKNOWLEDGMENTS

This work was financially supported by the National High Technology Research and Development Program (863 Program) 2009AA06A416 and 2010GXNSFE 013006, Guangxi Scientific Research and Technological Development Project No: 11107021-4-5 & No: 10123010-5. This work was also financially supported by the Natural Science Foundation of China (Project no 51108261).

REFERENCES

1. Boufi, S., and Belgacem, M. N. (2006). ″Modified cellulose fibres for adsorption of dissolved organic solutes,” *Cellulose 13*(1), 81–94. http://dx.doi.org/10.1007/s10570-005-9019-y
2. Dwivedi, A.D., Dubey, S.P., Hokkanen, S., Fallah, R.N., and Sillanpää, M. (2014). ″Recovery of gold from aqueous solutions by taurine modified cellulose: An adsorptive–reduction pathway” *Chemical Engineering Journal*, *255*, 97–106. http://dx.doi.org/10.1016/j.cej.2014.06.017
3. Seavey, K.C., and Glasser, W.G. (2001). ″Continuous cellulose fiber-reinforced cellulose ester composites. II. Fiber surface modification and consolidation conditions,” *Cellulose 8*(2), 161–169. http://dx.doi.org/10.1023/A:1016751015921
4. Casarano, R., Pires, P.A. R., Borin, A.C., and Seoud, O A. E. (2014). ″Novel solvents for cellulose: Use of dibenzyldimethylammonium fluoride/dimethyl sulfoxide (DMSO) as solvent for the etherification of the biopolymer and comparison with tetra(1-butyl)ammonium fluoride/DMSO,” *Industrial Crops and Products 54*: 185–191. http://dx.doi.org/10.1016/j.indcrop.2014.01.031
5. Takaichi, S., and Isogai, A. (2013). ″Oxidation of wood cellulose using 2-azaadamantane N-oxyl (AZADO) or 1-methyl-AZADO catalyst in NaBr/NaClO system,” *Cellulose 20*(4): 1979–1988. http://dx.doi.org/10.1007/s10570-013-9932-4
6. Dankovich, T., and Hsieh, Y.-L. (2007). ″Surface modification of cellulose with plant triglycerides for hydrophobicity,” *Cellulose 14*(5), 469–480. http://dx.doi.org/10.1007/s10570-007-9132-1
7. Zhuo, J., and Sun, G. (2014).″Light-induced surface graft polymerizations initiated by an anthraquinone dye on cotton fibers,” *Carbohydrate Polymers 112*, 158–64. http://dx.doi.org/10.1016/j.carbpol.2014.05.084
8. Hubbe, M.A., Rojas, O.J., Lucia, L.A. and Sain, M. (2008).″Cellulosic nanocomposites: A review,” *Bioresources 3*, 929–980.
9. Yiğitoğlu, M., and Arslan, M. (2007). ″4-Vinylpyridine and 2-hydroxyethylmethacrylate monomer mixture graft copolymerization onto poly (ethylene terephthalate) fibers using benzoyl peroxide,” *Polymer Bulletin 58*(5), 785–798. http://dx.doi.org/10.1007/s00289-006-0719-8
10. Cho, D., Lee, S., and Frey, M. W. (2012). ″Characterizing zeta potential of functional nano-fibers in a microfluidic device,” *Journal of Colloid and Interface Science 372*(1), 252–260. http://dx.doi.org/10.1016/j.jcis.2012.01.007
11. Li, H., Fu, S. Y., Peng, L. C., and Zhan, H. Y. (2012). ″Surface modification of cellulose fibers with layer-by-layer self-assembly of lignosulfonate and polyelectrolyte: Effects on fibers wetting properties and paper strength,” *Cellulose 19*(2), 533–546. http://dx.doi.org/10.1007/s10570-011-9639-3
12. Hokkanen, S., Repo, E., Suopajärvi, T., Liimatainen, H., Niinimaa, J. and Sillanpää, M. (2014). ″Adsorption of Ni(II), Cu(II) and Cd(II) from aqueous solutions by amino modified nanostructured microfibrillated cellulose,” *Cellulose 21*(3): 1471–1487. http://dx.doi.org/10.1007/s10570-014-0240-4
13. Correa, A. C., de Teixeira, E. M., Pessan, L. A., and Mattoso, L. H. C. (2010). ″Cellulose nanofibers from curaua fibers,” *Cellulose 17*(6), 1183–1192. http://dx.doi.org/10.1007/s10570-010-9453-3
14. Deshmukh, S. R., and Sing, R. P. (1987). ″Drag reduction effectiveness, shear stability and biodegradation resistance of guargum-based graft copolymers,” *Journal of Applied Polymer Science 33*(6), 1963–1975. http://dx.doi.org/10.1002/app.1987.070330610
15. Carrillo, F., Defays B., and Colom, X. (2008). ″Surface modification of lyocell fibres by graft copolymerization of thermo-sensitive poly-N-isopropylacrylamide,” *European Polymer Journal 44*(12), 4020–4028. http://dx.doi.org/10.1016/j.eurpolymj.2008.09.033
16. Kumar, V., Naithani, S., and Pandey, D. (2011). ″Optimization of reaction conditions for grafting of α-cellulose isolated from Lantana camara with acrylamide,” *Carbohydrate Polymers 86*(2), 760–768. http://dx.doi.org/10.1016/j.carbpol.2011.05.019
17. Naguib, H. F. (2002). ″Chemically induced graft copolymerization of itaconic acid onto sisal fibers,” *Journal of Polymer Research 9*(3), 207–211. http://dx.doi.org/10.1023/A:1021399826969
18. Yadav, M., Sand, A., and Behari, K. (2010). ″Synthesis and characterization of graft copolymer (alginate-g-poly (N,N-dimethylacrylamide)),” *Chinese Journal of Polymer Science 28*(5), 673–683. http://dx.doi.org/10.1007/s10118-010-9114-x
19. Chen, S. H, Yue, Q. Y., Gao, B. Y., and Li, Q. X. (2011). ″Preparation and characteristics of anion exchanger from corn stalks,” *Desalination 274*(1-3), 113–119. http://dx.doi.org/10.1016/j.desal.2011.01.080
20. Wang, L., and Xu Y. (2006). ″Preparation and characterization of graft copolymerization of ethyl acrylate onto hydroxypropyl methylcellulose in aqueous medium,” *Cellulose 13*(2), 191–200. http://dx.doi.org/10.1007/s10570-005-9043-y